

BSC**Design Calculation or Analysis Cover Sheet**

1. QA: QA

2. Page 1

Complete only applicable items.

3. System Naval SNF				4. Document Identifier 000-00C-DNF0-00100-000-00C			
5. Title Naval Long Waste Package Vertical Impact on Emplacement Pallet and Invert							
6. Group Thermal/Structural Analysis							
7. Document Status Designation <input type="checkbox"/> Preliminary <input checked="" type="checkbox"/> Committed <input type="checkbox"/> Confirmed <input type="checkbox"/> Cancelled/Superseded							
8. Notes/Comments None							
Attachments							Total Number of Pages
See Section 5							
RECORD OF REVISIONS							
9. No.	10. Reason For Revision	11. Total # of Pgs.	12. Last Pg. #	13. Originator (Print/Sign/Date)	14. Checker (Print/Sign/Date)	15. EGS (Print/Sign/Date)	16. Approved/Accepted (Print/Sign/Date)
00A	Initial issue.	39	II-13	D. G. McKenzie IV	Adam K. Scheider	N/A	M. J. Anderson 11/06/02
ECN 1	Changed status to committed since results are not expected to change.	1	1	T. Schmitt	M. Mullin	N/A	M. J. Anderson 8/12/05
00B	Change in format due to procedure change. Increased drop height to agree with latest requirements. Adjusted dimensions, masses and FER details to agree with latest sketches and drawings. Considered non-centered and angled orientations per latest requirements. Restructured temperature considerations as a sensitivity study. Added sensitivity studies of friction values and data collection time steps per reviewer comments. Major revision affecting all pages.	92	92	Kenneth Jaquay	Mohan Durani	N/A	Michael Anderson 11/17/06
00C	Eliminated middle lid and slotted sleeves to agree with latest sketches and drawings. Reduced deterministic drop height to agree with latest requirements. Ran vertical impact Capability simulations for PRA evaluations of response to impacts on drift invert steel structures with and without emplacement pallet. Special studies of temperature and invert steel material are added. Title change. This is a major revision affecting all pages.	166	166	Kenneth Jaquay <i>Kenneth Jaquay</i> 10/16/07	Mohan Durani <i>Mohan Durani</i> 10/16/07	Jason Viggato <i>Jason Viggato</i> 10/16/07	Michael Anderson <i>Michael Anderson</i> 10/16/07

DISCLAIMER

The calculations contained in this document were developed by Bechtel SAIC Company, LLC (BSC) and are intended solely for the use of BSC in its work for the Yucca Mountain Project.

CONTENTS

1. PURPOSE	12
2. REFERENCES.....	14
2.1 PROJECT PROCEDURES/DIRECTIVES.....	14
2.2 DESIGN INPUTS	14
2.3 DESIGN CONSTRAINTS.....	18
2.4 DESIGN OUTPUTS	18
3. ASSUMPTIONS.....	19
3.1 ASSUMPTIONS REQUIRING VERIFICATION	19
3.2 ASSUMPTIONS NOT REQUIRING VERIFICATION	19
4. METHODOLOGY	27
4.1 QUALITY ASSURANCE	27
4.2 USE OF SOFTWARE	27
4.3 STRESS ANALYSIS APPROACH	28
5. LIST OF ATTACHMENTS.....	30
6. BODY OF CALCULATION	37
6.1 MATERIAL PROPERTIES.....	37
6.1.1 Deterministic Calculation	37
6.1.2 Capability Calculation	42
6.2 TANGENT MODULI CALCULATIONS.....	44
6.3 IMPACT VELOCITY	45
6.4 FINITE ELEMENT REPRESENTATIONS.....	46
6.4.1 WP with EP Impact on Flat Target Surface.....	46
6.4.2 Worst Case WP with EP Flat Impact on Invert Steel	70
6.4.3 WP Impact on Invert Steel	74
7. RESULTS AND CONCLUSIONS	80
7.1 MESH VERIFICATION.....	80
7.1.1 WP Impact on EP.....	80
7.1.2 WP Impact on Invert.....	84
7.2 DETERMINISTIC CALCULATIONS.....	84
7.2.1 Offset WP Impacts	84
7.2.2 Short-Side Angled EP Impacts	95
7.2.3 Offset WP with Short-Side Angled EP Impacts	100
7.2.4 Long-Side Angled EP Impacts.....	101
7.2.5 EP Corner Impacts	102
7.2.6 Angled WP Impacts	103
7.2.7 Worst Case Impacts	104

7.3 DETERMINISTIC CALCULATIONS SENSITIVITY STUDIES	112
7.3.1 Temperature	112
7.3.2 Friction	113
7.3.3 Data Collection Rate	115
7.4 CAPABILITY CALCULATIONS	116
7.4.1 WP on EP on Flat Surface Impact	117
7.4.2 Worst Case WP on EP on Invert Impact.....	125
7.4.3 WP on Invert Impact.....	134
7.5 CAPABILITY CALCULATIONS SENSITIVITY STUDIES	152
7.5.1 Temperature	152
7.5.2 Invert Steel Material	158
7.6 MATERIAL STRENGTH VARIABILITY	162
7.7 DETERMINISTIC AND CAPABILITY CALCULATIONS SUMMARY	162

TABLES

Table 5-1 List of Electronic Files in Attachment I	30
Table 6-1 Elevated Temperature Vendor Data, Alloy 22	43
Table 6-2 Tangent Moduli	45
Table 7-1 WP Mesh Verification, 1 <i>m</i> Flat Drop on EP	81
Table 7-2 EP Mesh Verification, 1 <i>m</i> Worst Case Drop on EP	82
Table 7-3 OCB and Invert Mesh Verification, 4 <i>m/s</i> Worst Case Impact on Invert.....	84
Table 7-4 Comparative $\tau_{avg,max}$ in the OCB for WP Offset.....	93
Table 7-5 Comparative $\tau_{avg,max}$ Ratio to Flat for EP Z-Axis Rotation	99
Table 7-6 Comparative $\tau_{avg,max}$ Ratio to Centered-Flat for WP Offset and EP Z-Axis Rotation.....	101
Table 7-7 Comparative $\tau_{avg,max}$ Ratio to Flat for EP X-Axis Rotation.....	102
Table 7-8 Comparative $\tau_{avg,max}$ Ratio to Flat for EP X-Axis Rotation.....	103
Table 7-9 Comparative $\tau_{avg,max}$ Ratio to Flat for WP X-Axis Rotation	104
Table 7-10 Comparison Table for Worst Case Drops	105
Table 7-11 OCB Governing Location Stresses, 20 <i>in</i> Drop	109
Table 7-12 Temperature Sensitivity of OCB Stress Evaluation	113
Table 7-13 Friction Sensitivity of OCB Stress Evaluation.....	114
Table 7-14 Data Collection Rate Sensitivity of OCB Stress Evaluation	115
Table 7-15 WP on EP on Flat Surface Impact Capability Summary.....	117
Table 7-16 Worst Case WP on EP on Invert Impact Capability Summary	125
Table 7-17 WP on Invert Impact Capability Summary	135
Table 7-18 Temperature Effect on WP on Invert Impact Capability.....	153
Table 7-19 Invert Steel Material Choice Effect on WP on Invert Impact Capability.....	158

FIGURES

Figure 3-1	Maximum EWA Von Mises Strain Rate.....	20
Figure 6-1	Overview Model of Half FER.....	47
Figure 6-2	Centered WP w/ Trunnion Sleeve Hidden.....	48
Figure 6-3	0.75 in WP Offset w/ Trunnion Sleeve Hidden.....	48
Figure 6-4	1.5 in WP Offset w/ Trunnion Sleeve Hidden.....	49
Figure 6-5	1.75 in WP Offset w/ Trunnion Sleeve Hidden.....	49
Figure 6-6	2 in WP Offset w/ Trunnion Sleeve Hidden.....	50
Figure 6-7	2.5 in WP Offset w/ Trunnion Sleeve Hidden.....	50
Figure 6-8	2.7 in WP Offset w/ Trunnion Sleeve Hidden.....	51
Figure 6-9	2.8 in WP Offset w/ Trunnion Sleeve Hidden.....	51
Figure 6-10	2.9 in WP Offset w/ Trunnion Sleeve Hidden.....	52
Figure 6-11	3 in WP Offset w/ Trunnion Sleeve Hidden.....	52
Figure 6-12	4 in WP Offset w/ Trunnion Sleeve Hidden.....	53
Figure 6-13	2 deg Z-Axis EP rotation, Centered WP.....	54
Figure 6-14	3 deg Z-Axis EP Rotation, Centered WP.....	54
Figure 6-15	3.5 deg Z-Axis EP Rotation, Centered WP.....	54
Figure 6-16	4 deg Z-Axis EP Rotation, Centered WP.....	54
Figure 6-17	4.5 deg Z-Axis EP Rotation, Centered WP.....	55
Figure 6-18	5 deg Z-Axis EP Rotation, Centered WP.....	55
Figure 6-19	6 deg Z-Axis EP Rotation, Centered WP.....	55
Figure 6-20	3 in WP Offset w/ 4 deg EP Z-Axis Rotation.....	56
Figure 6-21	2 deg X-Axis EP Rotation, Centered WP.....	57
Figure 6-22	2 deg X-Axis and 4 deg Z-Axis EP Rotation, Centered WP.....	58
Figure 6-23	Flat EP, 2 deg X-Axis WP Rotation.....	59
Figure 6-24	Flat EP, 2.8 in Offset Y-Axis WP Rotation.....	60
Figure 6-25	Flat EP, 2.8 in Offset Y-Axis WP Rotation and Z-Axis WP Translation.....	61
Figure 6-26	Standard WP FER, Overview of WP Impact Region.....	63
Figure 6-27	Standard WP FER, Enlarged View of WP Impact Region.....	63
Figure 6-28	Standard WP FER, WP Impact Region Mesh Detail.....	64
Figure 6-29	Standard WP FER, Cross-section of Impact Region.....	64
Figure 6-30	Standard WP FER, Earlier Design Detail.....	65
Figure 6-31	Standard WP FER, Current Design Detail (With Shifted Inner Vessel).....	65
Figure 6-32	Standard EP FER Overview.....	66
Figure 6-33	Standard EP FER Inside View.....	66
Figure 6-34	Mesh Detail Near Standard EP FER Support Tube.....	67
Figure 6-35	Refined WP FER, Overview of WP Impact Region.....	67
Figure 6-36	Refined WP FER, Enlarged View of WP Impact Region.....	68
Figure 6-37	Refined WP FER, WP Impact Region Mesh Detail.....	68
Figure 6-38	Refined WP FER, Cross-section of Impact Region.....	69
Figure 6-39	Refined EP FER, Mesh Detail near EP Support Tube.....	69
Figure 6-40	Full FER of WP on EP on Invert Steel.....	70
Figure 6-41	End of FER above Transverse Beam.....	71

Figure 6-42 Meshing at End of FER above Transverse Beam	71
Figure 6-43 Quarter-Symmetry WP on EP Bridging Stiff Invert.....	72
Figure 6-44 FER of EP and WP Top Plug on either Side of Transverse Beam.....	73
Figure 6-45 Worst Case Alignment of WP, EP and Transverse Beam	73
Figure 6-46 FER Mesh of OCB and Invert Steel in Region of Contact	74
Figure 6-47 Worst Case WP on Stiff Invert Flat Impact without EP, 1 Inch Plug Offset.....	75
Figure 6-48 WP on Stiff Invert Flat Impact without EP, Maximum Offset	75
Figure 6-49 Angle Calculation.....	76
Figure 6-50 WP 5 Degree Impact on Stiff Invert	77
Figure 6-51 WP 10 Degree Impact on Stiff Invert	78
Figure 6-52 WP 18 Degree Impact on Stiff Invert	78
Figure 6-53 Standard FER, WP 18 Degree Impact on Stiff Invert.....	79
Figure 6-54 Refined FER, WP 18 Degree Impact on Stiff Invert	79
Figure 7-1 EWA MSS in the OCB, Flat Drop on EP, Standard WP Mesh	81
Figure 7-2 EWA MSS in the OCB, Flat Drop on EP, Refined WP Mesh.....	82
Figure 7-3 EWA MSS in the OCB, Worst Case Drop on EP, Standard EP Mesh	83
Figure 7-4 EWA MSS in the OCB, Worst Case Drop on EP, Refined EP Mesh.....	83
Figure 7-5 VM Stresses, 4 <i>m/s</i> Impact on 18 <i>deg</i> Invert, Standard Mesh	85
Figure 7-6 EWA VM Stress, 4 <i>m/s</i> Impact on 18 <i>deg</i> Invert, Standard Mesh.....	85
Figure 7-7 EWA VM Strain, 4 <i>m/s</i> Impact on 18 <i>deg</i> Invert, Standard Mesh.....	86
Figure 7-8 VM Stresses, 4 <i>m/s</i> Impact on 18 <i>deg</i> Invert, Refined Mesh.....	86
Figure 7-9 EWA VM Stress, 4 <i>m/s</i> Impact on 18 <i>deg</i> Invert, Refined Mesh	87
Figure 7-10 EWA VM Strain, 4 <i>m/s</i> Impact on 18 <i>deg</i> Invert, Refined Mesh	87
Figure 7-11 Centered (No Offset) WP w/ Flat EP, EWA MSS.....	88
Figure 7-12 0.75 <i>in</i> Offset WP w/ Flat EP, EWA MSS.....	88
Figure 7-13 1.5 <i>in</i> Offset WP w/ Flat EP, EWA MSS.....	89
Figure 7-14 1.75 <i>in</i> Offset WP w/ Flat EP, EWA MSS.....	89
Figure 7-15 2 <i>in</i> Offset WP, Flat EP, EWA MSS.....	90
Figure 7-16 2.5 <i>in</i> Offset WP w/ Flat EP, EWA MSS.....	90
Figure 7-17 2.7 <i>in</i> Offset WP w/ Flat EP EWA MSS.....	91
Figure 7-18 2.8 <i>in</i> Offset WP w/ Flat EP, EWA MSS.....	91
Figure 7-19 2.9 <i>in</i> Offset WP w/ Flat EP EWA MSS.....	92
Figure 7-20 3 <i>in</i> Offset WP w/ Flat EP EWA MSS.....	92
Figure 7-21 4 <i>in</i> Offset WP w/ Flat EP EWA MSS.....	93
Figure 7-22 Excel Plot of Table 7-4, $\tau_{avg,max}$ Ratio to Centered versus WP Vertical Offset	94
Figure 7-23 High Stress OCB Location for 2.8 <i>in</i> Offset WP with Flat EP Drop, <i>Pa</i>	94
Figure 7-24 2 <i>deg</i> EP Z-Axis Rotation, EWA MSS	95
Figure 7-25 3 <i>deg</i> EP Z-Axis Rotation, EWA MSS	96
Figure 7-26 3.5 <i>deg</i> EP Z-Axis Rotation, EWA MSS	96
Figure 7-27 4 <i>deg</i> EP Z-Axis Rotation, EWA MSS	97
Figure 7-28 4.5 <i>deg</i> EP Z-Axis Rotation, EWA MSS	97
Figure 7-29 5 <i>deg</i> EP Z-Axis Rotation, EWA MSS	98
Figure 7-30 6 <i>deg</i> EP Z-Axis Rotation, EWA MSS	98
Figure 7-31 Excel Plot of Table 7-5, $\tau_{avg,max}$ Ratio to Flat for EP Z-Axis Rotation	99
Figure 7-32 High Stress OCB Location for Centered WP on 4 <i>deg</i> EP Z-Axis Rotation, <i>Pa</i>	100

Figure 7-78	14 <i>m/s</i> WP on EP on Invert Impact, 5 <i>ms</i> Back View.....	131
Figure 7-79	14 <i>m/s</i> WP on EP on Invert Impact, 25 <i>ms</i> Back View.....	131
Figure 7-80	14 <i>m/s</i> WP on EP on Invert Impact, 10 <i>ms</i> , EP Only.....	131
Figure 7-81	14 <i>m/s</i> WP on EP on Invert Impact, t_{unload} , EP Only.....	131
Figure 7-82	14 <i>m/s</i> WP on EP on Invert Impact, 10 <i>ms</i> , <i>Pa</i>	132
Figure 7-83	14 <i>m/s</i> WP on EP on Invert Impact, t_{unload} , <i>Pa</i>	132
Figure 7-84	14 <i>m/s</i> WP on EP on Invert Impact, t_{unload} , <i>Pa</i>	132
Figure 7-85	14 <i>m/s</i> WP on EP on Invert Impact, t_{unload}	132
Figure 7-86	14 <i>m/s</i> WP on EP on Invert Impact, t_{unload} , Failure Zone.....	133
Figure 7-87	14 <i>m/s</i> WP on EP on Invert Impact, 23 <i>ms</i> , OCB, <i>Pa</i>	133
Figure 7-88	14 <i>m/s</i> WP on EP on Invert Impact, t_{unload} , OCB, <i>Pa</i>	133
Figure 7-89	14 <i>m/s</i> WP on EP on Invert Impact, t_{unload} , OCB, <i>Pa</i>	133
Figure 7-90	WP on EP on Invert Worst Case Impact Velocity Capability Trend.....	134
Figure 7-91	Flat 8 <i>m/s</i> Impact, 8 <i>in</i> Offset, EWA VM Stress.....	135
Figure 7-92	Flat 8 <i>m/s</i> Impact, 8 <i>in</i> Offset, t_{max} of EWA VM Stress.....	136
Figure 7-93	Flat 8 <i>m/s</i> Impact, 8 <i>in</i> Offset, EWA VM Strain.....	136
Figure 7-94	Flat 8 <i>m/s</i> Impact, 8 <i>in</i> Offset, EWA VM Strain at t_{max}	137
Figure 7-95	Flat 4 <i>m/s</i> Impact, 1 <i>in</i> Offset, EWA VM Stress.....	137
Figure 7-96	Flat 4 <i>m/s</i> Impact, 1 <i>in</i> Offset, t_{max} of EWA VM Stress.....	138
Figure 7-97	Flat 4 <i>m/s</i> Impact, 1 <i>in</i> Offset, EWA VM Strain.....	138
Figure 7-98	Flat 4 <i>m/s</i> Impact, 1 <i>in</i> Offset, EWA VM Strain at t_{max}	139
Figure 7-99	Flat 8 <i>m/s</i> Impact, 1 <i>in</i> Offset, EWA VM Stress.....	139
Figure 7-100	Flat 8 <i>m/s</i> Impact, 1 <i>in</i> Offset, t_{max} of EWA VM Stress.....	140
Figure 7-101	Flat 8 <i>m/s</i> Impact, 1 <i>in</i> Offset, EWA VM Strain.....	140
Figure 7-102	Flat 8 <i>m/s</i> Impact, 1 <i>in</i> Offset, EWA VM Strain at t_{max}	141
Figure 7-103	Flat 10 <i>m/s</i> Impact, 1 <i>in</i> Offset, VM Stresses.....	141
Figure 7-104	Flat 10 <i>m/s</i> Impact, 1 <i>in</i> Offset, t_{flow} and t_{unload} of VM Stresses.....	142
Figure 7-105	Flat 10 <i>m/s</i> Impact, 1 <i>in</i> Offset, EWA VM Stress.....	142
Figure 7-106	Flat 10 <i>m/s</i> Impact, 1 <i>in</i> Offset, EWA VM Strain.....	143
Figure 7-107	Flat 10 <i>m/s</i> Impact, 1 <i>in</i> Offset, EWA VM Strains at t_{flow} and t_{unload}	143
Figure 7-108	5 <i>deg</i> 4 <i>m/s</i> Impact, 1 <i>in</i> Offset, EWA VM Stress.....	144
Figure 7-109	5 <i>deg</i> 4 <i>m/s</i> Impact, 1 <i>in</i> Offset, t_{max} of EWA VM Stress.....	144
Figure 7-110	5 <i>deg</i> 4 <i>m/s</i> Impact, 1 <i>in</i> Offset, EWA VM Strain.....	145
Figure 7-111	5 <i>deg</i> 4 <i>m/s</i> Impact, 1 <i>in</i> Offset, EWA VM Strain at t_{max}	145
Figure 7-112	10 <i>deg</i> 4 <i>m/s</i> Impact, 1 <i>in</i> Offset, EWA VM Stress.....	146
Figure 7-113	10 <i>deg</i> 4 <i>m/s</i> Impact, 1 <i>in</i> Offset, t_{max} of EWA VM Stress.....	146
Figure 7-114	10 <i>deg</i> 4 <i>m/s</i> Impact, 1 <i>in</i> Offset, EWA VM Strain.....	147
Figure 7-115	10 <i>deg</i> 4 <i>m/s</i> Impact, 1 <i>in</i> Offset, EWA VM Strain at t_{max}	147
Figure 7-116	18 <i>deg</i> 5 <i>m/s</i> Impact, 1 <i>in</i> Offset, VM Stresses.....	148
Figure 7-117	18 <i>deg</i> 5 <i>m/s</i> Impact, 1 <i>in</i> Offset, t_{flow} and t_{unload} of VM Stresses.....	148
Figure 7-118	18 <i>deg</i> 5 <i>m/s</i> Impact, 1 <i>in</i> Offset, EWA VM Stress.....	149
Figure 7-119	18 <i>deg</i> 5 <i>m/s</i> Impact, 1 <i>in</i> Offset, EWA VM Strain.....	149
Figure 7-120	18 <i>deg</i> 5 <i>m/s</i> Impact, 1 <i>in</i> Offset, EWA VM Strain at t_{flow} and t_{unload}	150
Figure 7-121	VM Stresses at t_{unload} , Full FER, <i>Pa</i>	150
Figure 7-122	VM Stresses at t_{unload} , Full FER, Failure Location, <i>Pa</i>	151

Figure 7-123 VM Stresses at t_{unload} , OCB, Inner View, Pa	151
Figure 7-124 VM Stresses at t_{unload} , OCB Close-up, Pa	151
Figure 7-125 VM Stress at t_{unload} , OCB, Section View, Pa	151
Figure 7-126 WP on Invert Impact Velocity Capability Trend	152
Figure 7-127 300°C WP on Invert 4 m/s Impact, EWA VM Stress	153
Figure 7-128 300°C WP on Invert 4 m/s Impact, t_{max} of EWA VM Stress	154
Figure 7-129 300°C WP on Invert 4 m/s Impact, EWA VM Strain	154
Figure 7-130 300°C WP on Invert 4 m/s Impact, EWA VM Strain	155
Figure 7-131 300°C WP on Invert 5 m/s Impact, VM Stresses	155
Figure 7-132 300°C WP on Invert 5 m/s Impact, t_{max} of VM Stresses	156
Figure 7-133 300°C WP on Invert 5 m/s Impact, EWA VM Stress	156
Figure 7-134 300°C WP on Invert 5 m/s Impact, EWA VM Strain	157
Figure 7-135 300°C WP on Invert 5 m/s Impact, EWA VM Stress at t_{max}	157
Figure 7-136 Sensitivity of RT versus 300°C WP on Impact Capability	158
Figure 7-137 WP on A588 Invert 5 m/s Impact, VM Stresses	159
Figure 7-138 WP on A588 Invert 5 m/s Impact, t_{flow} and t_{unload} of VM Stresses	159
Figure 7-139 WP on A588 Invert 5 m/s Impact, EWA VM Stress	160
Figure 7-140 WP on A588 Invert 5 m/s Impact, EWA VM Strain	160
Figure 7-141 WP on A588 Invert 5 m/s Impact, VM Strain at t_{flow} and t_{unload}	161
Figure 7-142 WP on A588 Invert 5 m/s Impact, Deformation and VM Stresses at t_{unload} , Pa	161
Figure 7-143 18 deg tilted 20 in drop on Invert, ASME Properties, Governing Location	163
Figure 7-144 18 deg tilted 20 in drop on Invert, ASME Properties, $\sqrt{R \cdot t}$ Location	163
Figure 7-145 Mean Capability for Worst Case Impacts	164
Figure 7-146 Mean and 2σ Capability for WP Worst Case Impacts	165

ACRONYMS

ACC:	Project Accession Number for a Reference
ASM	American Society for Metals
ASME	American Society of Mechanical Engineers
ASTM	American Society for Testing and Materials
BSC	Bechtel SAIC Company, LLC.
CS	Carbon Steel
DOE	United States Department of Energy
EP	Emplacement Pallet
ETF	Expended Toughness Fraction
EWA	Element Wall-Averaged
FER	Finite Element Representation
HP	Hewlett-Packard
MSS	Maximum Shear Stress
OCB	Outer Corrosion Barrier
PRA	Probabilistic Risk Assessment
RT	Room Temperature
SNF	Spent Nuclear Fuel
SI	(ASME) Stress Intensity
SS	Stainless Steel
TEV	Transport and Emplacement Vehicle
VM	Von Mises Effective (Stress or Strain)
WP	Waste Package

1. PURPOSE

The purpose of this calculation is to determine the structural response of the Naval Long waste package (WP) with the emplacement pallet (EP) when they are subjected to event sequence impacts onto horizontal surfaces including the drift invert steel structure. This calculation includes considerations of non-centered and angled orientations of the WP, EP and invert steel. This calculation is addressing either a drop by the Transport and Emplacement Vehicle (TEV) or vertical impacts in the drift due to a seismic event. This calculation addresses both EP and invert steel contacts with the outer corrosion barrier (OCB) between its end sleeves.

There are three event sequence configurations and three types of calculations. The first configuration is the WP orientated in different positions on the EP and together impacting on an unyielding horizontal surface. The concern is the stresses in the WP at the OCB-to-EP contact zone. It only considers realistic orientations between the WP and EP that can occur during a drop of the WP on the EP from the TEV or in the drifts during vertical motion dominated seismic events. The EP is modeled without eroding elements to induce maximum stresses into the OCB.

Two types of calculations are performed on the first configuration; a deterministic calculation and a Capability calculation. The deterministic calculation is for a fixed drop height and uses the worst case orientation, minimum strength properties and conservative acceptable stress limits. The Capability calculation is at the same worst case orientation for several impact velocities to permit a damage magnitude prediction and uses average strength properties and response scatter accounting for material strength uncertainties.

The second configuration is the WP laterally centered on the EP which in turn is centered on the longitudinal beams of the invert steel structure. The lateral centering of the WP and EP is a representative “median” lateral position for the WP impacting the EP and invert steel. The EP is modeled with eroding elements to induce more realistic downward displacements and velocities of the WP when the OCB reaches the transverse beams of the invert steel structure. Different axial positions of the WP, EP and invert steel are used to determine the positional sensitivity of stresses in the OCB at the OCB-to-invert steel contact zone.

A Capability calculation is conducted using several axial positions and impact velocities and the final worst case location Capability includes response scatter accounting for material strength uncertainties.

The last configuration is the most extensively studied and is the WP without the EP and addresses angled vertical impacts of the WP directly on the drift invert steel structure’s transverse beams. This is intended to represent severe seismic events that separate the EP away from its starting location between the WP and invert steel structure.

This calculation also determines the sensitivity of the structural response to temperature, friction coefficient values, data collection time steps and invert steel material. The scope of this document is limited to reporting the calculation results for the OCB in terms of ASME stress

intensity (SI) ratios based on element wall-averaged (EWA) maximum shear stress (MSS) and in terms of strain energy ratios based on EWA von Mises effective (VM) stresses and strains. This calculation is intended for use in support of the design activities for the license application design of the Naval Long WP. The information regarding the EP, Naval Long WP and invert steel structure used in this calculation is based on the proposed/potential design presented by the drawings and sketches in References 2.2.16 to 2.2.18, 2.2.27 to 2.2.39 and 2.2.41 to 2.2.43.

2. REFERENCES

2.1 PROJECT PROCEDURES/DIRECTIVES

- 2.1.1 EG-PRO-3DP-G04B-00037, Rev. 9. *Calculations and Analyses*. Las Vegas, Nevada: Bechtel SAIC Company. ACC: ENG.20070717.0004
- 2.1.2 IT-PRO-0011, Rev. 7. *Software Management*. Las Vegas, Nevada: Bechtel SAIC Company. ACC: DOC.20070905.0007
- 2.1.3 ORD (Office of Repository Development) 2007. *Repository Project Management Automation Plan*. 000-PLN-MGR0-00200-000, Rev. 00E. Las Vegas, Nevada: U.S. Department of Energy, Office of Repository Development. ACC: ENG.20070326.0019

2.2 DESIGN INPUTS

- 2.2.1 Allegheny Ludlum 2006. Technical Data Blue Sheet, Stainless Steels Chromium-Nickel-Molybdenum, Types 316 (S31600), 316L (S31603), 317 (S31700), 317L (S31703). Technical Data Blue Sheet. [Brackenridge, Pennsylvania]: Allegheny Ludlum. TIC: 259471.
- 2.2.2 BSC (Bechtel SAIC Company) 2007. *Basis of Design for the TAD Canister-Based Repository Design Concept*. 000-3DR-MGR0-00300-000-001. Las Vegas, Nevada: Bechtel SAIC Company. ACC: ENG.20071002.0042
- 2.2.3 ASM (American Society for Metals) 1980. *Properties and Selection: Stainless Steels, Tool Materials and Special-Purpose Metals*. Volume 3 of *Metals Handbook*. 9th Edition. Benjamin, D., ed. Metals Park, Ohio: American Society for Metals. TIC: 209801. ISBN: 0-87170-009-3
- 2.2.4 ASM International 1990. *Properties and Selection: Irons, Steels, and High-Performance Alloys*. Volume 1 of *Metals Handbook*. 10th Edition. Materials Park, Ohio: ASM International. TIC: 245666. ISBN: 0-87170-377-7
- 2.2.5 ASME (American Society of Mechanical Engineers) 2001. *2001 ASME Boiler and Pressure Vessel Code (includes 2002 addenda)*. New York, New York: American Society of Mechanical Engineers. TIC: 251425.
- 2.2.6 ASTM G 1-03. 2003. *Standard Practice for Preparing, Cleaning, and Evaluating Corrosion Test Specimens*. West Conshohocken, Pennsylvania: American Society for Testing and Materials. TIC: 259413.
- 2.2.7 Avallone, E.A. and Baumeister, T., III, eds. 1987. *Marks' Standard Handbook for Mechanical Engineers*. 9th Edition. New York, New York: McGraw-Hill. TIC: 206891. ISBN: 0-07-004127-X

- 2.2.8 Boyer, H.E., ed. 2000. *Atlas of Stress-Strain Curves*. Metals Park, Ohio: ASM International. TIC: 248901. ISBN: 0-87170-240-1
- 2.2.9 BSC 2002. *Waste Package Tip-Over of 5-DHLW/DOE Short*. CAL-DDC-ME-000004 REV A. Las Vegas, Nevada: Bechtel SAIC Company. ACC: MOL.20020614.0038.
- 2.2.10 LS-DYNA. V.970.3858 D MPP. 2003. HP-UX 11.22. STN: 10300-970.3858 D MPP-00.
- 2.2.11 DOE 2003. *Validation Test Report for LS-DYNA Version 970.3858 D MPP*. 10300-VTR-970.3858 D MPP-00. Las Vegas, Nevada: U.S. Department of Energy, Office of Repository Development. ACC: MOL.20031218.0337.
- 2.2.12 Livermore Software Technology Corporation. 2003. LS-DYNA Keyword User's Manual. Version 970. Livermore, California: Livermore Software Technology Corporation. TIC: 254203.
- 2.2.13 Naples, E.M. 1999. Thermal, Shielding, and Structural Information on the Naval Spent Nuclear Fuel (SNF) Canister. Letter from E.M. Naples (Department of the Navy) to D.C. Haught (DOE/YMSCO), August 6, 1999, with enclosures. ACC: MOL.19991001.0133.
- 2.2.14 DOE (U.S. Department of Energy) 2007. "High-Level Radioactive Waste and U.S. Department of Energy and Naval Spent Nuclear Fuel to the Civilian Radioactive Waste Management System." Volume 1 of *Integrated Interface Control Document*. DOE/RW-0511, Rev. 3. Washington, D.C.: U.S. Department of Energy, Office of Civilian Radioactive Waste Management. ACC: DOC.20070125.0002.
- 2.2.15 Alemu, N. ed. 2007. *Waste Package Component Design Methodology Report*. 000-30R-WIS0-00100-000-003. Las Vegas, Nevada: Bechtel SAIC Company. ACC: ENG.20070927.0034.
- 2.2.16 BSC 2007. *Design and Engineering, Repository Subsurface Emplacement Drifts Steel Invert Structure Plan & Elevation*. 800-SS0-SSE0-00201-000-00C. Las Vegas, Nevada: Bechtel SAIC Company. ACC: ENG.20071002.0056.
- 2.2.17 BSC 2007. *Design and Engineering, Repository Subsurface Emplacement Drifts Steel Invert Structure Section & Materials*. 800-SS0-SSE0-00202-000-00C. Las Vegas, Nevada: Bechtel SAIC Company. ACC: ENG.20071002.0057.
- 2.2.18 BSC 2007. *Design and Engineering, Repository Subsurface Emplacement Drifts Steel Invert Structure Sections & Details*. 800-SS0-SSE0-00203-000-00C. Las Vegas, Nevada: Bechtel SAIC Company. ACC: ENG.20071002.0058.
- 2.2.19 Dieter, G.E. 1976. *Mechanical Metallurgy*. 2nd Edition. Materials Science and Engineering Series. New York, New York: McGraw-Hill Book Company. TIC: 247879. ISBN: 0-07-016891-1

- 2.2.20 Nicholas, T. 1980. *Dynamic Tensile Testing of Structural Materials Using a Split Hopkinson Bar Apparatus*. AFWAL-TR-80-4053. Wright-Patterson Air Force Base, Ohio: Air Force Wright Aeronautical Laboratories. TIC: 249469.
- 2.2.21 Halliday, D., et. al. 1988. *Fundamentals of Physics*. 3rd Edition Extended. New York, New York: John Wiley & Sons. TIC: 234765. ISBN: 0-471-81995-6
- 2.2.22 Haynes International. 1997. Hastelloy C-22 Alloy. Kokomo, Indiana: Haynes International. TIC: 238121.
- 2.2.23 Hechmer, J.L. and Hollinger, G.L. 1998. *3D Stress Criteria Guidelines for Application*. WRC Bulletin 429. New York, New York: Welding Research Council. TIC: 254432. ISBN: 1-58145-436-8
- 2.2.24 Roark, R.J. and Young, W.C. 1975. *Formulas for Stress and Strain*. 5th Edition. New York, New York: McGraw-Hill. TIC: 240746. ISBN: 0-07-053031-9
- 2.2.25 LL020603612251.015. Slow Strain Rate Test Generated Stress Corrosion Cracking Data. Submittal date: 08/27/2002.
- 2.2.26 BSC 2004. *Stress Intensity Classification: Waste Package Outer Corrosion Barrier Stresses due to Horizontal Drop Event*. 000-00C-MGR0-01600-000-00A. Las Vegas, Nevada: Bechtel SAIC Company. ACC: ENG.20041122.0001.
- 2.2.27 BSC 2004. *Design and Engineering, Emplacement Pallet Assembly Exploded*. 000-M00-SSE0-00302-000-00A. Las Vegas, Nevada: Bechtel SAIC Company. ACC: ENG.20040224.0006.
- 2.2.28 BSC 2004. *Design and Engineering, Emplacement Pallet Assembly Plate 1*. 000-M00-SSE0-00304-000-00A. Las Vegas, Nevada: Bechtel SAIC Company. ACC: ENG.20040224.0008.
- 2.2.29 BSC 2004. *Design and Engineering, Emplacement Pallet Assembly Plate 2*. 000-M00-SSE0-00305-000-00A. Las Vegas, Nevada: Bechtel SAIC Company. ACC: ENG.20040224.0009.
- 2.2.30 BSC 2004. *Design and Engineering Emplacement Pallet Assembly Plate 3*. 000-M00-SSE0-00306-000-00A. Las Vegas, Nevada: Bechtel SAIC Company. ACC: ENG.20040224.0010.
- 2.2.31 BSC 2004. *Design and Engineering Emplacement Pallet Assembly Plate 4*. 000-M00-SSE0-00307-000-00A. Las Vegas, Nevada: Bechtel SAIC Company. ACC: ENG.20040224.0011.

- 2.2.32 BSC 2004. *Design and Engineering Emplacement Pallet Assembly Plate 5*. 000-M00-SSE0-00308-000-00A. Las Vegas, Nevada: Bechtel SAIC Company. ACC: ENG.20040224.0012.
- 2.2.33 BSC 2004. *Design and Engineering, Emplacement Pallet Assembly Plate 6*. 000-M00-SSE0-00309-000-00A. Las Vegas, Nevada: Bechtel SAIC Company. ACC: ENG.20040224.0013.
- 2.2.34 BSC 2004. *Design and Engineering, Emplacement Pallet Assembly Plate 7*. 000-M00-SSE0-00310-000-00A. Las Vegas, Nevada: Bechtel SAIC Company. ACC: ENG.20040224.0014.
- 2.2.35 BSC 2004. *Design and Engineering, Emplacement Pallet Assembly Plate 8*. 000-M00-SSE0-00311-000-00A. Las Vegas, Nevada: Bechtel SAIC Company. ACC: ENG.20040224.0015.
- 2.2.36 BSC 2004. *Design and Engineering, Emplacement Pallet Assembly Plate 9*. 000-M00-SSE0-00312-000-00A. Las Vegas, Nevada: Bechtel SAIC Company. ACC: ENG.20040224.0016.
- 2.2.37 BSC 2004. *Design and Engineering, Emplacement Pallet Assembly Tube 1*. 000-M00-SSE0-00313-000-00A. Las Vegas, Nevada: Bechtel SAIC Company. ACC: ENG.20040224.0017.
- 2.2.38 BSC 2004. *Design and Engineering, Emplacement Pallet Assembly Tube 2*. 000-M00-SSE0-00314-000-00A. Las Vegas, Nevada: Bechtel SAIC Company. ACC: ENG.20040224.0018.
- 2.2.39 BSC 2004. *Design and Engineering, Emplacement Pallet Assembly Tube 3*. 000-M00-SSE0-00315-000-00A. Las Vegas, Nevada: Bechtel SAIC Company. ACC: ENG.20040224.0019.
- 2.2.40 BSC 2005. *IED Waste Package Processes, Ground Motion Time Histories, and Testing and Materials*. 800-IED-WIS0-00501-000-00A. Las Vegas, Nevada: Bechtel SAIC Company. ACC: ENG.20050406.0004.
- 2.2.41 BSC 2007. *Design and Engineering, Naval Long Waste Package Sketch*. 000-MWK-DNF0-00301-000-00B. Las Vegas, Nevada: Bechtel SAIC Company. ACC: ENG.20070227.0001
- 2.2.42 BSC 2007. *Design and Engineering, Naval Long Waste Package Sketch*. 000-MWK-DNF0-00302-000-00B. Las Vegas, Nevada: Bechtel SAIC Company. ACC: ENG.20070227.0002

- 2.2.43 BSC 2007. *Design and Engineering, Naval Long Waste Package Sketch*. 000-MWK-DNF0-00303-000-00B. Las Vegas, Nevada: Bechtel SAIC Company. ACC: ENG.20070227.0003
- 2.2.44 Special Metals 2006. INCONEL® Alloy 22. Publication Number SMC-049. Huntington, West Virginia: Special Metals. TIC: 259169.
- 2.2.45 ASTM 2005. A 588/A 588M – 05. *Standard Specification for High-Strength Low-Alloy Structural Steel, up to 50 ksi [345 MPa] Minimum Yield Point, with Atmospheric Corrosion Resistance*. West Conshohocken, Pennsylvania: American Society for Testing and Materials. TIC: 258058.
- 2.2.46 BSC 2007. *Design and Engineering, Stress Intensity Classification: Waste Package Outer Corrosion Barrier Stresses due to Drop with Emplacement Pallet*. 000-00C-MGR0-03200-000-00A. Las Vegas, Nevada: Bechtel SAIC Company. ACC: ENG.20070221.0001
- 2.2.47 BSC 2007. *Design and Engineering, Material Modeling of Alloy 22 Test Specimen Data*. 000-00C-WIS0-03200-000-00A. Las Vegas, Nevada: Bechtel SAIC Company. ACC: ENG.20070711.0001
- 2.2.48 Allegheny Technologies 2004. 004223-0069-001-2, *Nickel-Based Alloy Weld Filler Material and Base Metal Composition Test Program, Volume #1 Final Technical Report Appendices [sic] A-C*. 004223-0069-001-2, Rev 000. Albany, Oregon: Allegheny Technologies. ACC: ENG.20040507.0005

2.3 DESIGN CONSTRAINTS

None

2.4 DESIGN OUTPUTS

The results of this calculation will be used to update or develop these references.

- 2.4.1 BSC 2004. *Naval Waste Package Design Report*. 000-00C-DNF0-00800-000, REV 00B. Las Vegas, Nevada: Bechtel SAIC Company
- 2.4.2 BSC 2007. *TAD Waste Package Design Report*. 000-00C-DSC0-00100-000, REV 00A. Las Vegas, Nevada: Bechtel SAIC Company
- 2.4.3 BSC 2007. *Preliminary Preclosure Nuclear Safety Design Bases*. 000-PSA-MGR0-01000-000 Rev 001. Las Vegas, Nevada: Bechtel SAIC Company. ACC: ENG.20071015.0008

3. ASSUMPTIONS

In the course of developing this document, the following assumptions are made regarding the WP structural calculations.

3.1 ASSUMPTIONS REQUIRING VERIFICATION

- 3.1.1 The dimensions, masses and materials of the WP and EP used in the development of this calculation, corresponding to the drawings and sketches of References 2.2.27 to 2.2.39 and References 2.2.41 to 2.2.43 are assumed to be the same as the final definitive design. The rationale for this assumption is that the design of References 2.2.27 to 2.2.39 and References 2.2.41 to 2.2.43 is created for the License Application (LA). This assumption is used in Section 6.4 and will require verification at completion of the final definitive design.

3.2 ASSUMPTIONS NOT REQUIRING VERIFICATION

- 3.2.1 Strain-rate-dependent material properties are not published in traditional sources (e.g., the ASTM, ASME and ASM standards, codes and metal property data) for ASME SB-575 [UNS N06022], ASME SA-240 [UNS S31600, with modified N & C], ASME SA-36 [UNS K02600] and ASME SA-240 [UNS S31603], hereinafter termed Alloy 22, 316 stainless steel (SS), A36 carbon steel (CS) and 316L SS respectively. The material properties obtained under static loading conditions are assumed for these materials. The rationale for this assumption is that the material properties used in this calculation do not significantly change at the maximum EWA strain rates reached in the course of the event sequences. Figure 3-1 is a time plot of the EWA VM strain during the largest RT simulated impact (8 m/s) of the WP directly on the invert steel (see Section 7.4.3). The maximum EWA effective strain rate [slope of the curve between 1 and 3 ms] = $0.125/0.002 \text{ s} = 62.5 \text{ s}^{-1}$. The presented plot is for the OCB failure location. For this value of strain rate, Reference 2.2.20 (Figures 27 and 30, pages 42 and 45, respectively) indicates only a minor (less than 20%) strengthening of the higher strength steels. Therefore, the impact of using material properties obtained under static loading conditions will be a secondary effect and this assumption does not require verification. This assumption is used in Section 6.1 and is consistent with Section 6.1.1.2 in Reference 2.2.15.
- 3.2.2 The room temperature (RT) (20°C [68°F]) Poisson's ratio of Alloy 22 is not published in traditional sources. Therefore, the RT Poisson's ratio of ASME SB-443 [UNS N06625], hereinafter termed Alloy 625, is assumed for Alloy 22. The chemical compositions of Alloy 22 and Alloy 625 are similar since they are both 600 Series nickel-base alloys (Reference 2.2.5, Section II, Part B, SB-575, Table 1 and Reference 2.2.3, p. 143, respectively). Therefore, the difference in their Poisson's ratio is expected to be small. The rationale for this expectation is that Reference 2.2.3 pages 141, 143 and 145 indicate small differences in RT Poisson ratio values for the 600 Series nickel-base alloy family:

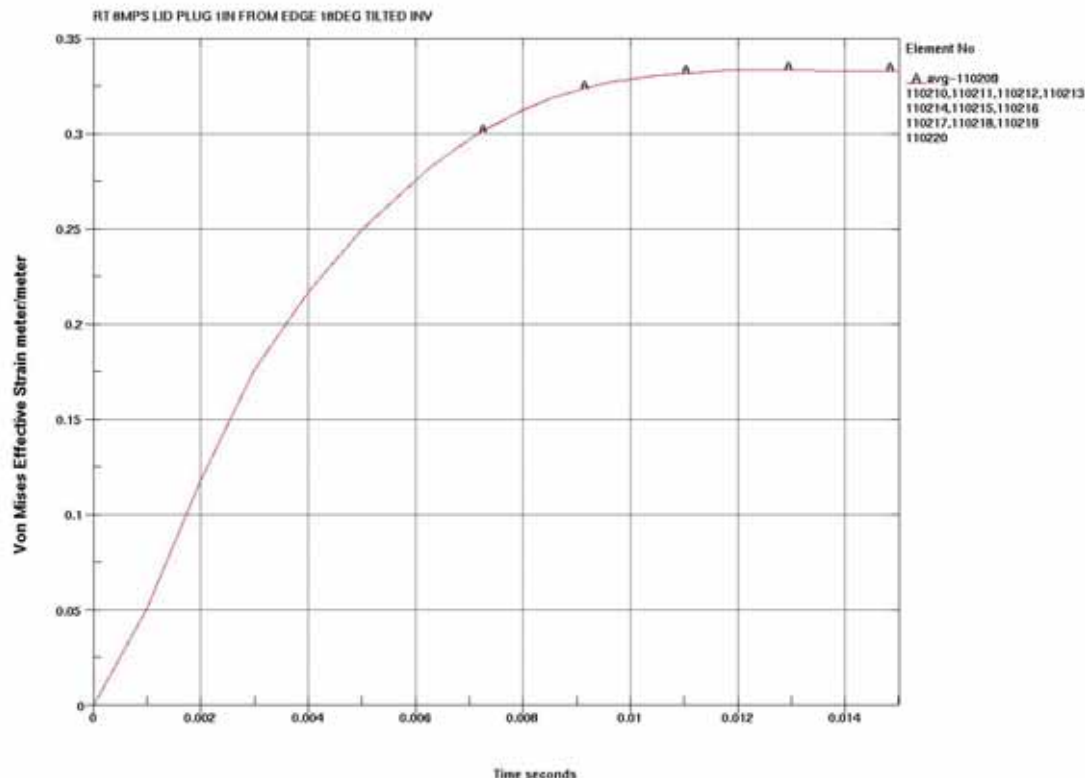


Figure 3-1 Maximum EWA Von Mises Strain Rate

Alloy 600 [UNS N06600] = 0.290

Alloy 625 [UNS N06625] = 0.278

Alloy 690 [UNS N06690] = 0.289

The impact on stress results of small differences in Poisson's ratio is anticipated to be negligible. The rationale for this anticipation is that the Reference 2.2.24 Table 30 stress formulas for cylindrical shells indicate insensitivity to Poisson's ratio. For the loading case of uniform radial shear loads (Case 8), the key breaching stress, the maximum hoop circumferential membrane stress, is proportional to Poisson's ratio, ν , through the term $(1 - \nu^2)^{1/4}$. Using the lowest and highest values of the three 600 Series nickel-base alloy ν values, 0.278 and 0.290, the difference in maximum hoop circumferential membrane stress values, all things being equal except ν , is a negligible 0.2%. Therefore, this study of parametric variations provides verification of this assumption per Reference 2.1.1 page 4 ("Verification may include . . . studies of parametric variations") and further verification of this assumption is not required. This assumption is used in Section 6.1 and is consistent with Section 6.1.1.7 of Reference 2.2.15.

- 3.2.3 The RT uniform strain (engineering strain corresponding to engineering tensile strength) of 316 SS and Alloy 22 is not listed in traditional sources. Therefore, it is assumed that the RT uniform strain is 90% of the RT elongation for both materials. The rationale for

this assumption is based the shape of RT engineering stress-strain curves for the materials (Reference 2.2.8, page 304 and Reference 2.2.25, S02234_001 Mechanical Deformation, file: "LL020603612251.015 Instron Data yr 2002"). The use of Reference 2.2.25 was approved as the appropriate data for the intended use in an Information Exchange Document (Reference 2.2.40). Therefore this assumption does not require verification. This assumption is used in Section 6.1 and corresponds to Section 6.1.1.5 of Reference 2.2.15.

- 3.2.4 The RT uniform strain of 316L SS is not listed in traditional sources. Therefore, it is assumed that the RT uniform strain is 60 percent of the RT elongation. The rationale for this assumption is based on measurements of engineering stress-strain curves for "as-received" 316L material at moderate strain rate (8 s^{-1}) (Reference 2.2.8, page 305). Therefore this assumption does not require verification. This assumption is used in Section 6.1 and corresponds to Section 6.1.1.4 of Reference 2.2.15.
- 3.2.5 The RT Poisson's ratio of 316L SS is not published in traditional sources. Therefore, the RT Poisson's ratio of 316 SS is assumed for 316L SS. The chemical compositions of 316L SS and 316 SS are similar (Reference 2.2.5, Section II, Part A, SA-240, Table 1) because they are both 300 Series (austenitic) stainless steels. Therefore, the difference in their Poisson's ratio is expected to be small. The rationale for this expectation is that Reference 2.2.3 page 755 Figure 15 indicates small differences in RT Poisson ratio values for the 300 Series SS family:

Type 304 SS [UNS S30400] = 0.290

Type 316 SS [UNS S31600] = 0.298

Type 310 SS [UNS S31000] = 0.308

The impact on stress results of small differences in Poisson's ratio is anticipated to be negligible. The rationale for this anticipation is that the Reference 2.2.24 Table 30 stress formulas for cylindrical shells indicate insensitivity to Poisson's ratio. For the loading case of uniform radial shear loads (Case 8), the key breaching stress, the maximum hoop circumferential membrane stress, is proportional to Poisson's ratio, ν , through the term $(1 - \nu^2)^{1/4}$. Using the lowest and highest values of the three 300 Series SS ν values, 0.290 and 0.308, the difference in maximum hoop circumferential membrane stress values, all things being equal except ν , is a negligible 0.3%. Therefore, this study of parametric variations provides verification of this assumption per Reference 2.1.1 page 4 (*"Verification may include . . . studies of parametric variations"*) and further verification of this assumption is not required. This assumption is used in Section 6.1 and is consistent with Section 6.1.1.9 of Reference 2.2.15.

- 3.2.6 The friction coefficients for contacts occurring between the materials used in this calculation are not published in traditional sources. It is, therefore, assumed that the dynamic (sliding) friction coefficient is 0.4 for all contacts. The rationale for this assumption is that this friction coefficient represents a reasonable lower bound value for most metal-on-metal contacts (see Reference 2.2.7, Table 3.2.1, page 3-26). A sensitivity

study is conducted in this calculation with the friction coefficient revised to 0.2 and 1.0 (see Section 7.3.2). The simulations using 0.4 and 1.0 result in exactly the same maximum stress response (critical contact surfaces lock-up identically in both simulations) at the governing OCB location and the simulation using 0.2 results in lower stress response (the sliding surfaces dissipate energy and reduce the impact load). Therefore the assumption of a 0.4 value is reasonable and does not require verification. This assumption is used in Section 6.4 and is consistent with Section 6.1.1.15 and 6.1.1.16 of Reference 2.2.15.

- 3.2.7 The exact mass and geometry of the Naval Long canister is simplified for the purpose of this calculation. The maximum recordable weight, 49,320 kilogram (*kg*) (54.25 tons) (Reference 2.2.14, Figure C-17, Note 3), is assumed to be distributed in a thick-walled (9.1 inch [*in*]) hollow cylinder with a 15 *in* top plug, 3.5 *in* bottom lid (Reference 2.2.13, Enclosure 3B, Drawing 6251E52) and properties of 316L SS (Reference 2.2.13, Enclosure 3, page 4). The increased wall thickness is back-calculated from the targeted weight. The increased canister stiffness by the increased wall thickness is offset by the ignored SNF stiffness and is inconsequential (see Assumption 3.2.12). The bottom lid is replaced with a 15 *in* end plug to facilitate the computational simplification and reduced computer demand through use of model reflections and symmetry boundary conditions. This increase of bottom end weight will not significantly affect the governing top end OCB stress location stresses. Section 5.6 of Reference 2.2.9 indicates that higher stresses occur when gaps are closed in load paths, therefore the axial gaps between the canister and inner vessel are removed by lengthening the canister (while preserving model symmetry). These simplifications slightly increase the weight of the canister to 53,053 *kg*. This assumption provides a set of bounding results for the deterministic calculation and reasonable results for the Capability calculations, while simplifying the finite element representation (FER). Therefore this assumption does not require verification. This assumption is used in Sections 6.1.1 and 6.4. Additionally, the overall center of gravity of the total mass of the canister is located 108 *in* from the bottom external surface and satisfies the Reference 2.2.13, Enclosure 3, page 3 requirement to be between 103 and 123 *in*.
- 3.2.8 The target surface for the deterministic calculation of the WP with EP drop event is the top surface of a 1.95 *m* (77 *in*) length x 0.64 *m* (25 *in*) width x 0.20 *m* (8 *in*) depth base-anchored block (see Figure 6-1) that is assumed to be unyielding (i.e., elastic), and comprised of RT A36 CS material. The rationale for this assumption is that lack of inelastic (energy dissipating) distortion of the target surface maximizes the stresses in the falling WP and is therefore bounding. This assumption is used in Sections 6.1.1 and 6.4.1 and is consistent with Section 7.1.2.6 of Reference 2.2.15.
- 3.2.9 The variation of functional friction coefficient between the static and dynamic value as a function of relative velocity of the surfaces in contact (see Reference 2.2.12, page 6.9) is not published in traditional sources for the materials used in this calculation. Therefore, the effect of relative velocity of the surfaces in contact is not included in this calculation by assuming that the functional friction coefficient and static friction coefficient are both

equal to the dynamic friction coefficient. This will provide a constant lower bound friction coefficient. A sensitivity study on friction coefficient values is conducted in this calculation (Section 7.3.2) that indicates that the lower bound friction coefficient used (0.4) is high enough to create lock-up of the critical contact surfaces and therefore the impact of this assumption on results presented in this document is negligible (see Section 7.3.2 and Assumption 3.2.6). This assumption is used in Section 6.4 and is consistent with Section 6.1.1.16 of Reference 2.2.15.

- 3.2.10 The Poisson's ratio and density at elevated temperatures are not published in traditional sources for Alloy 22, 316 SS and 316L SS. The RT Poisson's ratio and density are assumed for these materials. The impact of using RT Poisson's ratio and density is anticipated to be small. The rationale for this assumption is that temperature sensitivities of these material properties are expected to be small and small variations will have negligible affect on the calculation's stress results. Assumptions 3.2.2 and 3.2.5 provide parametric studies in this calculation that verify this for Poisson's Ratio. The change in density will be downward as the material expands, inversely related to the volumetric expansion term $(1+\Delta T\alpha)^3$, where ΔT is the temperature increase above RT and α is the relative (to RT) coefficient of thermal expansion. Using $\Delta T = 280^\circ\text{C}$ and a clearly upper bound value of $10^{-6} (\text{C})^{-1}$ for the materials' α values from 20°C to 300°C , leads to a density change of less than 0.1 %. The total mass will remain unchanged, so the effect of density change on stress is unclear, however even in the unlikely event that the resulting stress effect is a magnitude greater than the density change, it will be negligible. These studies of variations in Poisson's ratio and density provides verification of this assumption per Reference 2.1.1 page 4 (*"Verification may include . . . studies of parametric variations"*). Further verification of this assumption is not required. This assumption is used in Section 6.1 and is consistent with Section 6.1.1.11 of Reference 2.2.15.
- 3.2.11 The changes of minimum elongation with an increase of temperature for Alloy 22 and 316 SS are not published in traditional sources. The magnitude of these changes from RT to 300°C for Alloy 22 and 316 SS is assumed to be +10% and -30%, respectively, based on the relative changes of typical elongation for these materials available in vendor catalogues (see Reference 2.2.22, page 15, "Average Tensile Data, Solution Heat-Treated" and Reference 2.2.1, page 8). The rationale for this assumption is that the relative change of minimum elongation with temperature will be reasonably close to the relative change of typical elongation with temperature. Therefore this assumption does not require verification. This assumption is used in Section 6.1 and is consistent with Section 6.1.1.12 of Reference 2.2.15.
- 3.2.12 The minimum elongation of 316L SS at elevated temperatures is not published in traditional sources. Use of this material is limited to the naval canister. For the purpose of this calculation, the RT minimum elongation is assumed for this material. The rationale for this assumption is that stress levels in the naval canister are unrealistic (due to the assumption of a heavier than actual wall thickness – see Assumption 3.2.7) and generally inconsequential. The canister is only important as a mass loading and stiffener.

A change in elongation value results only in a change in the Section 6.2 calculated Tangent Modulus. Reference 2.2.26 Attachment V studied the effect of canister Tangent Modulus on OCB stress response for the horizontal drop event which produces a similar momentum loading on the OCB by the mass of the naval canister. A factor of 10 (900%) change in naval canister Tangent Modulus resulted in only 7.5% change in maximum EWA SI (Reference 2.2.26 Attachment VI Sensitivity Study, data files: Attachment VII, folder c_EvsE10.xls, worksheet 50EP versus worksheet E10EP, H35 values). The expected magnitude of Tangent Modulus change due to temperature change in elongation of 316L SS is clearly much less than 900% and arguably less than 90%. The rationale for this is the good correlation between the 30% temperature change in elongation in a similar 300 Series austenitic SS (316 SS) in Assumption 3.2.11 and its 30% temperature change in Tangent Modulus in Table 6-1. It is reasonable to expect that the temperature changes in the 316L SS values will be less than three times the temperature changes in the 316 SS values (therefore, less than 90% in Type 316 SS). And it is reasonable to expect that the 7.5% stress effect observed in Reference 2.2.26 will be reduced below 1% when the Tangent Modulus change is reduced by a factor of 10 (from 900% to 90%). These studies of variations in minimum elongation provides verification of this assumption per Reference 2.1.1 page 4 (*“Verification may include . . . studies of parametric variations”*). Further verification of this assumption is not required. This assumption is used in Section 6.1.

- 3.2.13 The calculations are performed at room temperature. Temperature sensitivity studies for the worst case deterministic calculations and the most severe Capability calculation were performed. In the deterministic calculations, slightly greater OCB damage occurred for RT impacts versus 300°C impacts (see Section 7.3.1). For Alloy 22 in this temperature range, a slight elevated temperature decrease in the primary stress intensity ratio to ultimate strength is created by the disproportionate lowering of the yield strength versus ultimate strength at elevated temperatures. In the Capability calculation, slightly greater OCB damage occurred for the 300°C impacts at lower load levels, but the difference reversed at the failure load levels (see Section 7.5.1). This assumption is used in Section 6.4.
- 3.2.14 The identification of worst case orientations of the WP on the EP for stresses in the WP at the EP contact points were based on the earlier BSC WP design defined by *Naval Long Waste Package Configuration*; 000-MW0-DNF0-00101-000-00A, 000-MW0-DNF0-00102-000-00A and 000-MW0-DNF0-00103-000-00A with ACC: ENG.20030929.0002, ENG.20030929.0003 and ENG.20030929.0004 respectively, and, *Naval Long Waste Package for Mass Assessment*; 000-MWK-DN00-00102-000-00A, 000-MWK-DN00-00103-000-00A and 000-MWK-DN00-00104-000-00A, with ACC: ENG.20050819.0007, ENG.20050819.0008 and ENG.20050819.0009, respectively. The only difference is a minor change in WP design details far away from the high stressed areas. Specifically, the existence of a middle lid in the Inner Vessel of the earlier design and cutouts (for a trunnion lifting collar) in the sleeves of the earlier design that were eliminated in the current design. Therefore, it is reasonable to assume that the identification of the worst

case orientations is correct and this assumption does not require verification. This assumption is used in Section 6.4.1.

- 3.2.15 The calculation only considers vertical input velocities and vertical impacts of the WP on the EP and invert steel. The rationale for this assumption is that these are the most damaging impacts. The addition of a horizontal component of impact velocity will tend to slide the EP out from under the WP and/or provide a glancing impact of the EP or WP on the invert steel. These effects will dissipate impact energy without adding to the stresses at the OCB highest stress location due to the vertical component of impact. The damage effects of horizontal velocities are secondary to the damage effects of vertical velocity up to the point that relative horizontal motions of the WP and drift lead to impacts between the WP and the drift walls. These WP on rock impacts are not considered in this calculation. Therefore this assumption does not require verification. This assumption is used in Section 6.4.
- 3.2.16 The structural resistance and energy absorption of the EP reduces the stresses in the OCB at the invert steel contact region when high level velocity events occur that crush the EP prior to the WP striking the invert steel. It is assumed that the EP will exhibit material failure during these events and that the lack of additional load carrying capacity post-failure can be reasonably modeled using the eroding element option of LS-DYNA. The shell elements in the EP are removed from the simulation when the peak von Mises effective strains reach the material's Code minimum elongation value. This will conservatively increase the simulations' impact velocity of the OCB on the invert steel. Therefore this assumption does not require verification. This assumption is used in Section 6.4.2.
- 3.2.17 The RT uniform strain of A36 CS and A588 alloy steel [UNS K11430] is not listed in traditional sources. Therefore, it is assumed that the uniform strain is 2/3 of the elongation. The rationale for this assumption is based on measurements of RT engineering stress-strain curves for structural steels (Reference 2.2.8, pages 186 and 189). Therefore this assumption does not require verification. This assumption is used in Section 6.1.
- 3.2.18 The invert steel material was changed from A36 CS to A588 alloy steel for corrosion reasons during the calculation. The FER was built using A36 CS and not changed. The choice of A36 CS or A588 alloy steel for the structural steel in the deterministic analyses is inconsequential because it is assumed to be an unyielding target surface (see Assumption 3.2.8). The small differences in RT modulus of elasticity, Poisson's ratio and density values are anticipated to be inconsequential. However, the choice for some of the Capability calculations requires consideration of post-yield behavior. A36 CS was assumed; however, a sensitivity calculation was performed for the worst case orientation WP-on-invert-steel impact at near-failure level using both the A36 CS and A588 alloy steel RT yield strength, tensile strength and elongation values. This study indicates that the Capability level of the OCB is not significantly effected (only 6% difference) by the

choice of structural steel (see Section 7.5.2). Therefore this assumption does not require verification. This assumption is used in Sections 6.1.1 and 6.4.

- 3.2.19 Although the top flanges of the transverse beams in the invert steel structure have standard fabrication radii, it is conservatively assumed that the top flange corner does not have any starting radii. The rationale for this assumption is that the plastic flow of the flange at the impact locations severely rounds the corner and the effect of starting radii is minimal. Therefore this assumption does not require verification. This assumption is used in Section 6.4.2.
- 3.2.20 It is assumed that the top flanges of the transverse beams in the invert steel structure are fully restrained vertically on their bottom surface and therefore will not bend under WP impact to the extent that the web deformation and underlying ballast permits. An accurate modeling of the ballast restraint on flange deformation is not possible, and after initial flange distortions, the load path will shift to the web which will provide considerable vertical constraint considering the beam stiffness and underlying ballast. This simplification will provide reasonable simulation results without being overly conservative. Therefore this assumption does not require verification. This assumption is used in Section 6.4.2.
- 3.2.21 It is assumed that the invert ballast backfill does not exist. This will permit the EP to distort more when bridging the invert steel longitudinal beams under WP impact loading and therefore conservatively increase the stresses in the OCB when it impacts the invert steel at higher velocity. Ignoring the ballast will also conservatively increase the stresses in the OCB by ignoring the impact velocity reduction due to the WP sleeves digging into the ballast. Therefore this assumption does not require verification. This assumption is used in Section 6.4.2.
- 3.2.22 The size of the invert steel was reduced in References 2.2.16, 2.2.17 and 2.2.18 (Rev. 00C) from 12x210 and 12x72 (Rev. 00B) for the transverse and longitudinal beams to 12x65 and 12x40, respectively, after the calculations were completed and in check. The 5 *ft* (0.305 *m*) by 5 *ft* (0.305 *m*) pattern was not changed, therefore the distances between flange edges will change insignificantly. The reduction in transverse beam section size will in actuality reduce the stresses in the OCB (due to a softer impact surface) but will not change the FER response prediction due to the conservative modeling in Assumption 3.2.20. The reduction in longitudinal beam section size will only affect the WP on EP on invert FER response, but the changed response will be negligible because the beam flange offers small resistance to the EP distortion and the fixed web boundary condition will provide the same restraint regardless of beam section size. Therefore it is assumed the FER OCB response prediction is reasonably predicted using the original beam section sizes. Therefore this assumption does not require verification. This assumption is used in Section 6.4.2.

4. METHODOLOGY

4.1 QUALITY ASSURANCE

This calculation is associated with the WP design and is performed by the Thermal/Structural Analysis Group in accordance with EG-PRO-3DP-G04B-00037, *Calculations and Analyses* (Reference 2.1.1). The Naval Long WP is classified as important to safety (ITS) and important to waste isolation (ITWI) per Section 12.1.2 of Reference 2.2.2. The EP is classified as ITWI per Section 8.1.2 of Reference 2.2.2. The emplacement drifts steel invert is classified as non-ITS and non-ITWI per Section 8.1.2 of Ref. 2.2.2. The TEV is classified as ITS per Section 14.1.2 of Reference 2.2.2. Therefore, the approved version of this calculation is designated as QA: QA.

Reference 2.2.16 through 2.2.18 are QA:N/A sources. However, these are suitable for use in this calculation as conservative non-failing impact surfaces (see Assumptions 3.2.18 to 3.2.22) since emplacement drifts steel invert are classified as non-ITS and non-ITWI. Sensitivity studies on material choice, contact angle and the conservative considerations of section stiffness, corner details and ballast restraint indicate the final details of the emplacement drifts invert, provided it has a similar-sized (5 ft x 5 ft [0.3 m x 0.3 m]) square-lattice-frame layout (without a central longitudinal beam), will have only minor effect on the calculation results.

4.2 USE OF SOFTWARE

The finite element solution portion of the calculation is performed by using the commercially available LS-DYNA Version 970.3858 D MPP finite element code (Reference 2.2.10), hereinafter referred to as “LS-DYNA”. LS-DYNA is obtained from Software Configuration Management in accordance with IT-PRO-0011, *Software Management* (Reference 2.1.2). LS-DYNA is identified by the Software Tracking Number 10300-970.3858 D MPP-00. LS-DYNA is appropriate for this calculation. Test problems with known solutions were successfully performed to validate the LS-DYNA application (Reference 2.2.11, Section 4 and 5). The LS-DYNA evaluation performed for this calculation is fully within the range of this validation. The calculations using the LS-DYNA software are executed on the Hewlett-Packard Itanium2 (IA64) series UNIX workstations (Operating System HP-UX 11.22), identified with Yucca Mountain Project tag number 501711, located in Las Vegas, Nevada. Access to the code is granted by the Software Configuration Management in accordance with appropriate procedures.

TrueGrid Version 2.2 (hereinafter referred to as “TrueGrid”) is used in this calculation solely to mesh geometric representations of the WP in the simulations. The meshing is executed on the Hewlett-Packard 9000 series UNIX workstation (Operating System HP-UX 11.0), identified with Yucca Mountain Project tag number 150690, located in Las Vegas, Nevada. The suitability and adequacy of this mesh is based on visual examination, engineering judgment, and the results of mesh verification in Section 7.1. The mesh has been evaluated in accordance with EG-PRO-3DP-G04B-00037 (Reference 2.1.1), and determined to be suitable and adequate for use as input to LS-DYNA. TrueGrid is Level 2 software as defined in Reference 2.1.2, Attachment 12 and is listed in the *Repository Project Management Automation Plan* (Reference 2.1.3, Table 6-1).

LS-PREPOST V1.0 (Livermore Software Technology Corporation) is the postprocessor used only for visual display and graphical representation of LS-DYNA FERs and results and therefore is Level 2 software as defined in Reference 2.1.2, Attachment 12 and is listed in the *Repository Project Management Automation Plan* (Reference 2.1.3, Table 6-1). The suitability and adequacy of the displayed results is based on visual examination and engineering judgment. The post processing is performed on the Hewlett-Packard Itanium2 (IA64) series UNIX workstations (Operating System HP-UX 11.22), identified with Yucca Mountain Project tag number 501711, and located in Las Vegas, Nevada.

The commercially available Microsoft Office Excel 2003 (11.8105.8107 SP2) (hereinafter referred to as "Excel") spreadsheet code, which is a component of Microsoft Office 2003, is used to perform plots of LS-DYNA results in Section 7 to provide visual indication that the maximum response orientation has been determined. These plots were verified by visual checks of the data points. Usage of Microsoft Office 2003 in this calculation constitutes Level 2 software usage, as defined in IT-PRO-0011 (Reference 2.1.2, Attachment 12). Microsoft Office Excel 2003 was executed on a PC running the Microsoft Windows XP Professional Version 2002 Service Pack 2 operating system.

All other calculations reported in this document are performed by hand.

The LS-DYNA input files, identified by .k and .inc file extensions, and LS-DYNA output files ("d3hsp") are provided in Attachment I. The input files for TrueGrid, identified by .tg file extensions are provided in Attachment I. The TrueGrid output files have the .inc extensions.

Due to the size of the files associated with this calculation, both input and output, some files have been electronically compressed using commercially available software packages. On the HP-UX platform computers the GZIP command is used to compress or uncompress files, this command comes packaged with the HP-UX 11.22 operating system. The HP-UX platform computer cluster where use of the GZIP command was performed is identified with one tag number: 501711. The files that were compressed were verified to uncompress correctly by hand check and visual inspection. The zipped files have a .gz extension.

4.3 STRESS ANALYSIS APPROACH

FERs of the WP on the EP are created and solved for vertical impact events using LS-DYNA. The OCB stress results are reviewed to determine the maximum response locations and magnitudes. Various orientations of the WP and EP are evaluated to determine the (worst case) orientation that leads to the highest OCB stress response. The governing OCB stress and strain responses for different impact velocities are compared to project deterministic structural acceptance criteria and/or used to compute Capability.

The design information regarding the WP and EP used in the finite element representation is based on the proposed/potential designs presented by the drawings and sketches of References 2.2.27 to 2.2.39 and References 2.2.41 to 2.2.43 (see Assumptions 3.1.1 and 3.2.14).

The Naval Long canister overall dimensions are consistent with the maximum values provided on page 3 of Enclosure 3 in Reference 2.2.13. The weight of the Naval Long canister is based on the maximum recordable weight (Reference 2.2.14, page C-17, Note 3). The details of the Naval Long canister and contents are simplified per Assumption 3.2.7.

The material strength properties (yield stress, tensile strength and elongation) used for the deterministic calculation against project structural acceptance criteria are based on ASME Code (Reference 2.2.5) minimum strength values. The OCB material strength properties used for the Capability calculations are based on the best estimate values in Table I-2 Appendix I of Reference 2.2.15 derived from published vendor expected (average) strength values using a worst case triaxiality factor per Section 7.1.7.2.4 of Reference 2.2.15. The best estimate material strength properties for components other than the OCB used for the Capability calculations are based on 1.1 times the ASME Code minimum strength values per Section 7.1.7.2.4 of Reference 2.2.15. The exception is the EP eroding material for the WP on EP bridging the invert steel Capability calculation (see Assumption 3.2.16).

The deterministic calculations are based on EWA maximum shear stress (MSS) as a conservative bound on ASME Code primary stress intensities per Section 7.1.4 of Reference 2.2.15 and Reference 2.2.46. The Capability calculations to support a Probabilistic Risk Assessment (PRA) are based on an Expended Toughness Fraction (ETF) using the material's Toughness Index (T_I) and the time histories of the EWA VM stresses and strains per Section 7.1.7.2.2 of Reference 2.2.15.

5. LIST OF ATTACHMENTS

Attachment I (2 DVDs, 4 CDs, 6 total): TrueGrid and LS-DYNA electronic files
(See Table 5-1)

Table 5-1 List of Electronic Files in Attachment I

Name	Date	Time	Size
Disc 1 - DVD			
Folder: EP short angles			
Subfolder: Center WP, 2deg EP			
d3hsp	7/18/2006	2:35 PM	133,442 KB
HALF_2DEG.k	7/18/2006	2:31 PM	5 KB
HALF_2DEG.tg	7/19/2006	9:08 AM	62 KB
HALF_2DEG_mod.inc	7/18/2006	2:33 PM	44,620 KB
Subfolder: Center WP, 3deg EP			
d3hsp	7/18/2006	2:38 PM	133,585 KB
HALF_3DEG.k	7/18/2006	2:37 PM	5 KB
HALF_3DEG.tg	7/19/2006	9:08 AM	62 KB
HALF_3DEG_mod.inc	7/18/2006	2:37 PM	44,615 KB
Subfolder: Center WP, 35deg EP			
d3hsp	7/18/2006	2:42 PM	133,607 KB
HALF_35DEG.k	7/18/2006	2:39 PM	5 KB
HALF_35DEG.tg	7/19/2006	9:08 AM	62 KB
HALF_35DEG_mod.inc	7/18/2006	2:41 PM	44,611 KB
Subfolder: Center WP, 4deg EP			
d3hsp	7/18/2006	2:50 PM	133,602 KB
HALF_4DEG.k	7/18/2006	2:44 PM	5 KB
HALF_4DEG.tg	7/19/2006	9:09 AM	62 KB
HALF_4DEG_mod.inc	7/18/2006	2:46 PM	44,571 KB
Subfolder: Center WP, 45deg EP			
d3hsp	7/18/2006	2:55 PM	133,876 KB
HALF_45DEG.k	7/18/2006	2:52 PM	5 KB
HALF_45DEG.tg	7/19/2006	9:09 AM	62 KB
HALF_45DEG_mod.inc	7/18/2006	2:52 PM	44,611 KB
Subfolder: Center WP, 5deg EP			
d3hsp	7/18/2006	4:22 PM	133,821 KB
HALF_5DEG.k	7/18/2006	4:26 PM	5 KB
HALF_5DEG.tg	7/19/2006	9:09 AM	62 KB
HALF_5DEG_mod.inc	7/18/2006	4:25 PM	44,605 KB
Subfolder: Center WP, 6deg EP			
d3hsp	7/18/2006	4:31 PM	133,642 KB
HALF_6DEG.k	7/18/2006	4:30 PM	5 KB
HALF_6DEG.tg	7/19/2006	9:09 AM	62 KB
HALF_6DEG_mod.inc	7/18/2006	4:29 PM	44,561 KB

Name	Date	Time	Size
Folder: Flat EP, centered WP, simple drop			
d3hsp	7/18/2006	12:36 PM	133,505 KB
HALF_0DEG.k	7/18/2006	12:33 PM	5 KB
HALF_0DEG.tg	7/19/2006	9:11 AM	62 KB
HALF_0DEG_mod.inc	7/18/2006	12:33 PM	44,584 KB
Folder: QTR FER			
d3hsp	7/18/2006	12:24 PM	69,277 KB
QTR_STD.tg	7/18/2006	12:25 PM	63 KB
QTR_STD_mod.inc	7/18/2006	12:22 PM	21,790 KB
QTR_STD2.k	7/18/2006	12:22 PM	6 KB
Folder: QTR RFER			
d3hsp	7/18/2006	11:39 AM	143,772 KB
QTR_REF2.k	7/18/2006	11:35 AM	6 KB
QTR_REF2.tg	7/18/2006	12:20 PM	62 KB
QTR_REF2_mod.inc	7/18/2006	11:37 AM	46,892 KB
Folder: Worst Case + translation			
28WPRY_WPZ.k	7/19/2006	8:21 AM	5 KB
d3hsp	7/19/2006	8:25 AM	243,000 KB
FULL_28WPRY_WPZ.inc	7/19/2006	8:23 AM	89,529 KB
FULL_28WPRY_WPZ.tg	7/19/2006	9:12 AM	62 KB
Folder: Worst Case 28 WP rotation			
28WPRY.k	7/19/2006	8:13 AM	5 KB
d3hsp	7/19/2006	8:19 AM	250,656 KB
FULL_28INWPRY.inc	7/19/2006	8:13 AM	89,502 KB
FULL_28INWPRY.tg	7/19/2006	9:11 AM	62 KB
Folder: WP horiz-offsets			
Subfolder: Flat EP, 075 WP			
d3hsp	7/18/2006	1:16 PM	132,917 KB
HALF_075IN_FLAT.k	7/18/2006	12:24 PM	5 KB
HALF_075IN_FLAT.tg	7/19/2006	9:12 AM	62 KB
HALF_075IN_FLAT_mod.inc	7/18/2006	12:46 PM	44,595 KB
Subfolder: Flat EP, 15 WP			
d3hsp	7/18/2006	1:40 PM	132,104 KB
HALF_15IN_FLAT.k	7/18/2006	1:37 PM	5 KB
HALF_15IN_FLAT.tg	7/19/2006	9:13 AM	61 KB
HALF_15IN_FLAT_mod.inc	7/18/2006	1:37 PM	44,598 KB
Subfolder: Flat EP, 175 WP			
d3hsp	7/18/2006	1:45 PM	131,790 KB
HALF_175IN_FLAT.k	7/18/2006	1:41 PM	5 KB
HALF_175IN_FLAT.tg	7/19/2006	9:13 AM	61 KB
HALF_175IN_FLAT_mod.inc	7/18/2006	1:42 PM	44,597 KB
Subfolder: Flat EP, 2 WP			
d3hsp	7/18/2006	2:04 PM	13,510 KB
HALF_2IN_FLAT.k	7/18/2006	2:02 PM	5 KB
HALF_2IN_FLAT.tg	7/19/2006	9:14 AM	61 KB
HALF_2IN_FLAT_mod.inc	7/18/2006	2:02 PM	44,602 KB

Name	Date	Time	Size
Subfolder: Flat EP, 25 WP			
d3hsp	7/18/2006	2:06 PM	131,236 KB
HALF_25IN_FLAT.k	7/18/2006	2:05 PM	5 KB
HALF_25IN_FLAT.tg	7/19/2006	9:14 AM	61 KB
HALF_25IN_FLAT_mod.inc	7/18/2006	2:05 PM	44,592 KB
Subfolder: Flat EP, 27 WP			
d3hsp	7/18/2006	2:09 PM	131,139 KB
HALF_27IN_FLAT.k	7/18/2006	2:07 PM	6 KB
HALF_27IN_FLAT.tg	7/19/2006	9:14 AM	61 KB
HALF_27IN_FLAT_mod.inc	7/18/2006	2:07 PM	44,593 KB
Subfolder: Flat EP, 28 WP			
d3hsp	7/18/2006	2:14 PM	131,034 KB
HALF_28IN_FLAT.k	7/18/2006	2:10 PM	6 KB
HALF_28IN_FLAT.tg	7/19/2006	9:14 AM	61 KB
HALF_28IN_FLAT_mod.inc	7/18/2006	2:12 PM	44,584 KB
Subfolder: Flat EP, 29 WP			
d3hsp	7/18/2006	2:19 PM	130,889 KB
HALF_29IN_FLAT.k	7/18/2006	2:15 PM	5 KB
HALF_29IN_FLAT.tg	7/19/2006	9:15 AM	61 KB
HALF_29IN_FLAT_mod.inc	7/18/2006	2:17 PM	44,588 KB
Subfolder: Flat EP, 3 WP			
d3hsp	7/18/2006	2:22 PM	130,788 KB
HALF_3IN_FLAT.k	7/18/2006	2:20 PM	5 KB
HALF_3IN_FLAT.tg	7/19/2006	9:15 AM	61 KB
HALF_3IN_FLAT_mod.inc	7/18/2006	2:20 PM	44,586 KB
Subfolder: Flat EP, 4 WP			
d3hsp	7/18/2006	2:26 PM	130,394 KB
HALF_4IN_FLAT.k	7/18/2006	2:23 PM	5 KB
HALF_4IN_FLAT.tg	7/19/2006	9:16 AM	61 KB
HALF_4IN_FLAT_mod.inc	7/18/2006	2:25 PM	44,588 KB
Disc 2 - DVD			
Folder: 2deg long WP, flat EP			
2DEGWP_FLAT.k	7/19/2006	7:59 AM	5 KB
d3hsp	7/19/2006	8:03 AM	250,730 KB
FULL_2DEGWP_FLAT.inc	7/19/2006	8:01 AM	89,570 KB
FULL_2DEGWP_FLAT.tg	7/19/2006	8:31 AM	62 KB
Folder: 3 WP, 4deg EP			
d3hsp	7/18/2006	4:37 PM	132,031 KB
HALF_3IN_4DEG.k	7/18/2006	4:34 PM	5 KB
HALF_3IN_4DEG.tg	7/19/2006	8:29 AM	62 KB
HALF_3IN_4DEG_mod.inc	7/18/2006	4:35 PM	44,608 KB
Folder: 4deg short + 2deg long EP			
4DEG_2CLEP.k	7/18/2006	5:22 PM	5 KB
d3hsp	7/18/2006	5:25 PM	257,205 KB
FULL_4DEG_2CLEP.inc	7/18/2006	5:23 PM	89,509 KB
FULL_4DEG_2CLEP.tg	7/19/2006	8:30 AM	62 KB

Name	Date	Time	Size
Folder Center WP, 2deg long EP			
d3hsp	7/18/2006	5:16 PM	249,534 KB
FULL_4PT_2CL.inc	7/18/2006	5:04 PM	89,576 KB
FULL_4PT_2CL.k	7/18/2006	5:04 PM	5 KB
FULL_4PT_2CL.tg	7/19/2006	9:07 AM	62 KB
Folder: Sensitivity Studies			
Subfolder: 2 WP Hi Friction			
28IN_NUONE.k	7/19/2006	10:30 AM	6 KB
d3hsp	7/19/2006	10:33 AM	130,942 KB
HALF_28IN_FLAT.tg	7/19/2006	10:35 AM	61 KB
HALF_28IN_FLAT_mod.inc	7/19/2006	10:30 AM	44,584 KB
Subfolder: 28 WP Hi THDT			
28IN_THDT.k	7/19/2006	10:37 AM	5 KB
d3hsp	7/19/2006	10:39 AM	130,942 KB
HALF_28IN_FLAT.tg	7/19/2006	10:40 AM	61 KB
HALF_28IN_FLAT_mod.inc	7/19/2006	10:37 AM	44,584 KB
Subfolder: 28 WP Low Friction			
28IN_NULOW.k	7/19/2006	10:16 AM	5 KB
d3hsp	7/19/2006	10:20 AM	131,402 KB
HALF_28IN_FLAT.tg	7/19/2006	10:29 AM	61 KB
HALF_28IN_FLAT_mod.inc	7/19/2006	10:18 AM	44,584 KB
Disc 3 - CD			
28WPRY_REF2.k	8/10/2006	4:59 PM	6 KB
d3hsp	8/10/2006	5:02 PM	300,719 KB
FULL_28INWPRY_REF.inc	8/10/2006	5:02 PM	117,228 KB
FULL_28INWPRY_REF.tg (restored)	10/11/2007	2:47 PM	64 KB
Disc 4 - CD			
Folder: ASME20in			
d3hsp.gz	7/31/2007	3:11 PM	25,040 KB
REVB_WCASE_NLEP3a.inc.gz	7/31/2007	3:12 PM	21,216 KB
REVB_WCASE_NLEP3a.tg	7/31/2007	3:12 PM	64 KB
REVB20in.k	7/31/2007	3:11 PM	5 KB
Folder: PRA10mps			
d3hsp.gz	7/31/2007	2:36 PM	25,301 KB
PRA10mpsBI.k	7/31/2007	2:37 PM	5 KB
REVB_WCASE_NLEP3a.inc	7/31/2007	2:38 PM	89,514 KB
REVB_WCASE_NLEP3a.tg	7/31/2007	2:57 PM	64 KB
Folder: PRA15mps			
d3hsp.gz	7/31/2007	2:59 PM	25,282 KB
PRA15mpsBI.k	7/31/2007	2:58 PM	5 KB
REVB_WCASE_NLEP3a.inc	7/31/2007	2:59 PM	89,514 KB
REVB_WCASE_NLEP3a.tg	7/31/2007	3:00 PM	64 KB

Name	Date	Time	Size
Folder: PRA20in			
d3hsp.gz	7/31/2007	3:02 PM	25,056 KB
PRA5msBl.k	7/31/2007	3:01 PM	5 KB
REVB_WCASE_NLEP3a.in.gz	7/31/2007	3:04 PM	21,216 KB
REVB_WCASE_NLEP3a.tg	7/31/2007	3:03 PM	64 KB
Folder: PRASmall			
d3hsp.gz	7/31/2007	3:07 PM	25,410 KB
PRA0mpsBl.k	7/31/2007	3:04 PM	5 KB
REVB_WCASE_NLEPa.inc.gz	7/31/2007	3:04 PM	21,216 KB
REVB_WCASE_NLEP3a.tg	7/31/2007	3:07 PM	64 KB
Disc 5 – CD (tg files are on Disc 6 and have same name w/o “_mod” as .inc files)			
Folder: 7.1.2 WP on INV MESH STUDY			
Subfolder: REF Mesh			
d3hsp.gz	10/04/2007	10:40 AM	32,316 KB
4TILT18degREF.k	10/04/2007	10:40 AM	5 KB
TILT18NOEPref_mod.inc.gz	10/04/2007	10:40 AM	22,683 KB
tg on Disc 6			
Subfolder: STD Mesh			
d3hsp.gz	10/04/2007	10:36 PM	22,552 KB
TILT18deg.k	10/04/2007	10:36 PM	5 KB
TILT18NOEP_mod.inc.gz	10/04/2007	10:36 PM	14,827 KB
tg on Disc 6			
Folder: 7.2.7 Worst Case EP 20in ASME			
d3hsp.gz	10/04/2007	12:03 PM	25,720 KB
REVB20in.k	10/04/2007	12:02 PM	5 KB
REVB_WCASE_NLEP3a.inc.gz	10/04/2007	12:02 PM	21,812 KB
tg on Disc 6			
Folder: 7.4.1 WP on FLAT EP			
REVB_WCASE_NLEP3a.inc.gz	10/04/2007	12:37 PM	21,812 KB
tg on Disc 6			
Subfolder: 1.5MPS			
d3hsp.gz	10/04/2007	12:37 PM	26,097 KB
PRA0mpsBl.k	10/04/2007	12:36 PM	5 KB
Subfolder: 10MPS			
d3hsp.gz	10/04/2007	12:38 PM	25,987 KB
PRA10mpsBl.k	10/04/2007	12:38 PM	5 KB
Subfolder: 15MPS			
d3hsp.gz	10/04/2007	12:39 PM	25,967 KB
PRA15mpsBl.k	10/04/2007	12:38 PM	5 KB
Subfolder: 20in (5mps actually)			
d3hsp.gz	10/04/2007	12:39 PM	25,736 KB
PRA5msBl.k	10/04/2007	12:38 PM	5 KB

Name	Date	Time	Size
FOLDER: 7.4.2 WP on EP on INV			
WP2inEP1inINV5mod.inc.gz	10/04/2007	12:43 PM	15,515 KB
tg on Disc 6			
Subfolder: 10MPS			
d3hsp.gz	10/04/2007	12:43 PM	21,681 KB
10WCTEPINV21.k	10/04/2007	12:42 PM	9 KB
Subfolder: 12MPS			
d3hsp.gz	10/04/2007	12:44 PM	21,641 KB
12WCTEPINV21.k	10/04/2007	12:43 PM	9 KB
Subfolder: 14MPS			
d3hsp.gz	10/04/2007	12:44 PM	21,642 KB
14WCTEPINV21.k	10/04/2007	12:44 PM	9 KB
Folder: 7.4.3 WP on INV			
Subfolder: 10DEG 4MPS			
d3hsp.gz	10/04/2007	2:36 PM	22,610 KB
4TILT10deg.k	10/04/2007	2:35 PM	5 KB
TILT10NOEP_mod.inc.gz	10/04/2007	2:35 PM	14,833 KB
tg on Disc 6			
Subfolder: 18DEG 5MPS			
d3hsp.gz	10/04/2007	3:00 PM	22,552 KB
5TILT18deg.k	10/04/2007	3:00 PM	5 KB
TILT18NOEP_mod.inc.gz	10/04/2007	3:00 PM	14,827 KB
tg on Disc 6			
Subfolder: 5DEG 4MPS			
d3hsp.gz	10/04/2007	2:35 PM	22,568 KB
4TILT5deg.k	10/04/2007	2:35 PM	5 KB
TILT5NOEP_mod.inc.gz	10/04/2007	2:35 PM	14,867 KB
tg on Disc 6			
Subfolder: FLAT 8in OFFSET 8MPS			
d3hsp.gz	10/04/2007	2:01 PM	14,907 KB
8offsetFLAT.k	10/04/2007	12:49 PM	5 KB
maxoff_flat_mod.inc.gz	10/04/2007	2:01 PM	10,543 KB
tg on Disc 6			
Subfolder: FLAT WC OFFSET			
last2NOEPINV1in.inc.gz	10/04/2007	2:29 PM	14,026 KB
tg on Disc 6			
sub-subfolder: 10MPS			
d3hsp.gz	10/04/2007	2:34 PM	19,862 KB
10WCT1in.k	10/04/2007	2:29 PM	5 KB
sub-subfolder: 4MPS			
d3hsp.gz	10/04/2007	2:26 PM	23,737 KB
4WCT1in.k	10/04/2007	2:26 PM	5 KB
sub-subfolder: 8MPS			
d3hsp.gz	10/04/2007	2:28 PM	21,403 KB
8WCT1in.k	10/04/2007	2:27 PM	6 KB

Name	Date	Time	Size
FOLDER: 7.5.1 18DEG 300C			
TILT18NOEP_mod.inc.gz	10/04/2007	2:46 PM	14,827 KB
tg on Disc 6			
Subfolder: 4MPS			
d3hsp.gz	10/04/2007	2:46 PM	23,350 KB
4TILT18deg300C.k	10/04/2007	2:45 PM	5 KB
Subfolder: 5MPS			
d3hsp.gz	10/04/2007	2:47 PM	23,383 KB
5TILT18deg300C.k	10/04/2007	2:47 PM	5 KB
FOLDER: 7.5.2 5MPS A588 MATL INV			
d3hsp.gz	10/04/2007	2:58 PM	22,552 KB
5mps18deg588.k	10/04/2007	2:58 PM	5 KB
TILT18NOEP_mod.inc.gz	10/04/2007	2:58 PM	14,827 KB
tg on Disc 6			
FOLDER: 7.7 WC INV 20in ASME			
d3hsp.gz	10/04/2007	3:12 PM	23,368 KB
ASME18TILT.k	10/04/2007	3:12 PM	6 KB
TILT18NOEP_mod.inc.gz	10/04/2007	3:12 PM	14,827 KB
tg on Disc 6			
Disc 6 – CD			
FOLDER: 7.4.3 18DEG 4MPS			
d3hsp.gz	10/10/2007	8:34 AM	3683 KB
4TILT18deg.k	10/10/2007	8:42 AM	6 KB
TILT18NOEP_mod.inc.gz	10/10/2007	8:44 AM	12,337 KB
tg in following folder			
FOLDER: TG Models			
last2NOEPINV1in.tg	10/10/2007	8:49 AM	69 KB
maxoff_flat.tg	10/10/2007	8:49 AM	67 KB
REVB_WCASE_NLEP3a.tg	10/10/2007	8:49 AM	66 KB
TILT5NOEP.tg	10/10/2007	8:49 AM	69 KB
TILT10NOEP.tg	10/10/2007	8:49 AM	69 KB
TILT18NOEP.tg	10/10/2007	8:49 AM	69 KB
TILT18NOEPref.tg	10/10/2007	8:49 AM	69 KB
WP2inEP1inINV5.tg	10/10/2007	8:49 AM	69 KB
FOLDER: Fixed TG Model			
TILT18FIX.tg	10/10/2007	8:51 AM	69 KB

NOTE: The file sizes and times may vary with operating system. Folder names may not be exactly as they appear on the discs and in different order (file names are exact).

6. BODY OF CALCULATION

6.1 MATERIAL PROPERTIES

6.1.1 Deterministic Calculation

Material properties used in the deterministic calculation are listed in this section. Stress units are Pascal (Pa), Mega Pascal ($MPa = 10^6 Pa$), Giga Pascal ($GPa = 10^9 Pa$), lb/in^2 (psi) and $ksi = 10^3 psi$.

Some strain-rate-dependent and temperature-dependent properties are not published in traditional sources. In these cases, static loading properties are used and either RT values or extrapolated elevated temperature values are used (see Assumptions 3.2.1 and 3.2.10).

The value of each material property is sought at both RT and $300^\circ C$ ($572^\circ F$). When elevated temperature data is available, the material properties are obtained by linear interpolation of the bounding temperature properties using the formula:

$$p = p(T) = p_l + \left(\frac{T - T_l}{T_u - T_l} \right) \cdot (p_u - p_l)$$

Subscripts u and l denote the upper and lower bounding values of generic material property p at the corresponding bounding temperatures T .

Alloy 22 (SB-575 [UNS N06022] for OCB, trunnion sleeves and EP):

- Density = $8690 kg/m^3$ ($0.314 lb/in^3$) at RT (Reference 2.2.5, Section II, Part B, SB-575, Section 7.1)
- Yield strength = $310 MPa$ ($45.0 ksi$) at RT (Reference 2.2.5, Section II, Part D, Table Y-1)
Yield strength = $216 MPa$ ($31.4 ksi$) at $288^\circ C$ ($550^\circ F$) (Reference 2.2.5, Section II, Part D, Table Y-1)
Yield strength = $211 MPa$ ($30.6 ksi$) at $316^\circ C$ ($600^\circ F$) (Reference 2.2.5, Section II, Part D, Table Y-1)
Yield strength = $214 MPa$ ($31.0 ksi$) at $300^\circ C$ ($572^\circ F$)
- Tensile strength = $689 MPa$ ($100 ksi$) at RT (Reference 2.2.5, Section II, Part D, Table U)
Tensile strength = $641 MPa$ ($92.9 ksi$) at $260^\circ C$ ($500^\circ F$) (Reference 2.2.5, Section II, Part D, Table U)
Tensile strength = $628 MPa$ ($91.1 ksi$) at $316^\circ C$ ($600^\circ F$) (Reference 2.2.5, Section II, Part D, Table U)
Tensile strength = $632 MPa$ ($91.7 ksi$) at $300^\circ C$ ($572^\circ F$)

- Elongation = 0.45 at RT (Reference 2.2.5, Section II, Part B, SB-575, Table 4)
- Poisson's ratio = 0.278 at RT (Reference 2.2.3, page 143; see Assumption 3.2.2)
- Modulus of elasticity = 206 *GPa* (29.9×10^6 *psi*) at RT (Reference 2.2.22, page 14, Table "Average Dynamic Modulus of Elasticity") This data is the best available and suitable for its use in this calculation.
Modulus of elasticity = 196 *GPa* (28.4×10^6 *psi*) at 204°C (400°F) (Reference 2.2.22, page 14, Table "Average Dynamic Modulus of Elasticity") This data is the best available and suitable for use in this calculation.
Modulus of elasticity = 191 *GPa* (27.6×10^6 *psi*) at 316°C (600°F) (Reference 2.2.22, page 14, Table "Average Dynamic Modulus of Elasticity") This data is the best available and suitable for use in this calculation.
Modulus of elasticity = 191 *GPa* (27.7×10^6 *psi*) at 300°C (572°F)

316 SS (SA-240 [UNS S31600 w/ modified N & C] for inner vessel and spread ring):

- Density = 7980 *kg/m*³ (0.288 *lb/in*³) at RT (Reference 2.2.6, Table X1.1, page 8)
- Yield strength = 207 *MPa* (30.0 *ksi*) at RT (Reference 2.2.5, Section II, Part D, Table Y-1)
Yield strength = 138 *MPa* (20.0 *ksi*) at 260°C (500°F) (Reference 2.2.5, Section II, Part D, Table Y-1)
Yield strength = 130 *MPa* (18.9 *ksi*) at 316°C (600°F) (Reference 2.2.5, Section II, Part D, Table Y-1)
Yield strength = 132 *MPa* (19.1 *ksi*) at 300°C (572°F)
- Tensile strength = 517 *MPa* (75.0 *ksi*) at RT (Reference 2.2.5, Section II, Part D, Table U)
Tensile strength = 495 *MPa* (71.8 *ksi*) at 260°C (500°F) (Reference 2.2.5, Section II, Part D, Table U)
Tensile strength = 495 *MPa* (71.8 *ksi*) at 316°C (600°F) (Reference 2.2.5, Section II, Part D, Table U)
Tensile strength = 495 *MPa* (71.8 *ksi*) at 300°C (572°F)
- Elongation = 0.40 at RT (Reference 2.2.5, Section II, Part A, SA-240, Table 2)
- Poisson's ratio = 0.30 at RT (Reference 2.2.3, Figure 15, page 755)
- Modulus of elasticity = 195 *GPa* (28.3×10^6 *psi*) at RT (Reference 2.2.5, Section II, Part D, Table TM-1)
Modulus of elasticity = 178 *GPa* (25.8×10^6 *psi*) at 260°C (500°F) (Reference 2.2.5, Section II, Part D, Table TM-1)
Modulus of elasticity = 174 *GPa* (25.3×10^6 *psi*) at 316°C (600°F) (Reference 2.2.5, Section II, Part D, Table TM-1)
Modulus of elasticity = 175 *GPa* (25.4×10^6 *psi*) at 300°C (572°F)

316L (SA-240 [UNS S31603] for Naval canister, see Assumption 3.2.7):

- Density = 7980 kg/m^3 (0.288 lb/in^3) at RT (Reference 2.2.6, Table X1.1, page 8)
- Yield strength = 172 MPa (25.0 ksi) at RT (Reference 2.2.5, Section II, Part D, Table Y-1)
Yield strength = 113 MPa (16.4 ksi) at 260°C (500°F) (Reference 2.2.5, Section II, Part D, Table Y-1)
Yield strength = 108 MPa (15.6 ksi) at 316°C (600°F) (Reference 2.2.5, Section II, Part D, Table Y-1)
Yield strength = 109 MPa (15.8 ksi) at 300°C (572°F)
- Tensile strength = 483 MPa (70.0 ksi) at RT (Reference 2.2.5, Section II, Part D, Table U)
Tensile strength = 426 MPa (61.8 ksi) at 260°C (500°F) (Reference 2.2.5, Section II, Part D, Table U)
Tensile strength = 425 MPa (61.7 ksi) at 316°C (600°F) (Reference 2.2.5, Section II, Part D, Table U)
Tensile strength = 426 MPa (61.7 ksi) at 300°C (572°F)
- Elongation = 0.40 at RT (Reference 2.2.5, Section II, Part A, SA-240, Table 2)
- Poisson's ratio = 0.3 at RT (Reference 2.2.3, Figure 15, page 755, see Assumption 3.2.5)
- Modulus of elasticity = 195 GPa ($28.3 \times 10^6 \text{ psi}$) at RT (Reference 2.2.5, Section II, Part D, Table TM-1)
Modulus of elasticity = 178 GPa ($25.8 \times 10^6 \text{ psi}$) at 260°C (500°F) (Reference 2.2.5, Section II, Part D, Table TM-1)
Modulus of elasticity = 174 GPa ($25.3 \times 10^6 \text{ psi}$) at 316°C (600°F) (Reference 2.2.5, Section II, Part D, Table TM-1)
Modulus of elasticity = 175 GPa ($25.4 \times 10^6 \text{ psi}$) at 300°C (572°F)

A36 CS (SA-36/36M [UNS K02600] target surface and invert steel (see Assumptions 3.2.8 and 3.2.18). Yield, ultimate and elongation properties used in the Capability calculations are included herein for completeness:

- Density = 7860 kg/m^3 (0.284 lb/in^3) at RT (Reference 2.2.6, Table X1.1, page 8)
- Yield strength = 250 MPa (36.0 ksi) at RT (Reference 2.2.5, Section II, Part D, Table Y-1)
- Tensile strength = 400 MPa (58.0 ksi) at RT (Reference 2.2.5, Section II, Part D, Table U)
- Elongation = 0.20 at RT (Reference 2.2.5, Section II, Part A, SA-36/SA-36M, Table 3)
- Poisson's ratio = 0.30 at RT (Reference 2.2.4, page 374)

- Modulus of elasticity = 203 *GPa* (29.5×10^6 *psi*) at RT (Reference 2.2.5, Section II, Part D, Table TM-1)

A588 alloy steel (ASTM A588, Grade 50 [UNS K11430]) structural steel (see Assumption 3.2.18; A36 CS density, Poisson's ratio and modulus of elasticity used)

- Density = 7860 *kg/m*³ (0.284 *lb/in*³) at RT (Reference 2.2.6, Table X1.1, page 8)
- Yield strength = 345 *MPa* (50.0 *ksi*) at RT (Reference 2.2.45, Table 2)
- Tensile strength = 483 *MPa* (70.0 *ksi*) at RT (Reference 2.2.45, Table 2)
- Elongation = 0.21 at RT (Reference 2.2.45, Table 2)
- Poisson's ratio = 0.30 at RT (Reference 2.2.4, page 374)
- Modulus of elasticity = 203 *GPa* (29.5×10^6 *psi*) at RT (Reference 2.2.5, Section II, Part D, Table TM-1)

Calculations for Elevated-Temperature Minimum Elongations

The values for minimum elongation at elevated temperatures are not listed in traditional sources. However, typical elongation values at elevated temperatures are available in vendors' data. The vendor data trends are used to project the minimum RT values from accepted codes to elevated temperatures (see Assumption 3.2.11).

For Alloy 22, the vendor's data shows an approximate 10% relative increase between RT and 300°C (572°F) (Reference 2.2.22, page 15, Table "Average Tensile Data, Solution Heat-Treated"). This data is the best available and suitable for use in this calculation. Therefore, the minimum elongation value for Alloy 22 at elevated temperature is:

$$\text{Minimum elongation} = 0.45 \cdot (1 + 0.1) = 0.49 \text{ at } 300^\circ\text{C} (572^\circ\text{F})$$

For 316 SS, the vendor's data shows an approximate 30% decrease between RT and 300°C (572°F) (Reference 2.2.1, page 8). This data is the best available and suitable for use in this calculation. Therefore, the minimum elongation values for 316 SS at elevated temperature is:

$$\text{Minimum elongation} = 0.40 \cdot (1 - 0.3) = 0.28 \text{ at } 300^\circ\text{C} (572^\circ\text{F})$$

The minimum elongation value of the only other material sometimes at elevated temperature in this calculation, Type 316L SS, the naval canister material, will have insignificant effect on the results of this calculation. Therefore, it is not necessary to perform similar calculations for the minimum elongation of this material at elevated temperature (see Assumption 3.2.12).

Calculations for True Measures of Ductility

The strength properties in this section so far have referred to engineering stress and strain definitions (see Reference 2.2.19, Chapter 9):

$$s = \frac{P}{A_0} \text{ and } e = \frac{L - L_0}{L_0}$$

where P stands for the force applied during a static tensile test, L is the deformed-specimen length, and L_0 and A_0 are the original length and cross-sectional area of the specimen, respectively. It is generally accepted that the engineering stress-strain curve does not give a true indication of the deformation characteristics of a material during plastic deformation since it is based entirely on the original dimensions of the specimen. Therefore, the LS-DYNA finite element code requires input in terms of true stress and true strain definitions:

$$\sigma = \frac{P}{A} \text{ and } \varepsilon = \ln\left(\frac{L}{L_0}\right)$$

The relationships between the true stress and true strain definitions and engineering stress and engineering strain definitions can be readily derived based on constancy of volume ($A_0 \cdot L_0 = A \cdot L$) and strain homogeneity during plastic deformation:

$$\sigma = s \cdot (1 + e) \text{ and } \varepsilon = \ln(1 + e)$$

These expressions are applicable only in the hardening region of the stress-strain curve before the onset of necking (before stresses reach the tensile strength).

The following parameters are used in the subsequent calculations:

$s_y \approx \sigma_y$ = yield strength

s_u = engineering tensile strength

σ_u = true tensile strength

$e_y \approx \varepsilon_y$ = strain corresponding to tensile yield strength

e_u = engineering strain corresponding to engineering tensile strength (uniform strain)

ε_u = true strain corresponding to true tensile strength (true uniform strain)

Uniform strain data are not listed in traditional sources and it needs to be estimated based on stress-strain curves and the minimum specified elongation. For Alloy 22 and 316 SS, the minimum elongation, reduced by 10% is used for the uniform strain (see Assumption 3.2.3). The minimum elongation for 316L SS is reduced by 40% and used for the uniform strain (see Assumption 3.2.4).

In the case of Alloy 22:

$$e_u = 0.9 \cdot \text{elongation} = 0.9 \cdot 0.45 = 0.41 \text{ at RT and}$$

$$e_u = 0.9 \cdot 0.49 = 0.44 \text{ at } 300^\circ\text{C (572}^\circ\text{F)}$$

$$\varepsilon_u = \ln(1 + e_u) = \ln(1 + 0.41) = 0.34 \text{ at RT}$$

$$\varepsilon_u = \ln(1 + e_u) = \ln(1 + 0.44) = 0.36 \text{ at } 300^\circ\text{C (572}^\circ\text{F)}$$

$$\sigma_u = s_u \cdot (1 + e_u) = 689 \cdot (1 + 0.41) = 971 \text{ MPa (141 ksi) at RT}$$

$$\sigma_u = s_u \cdot (1 + e_u) = 632 \cdot (1 + 0.44) = 910 \text{ MPa (132 ksi) at } 300^\circ\text{C (572}^\circ\text{F)}$$

For 316 SS:

$$e_u = 0.9 \cdot \text{elongation} = 0.9 \cdot 0.40 = 0.36 \text{ at RT}$$

$$e_u = 0.9 \cdot 0.28 = 0.25 \text{ at } 300^\circ\text{C (572}^\circ\text{F)}$$

$$\varepsilon_u = \ln(1 + e_u) = \ln(1 + 0.36) = 0.31 \text{ at RT}$$

$$\varepsilon_u = \ln(1 + e_u) = \ln(1 + 0.25) = 0.22 \text{ at } 300^\circ\text{C (572}^\circ\text{F)}$$

$$\sigma_u = s_u \cdot (1 + e_u) = 517 \cdot (1 + 0.36) = 703 \text{ MPa (102 ksi) at RT}$$

$$\sigma_u = s_u \cdot (1 + e_u) = 495 \cdot (1 + 0.25) = 619 \text{ MPa (89.8 ksi) at } 300^\circ\text{C (572}^\circ\text{F)}$$

For 316L SS:

$$e_u = 0.6 \cdot \text{elongation} = 0.6 \cdot 0.40 = 0.24 \text{ at RT and } 300^\circ\text{C (572}^\circ\text{F) (see Assumption 3.2.12)}$$

$$\varepsilon_u = \ln(1 + e_u) = \ln(1 + 0.24) = 0.22 \text{ at RT and } 300^\circ\text{C (572}^\circ\text{F)}$$

$$\sigma_u = s_u \cdot (1 + e_u) = 483 \cdot (1 + 0.24) = 599 \text{ MPa (86.9 ksi) at RT}$$

$$\sigma_u = s_u \cdot (1 + e_u) = 426 \cdot (1 + 0.24) = 528 \text{ MPa (76.6 ksi) at } 300^\circ\text{C (572}^\circ\text{F)}$$

6.1.2 Capability Calculation

The Capability calculation uses adjusted Section 6.1.1 material strength properties for all components except the OCB and vendor material strength data for the OCB. With one exception, the non-OCB material strength parameters, S_y , S_u and elongation are increased by 10% for the Capability calculation (Section 7.1.7.2.4 of Reference 2.2.15). The exception is for the Capability calculation of the WP on the EP bridging the invert steel. The EP material uses the Alloy 22 vendor average properties described below without triaxiality adjustment and the LS-DYNA eroding element option based on reaching a true VM strain corresponding to the Code minimum elongation value (see Assumption 3.2.16).

Additional material properties for the OCB used in the Capability calculation are listed in this section. Stress units are Pascal (Pa), Mega Pascal ($MPa = 10^6 Pa$), Giga Pascal ($GPa = 10^9 Pa$), lb/in^2 (psi) and $ksi = 10^3 psi$.

The following vendor averaged Alloy 22 RT material values and adjustments are directly from Table I-2 and Equations I-5 to I-9 of Reference 2.2.15.

Vendor Averaged Alloy 22 RT Properties

- Uniaxial yield strength, S_y and σ_y , = 356 MPa (52 ksi)
- Uniaxial engineering tensile strength, S_u , = 764 MPa (111 ksi)
- Uniform strain, e_u , = 0.61

Evaluations of the governing locations indicate the presence of more severe triaxiality gradients than VM stress and strain gradients, with some Triaxiality Ratios near the worst case value of 0.05. Therefore, the worst case triaxiality adjustment, $ADJ = 0.519$ (see Table I-3 of Reference 2.2.15) is used to obtain triaxiality-adjusted vendor-averaged true ultimate strain, ϵ_u' , and true ultimate (tensile) strength, σ_u' , values:

$$\epsilon_u' = \ln(1 + ADJ \cdot e_u) = \ln(1 + 0.519 \cdot 0.61) = 0.28$$

$$\sigma_u' = S_u \cdot (1 + ADJ \cdot e_u) = 764 \cdot (1 + 0.519 \cdot 0.61) = 1006 \text{ MPa (146 ksi)}$$

Vendor Averaged Alloy 22 properties at 300°C (572°F) are used in a temperature sensitivity study in Section 7.5.1. References 2.2.22 and 2.2.44 provide the elevated temperature data in Table 6-1 which is read directly off the plots or linearly interpolated from tabulated values to obtain 300°C values. This data is the best available and suitable for use in this calculation.

Table 6-1 Elevated Temperature Vendor Data, Alloy 22

Vendor, Source	Temperature °F (°C)	Yield Strength ksi (MPa)	Tensile Strength ksi (MPa)	Elongation %
Special Metals 2006, page 2, Figure 1	572 (300)	35.9 (248)	97.3 (671)	66
Haynes 1997, page 15, 0.25" to 0.75" Plate	400 (204)	41 (283)	98 (676)	66
	600 (316)	36 (248)	95 (655)	68
	572 (300)	36.7 (253)	95.4 (658)	67.7
Vendor Average	300°C	36.3 (250)	96.4 (664)	66.9

To provide consistency with the RT Capability calculation, the uniform engineering strain at 300°C is computed using the same fraction of the elongation, $0.61/0.66 = 0.92$, as in the representative RT test curve used in Appendix I of Reference 2.2.15. This is very close to the 0.9 fraction used in Assumption 3.2.3. Therefore, $e_u = 0.92 \times 0.669 = 0.615$. Again, the worst case triaxiality adjustment, $ADJ = 0.519$ (see Table I-3 of Reference 2.2.15) is used to obtain triaxiality-adjusted vendor-averaged ϵ_u' and σ_u' values at 300°C:

$$\epsilon_u' = \ln(1 + ADJ \cdot e_u) = \ln(1 + 0.519 \cdot 0.615) = 0.28$$

$$\sigma_u' = S_u \cdot (1 + ADJ \cdot e_u) = 664 \cdot (1 + 0.519 \cdot 0.615) = 876 \text{ MPa (127 ksi)}$$

6.2 TANGENT MODULI CALCULATIONS

When metals are driven into the plastic range, the slope of the stress-strain curve continuously changes. A simplification of this curve is used to incorporate plasticity into the FERs. A standard post-yield approximation commonly used in engineering is to use a straight line between the yield point and the ultimate tensile strength point of the material (bilinear elastoplastic representation). This is used in both the deterministic and Capability calculations.

The exception is the OCB material in the Capability calculations where a triaxiality-adjusted trilinear stress-strain curve is input point-by-point.

LS-DYNA solutions are conducted using true stress and true strain. Therefore, a bilinear true stress – true strain curve is constructed. The only new parameter in the subsequent calculations is the tangent (hardening) modulus (E_1), the plastic region slope of this bilinear true stress – true strain curve.

For example, in the case of Alloy 22 for the RT deterministic calculation (see Section 6.1.1), the strain corresponding to the yield strength is:

$$\varepsilon_y = \sigma_y / E = 310 \cdot 10^6 / 206 \cdot 10^9 = 1.5 \cdot 10^{-3}$$

Hence, the tangent modulus is:

$$E_1 = (\sigma_u - \sigma_y) / (\varepsilon_u - \varepsilon_y) = (0.971 - 0.310) / (0.34 - 1.5 \cdot 10^{-3}) = 1.95 \text{ GPa} \quad (0.283 \times 10^6 \text{ psi})$$

Another example is the case of 316 SS for the RT Capability calculation (see Section 6.1.2). The 10% adjusted strength values are:

$$\sigma_y \approx S_y = 1.1 \cdot 207 \text{ MPa} = 228 \text{ MPa}$$

$$S_u = 1.1 \cdot 517 \text{ MPa} = 569 \text{ MPa}$$

$$\text{elongation} = 1.1 \cdot 0.4 = 0.44$$

This leads to:

$$e_u = 0.9 \cdot \text{elongation} = 0.9 \cdot 0.44 = 0.396$$

$$\varepsilon_u = \ln(1 + e_u) = \ln(1 + 0.396) = 0.334$$

$$\sigma_u = S_u \cdot (1 + e_u) = 569 \cdot (1 + 0.396) = 794 \text{ MPa}$$

$$\varepsilon_y = \sigma_y / E = (228 / 195) \cdot 10^{-3} = 1.17 \cdot 10^{-3}$$

$$E_1 = (\sigma_u - \sigma_y) / (\epsilon_u - \epsilon_y) = (0.794 - 0.228) / (0.334 - 1.17 \cdot 10^{-3}) = 1.70 \text{ GPa} (0.246 \cdot 10^6 \text{ psi})$$

The values of tangent moduli used in this calculation are presented in Table 6-2.

Table 6-2 Tangent Moduli

Material	Tangent Modulus, E_t , GPa (10^6 psi)	
	RT	300°C (572°F)
Alloy 22⁽¹⁾	1.95 (0.283)	1.94 (0.281)
Alloy 22⁽²⁾	1.84 (0.267)	not used
316 SS⁽¹⁾	1.60 (0.232)	2.22 (0.322)
316 SS⁽³⁾	1.70 (0.246)	2.26 (0.328)
316L⁽¹⁾	1.95 (0.283)	1.90 (0.276)
316L SS⁽³⁾	2.07 (0.300)	2.02 (0.293)
A36 CS⁽³⁾	1.73 (0.251)	not used
A588 Alloy Steel⁽³⁾	1.65 (0.239)	not used

⁽¹⁾ Deterministic calculation, Section 6.1.1 properties used directly.

⁽²⁾ Capability calculation, EP material, unadjusted vendor properties.

⁽³⁾ Capability calculation; minimum yield, ultimate and elongation values increased by 10%

6.3 IMPACT VELOCITY

To reduce the computer execution time while preserving all dynamic loading features of the problem relevant to the structural calculation, the WP and EP are set in a position immediately before impact and given an appropriate impact velocity. The Capability calculations use arbitrary impact velocities, whereas, the stress sensitivity to WP-on-EP orientation and the deterministic calculation use impact velocities based on drop heights as follows.

Using earth's gravitational constant, g = acceleration due to gravity = 9.81 m/s^2 (32.2 ft/s^2) and Newton's equation of motion (Reference 2.2.21, page 20, equation 15),

$$V_f^2 = V_o^2 + 2 \cdot g \cdot (h_o - h_f),$$

the impact (final) velocity V_f , for any free fall ($V_o = 0$) with drop height, $h = h_o - h_f$, can be computed:

$$V_f^2 = 2 \cdot g \cdot h$$

For drop heights of 1 m (3.3 ft) and 20 in (0.508 m):

$$V_f = \sqrt{2 \cdot 9.81 \cdot 1} = 4.43 \text{ m/s} (14.5 \text{ ft/s}) \text{ for a 1 m (3.3 ft) drop height.}$$

$$V_f = \sqrt{2 \cdot 9.81 \cdot 0.508} = 3.16 \text{ m/s} (10.4 \text{ ft/s}) \text{ for a 20 in (0.508 m) drop height.}$$

6.4 FINITE ELEMENT REPRESENTATIONS

There are three event sequence configurations evaluated in this calculation. The first configuration is the WP orientated in different positions on the EP and together impacting on an unyielding horizontal surface. The concern is the stresses in the OCB at the OCB-to-EP contact zone. It only considers realistic orientations between the WP and EP that can occur during a drop of the WP on the EP from the TEV or in the drifts during vertical motion dominated seismic events. The EP is modeled without eroding elements to induce maximum stresses into the OCB.

The second configuration is the WP laterally centered on the EP which in turn is centered on the longitudinal beams of the invert steel structure. The lateral centering of the WP and EP is a representative “median” lateral position for the WP impacting the EP and invert steel. The EP is modeled with eroding elements to induce more realistic downward displacements and velocities of the WP when the OCB reaches the transverse beams of the invert steel structure. Different axial positions of the WP, EP and invert steel are used to determine the positional sensitivity of stresses in the OCB region of concern, the OCB-to-invert steel contact zone.

The last configuration is the WP without the EP and addresses angled vertical impacts of the WP directly on the drift invert steel structure’s transverse beams. This is intended to represent severe seismic events that separate the EP away from its starting location between the WP and invert. Again, the OCB region of concern is the OCB-to-invert steel contact zone.

All event sequence evaluations are conducted at RT (see Assumption 3.2.13). Impact velocities are applied in the vertical (Y) direction (see Assumption 3.2.15). The invert steel structure’s material properties are those of A36 CS (see Assumption 3.2.18).

6.4.1 WP with EP Impact on Flat Target Surface

This section describes the finite element representations (FERs) used to determine a worst case orientation for the OCB-to-EP contact region stresses. They are based on an earlier BSC WP design (see Assumption 3.2.14).

The WP is simplified in several ways. First, the Naval Long canister and contents are simplified to a hollow right cylinder with end plugs at both ends and a thickened wall. The thickness of the wall and end plugs is based on the bounding maximum mass and a set of conservative simplifications. (see Assumption 3.2.7). The WP lid lifting features are omitted. The EP is simplified by modeling the low stressed 316 SS cross-beams (Tube 1, Reference 2.2.37) as Alloy 22, allowing the beam ends to be merged with the remaining EP FER as one material. Quarter-Symmetry and Half-Symmetry FERs are used with symmetry boundary conditions when possible. The benefit of using these simplifications is to reduce the computer modeling and execution time while preserving all features of the problem relevant to the structural calculation. FERs are developed in conjunction with reviews of simulation results to evolve a worst case orientation of the WP and EP to each other and to the target surface.

WP Transverse Offset Positions

The transverse (X-Y) contact position of the WP on the EP is varied using 11 different FERs. The WP location ranges from centered on the EP to an offset 4 *in* above the centered position with a corresponding horizontal offset to make contact with the EP (referred to as “4 *in* WP offset”). The WP and EP longitudinal axes are parallel and horizontal. This permits the use of a Half-Symmetry FER (referred to as a “Half FER”) with an X-Y symmetry plane at the WP and EP mid-lengths. See Figures 6-1 to 6-12.

0 DEG NO OFFSET (4 PT LOAD)

Time = 0

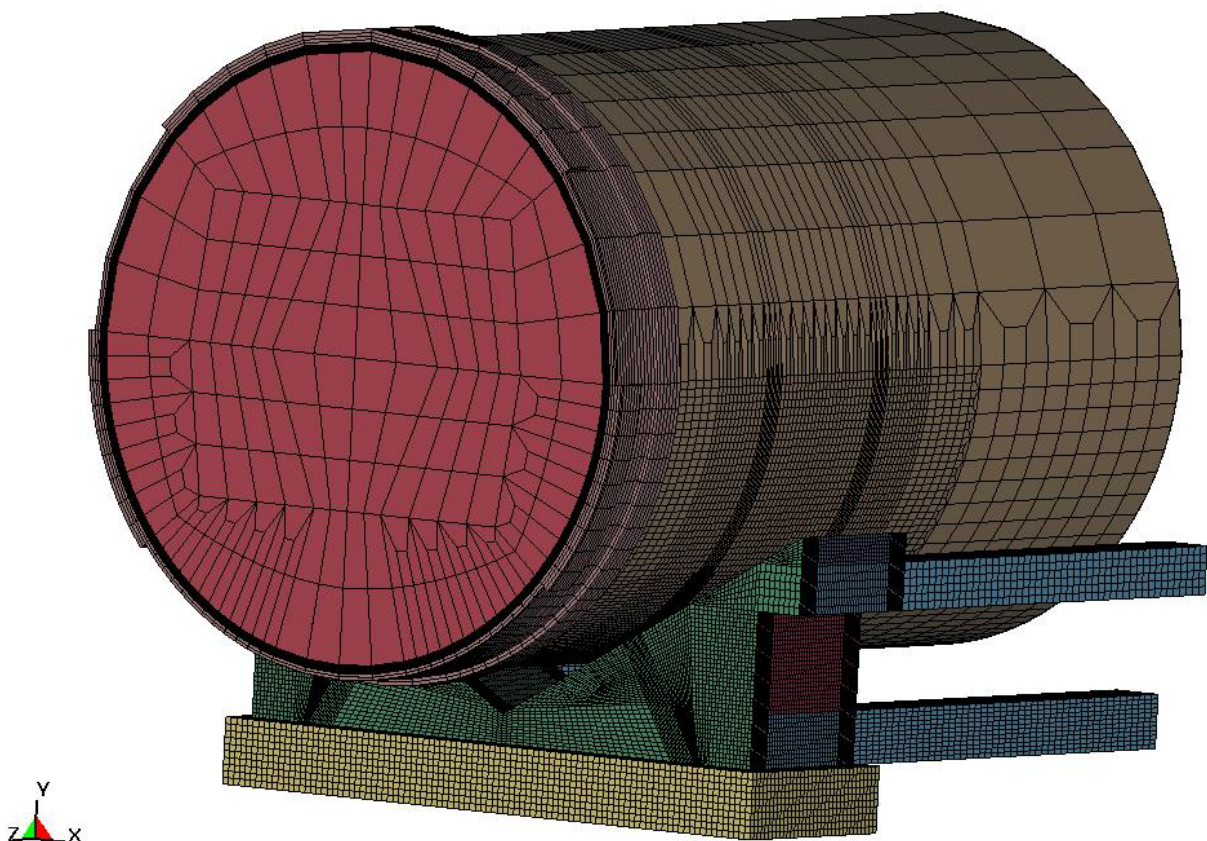


Figure 6-1 Overview Model of Half FER

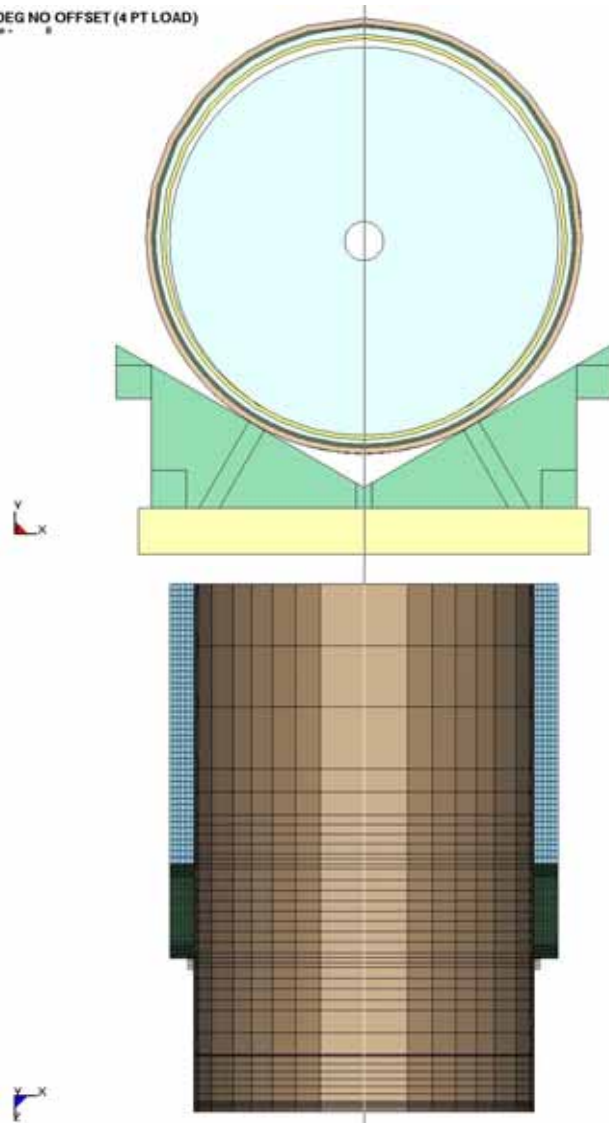
0 DEG NO OFFSET (4 PT LOAD)
Time = 0

Figure 6-2 Centered WP w/ Trunnion Sleeve Hidden

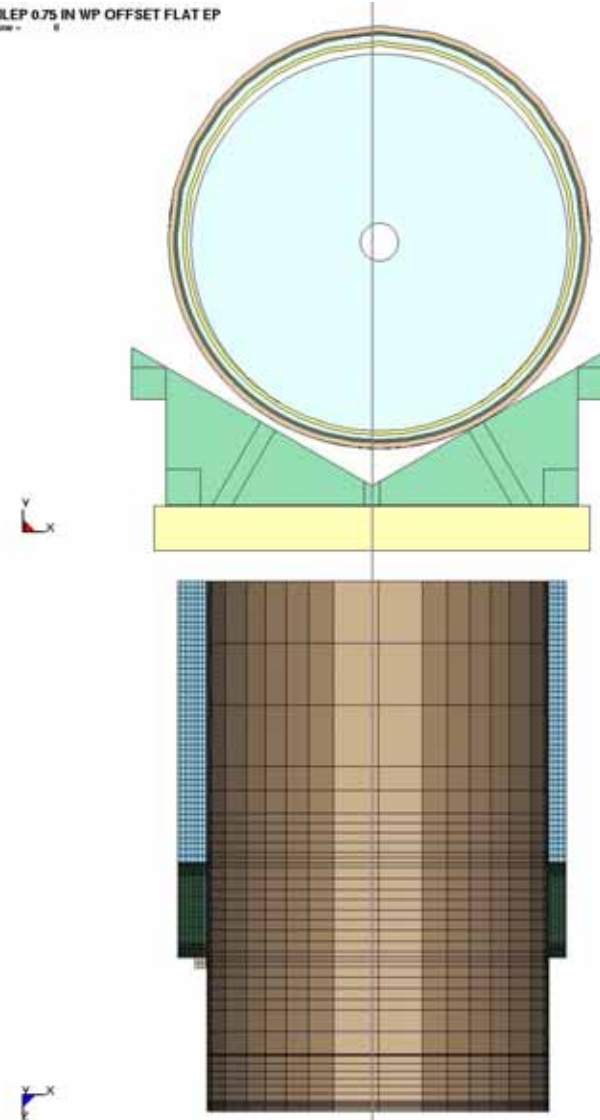
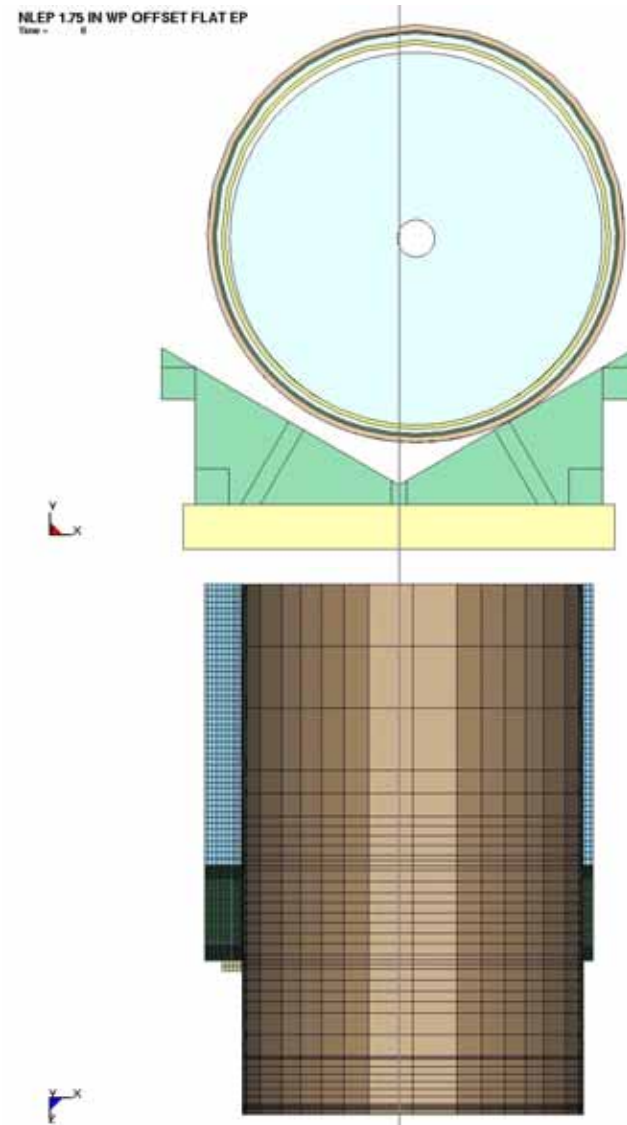
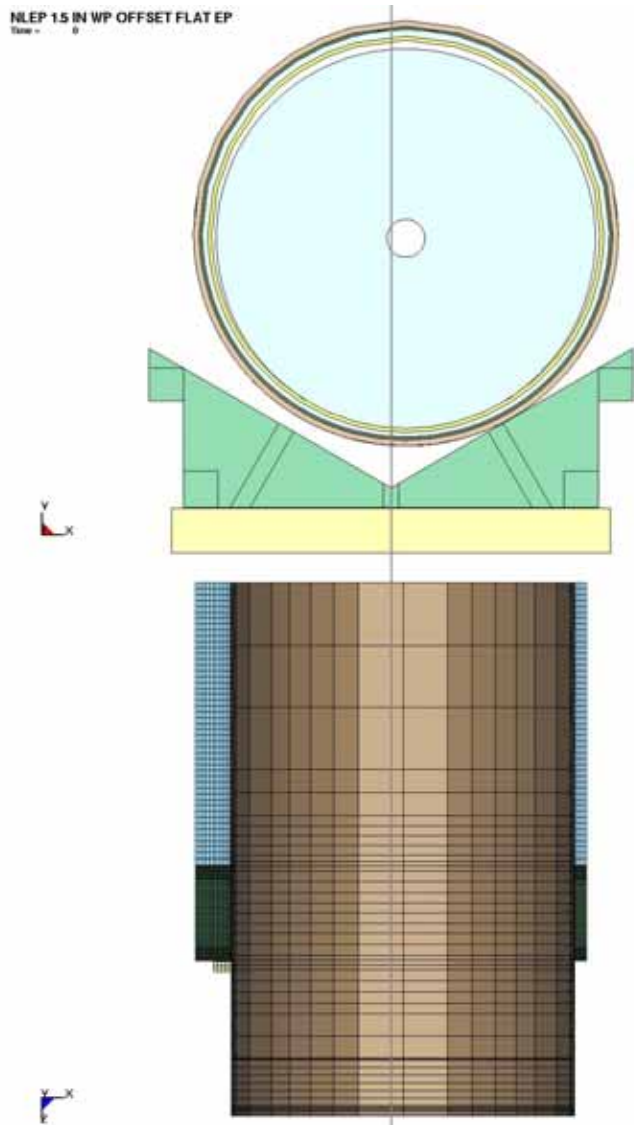
NLEP 0.75 IN WP OFFSET FLAT EP
Time = 0

Figure 6-3 0.75 in WP Offset w/ Trunnion Sleeve Hidden



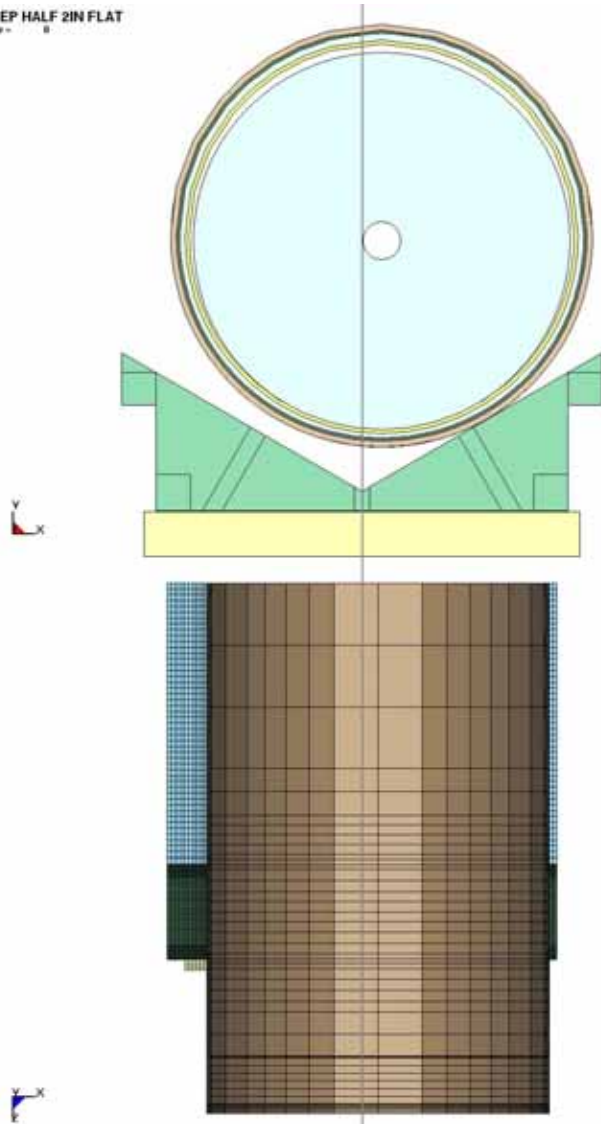
NLEP HALF 2IN FLAT
Time = 0

Figure 6-6 2 in WP Offset w/ Trunnion Sleeve Hidden

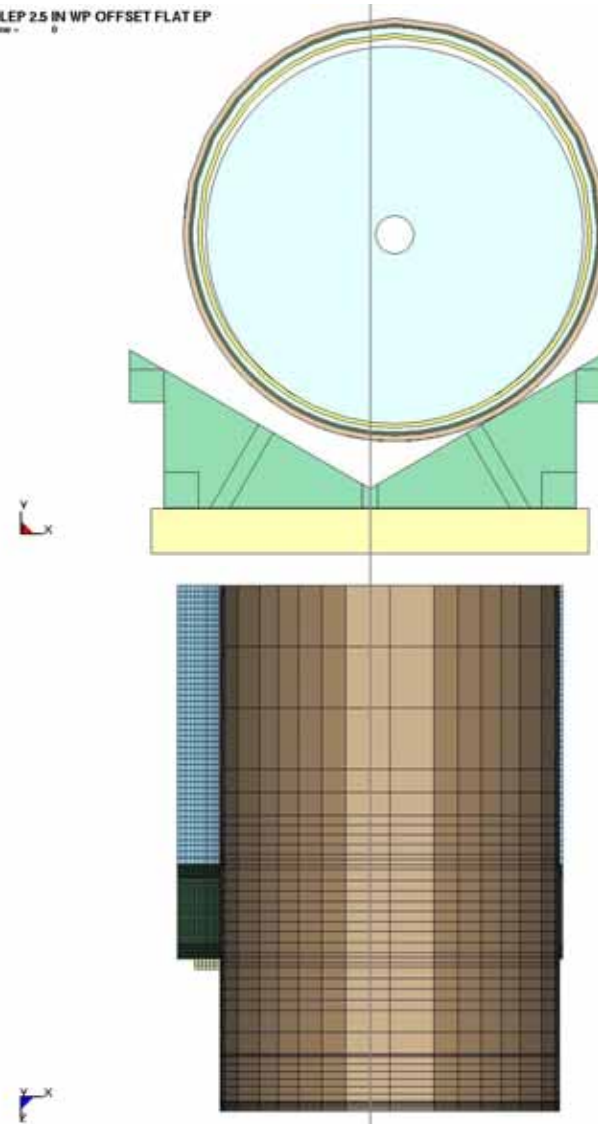
NLEP 2.5 IN WP OFFSET FLAT EP
Time = 0

Figure 6-7 2.5 in WP Offset w/ Trunnion Sleeve Hidden

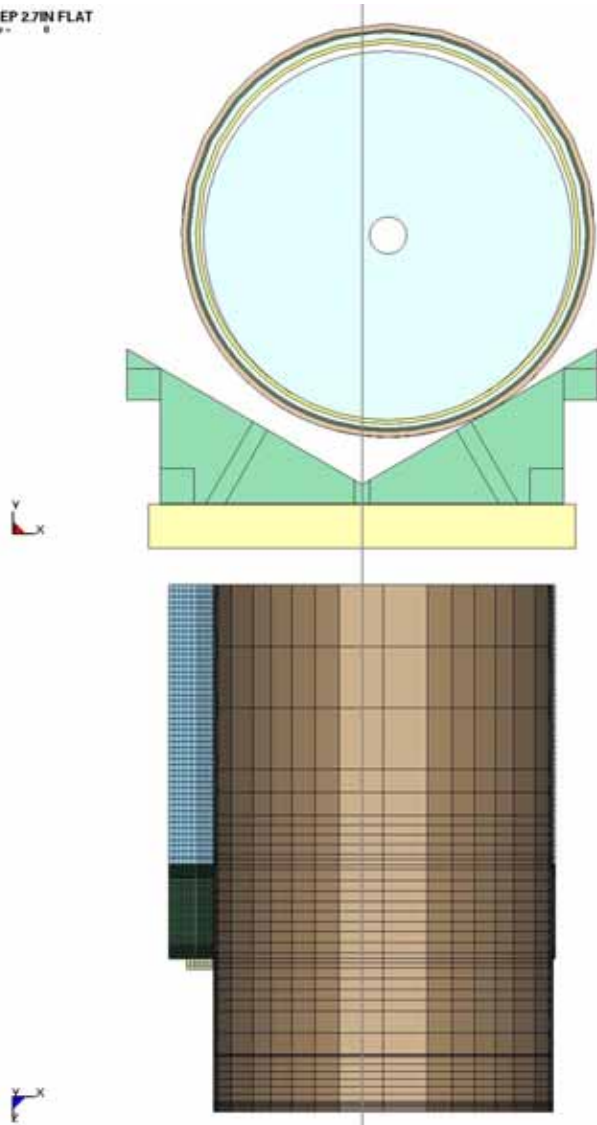
NLEP 2.7IN FLAT
Time = 0

Figure 6-8 2.7 in WP Offset w/ Trunnion Sleeve Hidden

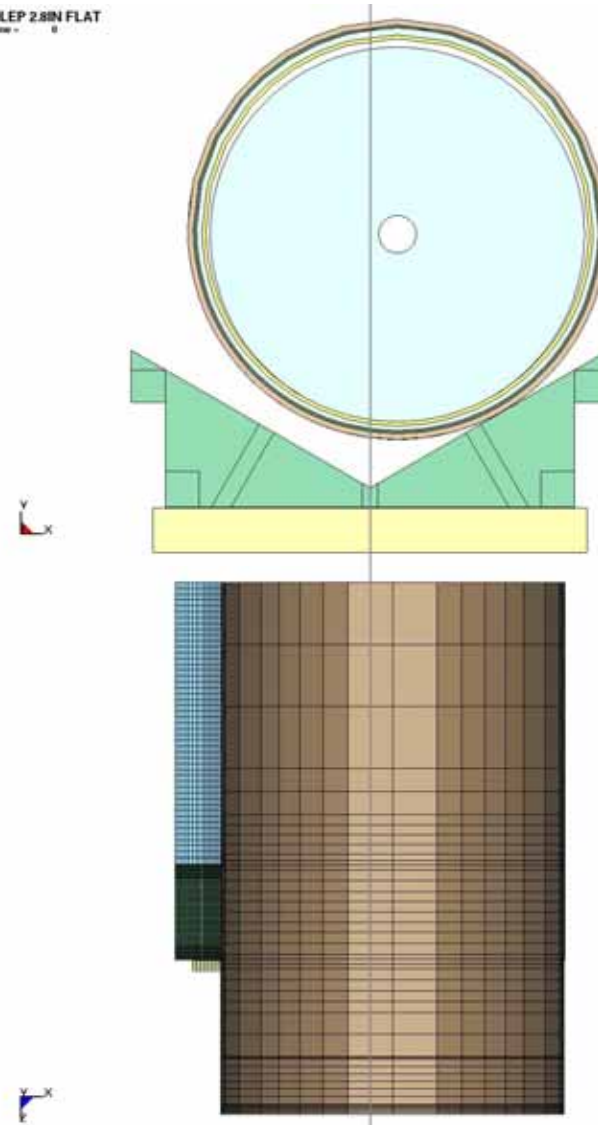
NLEP 2.8IN FLAT
Time = 0

Figure 6-9 2.8 in WP Offset w/ Trunnion Sleeve Hidden

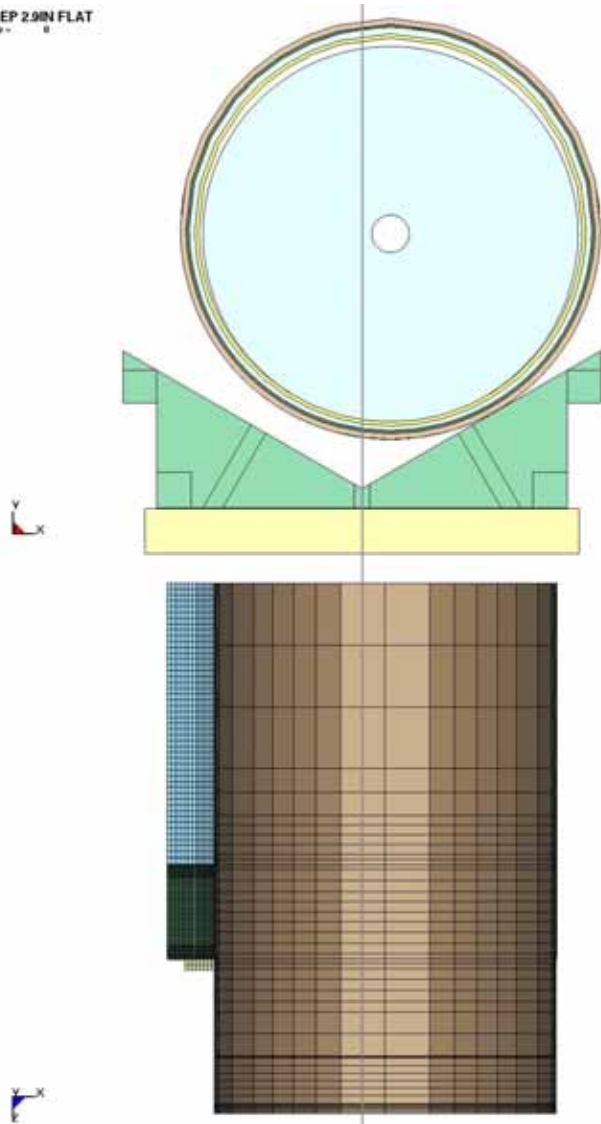
NLEP 2.9IN FLAT
Time = 0

Figure 6-10 2.9 in WP Offset w/ Trunnion Sleeve Hidden

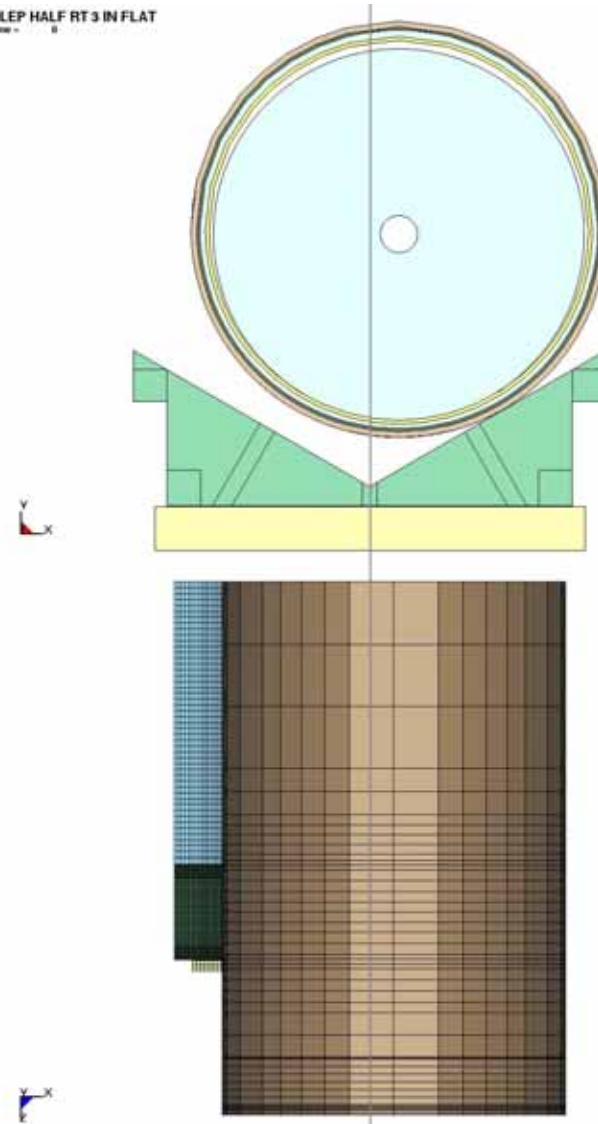
NLEP HALF RT 3 IN FLAT
Time = 0

Figure 6-11 3 in WP Offset w/ Trunnion Sleeve Hidden

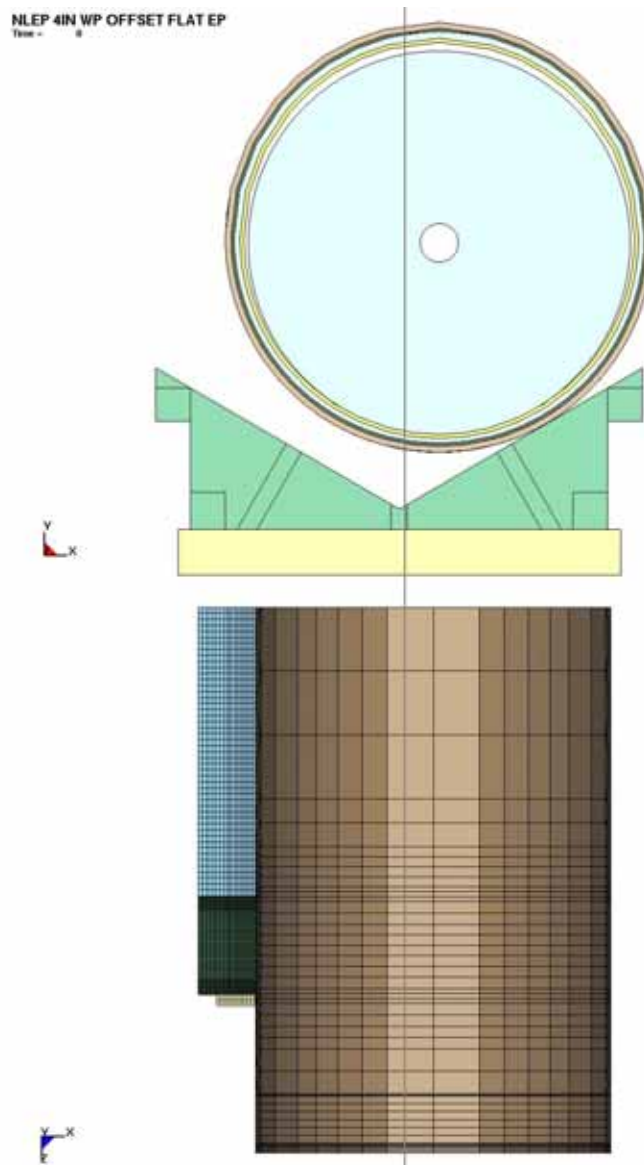


Figure 6-12 4 in WP Offset w/ Trunnion Sleeve Hidden

EP Axial Rotational Positions

The rotational (about the Z-axis) orientation of the EP to the target surface is varied using seven different FERs. The EP impact position varies from a perfectly flat impact to an impact with a 6 degree (*deg*) rotation of the bottom of the EP to the target surface. Both ends of the EP contact the target surface at the same time and the WP is perfectly centered on the EP. This again permits the use of a Half-Symmetry FER with an X-Y symmetry plane at the WP and EP mid-lengths. See Figures 6-13 to 6-19.

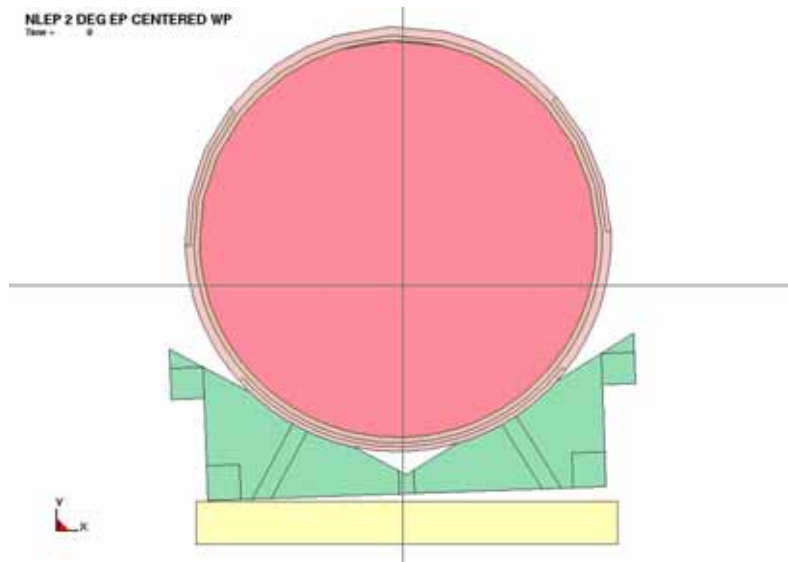


Figure 6-13 2 deg Z-Axis EP rotation, Centered WP

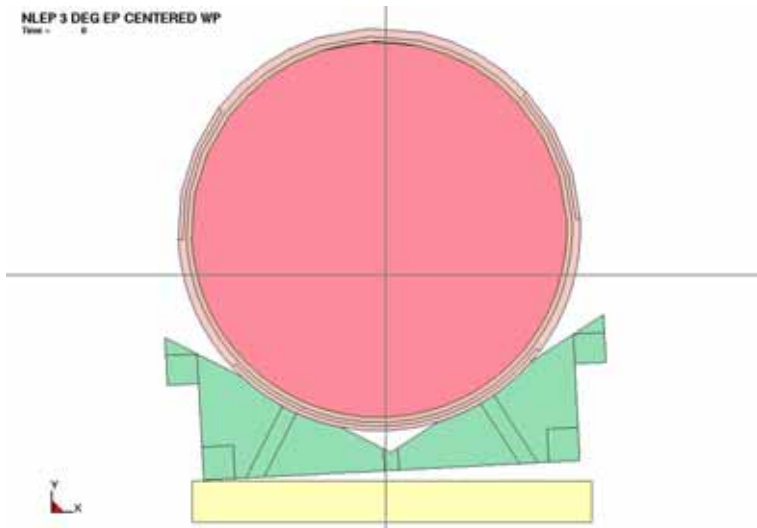


Figure 6-14 3 deg Z-Axis EP Rotation, Centered WP

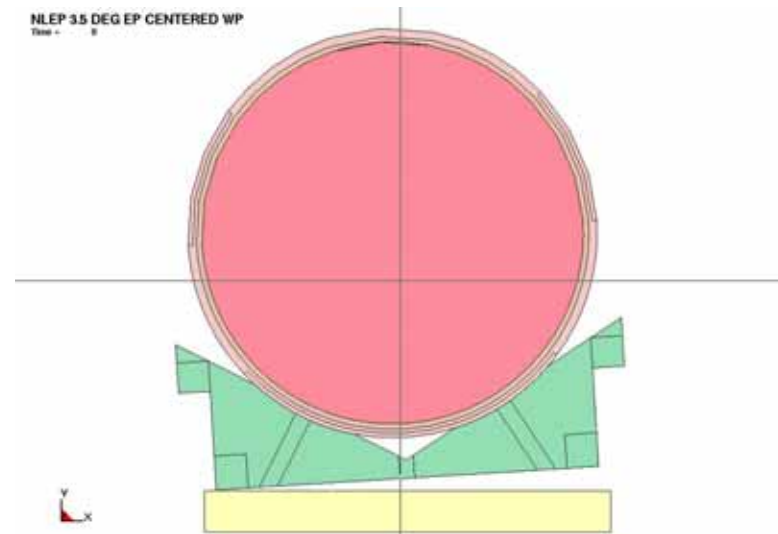


Figure 6-15 3.5 deg Z-Axis EP Rotation, Centered WP

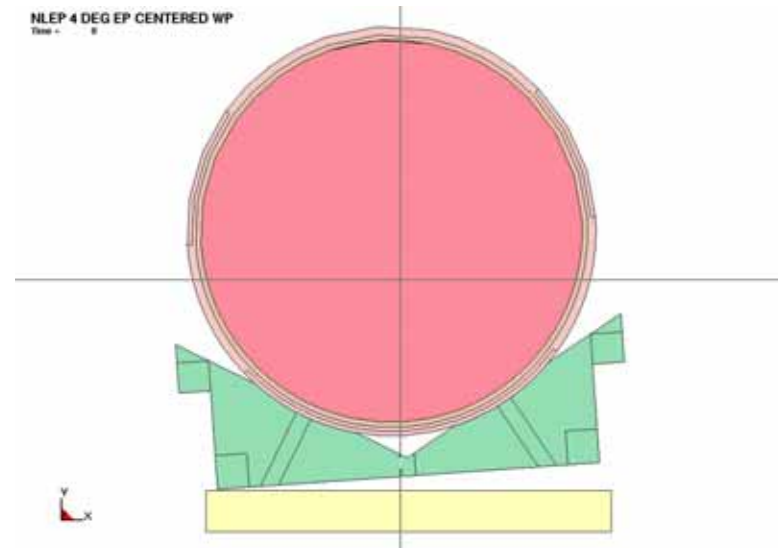


Figure 6-16 4 deg Z-Axis EP Rotation, Centered WP

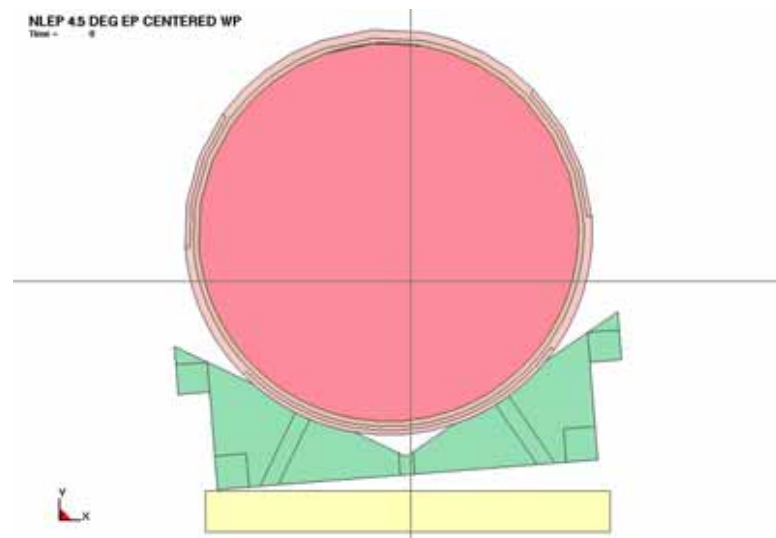


Figure 6-17 4.5 deg Z-Axis EP Rotation, Centered WP

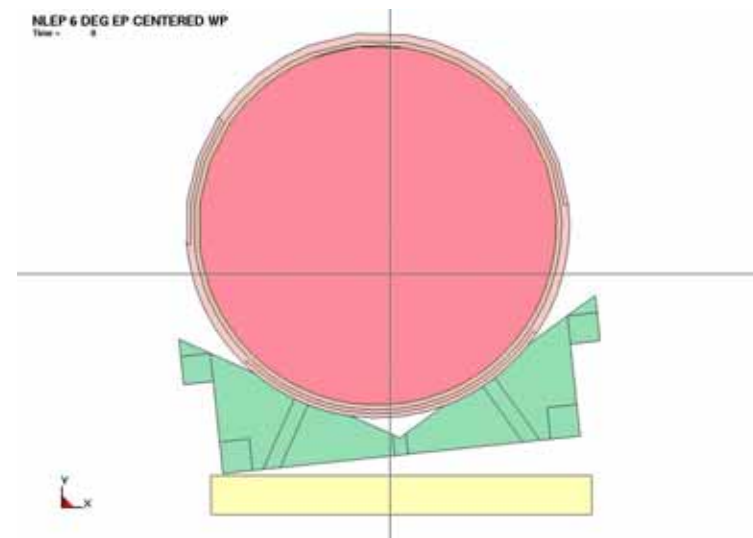


Figure 6-19 6 deg Z-Axis EP Rotation, Centered WP

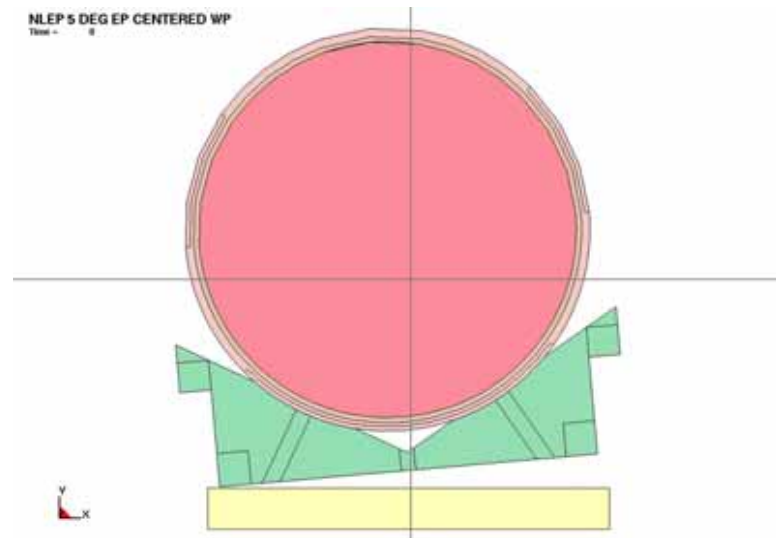


Figure 6-18 5 deg Z-Axis EP Rotation, Centered WP

A combined case of two previous cases features a 4 *deg* EP rotation with a 3 *in* WP offset. This still permits the use of a Half-Symmetry FER with an X-Y symmetry plane at the WP and EP mid-lengths. See Figure 6-20.

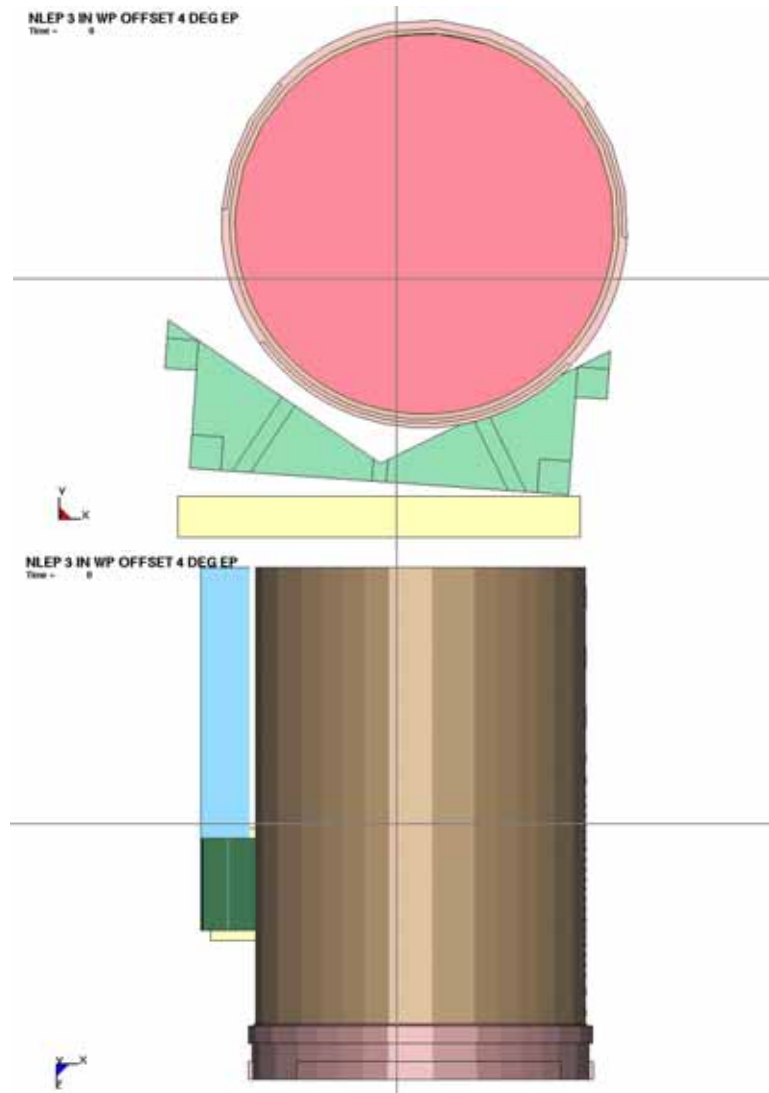


Figure 6-20 3 *in* WP Offset w/ 4 *deg* EP Z-Axis Rotation

EP Longitudinal Rotation Positions

The X-axis rotational orientation of the EP to the target surface is set at 2 degrees in two FERs. One FER has no rotation of the EP around the Z-axis. The other FER is rotated about the Z-axis at the angle that leads to the highest stresses for Z-axis rotation alone (4 *deg* rotation). This provides a “corner drop” of the EP. In both FERs the WP is perfectly centered on the EP. Fully 3-D FERs must be used for these representations. See Figures 6-21 and 6-22.

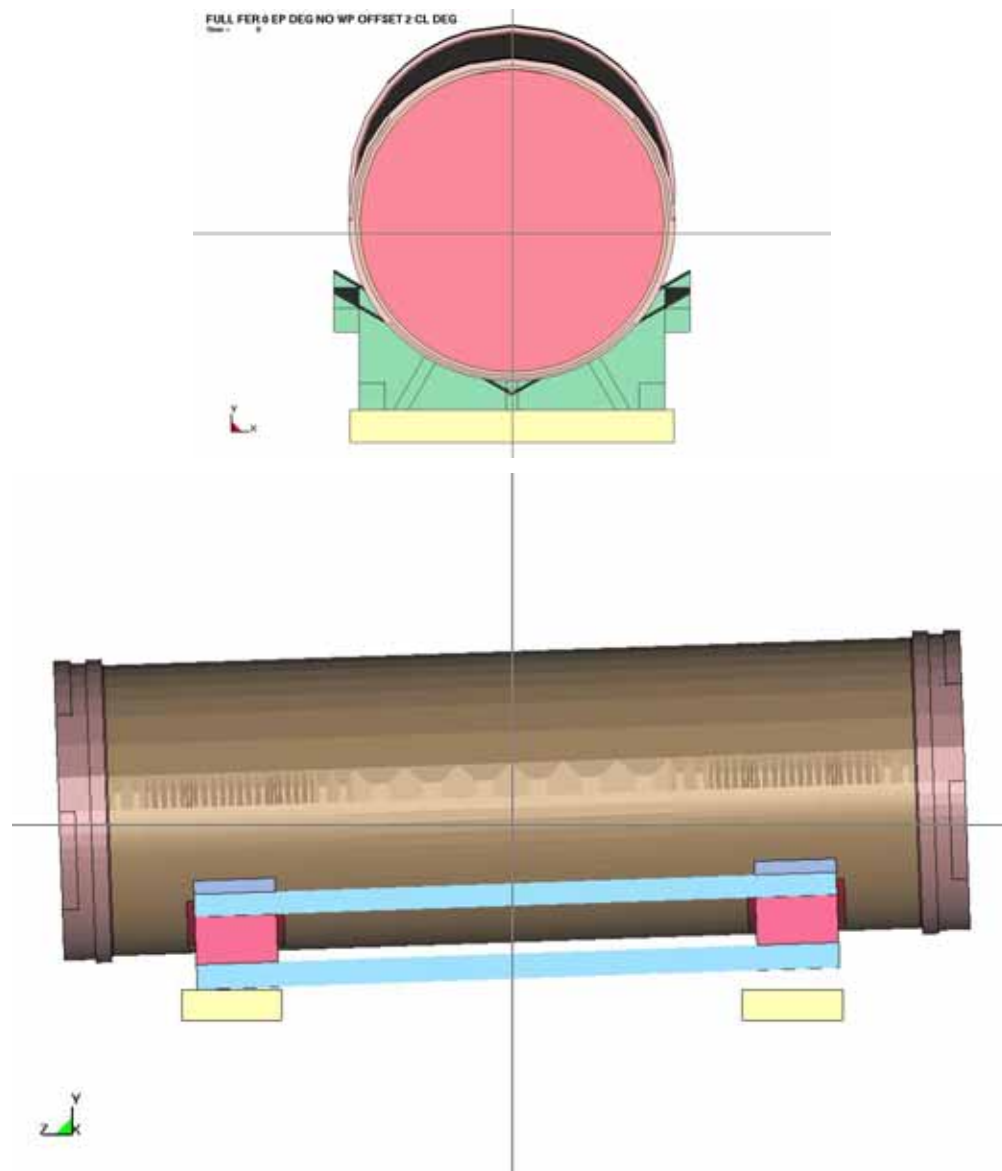


Figure 6-21 2 *deg* X-Axis EP Rotation, Centered WP

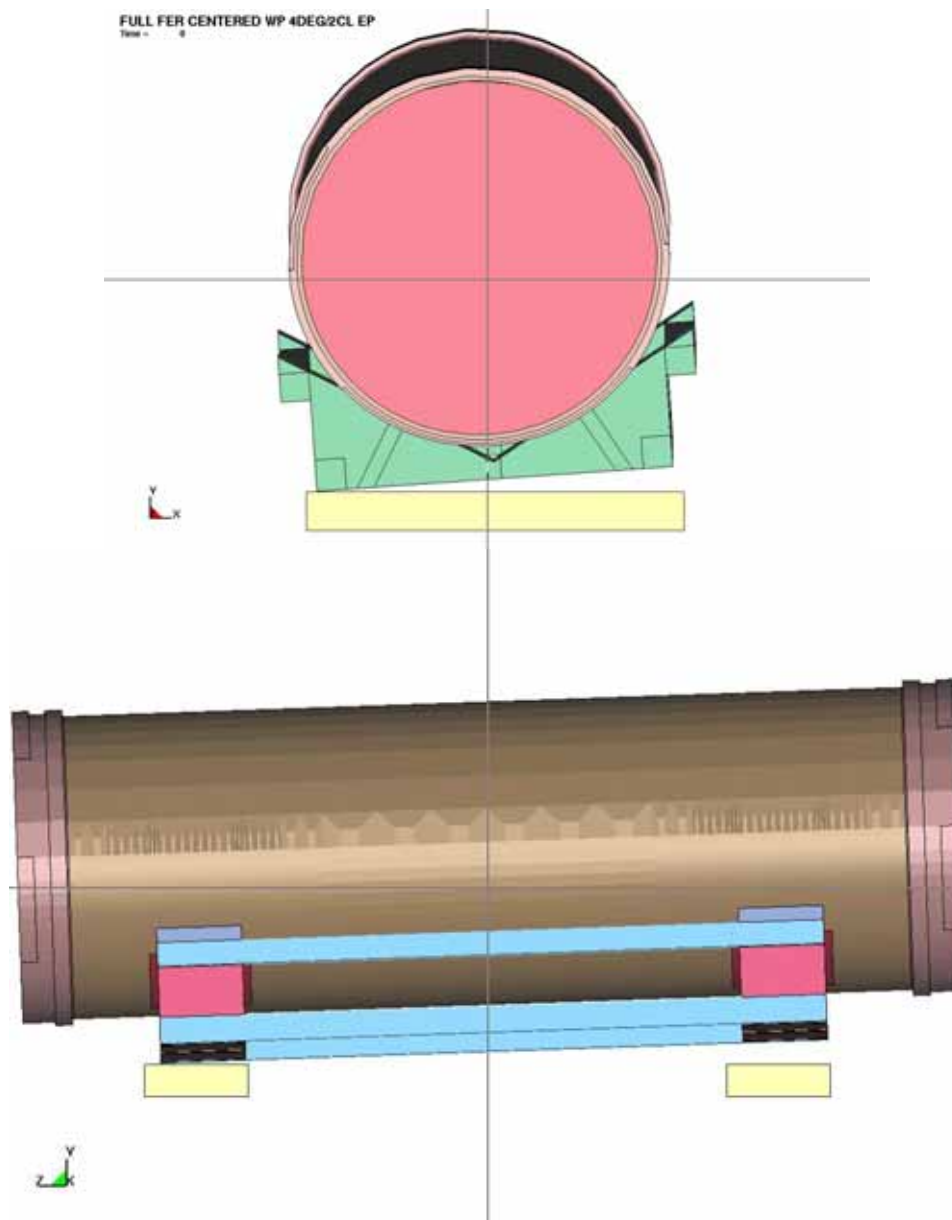


Figure 6-22 2 deg X-Axis and 4 deg Z-Axis EP Rotation, Centered WP

WP Rotated Positions

The remaining three fully 3-D standard mesh FERs are based on the EP impacting the target surface perfectly flat with the WP positioned off center and/or rotated on the EP.

The first of these FERs has the X-axis rotational orientation of the WP to the EP set at 2 degrees. See Figure 6-23.

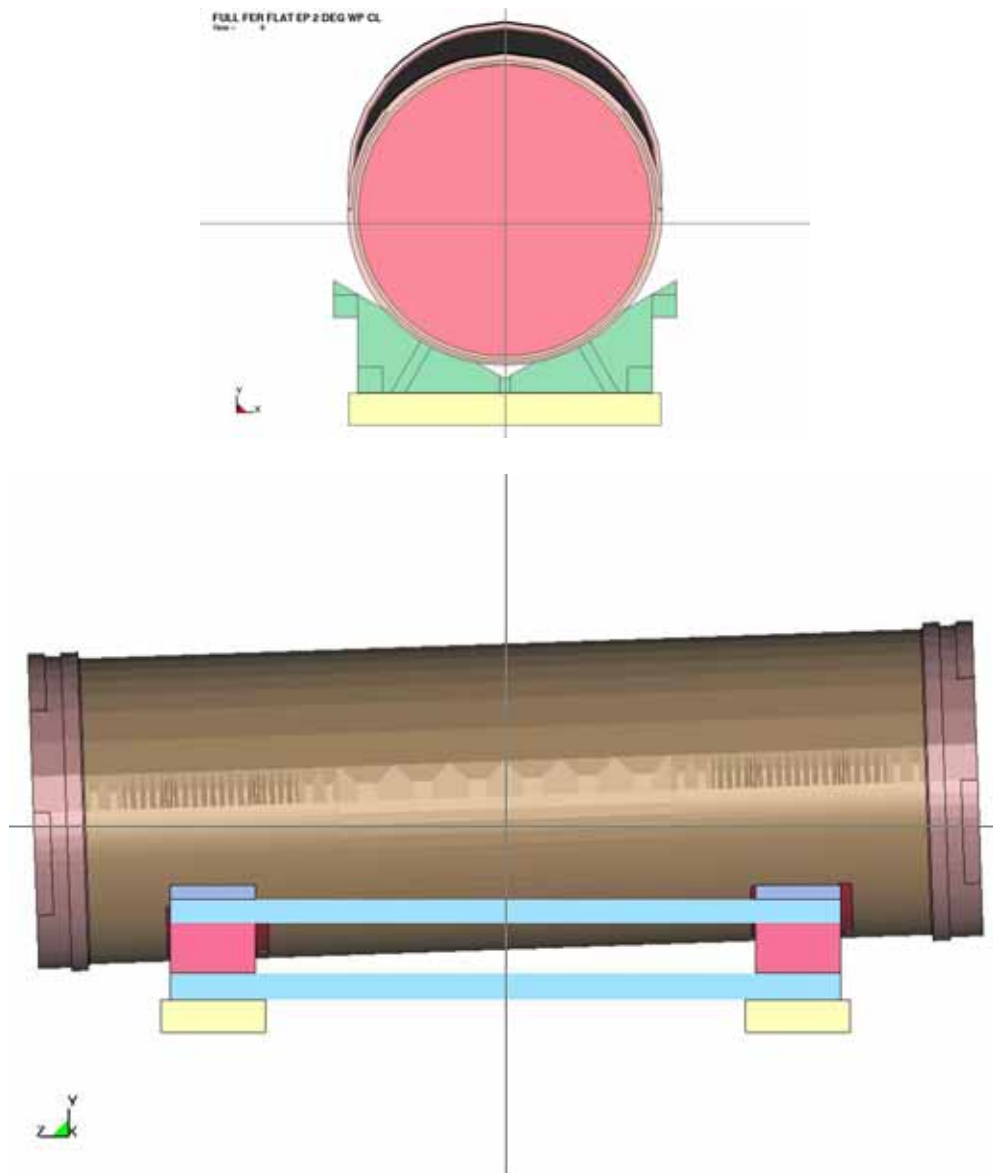


Figure 6-23 Flat EP, 2 deg X-Axis WP Rotation

Another has the WP rotated about the vertical (Y) axis so that it impacts the EP diagonally at the offset distance that led to the highest stresses for X-Y WP offsets alone (2.8 *in* vertical offset). See Figure 6-24.

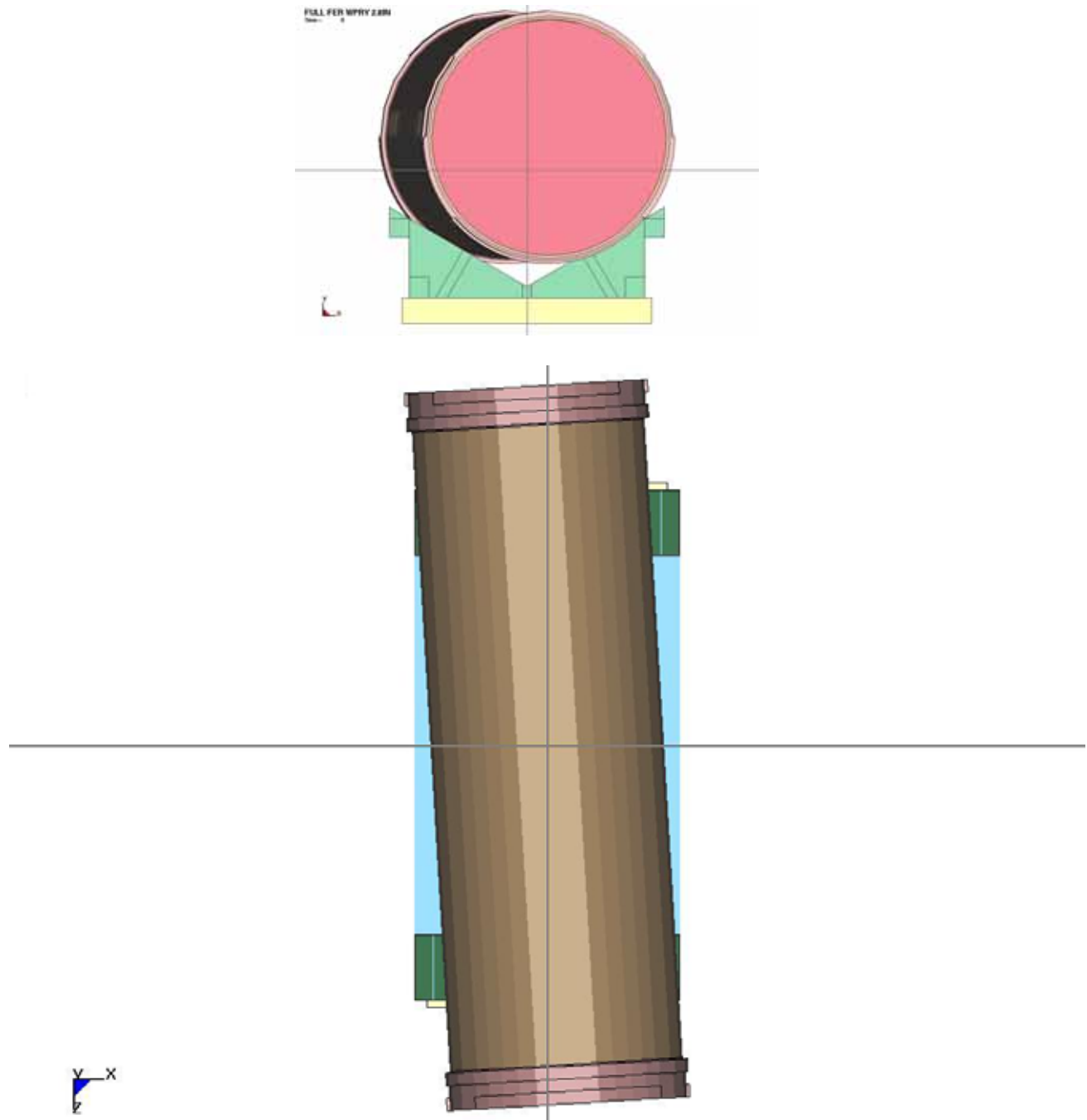


Figure 6-24 Flat EP, 2.8 *in* Offset Y-Axis WP Rotation

The final standard mesh FER is identical to the preceding FER except that the WP is also translated in the Z direction as far as the trunnion sleeves will permit. See Figure 6-25.

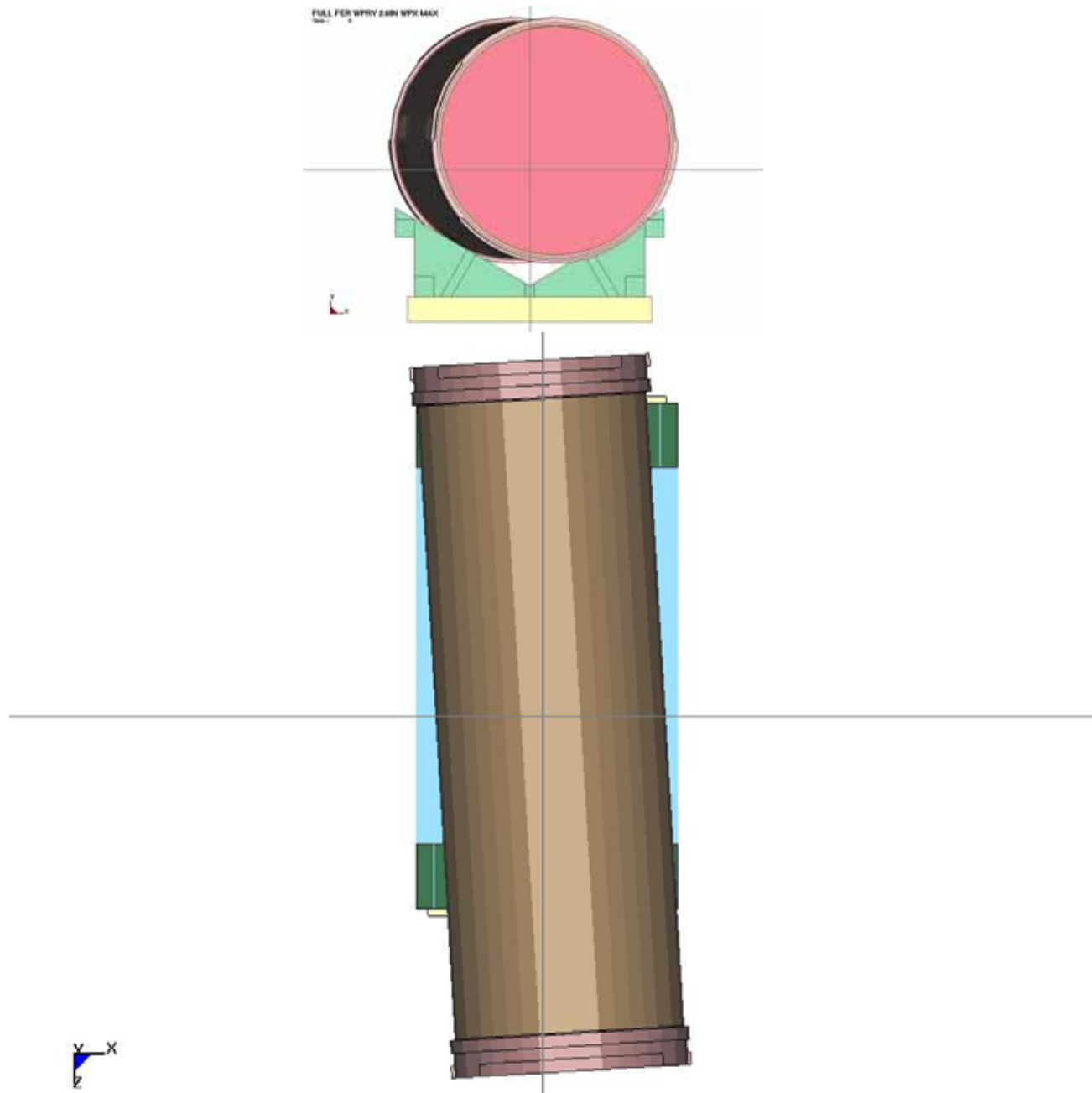


Figure 6-25 Flat EP, 2.8 in Offset Y-Axis WP Rotation and Z-Axis WP Translation

A static and dynamic friction coefficient of 0.4 is assumed for all contacts (Assumptions 3.2.6 and 3.2.9). A sensitivity study supporting this assumption is conducted (Section 7.3.2).

The WP and EP are positioned directly above the unyielding target surface (Assumption 3.2.8) and given an initial downward (-Y) velocity corresponding to their impact velocity (Section 6.3).

The standard mesh is generated using 8-node constant-stress brick elements and is refined in the regions of contact between the WP and EP. To capture realistic wall stresses, the OCB utilizes 9 brick elements across the wall thickness and is generated in each of the other directions (hoop and axial) to maintain an aspect ratio of approximately 1:1:1 in the regions of interest. The mesh is then gradually transitioned away from these areas of interest to reduce the number of elements and thus reduce the computer execution time.

The WP mesh is further refined to verify that the results are not WP mesh sensitive in accordance with Reference 2.2.15, Section 7.1.3. The number of brick elements across the thickness of the OCB is increased from 9 elements to 12 elements and the number of elements in the other directions is increased to maintain an aspect ratio of approximately 1:1:1 in the region of interest.

Mesh refinement comparison simulations are set up for a perfectly centered WP on a perfectly centered and flat impacting EP. This permits the use of Quarter-Symmetry FERs, one with a standard WP mesh, the other with a refined WP mesh. See Figures 6-26 to 6-34 (standard WP mesh) and Figures 6-35 through 6-38 (refined WP mesh). The EP mesh is the same in both FERs. Figures 6-30 and 6-31 show the design detail differences discussed in Assumption 3.2.14.

The comparative results for the two WP mesh refinements can be seen in Table 7-1 and confirms that the accuracy and representativeness of the results of this calculation using the standard WP mesh are acceptable for identifying the worst case loading.

Once the worst case loading is identified, the EP mesh is further refined in the WP impact region for the worst case loading to verify that the results are not EP mesh sensitive in accordance with Reference 2.2.15, Section 7.1.3. The number of plate elements in the EP at the WP contact region is increased significantly; compare Figure 6-34 to Figure 6-39. The comparative results for the two EP mesh refinements can be seen in Table 7-2 and confirms that the accuracy and representativeness of the results of this calculation using the standard WP mesh with the refined EP mesh are acceptable for predicting the worst case loading behavior.

Because of significant high frequency response, at least two runs are conducted for each simulation. The first uses slow data collection and longer times to identify the highest stressed locations and the time of maximum response. The second collects very high rate data at the highest stressed location near the time of maximum response. In some cases the more detailed data indicates that the maximum location or time is missed and a third run is conducted. Only the last run is kept. This approach is needed to keep the data storage requirements realistic. A stress sensitivity study of data collection rates is conducted to establish the optimum data collection rate (see Section 7.3.3).

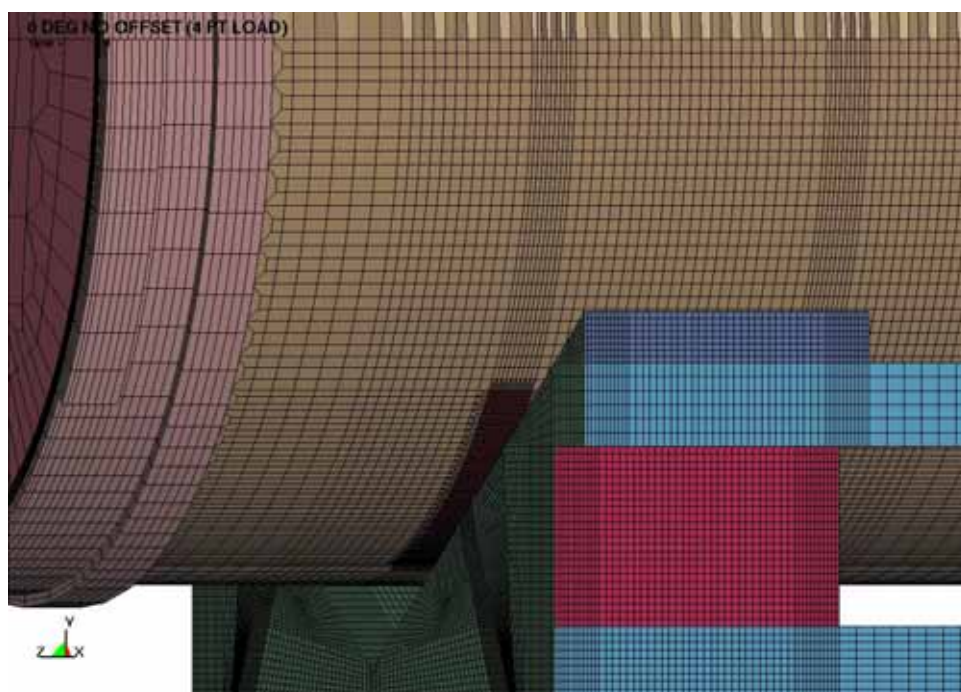


Figure 6-26 Standard WP FER, Overview of WP Impact Region

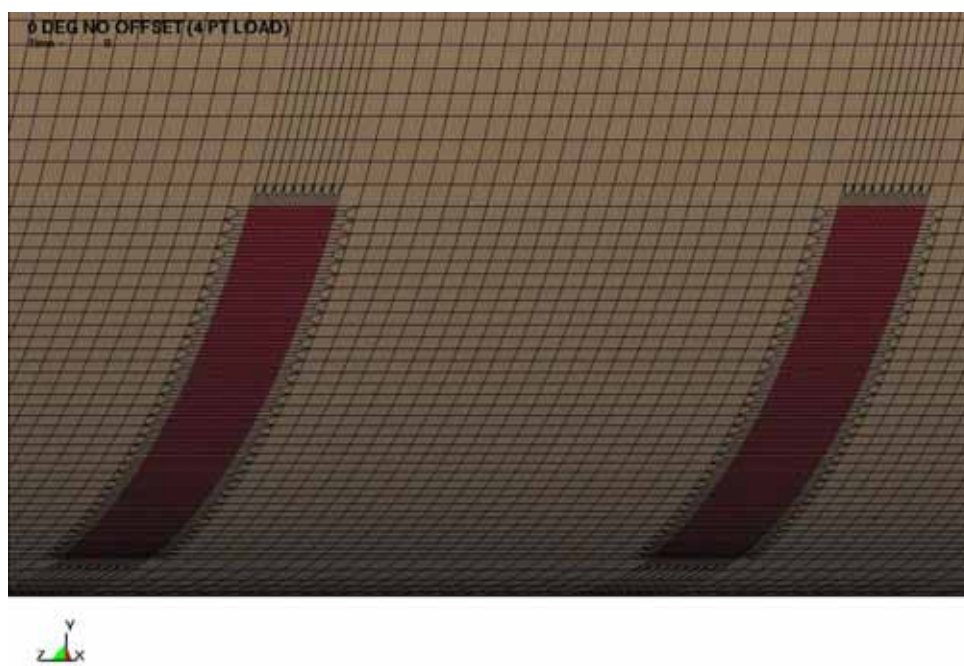


Figure 6-27 Standard WP FER, Enlarged View of WP Impact Region

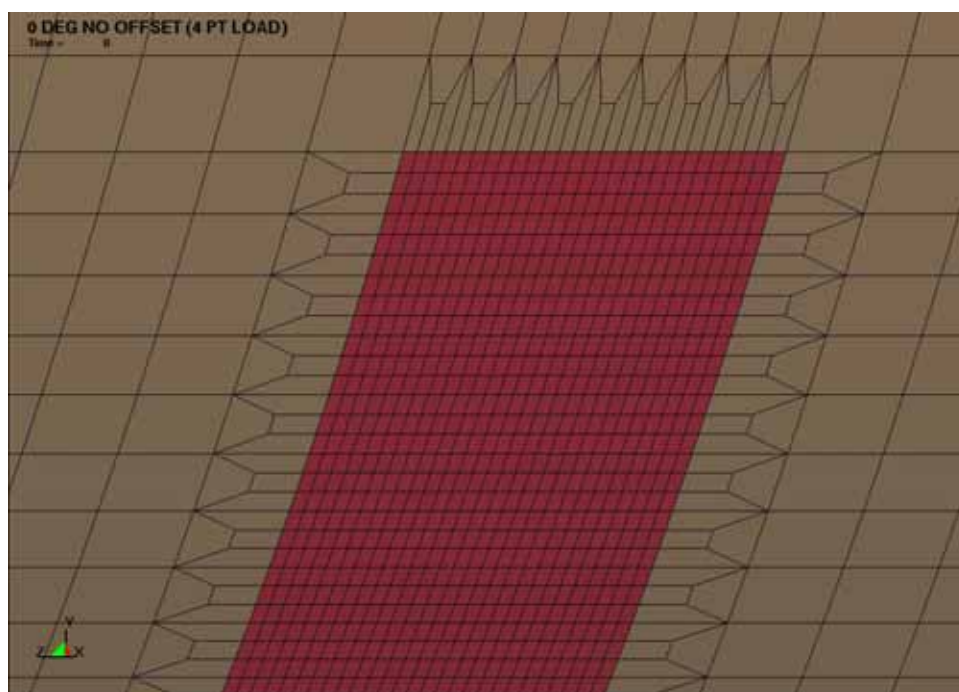


Figure 6-28 Standard WP FER, WP Impact Region Mesh Detail

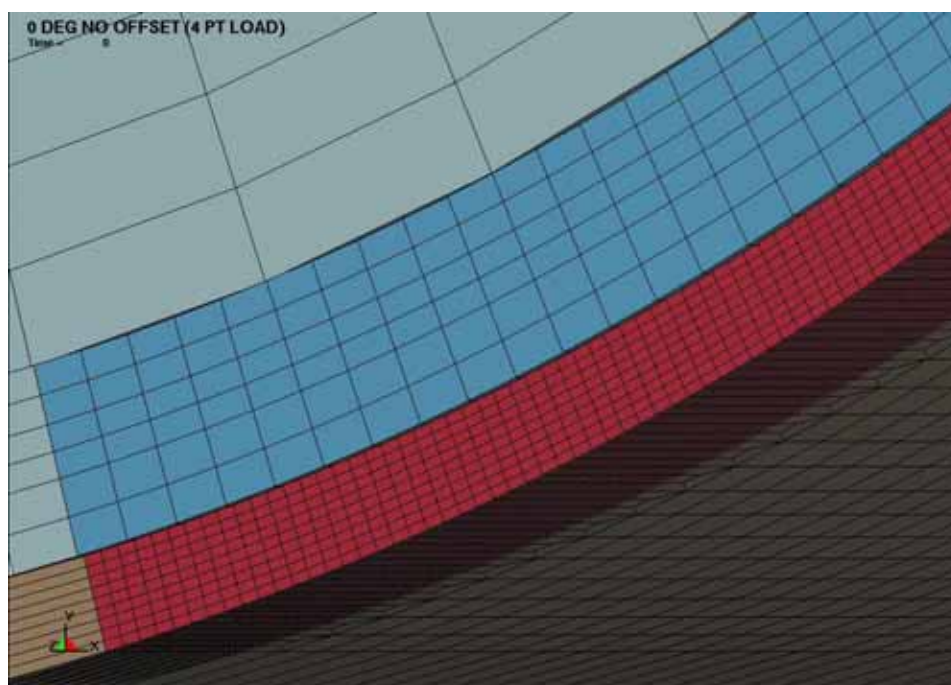


Figure 6-29 Standard WP FER, Cross-section of Impact Region

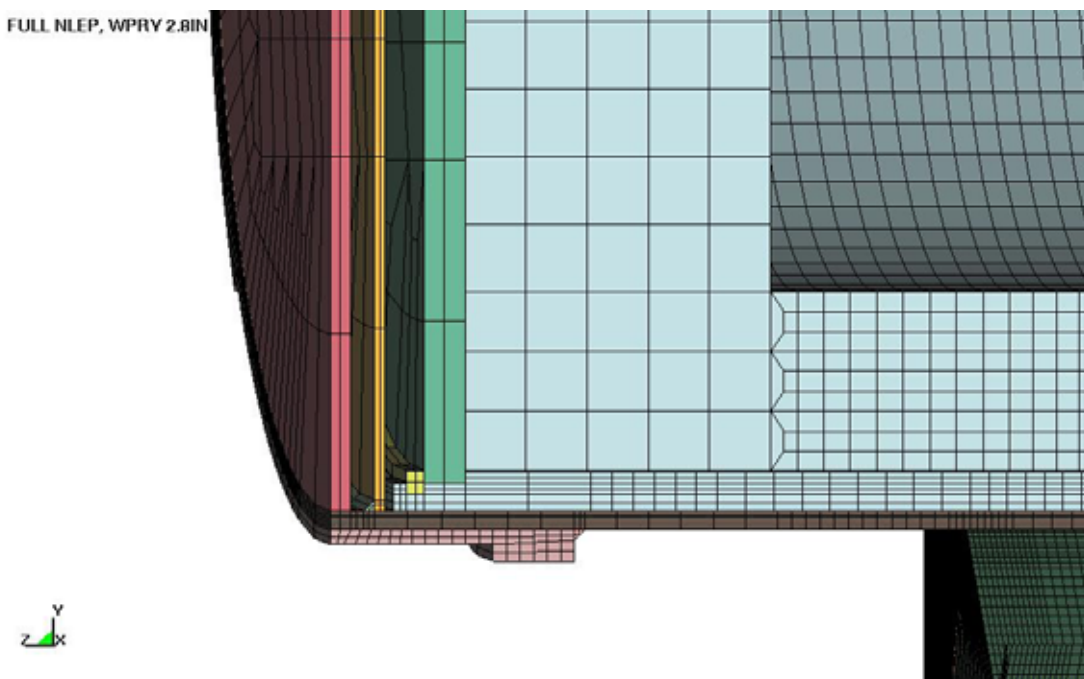


Figure 6-30 Standard WP FER, Earlier Design Detail

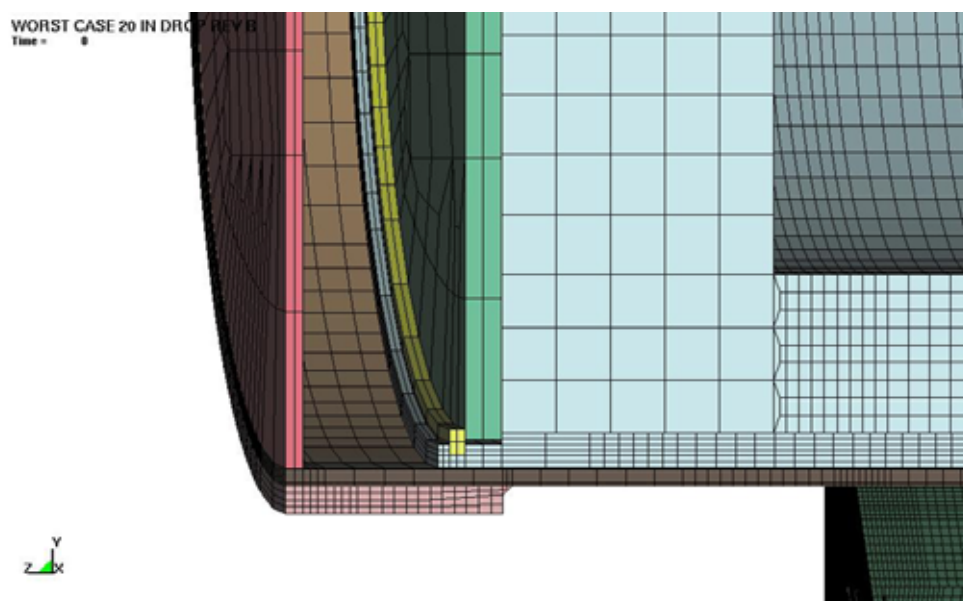


Figure 6-31 Standard WP FER, Current Design Detail (With Shifted Inner Vessel)

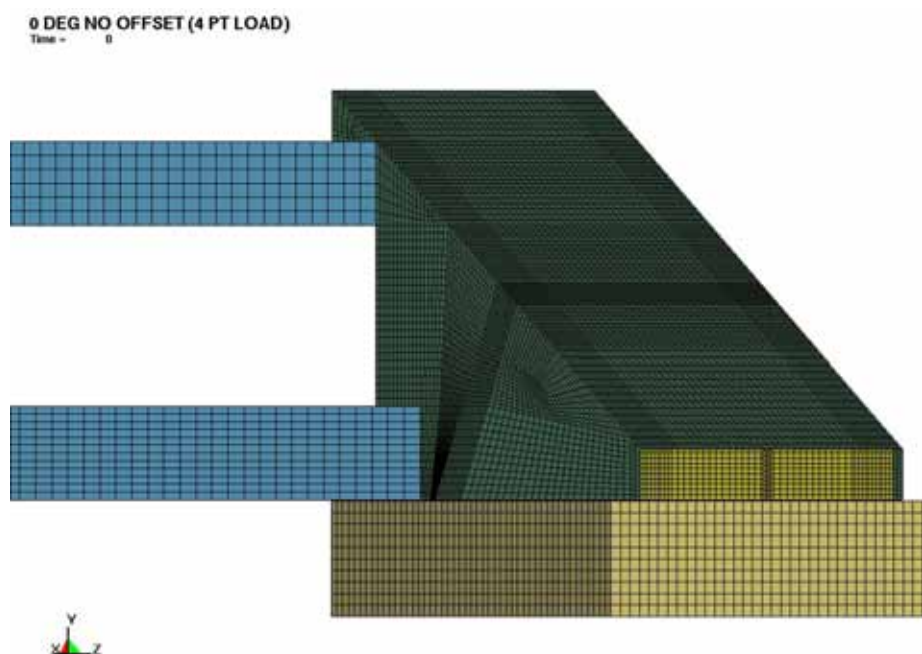


Figure 6-32 Standard EP FER Overview

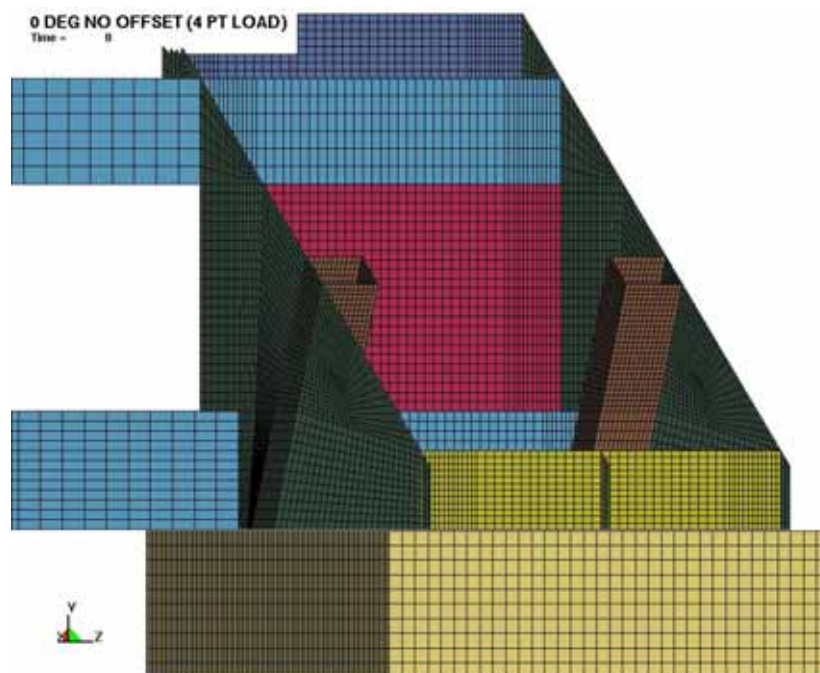


Figure 6-33 Standard EP FER Inside View

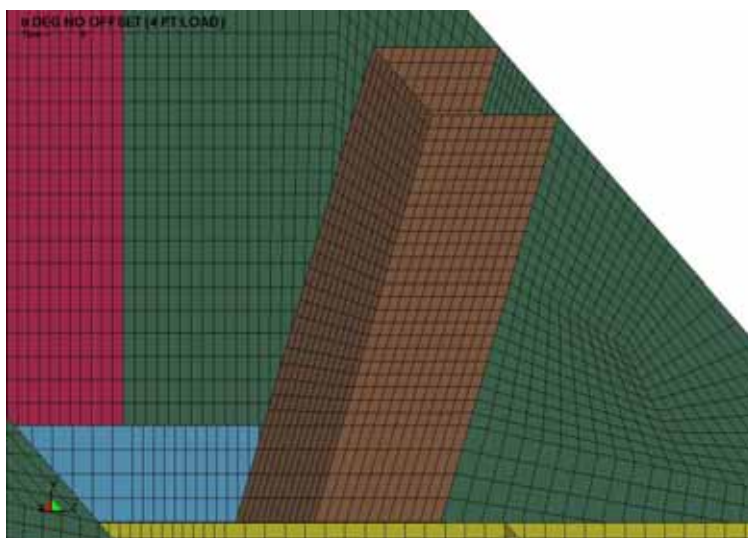


Figure 6-34 Mesh Detail Near Standard EP FER Support Tube

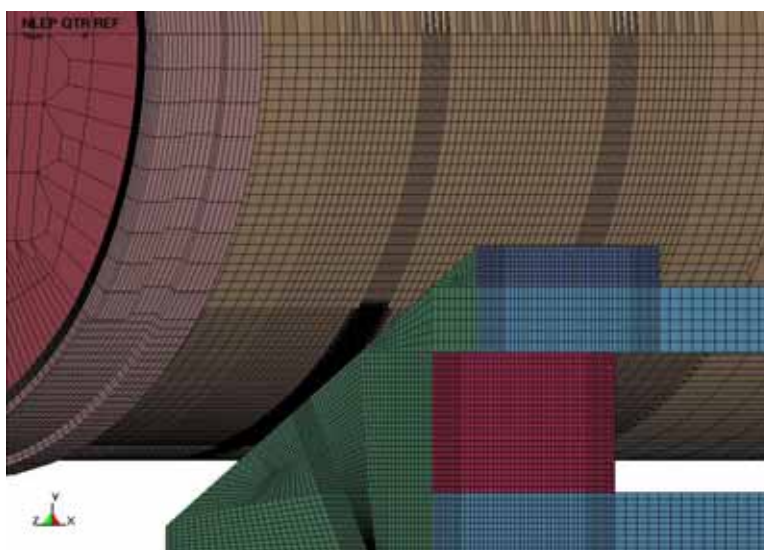


Figure 6-35 Refined WP FER, Overview of WP Impact Region

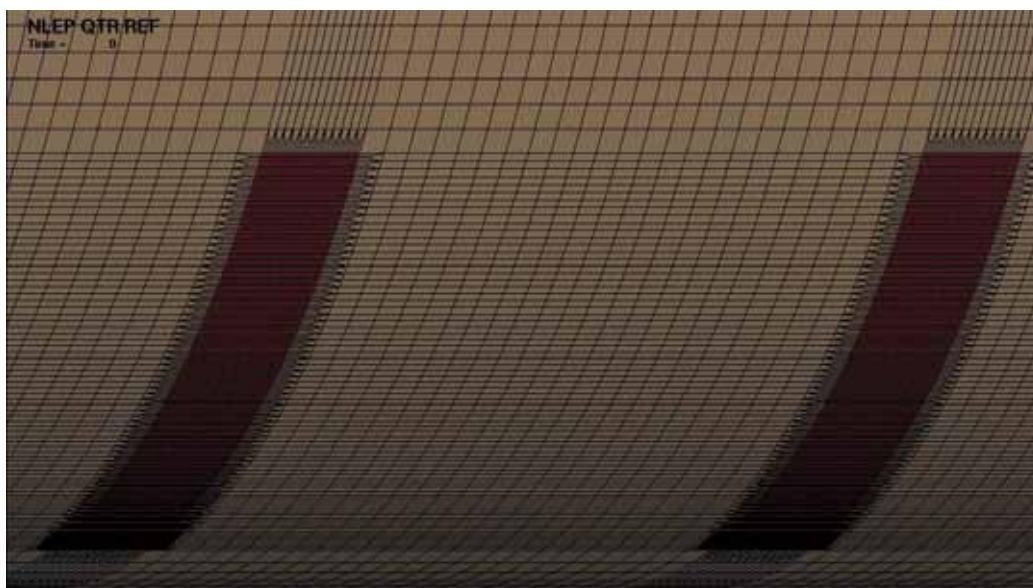


Figure 6-36 Refined WP FER, Enlarged View of WP Impact Region

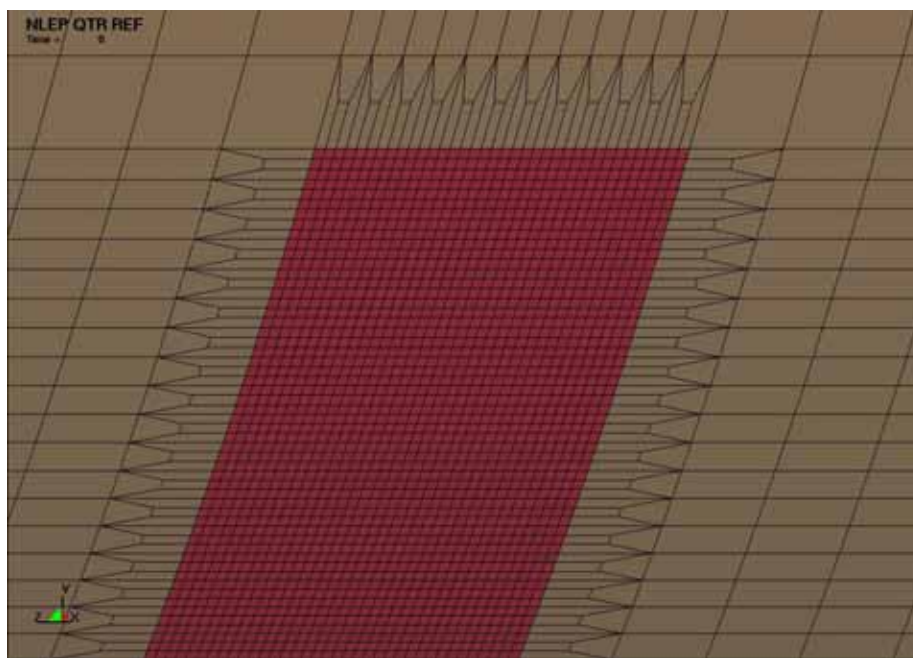


Figure 6-37 Refined WP FER, WP Impact Region Mesh Detail

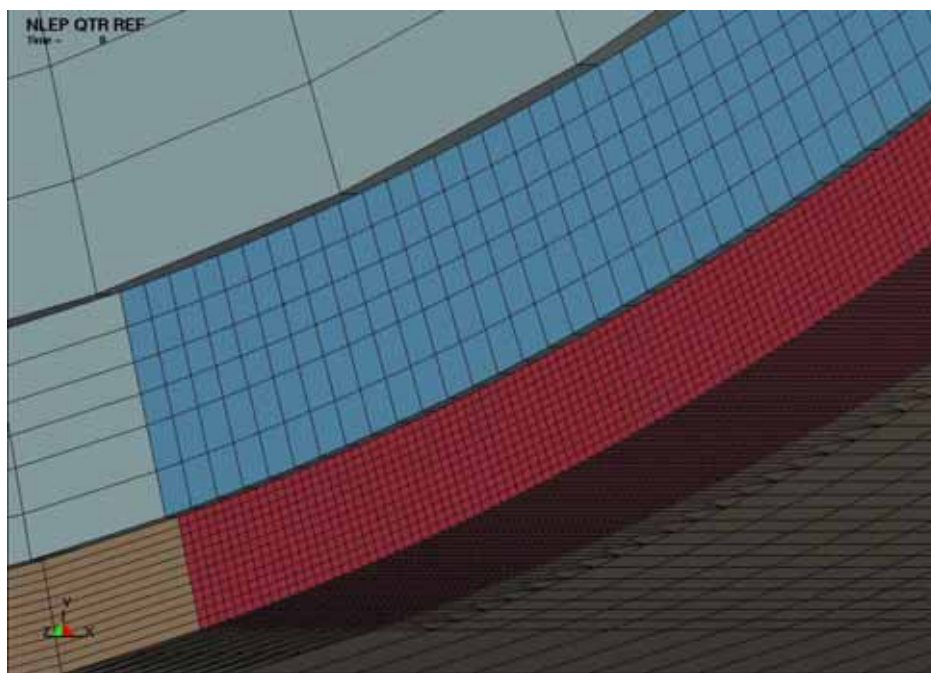


Figure 6-38 Refined WP FER, Cross-section of Impact Region

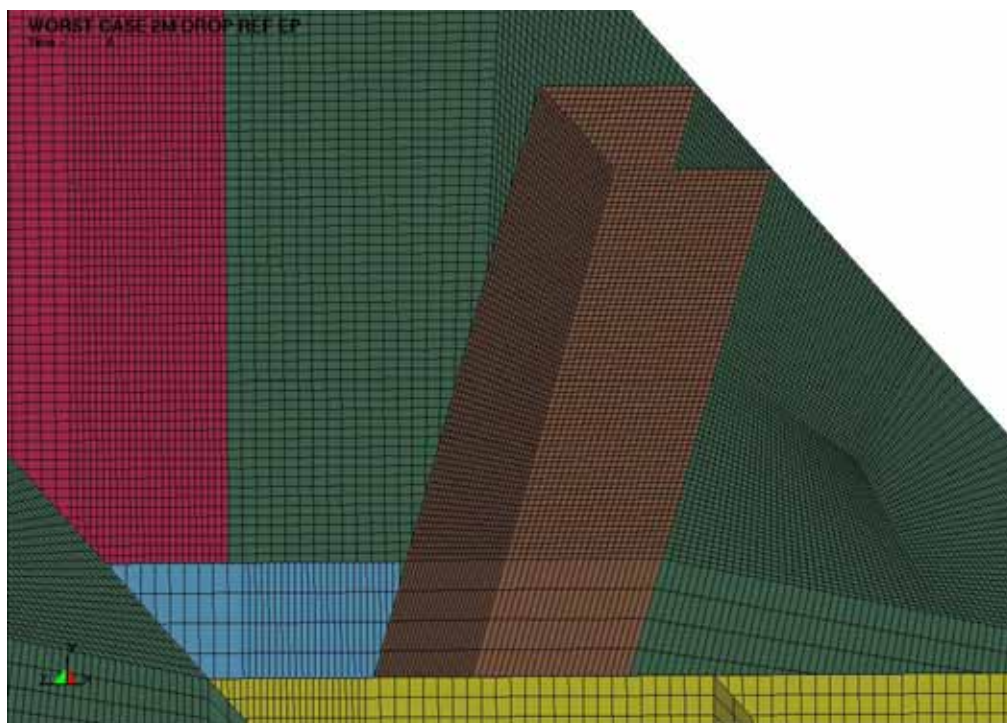


Figure 6-39 Refined EP FER, Mesh Detail near EP Support Tube

6.4.2 Worst Case WP with EP Flat Impact on Invert Steel

This section describes the FERs used to determine a worst case orientation and the failure level initial vertical velocity for the event sequence starting configuration depicted in Figures 6-40 to 6-42. The EP spans the invert steel structure's longitudinal beams and after it is crushed by the WP, the WP strikes the transverse beam. The crushing of the EP develops lower stresses at the OCB-EP contact region than that of the Section 6.4.1 configurations because the EP base is not supported between the longitudinal beams and the EP is modeled with eroding elements (see Assumptions 3.2.16 and 3.2.21). The highest OCB stresses are developed at the OCB-invert steel contact region after the EP has crushed sufficiently to create this contact. The FER shown in partial view in Figure 6-42 is close to the standard mesh described in Section 6.4.1 except it contains the latest WP design details in References 2.2.41 to 2.2.43 (i.e., no middle lid and no lifting trunnion undercuts in the sleeves) and the invert steel structure per References 2.2.16 to 2.2.18. Despite the invert FER missing the two central transverse beams, the number of elements is well over one million and the large simulation time needed to crush the EP ahead of the WP contacting the invert steel challenged the computing resources. The intent was to provide realistic invert steel flange, web and connector angle distortions. The full model was never completed, but is shown partially to familiarize the reader with the invert steel layout.

CENTERED SYM FLAT IMPACT ON INVERT

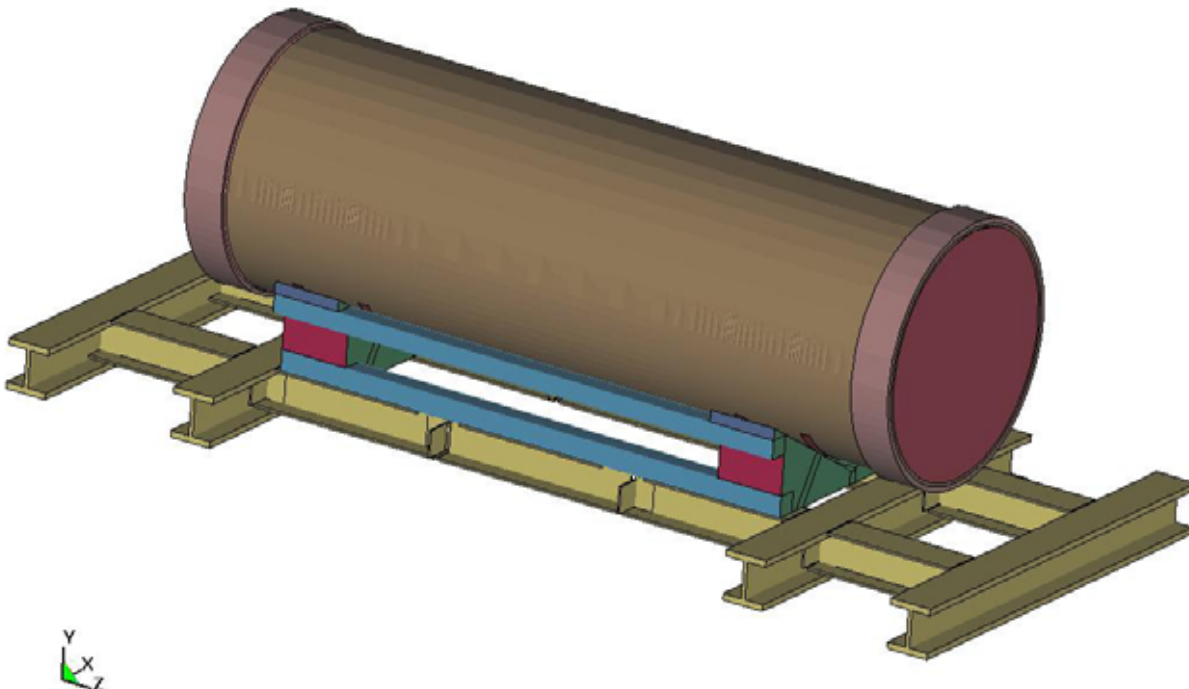


Figure 6-40 Full FER of WP on EP on Invert Steel

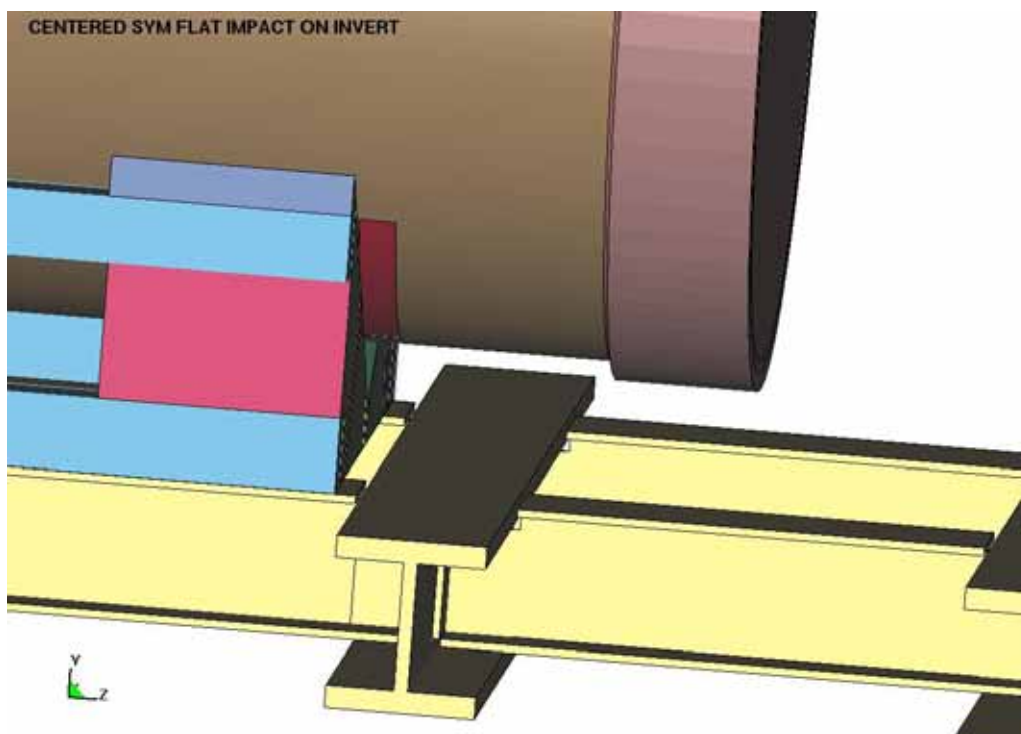


Figure 6-41 End of FER above Transverse Beam

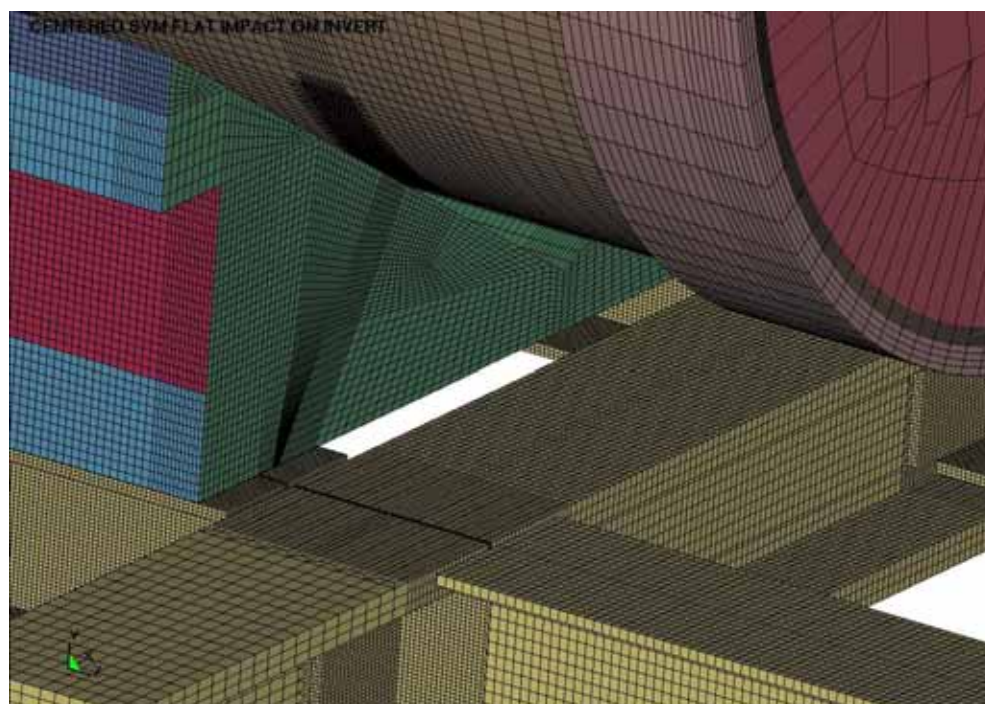


Figure 6-42 Meshing at End of FER above Transverse Beam

A Quarter-Symmetry FER with symmetry boundary conditions reduced the computer demands without sacrificing the basic physical phenomena of the simulation (see Assumption 3.2.22). The conservative use of restrained sharp edge top flanges for the transverse beams (see Assumptions 3.2.19 and 3.2.20) further reduced the computer demands. The starting position of the WP laterally centered in the bottom of the EP reduces the distortion needed (and energy absorption) of the EP before the WP strikes the invert steel. The longitudinal beams were restrained only at their webs. Searching for the worst case longitudinal location of the WP on the EP on the invert steel ended up with the bottom of the naval canister top plug lined up about an inch (25.4 mm) from the upper edge of the transverse beam and the EP lined up about two inches (50.8 mm) from the lower edge of the transverse beam as shown in Figures 6-43 to 6-45. This worst case location requires the WP to be shifted approximately 3 inches off the longitudinal center of the EP, which is possible in a seismic event. Additional FER refinement of the OCB and invert steel at their contact locations is provided as depicted in Figure 6-46. The adequacy of these mesh refinements is evaluated using the FERs without an intervening EP, discussed in the next section.

2 & 1 INCH EP & PLUG OFFSETS, 10MPG WCT

Time = 0

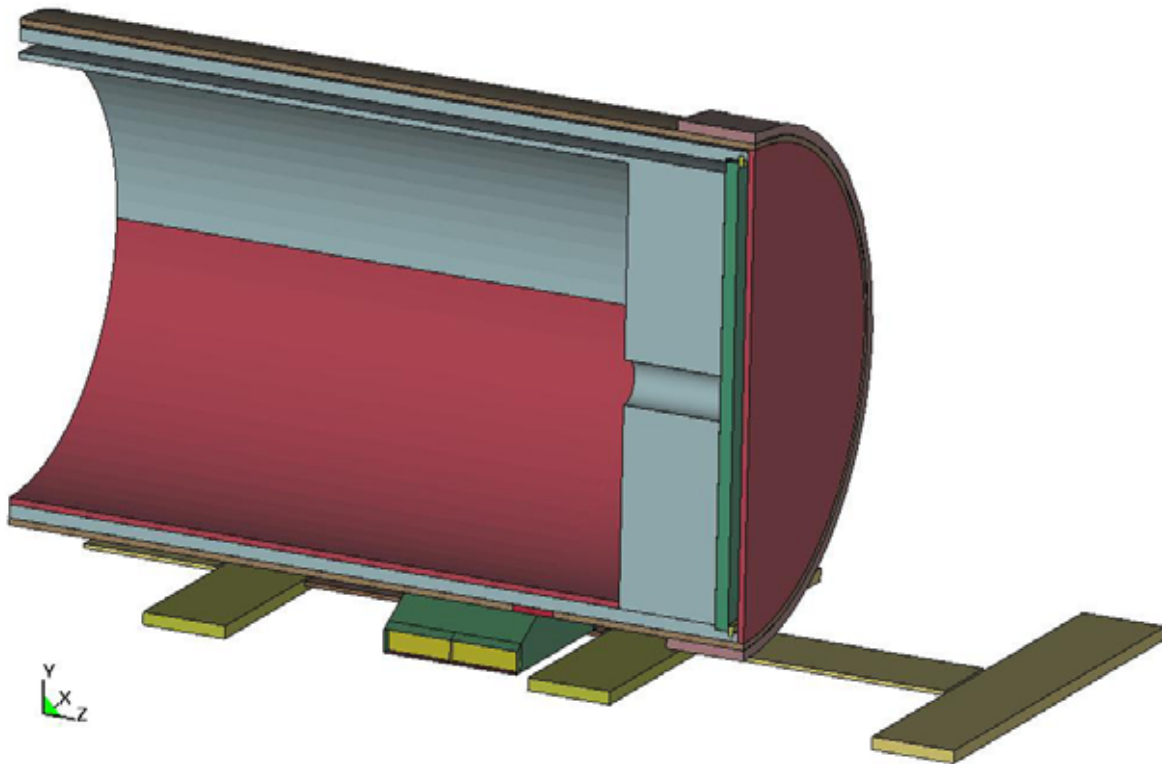


Figure 6-43 Quarter-Symmetry WP on EP Bridging Stiff Invert

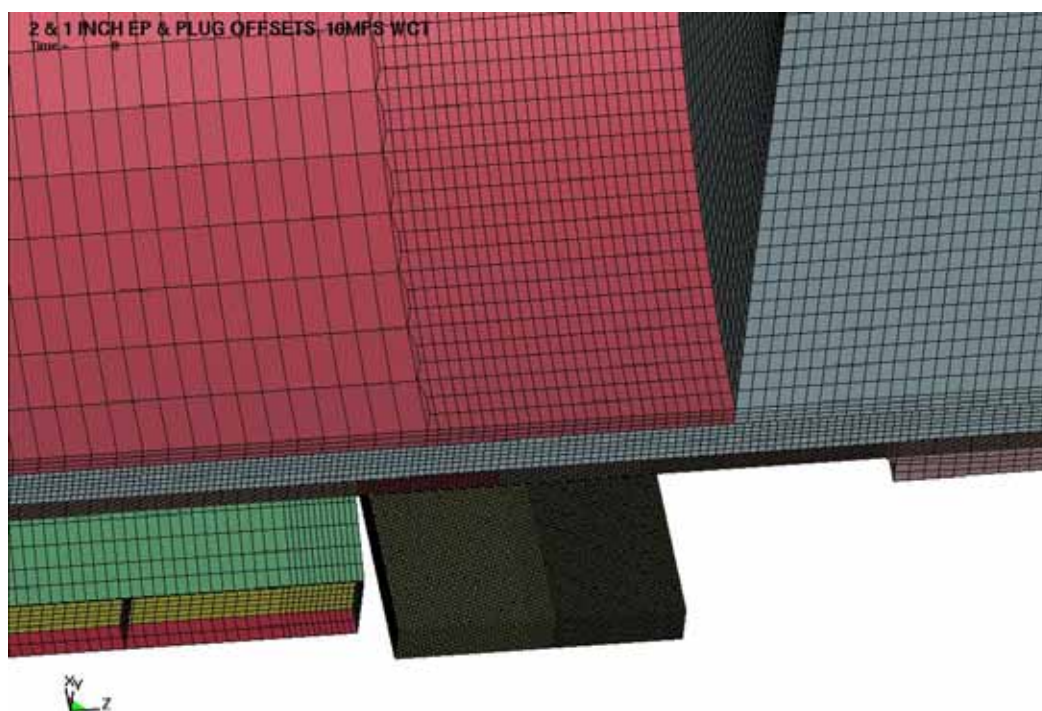


Figure 6-44 FER of EP and WP Top Plug on either Side of Transverse Beam

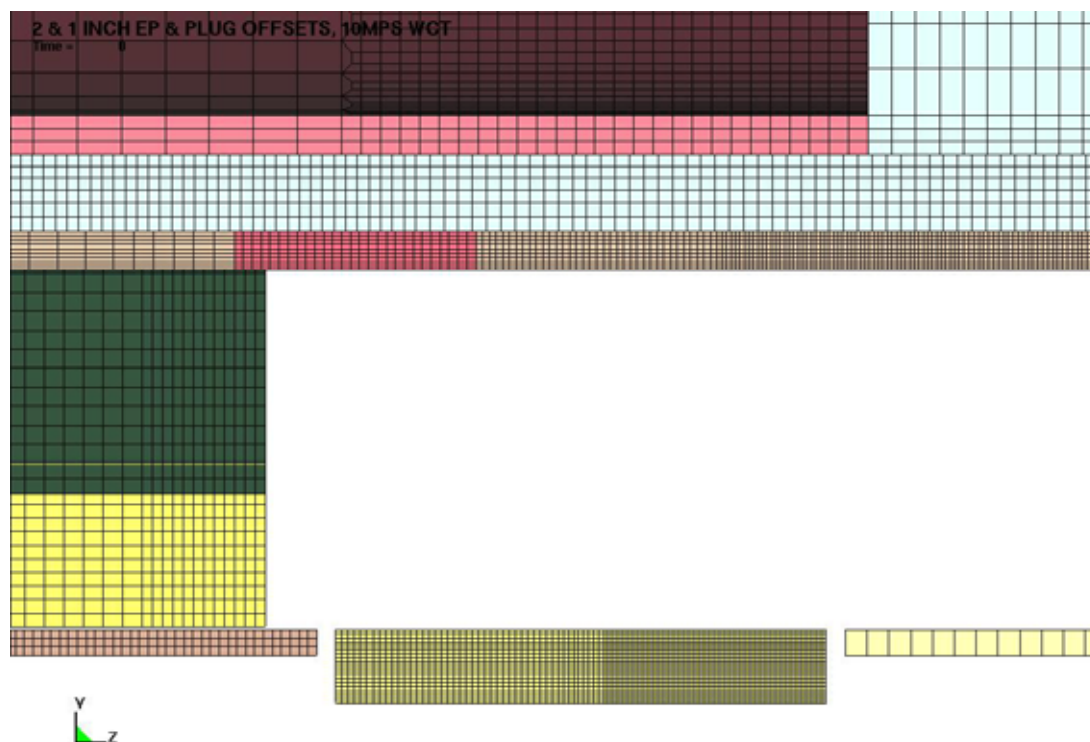


Figure 6-45 Worst Case Alignment of WP, EP and Transverse Beam

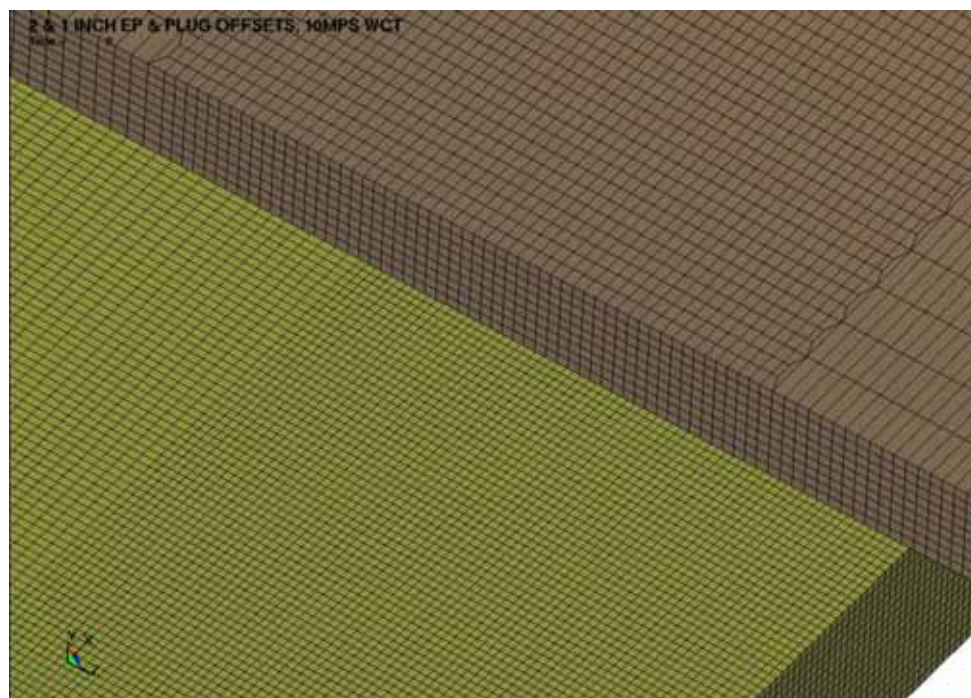


Figure 6-46 FER Mesh of OCB and Invert Steel in Region of Contact

6.4.3 WP Impact on Invert Steel

This section describes the FERs used to determine a worst case orientation and the failure level initial vertical velocity for the event sequence of the WP alone vertically impacting the invert steel structure's transverse beams. The EP is not included in the FER and this represents a severe seismic event during which the WP and EP become separated. The initial FERs used were for a flat impact at various longitudinal positions.

Again it was determined that the worst case is when the top plug of the naval canister is aligned just off the edge of the transverse beam. The stresses in the OCB decrease directly with the distance of the top plug from the edge of the transverse beam. When the top plug is over the transverse beam, the OCB stresses become very low. FER simulation results for the two extreme flat impact cases of the top plug between the transverse beams are presented in this calculation (Figures 6-47 and Figure 6-48).

The WP was then tilted at different impact angles to the transverse beam at the longitudinal worst case location, up to the maximum angle it could impact without the sleeve of the WP impacting the longitudinal beams (18 degrees). Figure 6-49 provides this maximum angle determination based on the invert steel structure's available space and the WP dimensions

OCB ON INVERT FLANGE, 1IN OFFSET

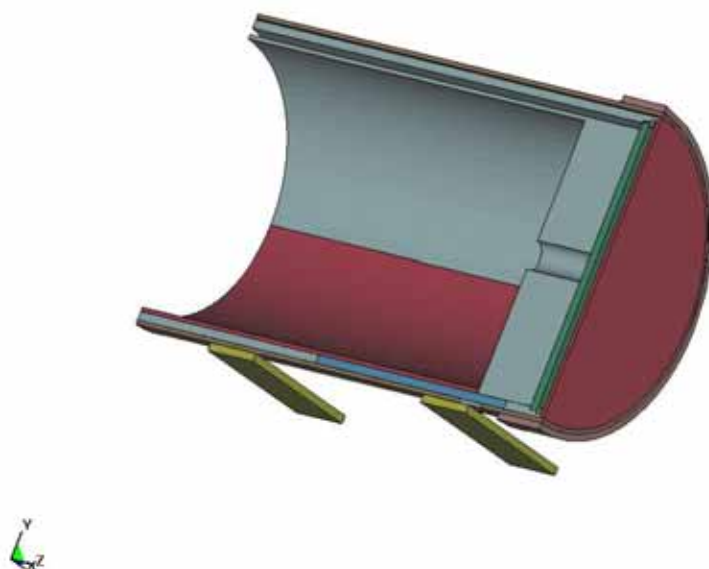


Figure 6-47 Worst Case WP on Stiff Invert Flat Impact without EP, 1 Inch Plug Offset

WP FLAT IMPACT ON INV, MAX OFFSET

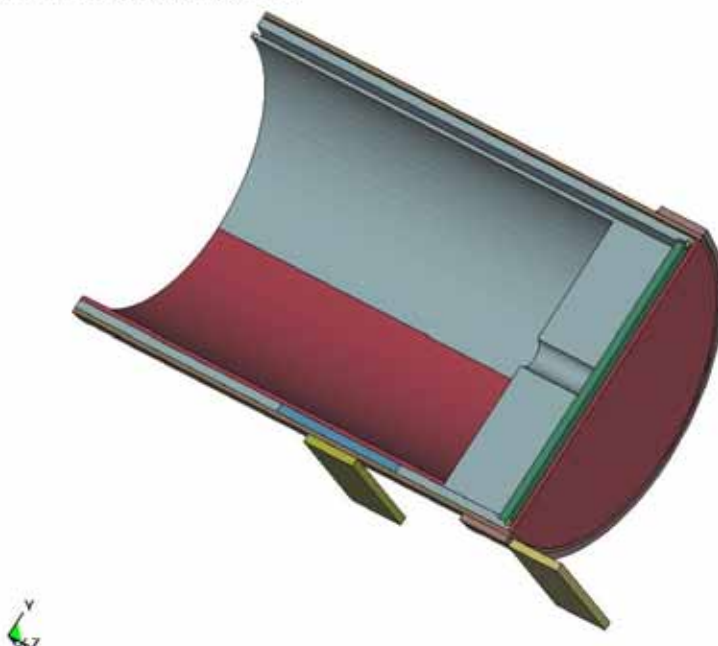
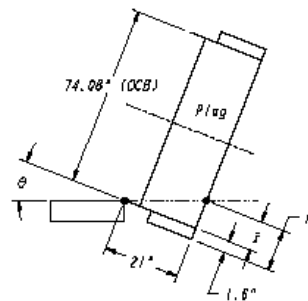
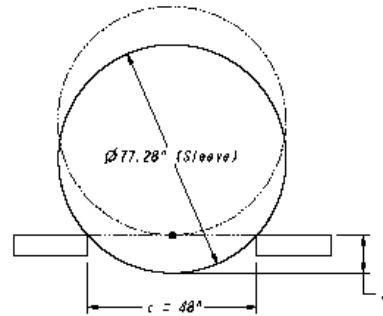
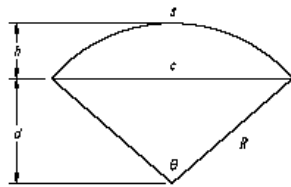


Figure 6-48 WP on Stiff Invert Flat Impact without EP, Maximum Offset



(units are inches)

$$d = \frac{1}{2} \sqrt{4R^2 - c^2}$$

$$h = R - d$$

$$R = \frac{77.28}{2} = 38.64$$

$$d = \frac{1}{2} \sqrt{4 \cdot 38.64^2 - 48^2} = 30.28$$

$$h = 38.64 - 30.28 = 8.36$$

$$x = 8.36 - 1.6 = 6.76$$

$$\tan \theta = \frac{6.76}{21} = 0.322$$

$$\theta = 18^\circ$$

Figure 6-49 Angle Calculation

Figures 6-50 to 6-52 depict the angle cases evaluated. The symmetry boundary condition creates two transverse beams absorbing the impact, one at each end. Deterministic calculations of horizontal drop events and oblique slap-down events indicate the shared two end loading will provide essentially identical stress responses near the contact regions as single end loadings with slap-downs. Therefore, the use of a mid-plane longitudinal symmetry provides a reasonable representation of stress and strain response in the contact region for the angled one end hit. The applied velocity in the Y-direction in these FERs includes minor in-drift off-vertical contributions that make the contact direction normal to the OCB surface. This is a conservative representation (see Assumption 3.2.22).

A refinement check is conducted for the governing 18 degree case using the standard and refined FERs depicted in Figures 6-53 and 6-54. The number of elements through the OCB wall is increased from 9 to 12 while keeping the element aspect ratios near cubic. The inner vessel and invert steel meshes are also refined. The comparative results for the two mesh refinements can be seen in Table 7-3 and confirms that the accuracy and representativeness of the results of this calculation using the standard WP and invert steel meshes are acceptable for predicting EWA stress and strain response in accordance with Reference 2.2.15, Section 7.1.3.

The TrueGrid developed meshes in some cases contained node sets with unintended additional nodes that were manually removed from the output .inc geometry files and identified with “mod” in the file title. This is due to a known bug in the program when using double TRBB transitions. Also, during final check, the top lid of the OCB opposite the contact region was found to have three elements not attached to the OCB shell. The maximum stress case (5 *mps* Figure 6-52) was rerun with the elements attached and there was no discernable difference in results. The fixed TrueGrid FER mesh is included on the data CD (Disc 6).

OCB ON 5DEG TILTED INVERT FLANGE, 1IN OFFSET

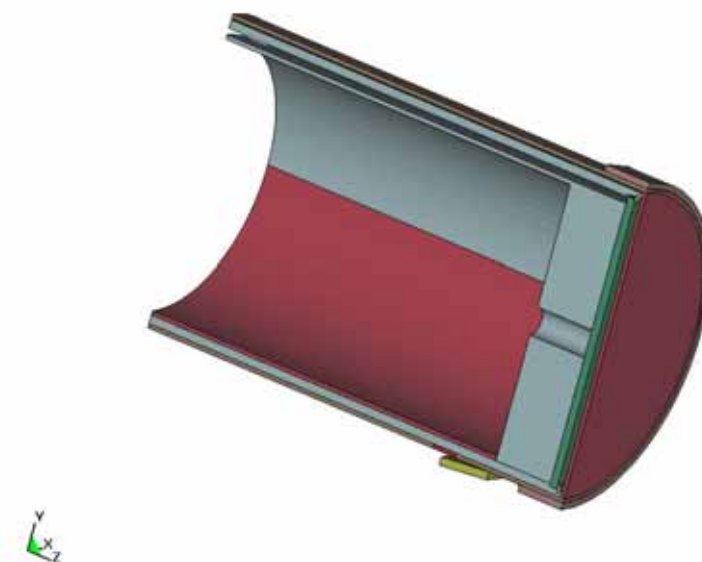


Figure 6-50 WP 5 Degree Impact on Stiff Invert

OCB ON 10DEG TILTED INVERT FLANGE, 1IN OFFSET

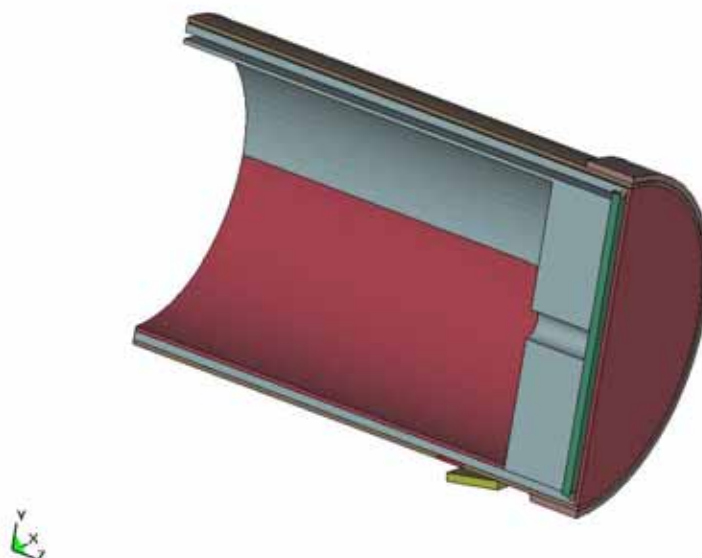


Figure 6-51 WP 10 Degree Impact on Stiff Invert

OCB ON 18DEG TILTED INVERT FLANGE, 1IN OFFSET

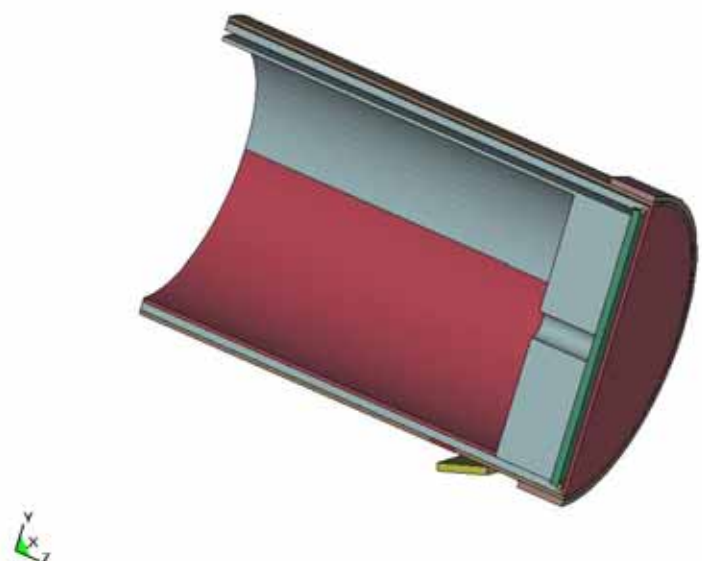


Figure 6-52 WP 18 Degree Impact on Stiff Invert

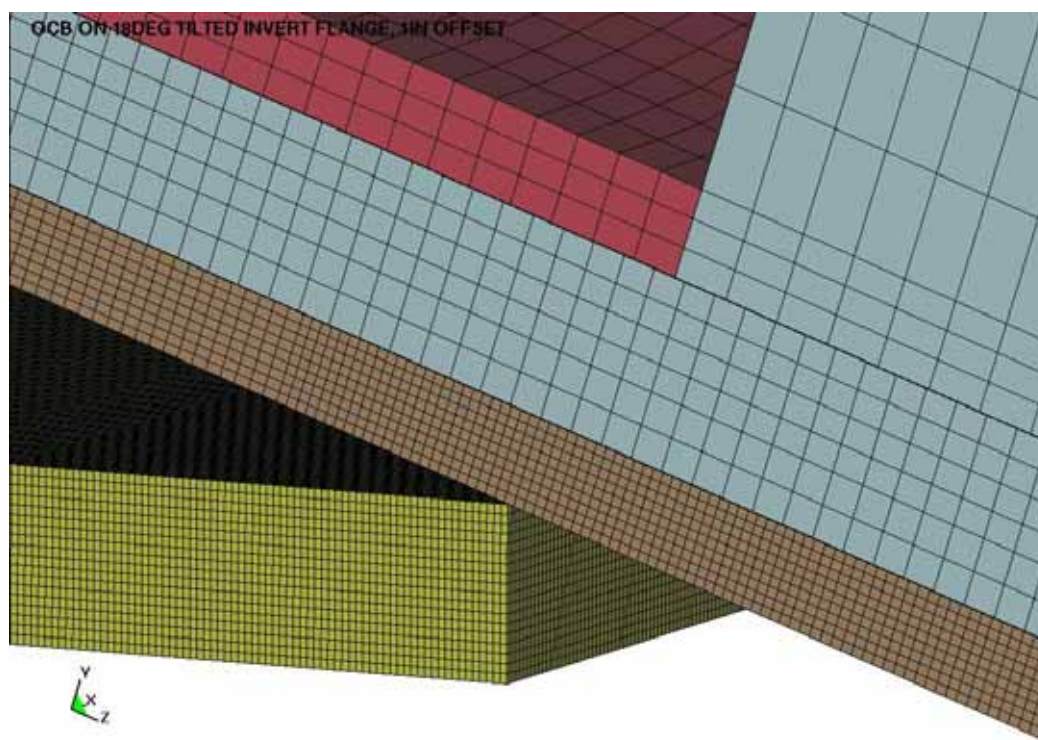


Figure 6-53 Standard FER, WP 18 Degree Impact on Stiff Invert

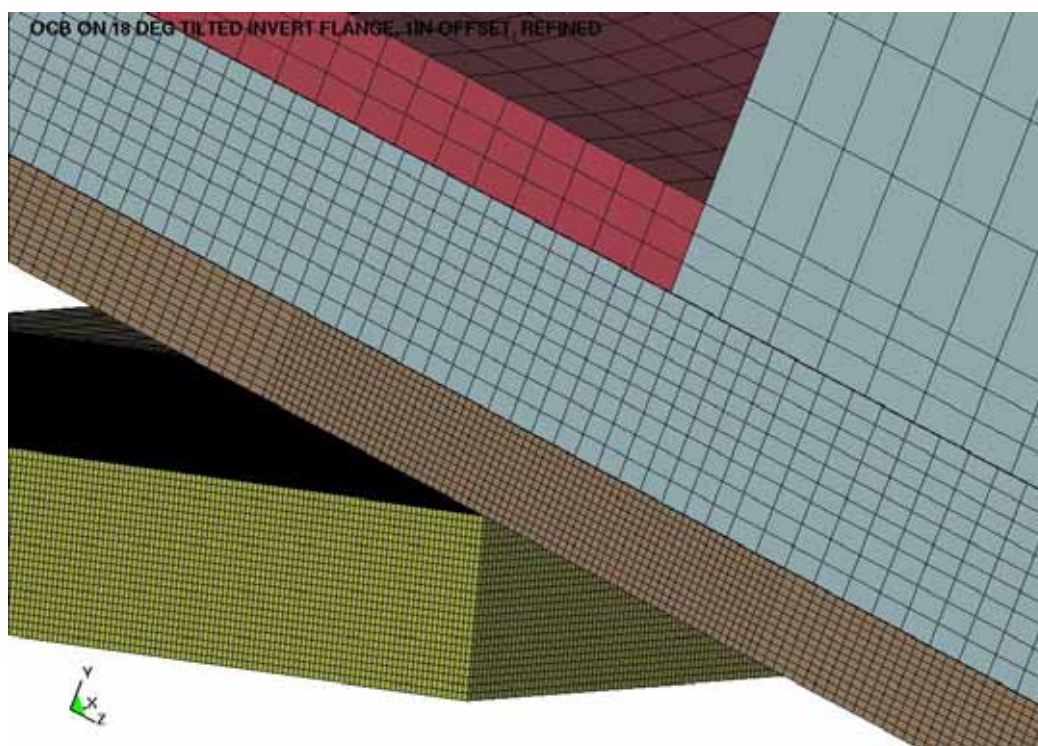


Figure 6-54 Refined FER, WP 18 Degree Impact on Stiff Invert

7. RESULTS AND CONCLUSIONS

The following results obtained from LS-DYNA are reasonable compared to the inputs and are suitable for the intended use of this calculation.

The results obtained from LS-DYNA for verifying mesh adequacy and deterministic calculations are reported herein in terms of maximum shear stress (MSS). Since ASME general primary membrane and maximum (membrane plus bending) primary stress intensities (SIs) are used for the deterministic calculations (see Reference 2.2.5 Section III, Division 1, Appendix F, F-1341.2.), in accordance with Reference 2.2.15, Section 7.1.4, the LS-DYNA results need to be converted. The MSS (see Reference 2.2.19, Chapter 3) is defined as one-half of the difference between the maximum and minimum principal stress. ASME SI is defined as the difference between the maximum and minimum principal stress (see Reference 2.2.5, Section III, Division 1, Appendix XIII, XIII-1123(a)).

Therefore, the MSS at a point, obtained from LS-DYNA, is multiplied by two to obtain the corresponding SI. Constant stress solid elements are used in the OCB FER, and therefore, the SI of an element is twice the MSS of the element. In ASME Code terminology, this is the total SI at a point that can contain primary, secondary and peak stress contributions. The stresses at all the elements on a wall section contribute to wall membrane and wall bending stress intensities. Classifying 3-D FEA stress fields into primary, secondary and peak contributions, and developing bending and membrane stress intensities is complex (see Reference 2.2.23) and required a stress classification calculation (Reference 2.2.46). This effort resulted in classifying the membrane stresses as fully primary and the bending stresses as fully secondary, and use of the element wall average (EWA) of the total stress intensities (twice the MSS) as a bound on the primary membrane stress intensity.

7.1 MESH VERIFICATION

7.1.1 WP Impact on EP

Table 7-1 shows the changes of volumes and time-maximum EWA MSS, $\tau_{avg,max}$, for the standard (Figures 6-6 to 6-34) and refined (Figures 6-35 to Figures 6-38) quarter symmetry WP mesh simulations of a flat 1 m drop (no offsets or angles). The elements in Table 7-1 are the elements at the highest stressed location near the governing location through the OCB for the worst case loading. This location includes high local bearing stresses due to the edge loading of the OCB by the EP. This calculation does not evaluate these local bearing stresses (see Reference 2.2.5, Section III, Division 1, Appendix F, F-1341.6), but only the EWA MSS. Four element strings are used for the refined WP mesh to provide a comparable EWA volume to the standard WP mesh. The initial volume (V) reported in Table 7-1 is for a representative individual element of the OCB element strings (initial volumes of elements in any string are essentially identical).

Table 7-1 WP Mesh Verification, 1 *m* Flat Drop on EP

	Element #s	Standard WP Mesh	Element #s	Refined WP Mesh	% Change
OCB	H 38030 to H 38038	$\tau_{avg,max} = 2.37e+8$ <i>Pa</i> (see Figure 7-1)	H 131781 to H 131804 H 134373 to H 134396	$\tau_{avg,max} = 2.34e+8$ <i>Pa</i> (see Figure 7-2)	Stress: 1.3%
	H 38038	$V = 4.44e-8$ <i>m</i> ³	H 131804	$V = 1.25e-8$ <i>m</i> ³	Volume: 255%

Figures 7-1 and 7-2 provide time plots of the EWA MSS. Time plots of stresses in this calculation use units of Pascal (*Pa*) and seconds (*s*). Table 7-1 shows that the change in time-maximum of the EWA MSS is more than two orders of magnitude lower than the corresponding change in element volume. This verifies that both WP meshes are appropriate (see Reference 2.2.15 Section 7.1.3). The standard WP mesh is used for all simulations.

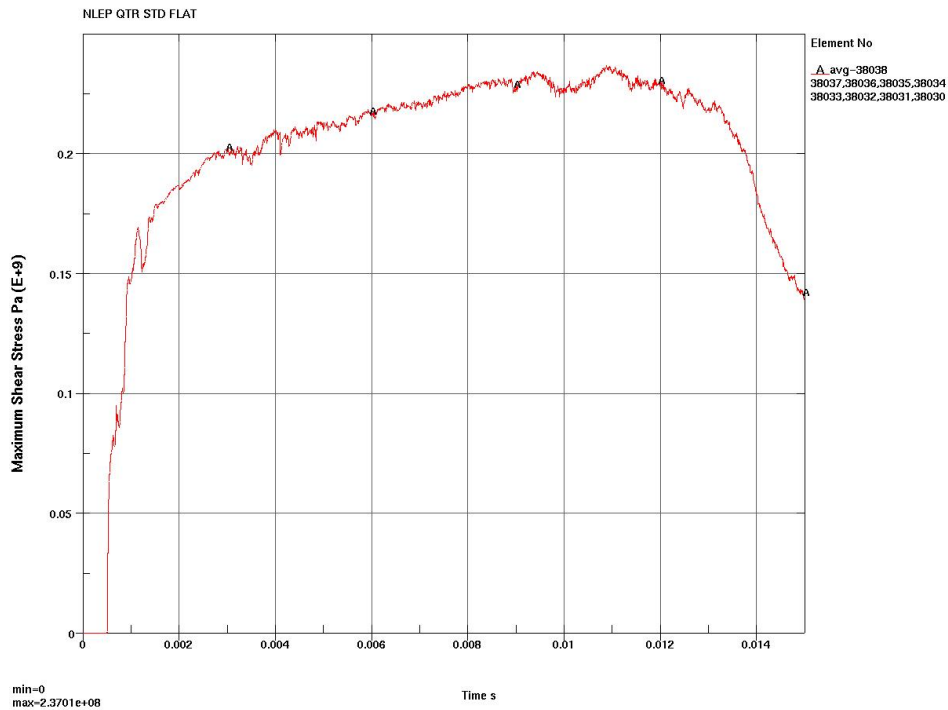


Figure 7-1 EWA MSS in the OCB, Flat Drop on EP, Standard WP Mesh

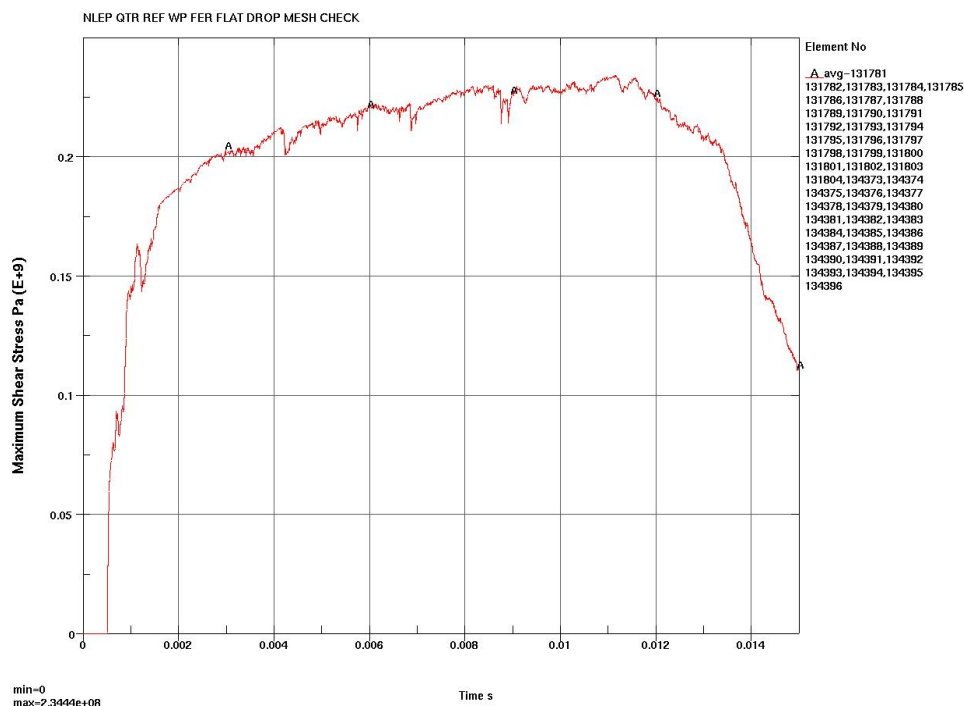


Figure 7-2 EWA MSS in the OCB, Flat Drop on EP, Refined WP Mesh

For the worst case drop orientation (Figure 6-24), a refined EP mesh (Figure 6-39) is developed and the difference in OCB stress results from this refinement is evaluated. Table 7-2 is an analogous table to Table 7-1 for this evaluation except it is a full FER and the same (standard) OCB mesh and element string is used for both simulations. “A” in Table 7-2 is the area of the EP plate element under the OCB governing location.

Table 7-2 EP Mesh Verification, 1 m Worst Case Drop on EP

	Element #s	Standard EP Mesh	Element #s	Refined EP Mesh	% Change
OCB	H 38780 to H 38788	$\tau_{avg,max} = 2.899e+8 \text{ Pa}$ (see Figure 7-3)	H 38780 to H 38788	$\tau_{avg,max} = 2.909e+8 \text{ Pa}$ (see Figure 7-4)	Stress: 0.3%
EP	S 77295	$A = 1.500e-5 \text{ m}^2$	S 234766	$A = 1.0591e-5 \text{ m}^2$	Area: 42%

Figures 7-3 and 7-4 provide time plots of the governing OCB location for a 1 m drop in the worst case drop orientation. Table 7-2 shows that the change in maximum OCB EWA MSS is more than two orders of magnitude lower than the change in EP element area. This verifies that both

EP meshes are appropriate. The refined EP mesh is used for the deterministic worst case 20 *in* (0.508 *m*) drop calculation and the Capability calculations.

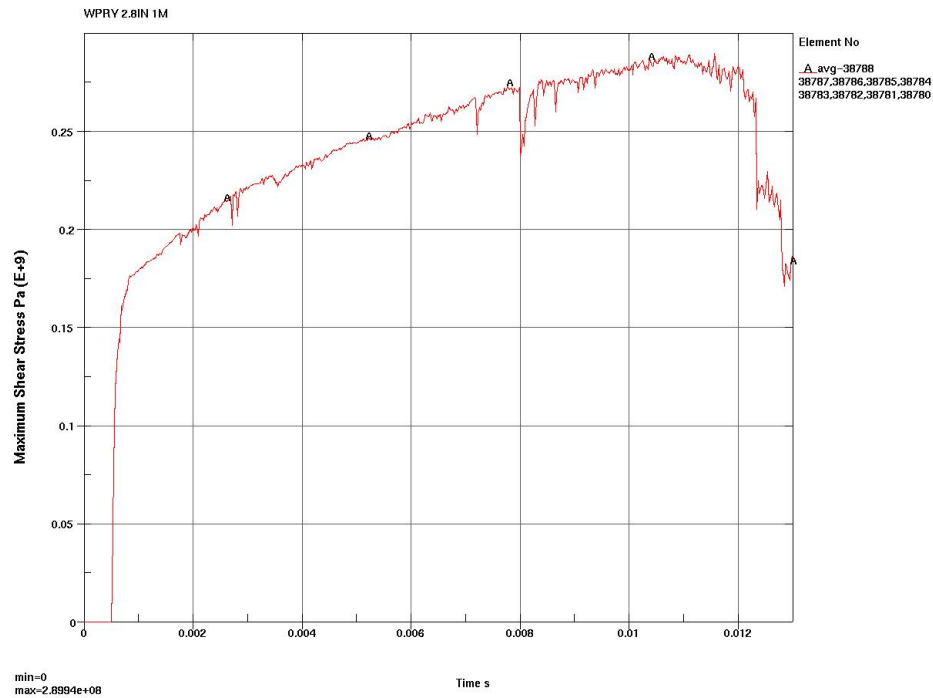


Figure 7-3 EWA MSS in the OCB, Worst Case Drop on EP, Standard EP Mesh

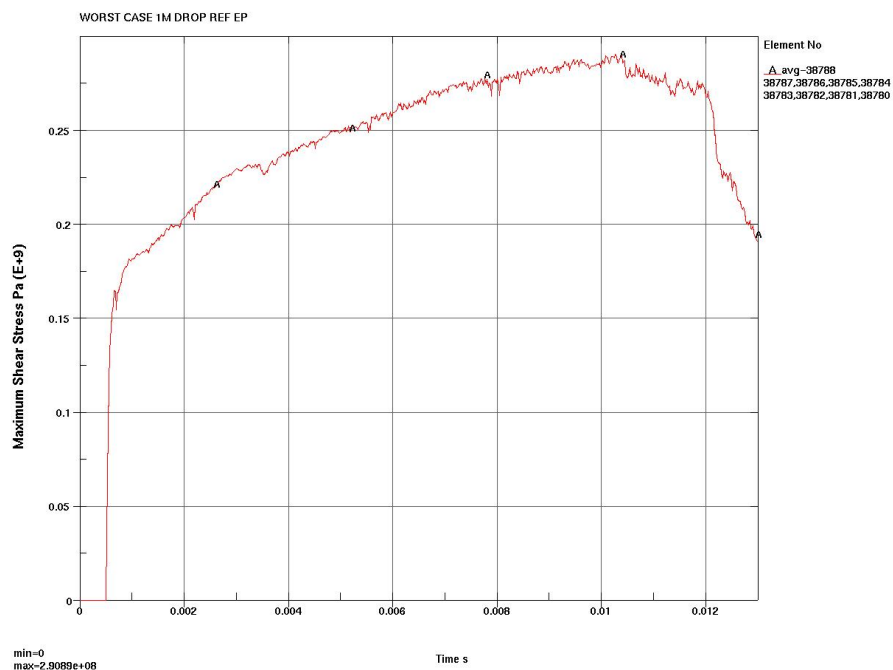


Figure 7-4 EWA MSS in the OCB, Worst Case Drop on EP, Refined EP Mesh

7.1.2 WP Impact on Invert

For the worst case 18 degree impact orientation (Figures 6-43 and 6-44), a refined OCB and invert mesh (Figure 6-45) is developed and the difference in OCB stress/strain results from this refinement is evaluated in Table 7-3 for a near-failure level 4 *m/s* impact Capability calculation. In this case, the Expanded Toughness Fraction (ETF) is compared at the time of maximum EWA VM stress (0.0136 *sec*). Section 7.4 discusses derivation of ETF values in detail. The element volumes are the starting element sizes at the contact location.

Table 7-3 OCB and Invert Mesh Verification, 4 *m/s* Worst Case Impact on Invert

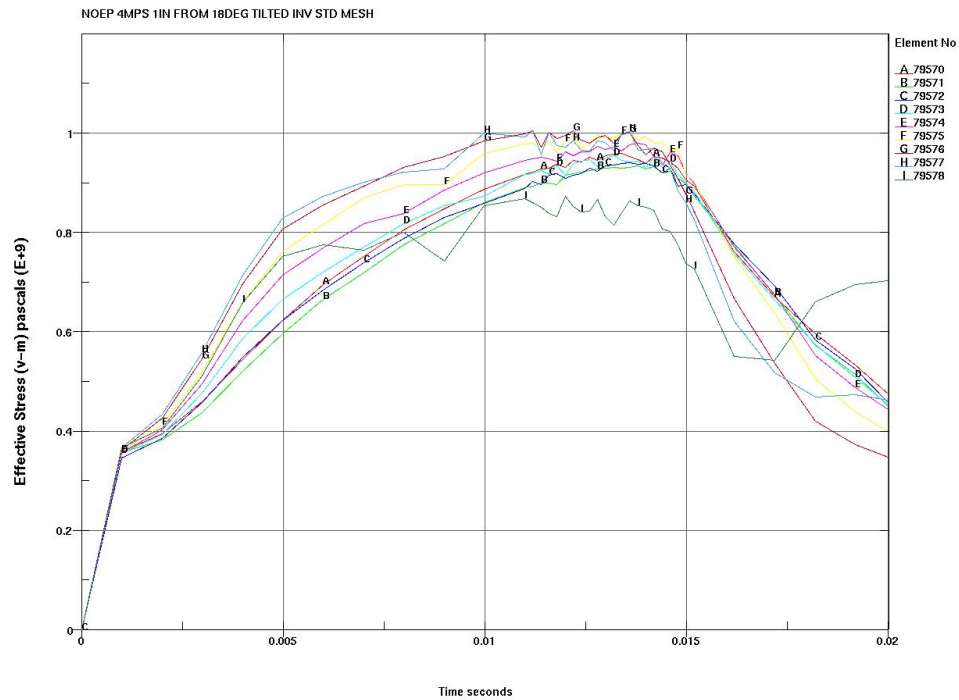
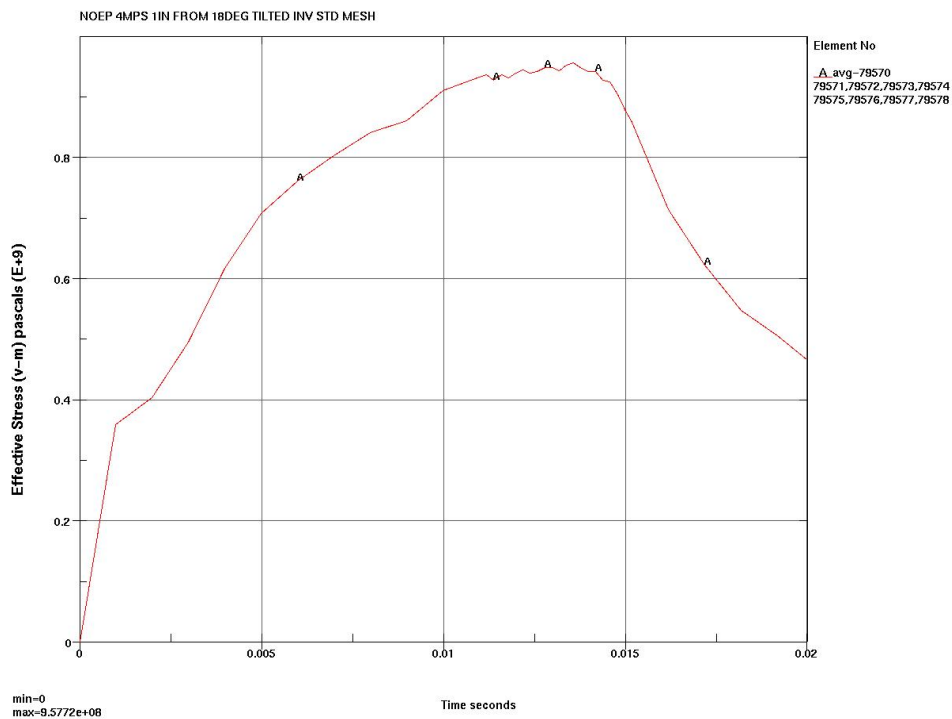
	Element #s	Standard Mesh	Element #s	Refined Mesh	% Change
OCB	H 79570 to H 79578	ETF = [(356+957.7)/2]·0.2472/191 = 0.850 (see Figures 7-5 to 7-7)	H 111517 to H 111528	ETF = [(356+962.8)/2]·0.2440/191 = 0.842 (see Figures 7-8 to 7-10)	ETF: 1.0%
OCB	H 79578	V = 3.8085e-8 <i>m</i> ³	H 111528	V = 1.1715e-8 <i>m</i> ³	Volume: 225%
Invert	H 611657	V = 1.2732e-8 <i>m</i> ³	H 906854	V = 0.71617e-8 <i>m</i> ³	Volume: 78%

Figures 7-5 to 7-10 provide time plots of the governing OCB locations for a 4 *m/s* impact in the worst case orientation. Table 7-3 shows that the change in ETF is almost two orders of magnitude lower than the change in the OCB and invert element volumes. This verifies that both meshes are appropriate. The standard mesh is used for the Capability calculations.

7.2 DETERMINISTIC CALCULATIONS

7.2.1 Offset WP Impacts

This section analyzes the stresses generated from X-Y plane offset WP 1 *m* drops. The visual representation of the WP offset positioning along the EP is shown in Figures 6-2 to 6-12. Figures 7-11 to 7-21 are the time plots of the EWA MSS at the governing location of the OCB for each offset WP drop case. Figure 7-11 is the time plot for the no-offset (centered) case to which the effect of offsetting is compared in Table 7-4 and Figure 7-22.

Figure 7-5 VM Stresses, 4 *m/s* Impact on 18 *deg* Invert, Standard MeshFigure 7-6 EWA VM Stress, 4 *m/s* Impact on 18 *deg* Invert, Standard Mesh

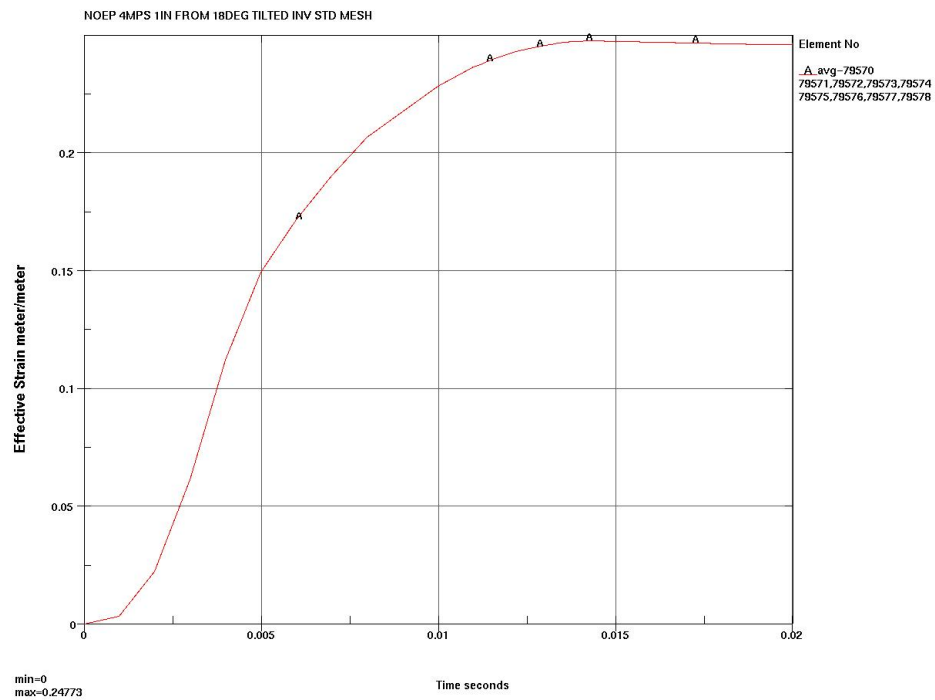


Figure 7-7 EWA VM Strain, 4 m/s Impact on 18 deg Invert, Standard Mesh

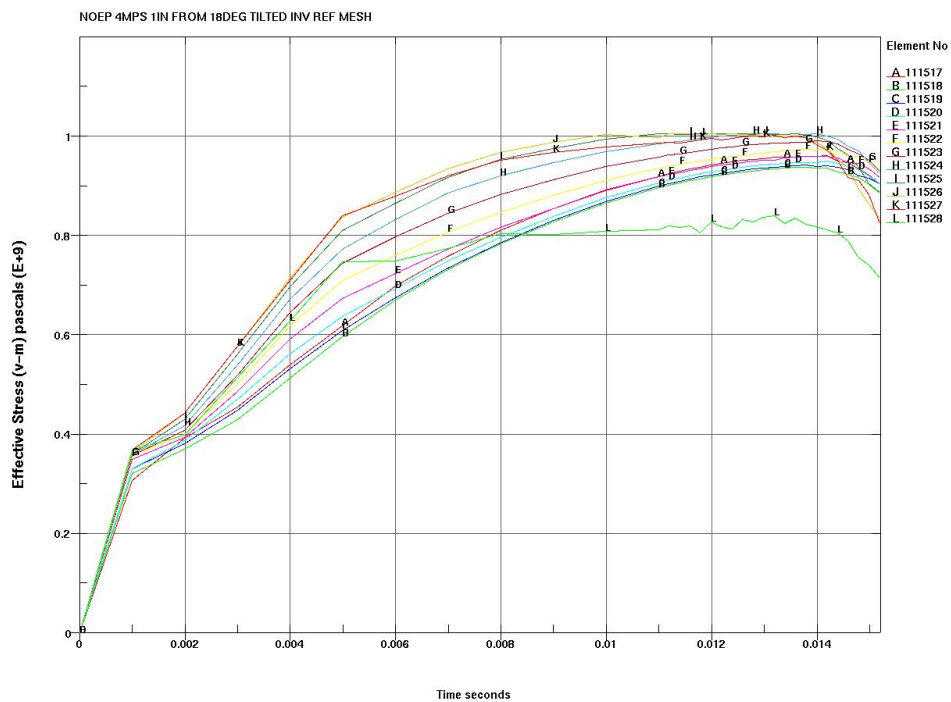


Figure 7-8 VM Stresses, 4 m/s Impact on 18 deg Invert, Refined Mesh

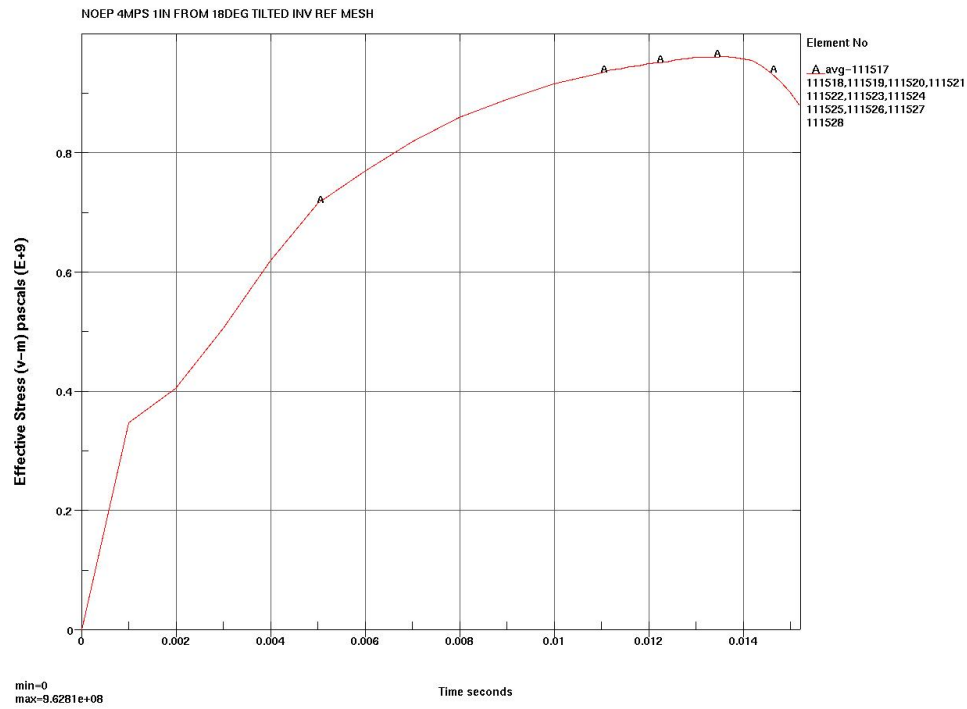


Figure 7-9 EWA VM Stress, 4 m/s Impact on 18 deg Invert, Refined Mesh

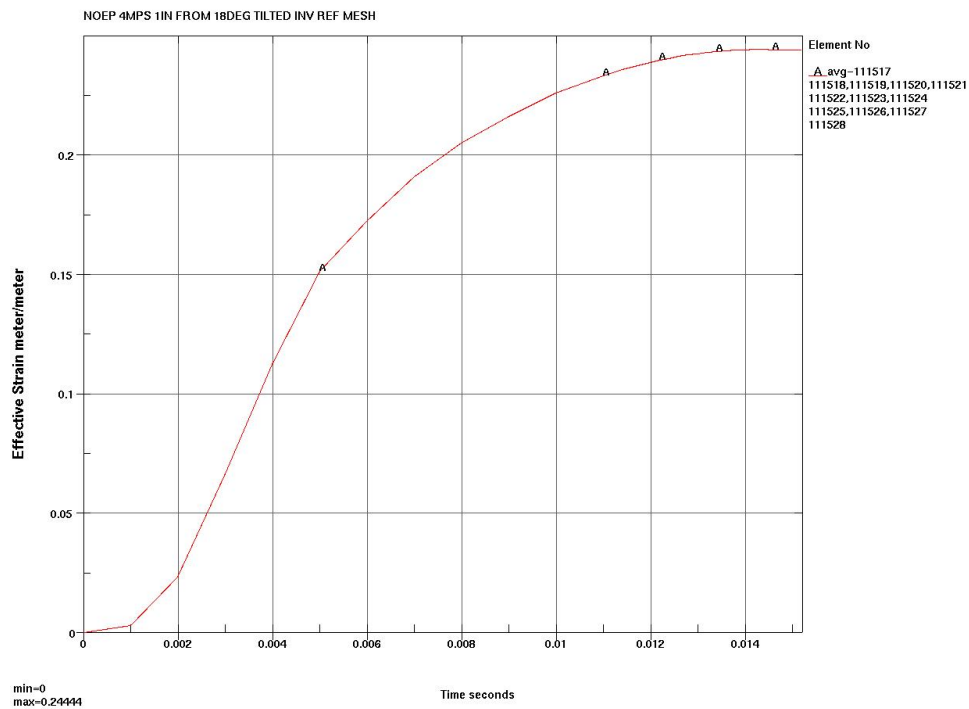


Figure 7-10 EWA VM Strain, 4 m/s Impact on 18 deg Invert, Refined Mesh

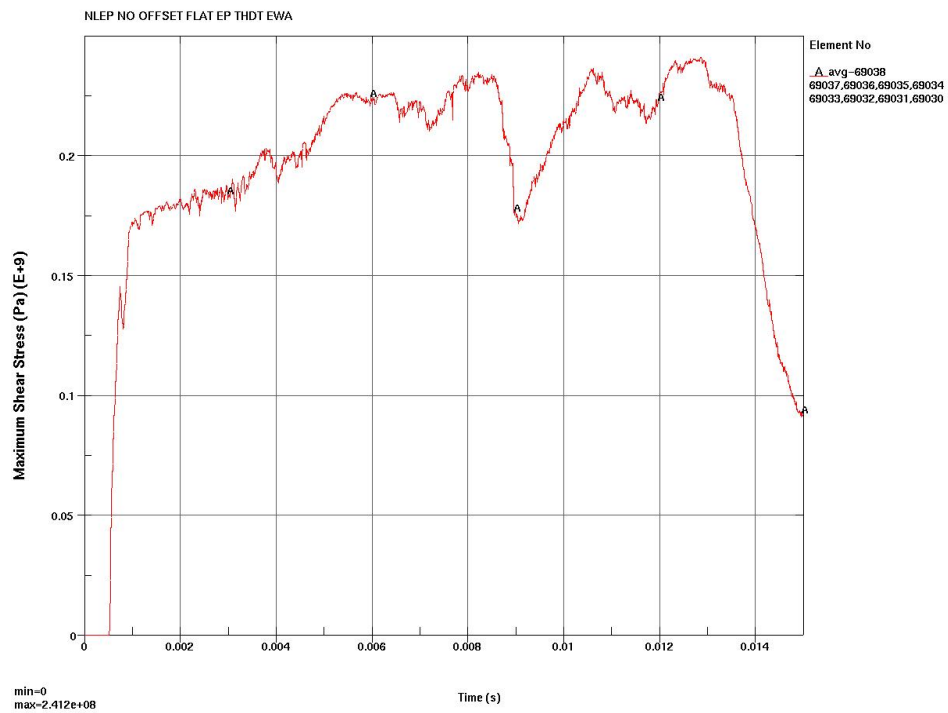


Figure 7-11 Centered (No Offset) WP w/ Flat EP, EWA MSS

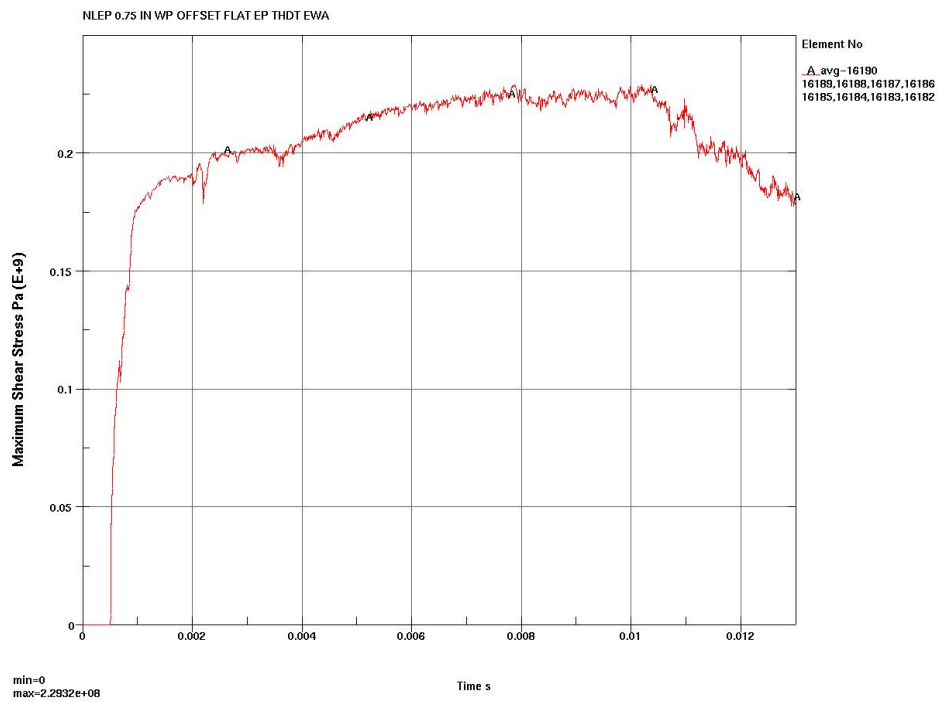


Figure 7-12 0.75 in Offset WP w/ Flat EP, EWA MSS

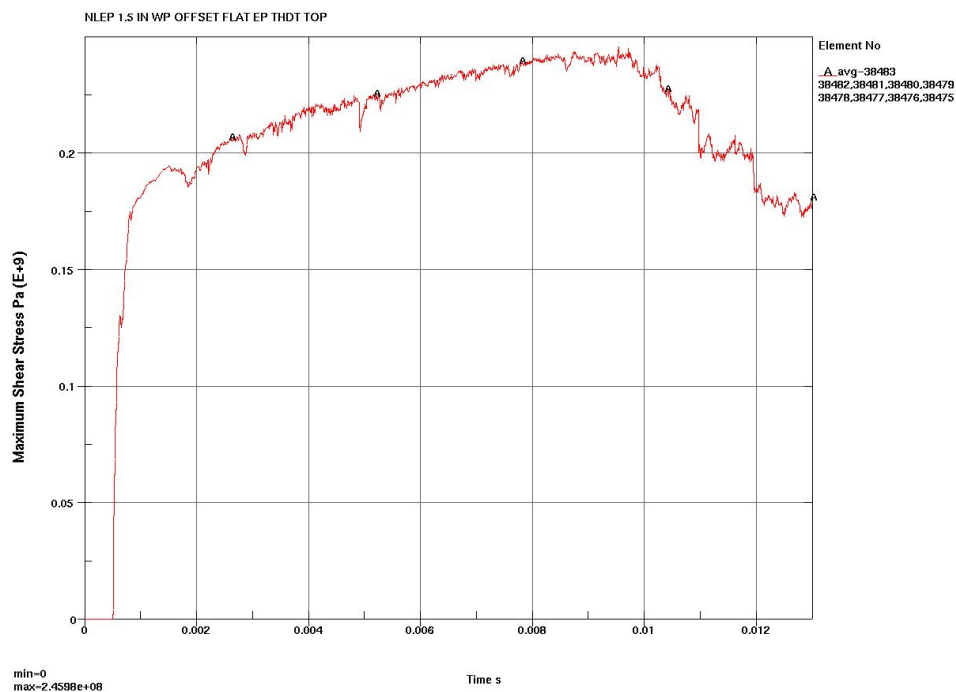


Figure 7-13 1.5 in Offset WP w/ Flat EP, EWA MSS

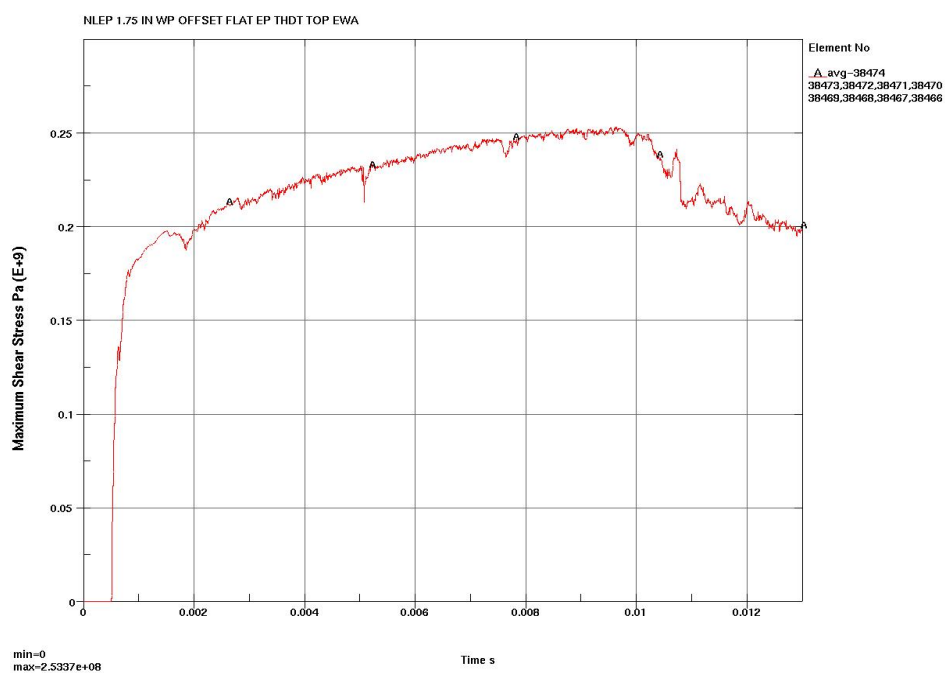


Figure 7-14 1.75 in Offset WP w/ Flat EP, EWA MSS

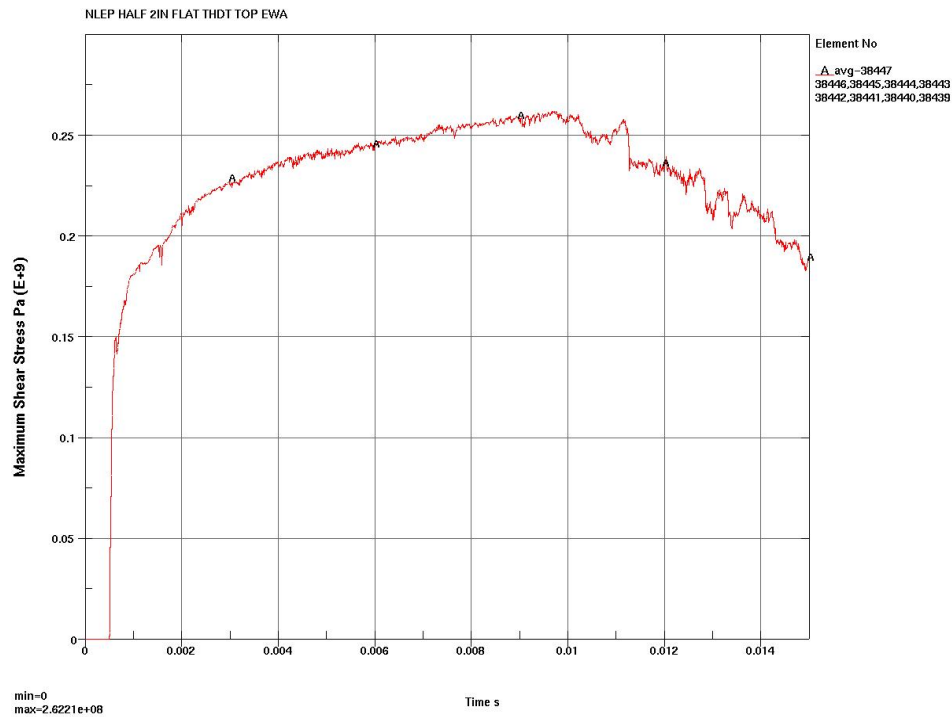


Figure 7-15 2 in Offset WP, Flat EP, EWA MSS

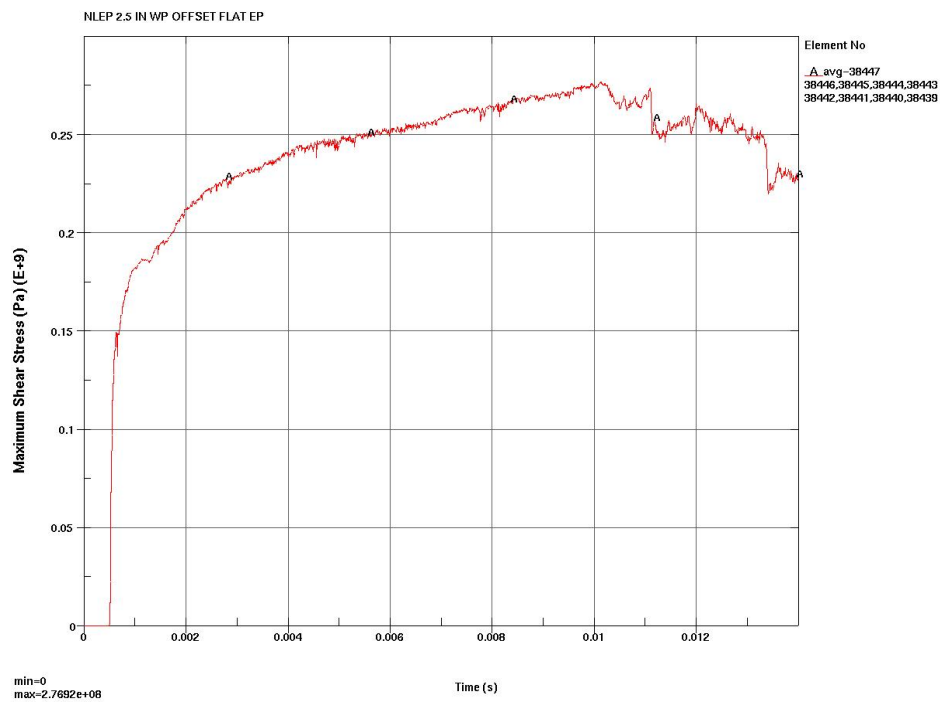


Figure 7-16 2.5 in Offset WP w/ Flat EP, EWA MSS

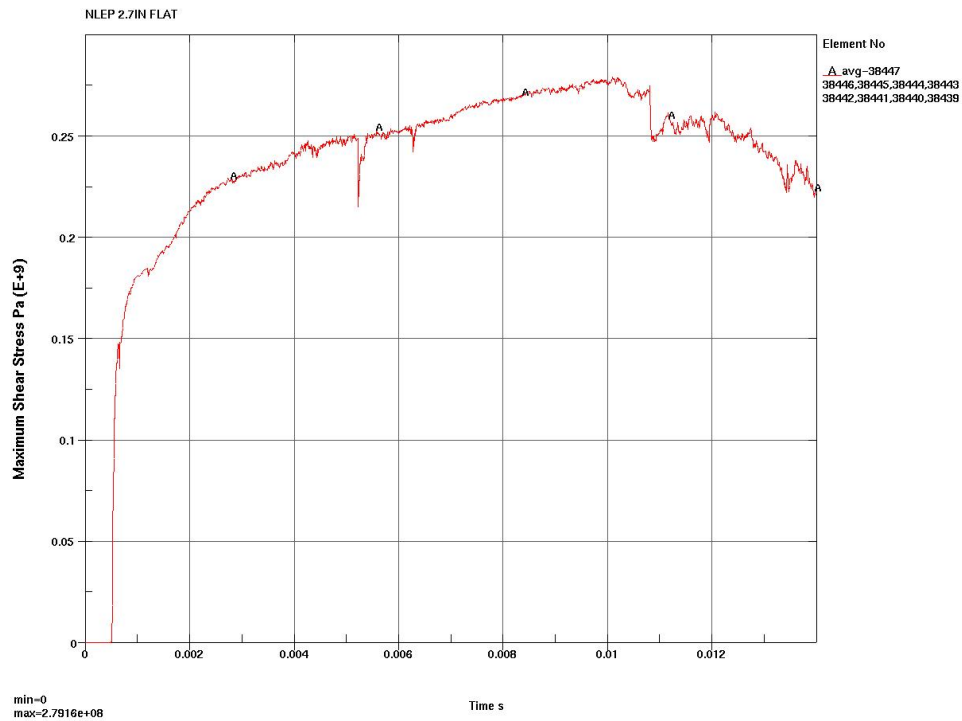


Figure 7-17 2.7 in Offset WP w/ Flat EP EWA MSS

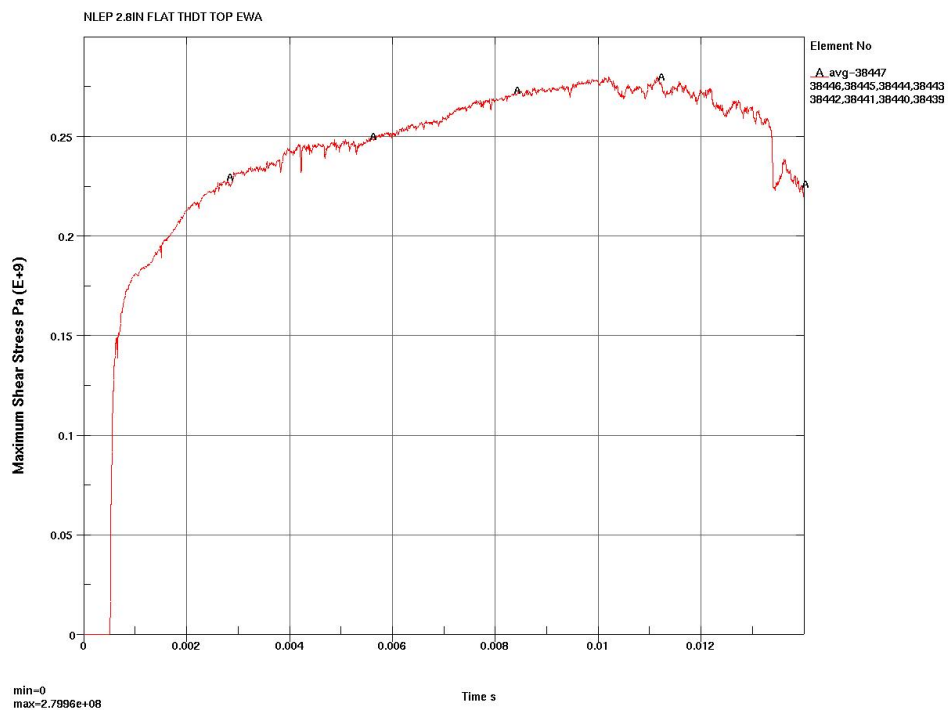


Figure 7-18 2.8 in Offset WP w/ Flat EP, EWA MSS

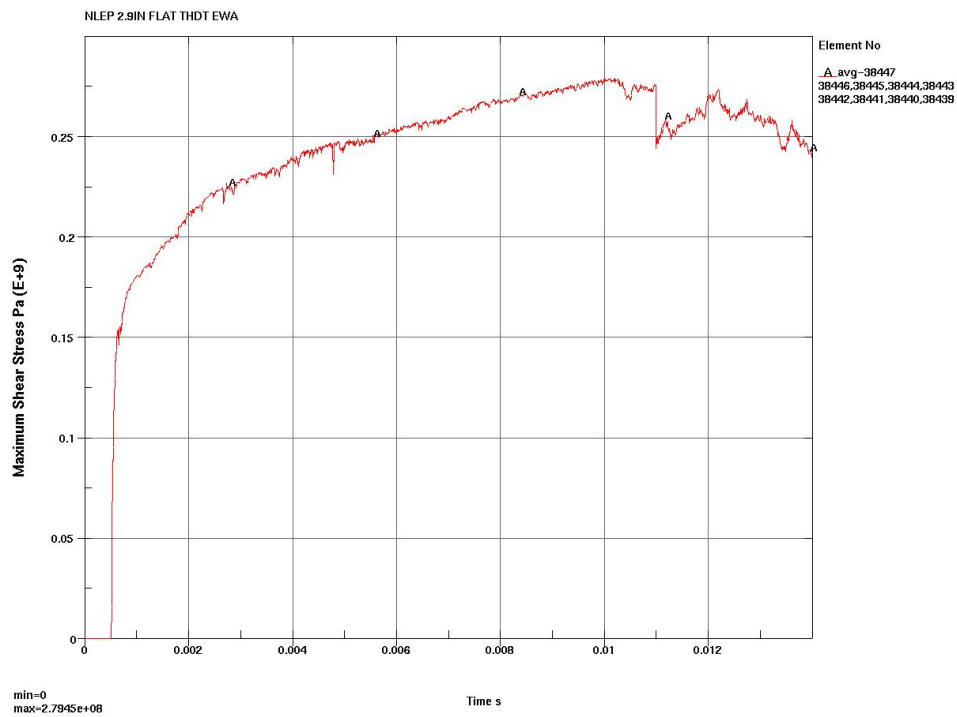


Figure 7-19 2.9 in Offset WP w/ Flat EP EWA MSS

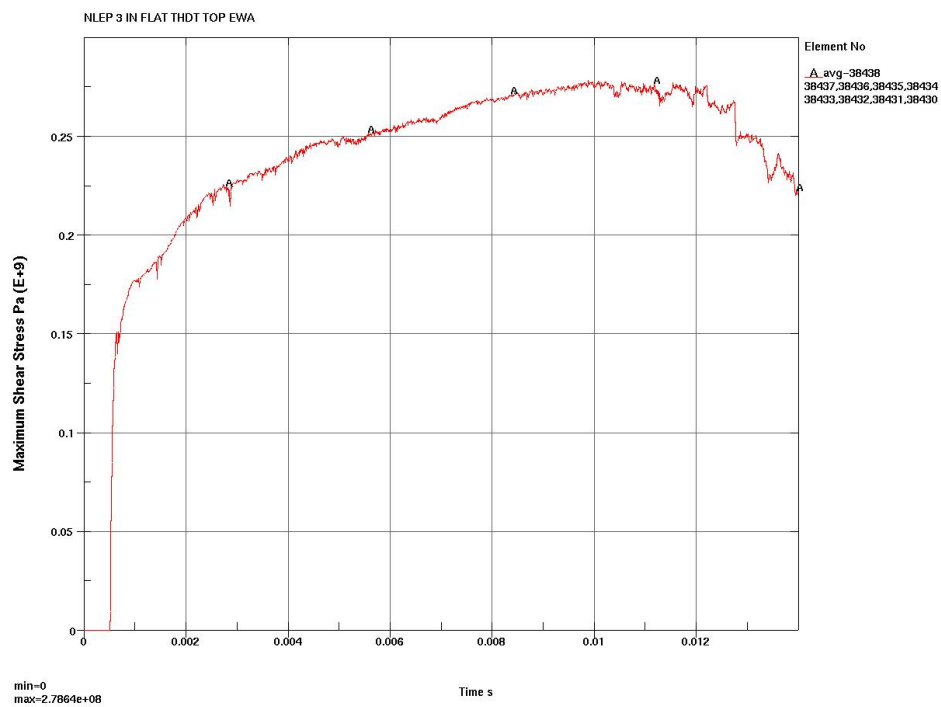


Figure 7-20 3 in Offset WP w/ Flat EP EWA MSS

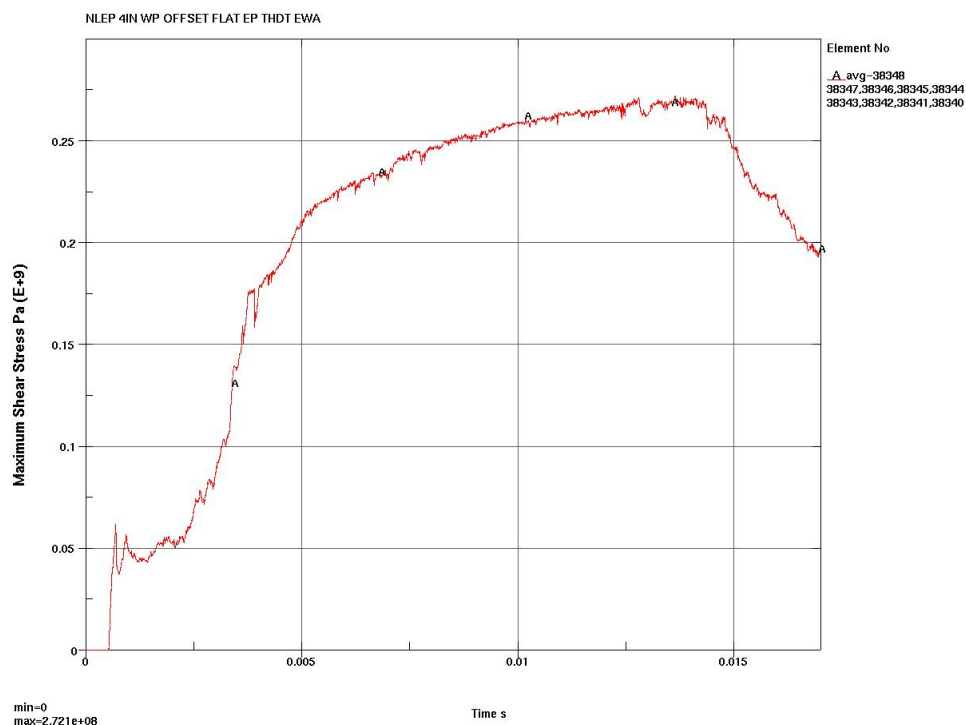


Figure 7-21 4 in Offset WP w/ Flat EP EWA MSS

Table 7-4 Comparative $\tau_{avg,max}$ in the OCB for WP Offset

Vertical Offset	$\tau_{avg,max}$	Ratio to Centered
None (Centered)	241.2 MPa (see Figure 7-11)	1
0.75 in	229.3 MPa (see Figure 7-12)	0.951
1.5 in	246.0 MPa (see Figure 7-13)	1.020
1.75 in	253.4 MPa (see Figure 7-14)	1.050
2 in	262.2 MPa (see Figure 7-15)	1.087
2.5 in	276.9 MPa (see Figure 7-16)	1.148
2.7 in	279.2 MPa (see Figure 7-17)	1.157
2.8 in	280.0 MPa (see Figure 7-18)	1.161
2.9 in	279.4 MPa (see Figure 7-19)	1.159
3 in	278.6 MPa (see Figure 7-20)	1.155
4 in	272.1 MPa (see Figure 7-21)	1.128

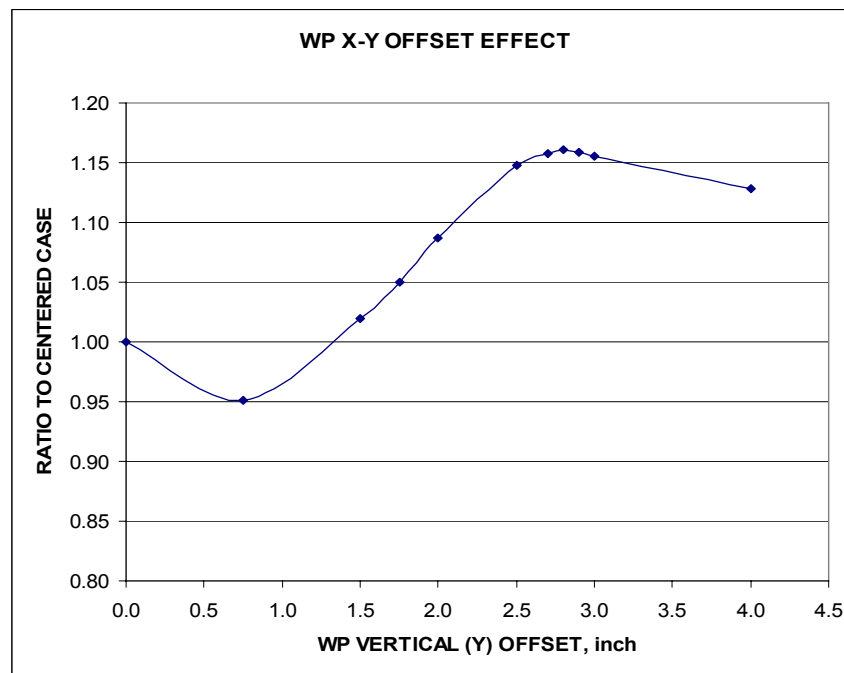


Figure 7-22 Excel Plot of Table 7-4, $\tau_{avg,max}$ Ratio to Centered versus WP Vertical Offset

From Figure 7-22, the worst case offset is near 2.8 in. Figure 7-18 indicates that $\tau_{avg,max}$ for this offset occurs near 10 ms. Figure 7-23 is a depiction of the distortions and surface MSS gradients near the governing OCB location (element string below the “H” of the element identifier on the figure) at 10 ms. The EP diagonal tube (behind the solid lines on the EP side plate) is creating a “hard spot” that increases the OCB stresses.

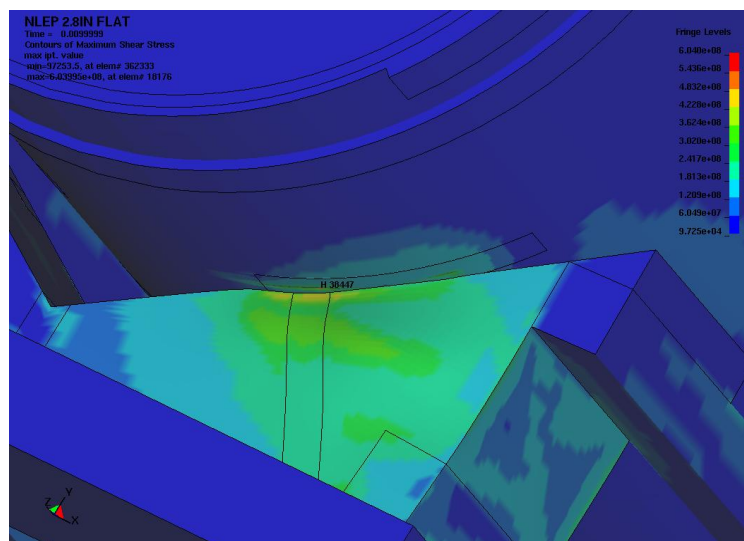


Figure 7-23 High Stress OCB Location for 2.8 in Offset WP with Flat EP Drop, Pa

7.2.2 Short-Side Angled EP Impacts

This section analyzes the stresses generated from Z-axis rotations of the EP under 1 *m* drops. The visual representation of the rotations is shown in Figures 6-13 to 6-19. The WP is centered on the EP. Figures 7-24 to 7-30 are the time plots of the EWA MSS at the governing location of the OCB for each angled EP drop case. Figure 7-11 is the time plot for the no-offset (centered) case to which the effect of EP rotation is compared in Table 7-5 and Figure 7-31.

The step change interruption of the stress plots in Figures 7-24 to 7-30 at increasingly later times is due to the EP angle to the target closing and the EP bottom striking the target surface. The WP is then partially supported by the opposite side of the EP, which unloads the initial load path. When the EP rebounds from the opposite side, the initial load path again carries the entire load, but the WP rebound has begun and the OCB stresses tail off.

From Figure 7-31, the worst case EP angulation is near 4 deg. Figure 7-27 indicates that $\tau_{avg,max}$ for this EP rotation occurs near 19 *ms*. Figure 7-32 is a depiction of the distortions and surface MSS gradients near this governing OCB location (at the element string below the “H” of the element identifier on the figure) at 19 *ms*. Again, the EP diagonal tube (behind the solid lines on the EP side plate) is creating a “hard spot” that increases the OCB stresses.

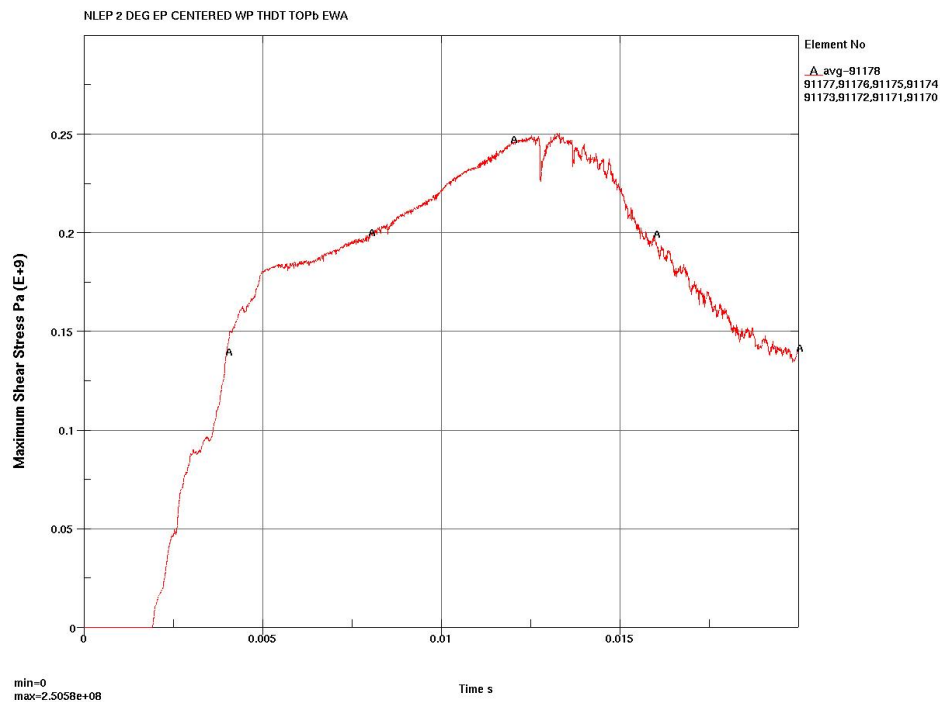


Figure 7-24 2 *deg* EP Z-Axis Rotation, EWA MSS

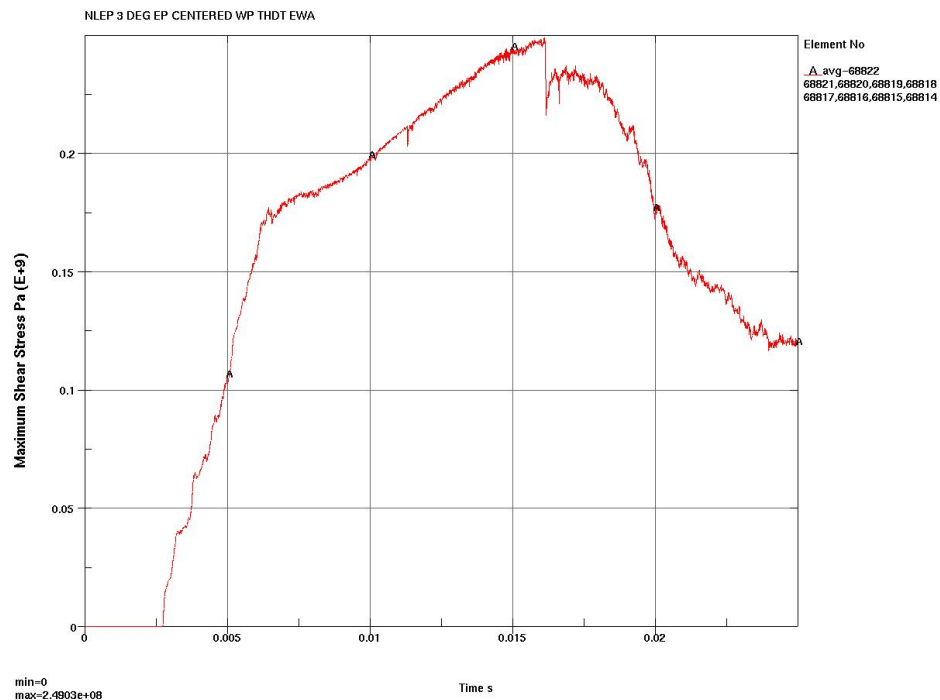


Figure 7-25 3 deg EP Z-Axis Rotation, EWA MSS

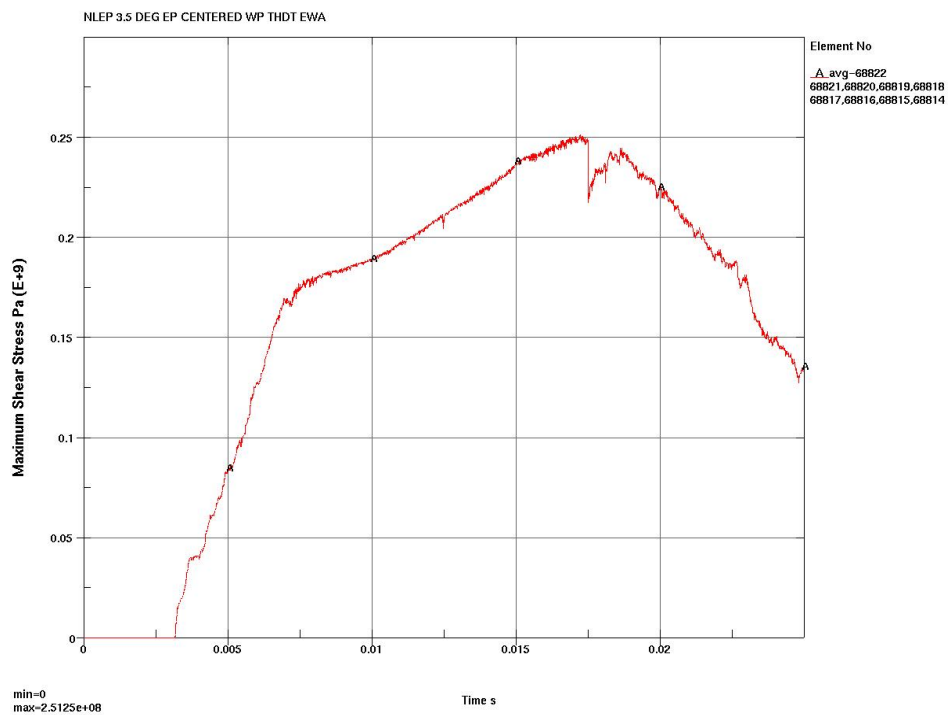


Figure 7-26 3.5 deg EP Z-Axis Rotation, EWA MSS

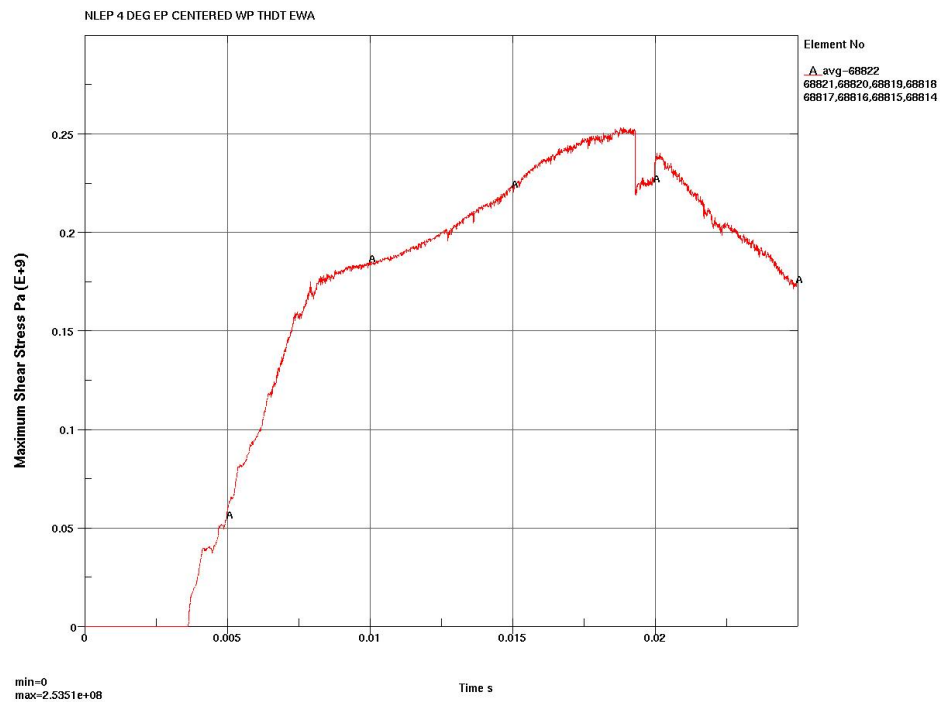


Figure 7-27 4 deg EP Z-Axis Rotation, EWA MSS

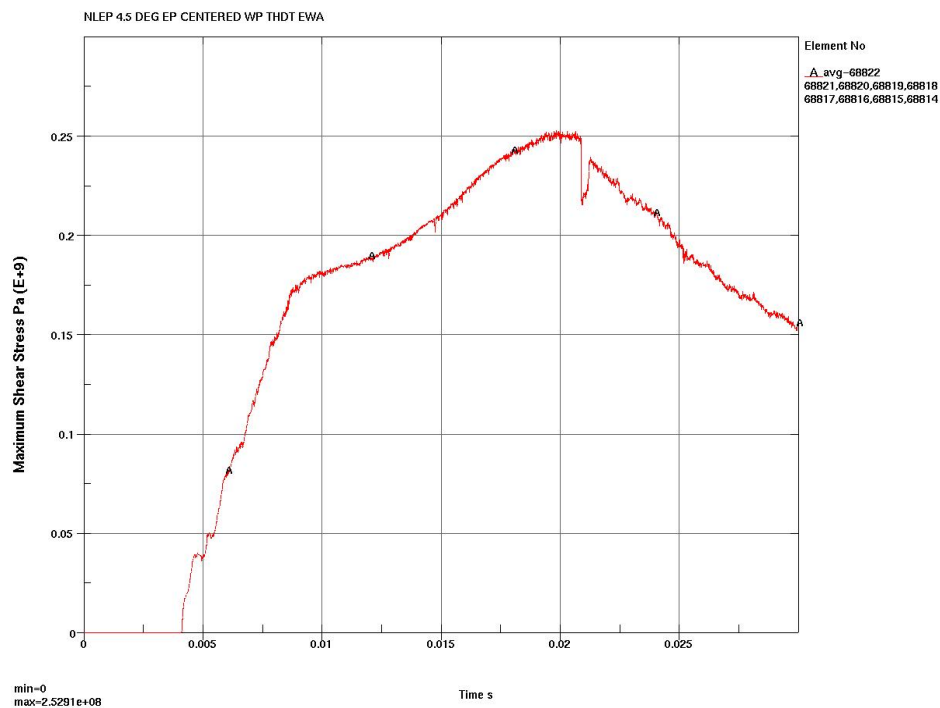


Figure 7-28 4.5 deg EP Z-Axis Rotation, EWA MSS

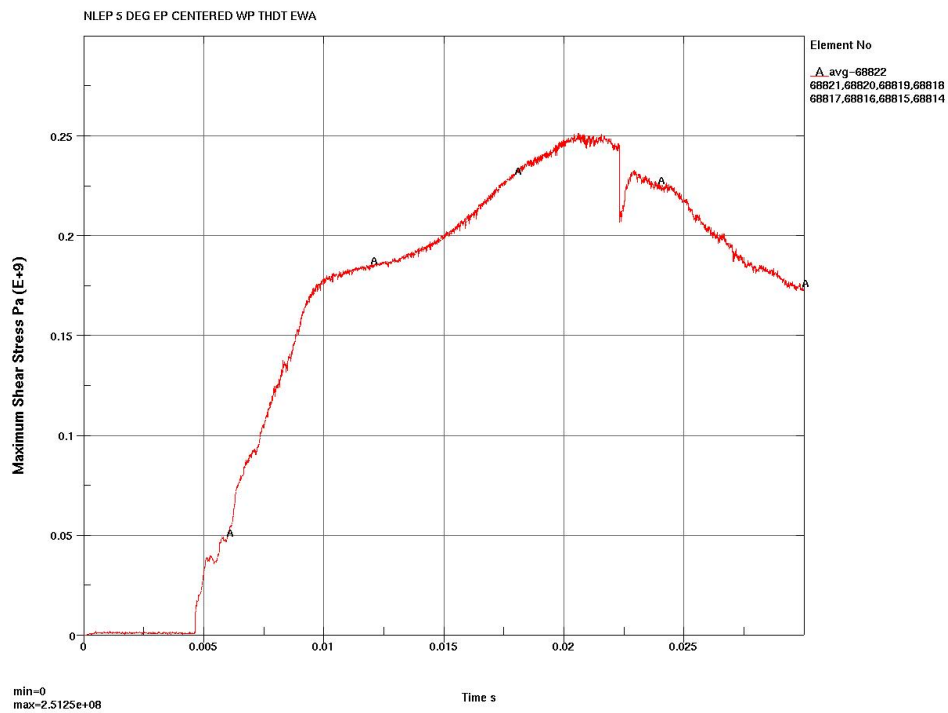


Figure 7-29 5 deg EP Z-Axis Rotation, EWA MSS

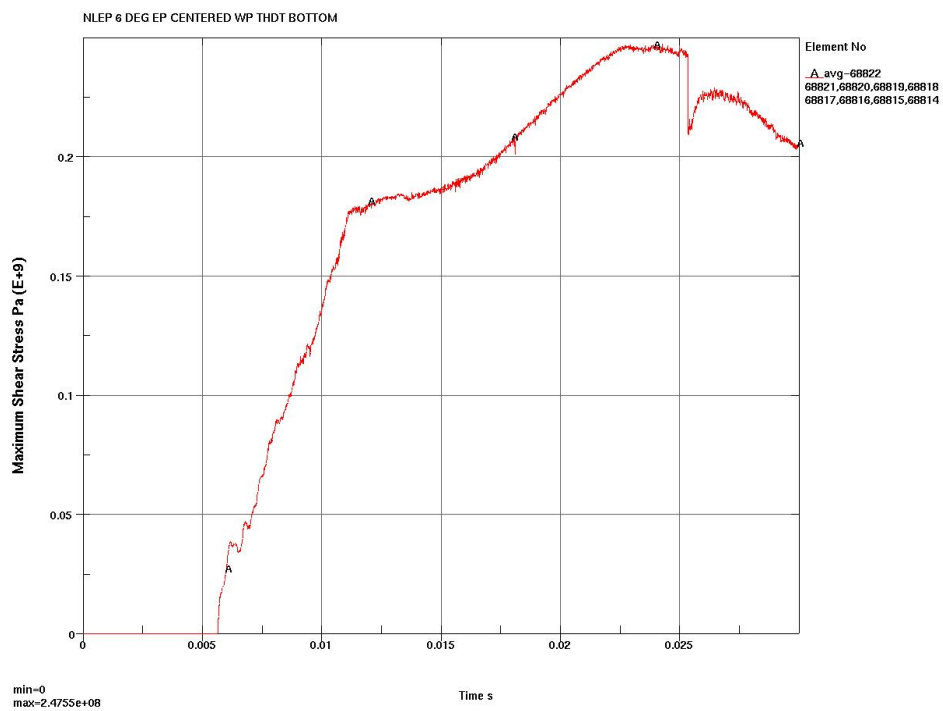
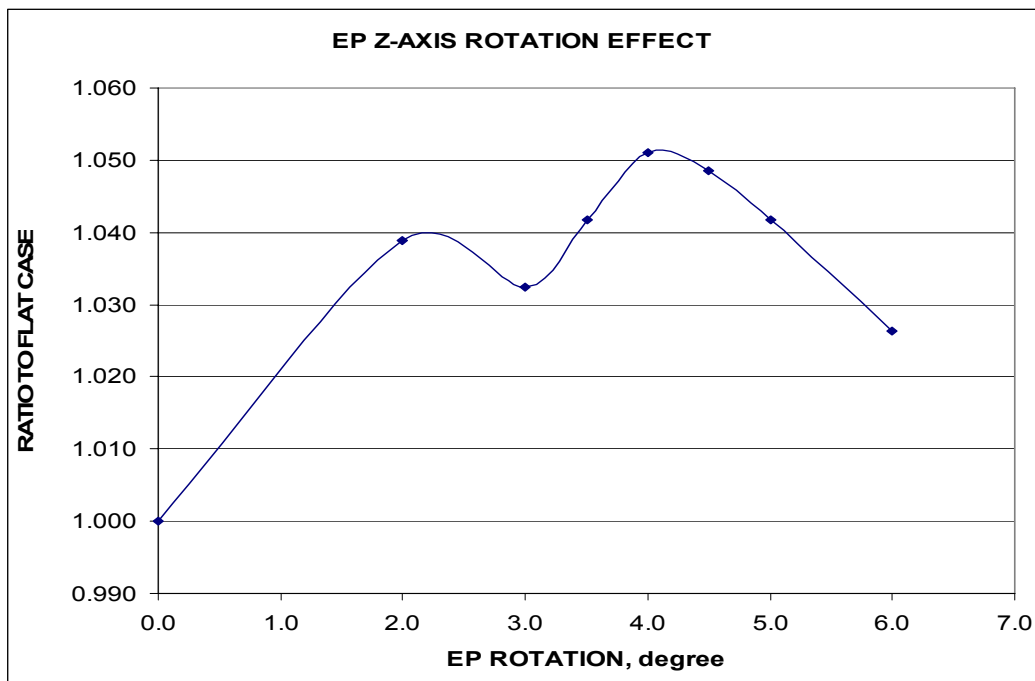


Figure 7-30 6 deg EP Z-Axis Rotation, EWA MSS

Table 7-5 Comparative $\tau_{avg,max}$ Ratio to Flat for EP Z-Axis Rotation

EP Z-Axis Rotation	$\tau_{avg,max}$	Ratio to Flat
0 deg (Flat)	241.2 MPa (see Figure 7-11)	1
2 deg	250.6 MPa (see Figure 7-24)	1.039
3 deg	249.0 MPa (see Figure 7-25)	1.032
3.5 deg	251.2 MPa (see Figure 7-26)	1.042
4 deg	253.5 MPa (see Figure 7-27)	1.051
4.5 deg	252.9 MPa (see Figure 7-28)	1.048
5 deg	251.2 MPa (see Figure 7-29)	1.042
6 deg	247.6 MPa (see Figure 7-30)	1.026

Figure 7-31 Excel Plot of Table 7-5, $\tau_{avg,max}$ Ratio to Flat for EP Z-Axis Rotation

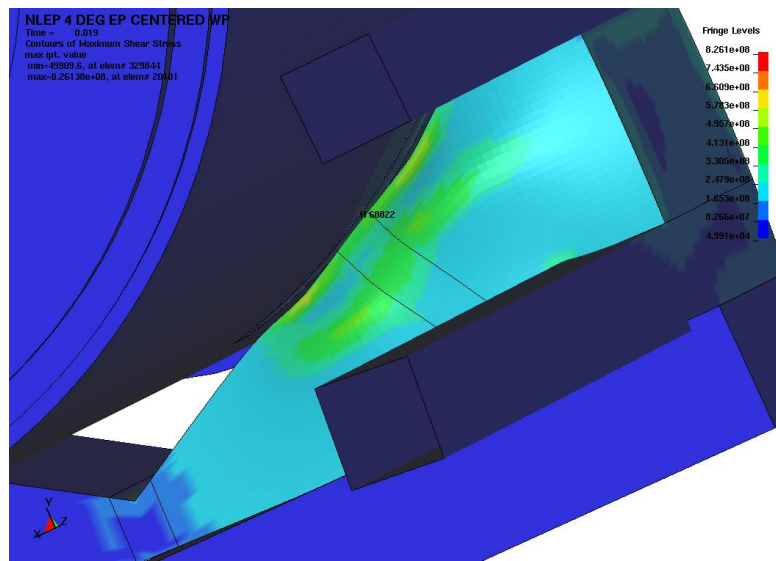


Figure 7-32 High Stress OCB Location for Centered WP on 4 deg EP Z-Axis Rotation, Pa

7.2.3 Offset WP with Short-Side Angled EP Impacts

This case is a combination of the near worst case X-Y offset of the WP along the EP with the worst case Z-axis rotation (4 deg) of the EP. Visual representation of the case is shown in Figure 6-20. Figure 7-33 shows the EWA MSS of the OCB for the combined case.

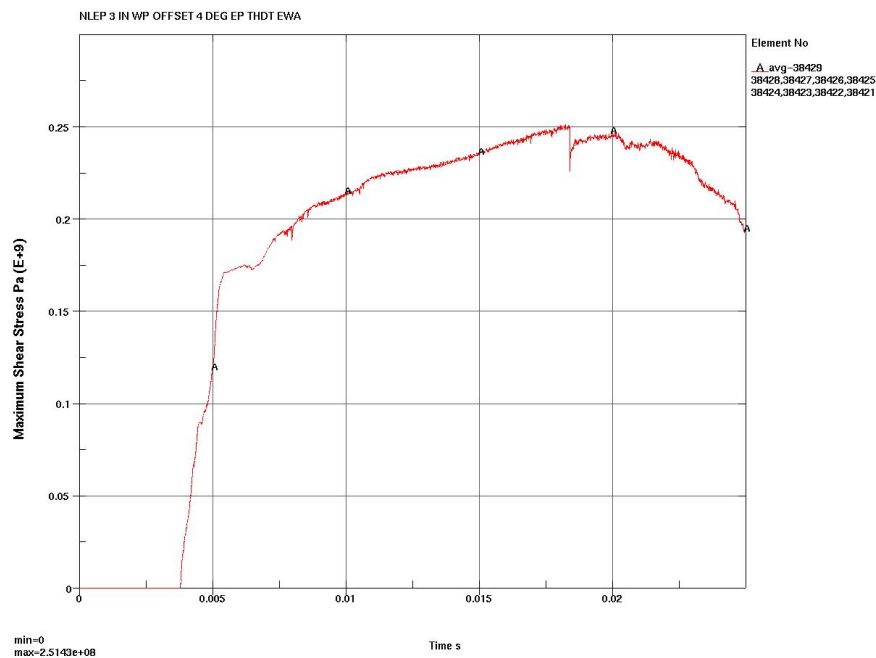


Figure 7-33 3 in Offset WP, 4 deg Z-Axis Rotation, Pa

Table 7-6 provides stress response comparisons between the individual cases, the combined case and the centered – flat case. The combination of the two cases reduces the stresses below those which exist in each individual case.

Table 7-6 Comparative $\tau_{avg,max}$ Ratio to Centered-Flat for WP Offset and EP Z-Axis Rotation

Offset + Rotation	$\tau_{avg,max}$	Ratio to Flat
Centered WP Flat EP	241.2 MPa (see Figure 7-11)	1
3 in Offset WP	278.6 MPa (see Figure 7-20)	1.155
4 deg Z-Axis EP	253.5 MPa (see Figure 7-27)	1.051
3 in Offset WP 4 deg Z-Axis EP	251.4 MPa (see Figure 7-33)	1.042

7.2.4 Long-Side Angled EP Impacts

Visual representation of the orientation is shown in Figure 6-21. This is a 2 deg rotation of the EP about the X-axis. The WP is centered on the EP. Figure 7-34 shows the governing EWA MSS response of the OCB for this drop event.

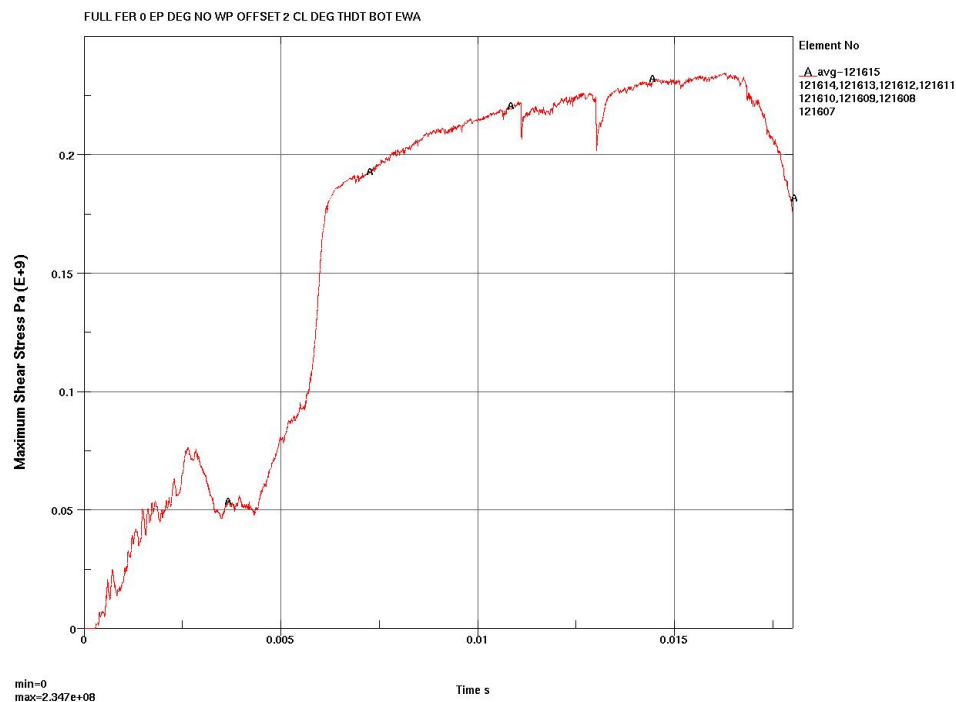


Figure 7-34 2 deg X-Axis EP Rotation, EWA MSS

Table 7-7 provides a stress response comparison between the rotated EP case and the flat impact case. The X-axis rotation of the EP reduces the stress response.

Table 7-7 Comparative $\tau_{avg,max}$ Ratio to Flat for EP X-Axis Rotation

Rotation	$\tau_{avg,max}$	Ratio to Flat
0 deg (Flat)	241.2 MPa (see Figure 7-11)	1
2 deg X-axis	234.7 MPa (see Figure 7-34)	0.973

7.2.5 EP Corner Impacts

The visual representation of the angulations in this case is shown in Figure 6-22. This is a double rotation of the EP so that it impacts on a corner. The WP is centered on the EP. Figure 7-35 shows the governing EWA MSS of the OCB during the impact.

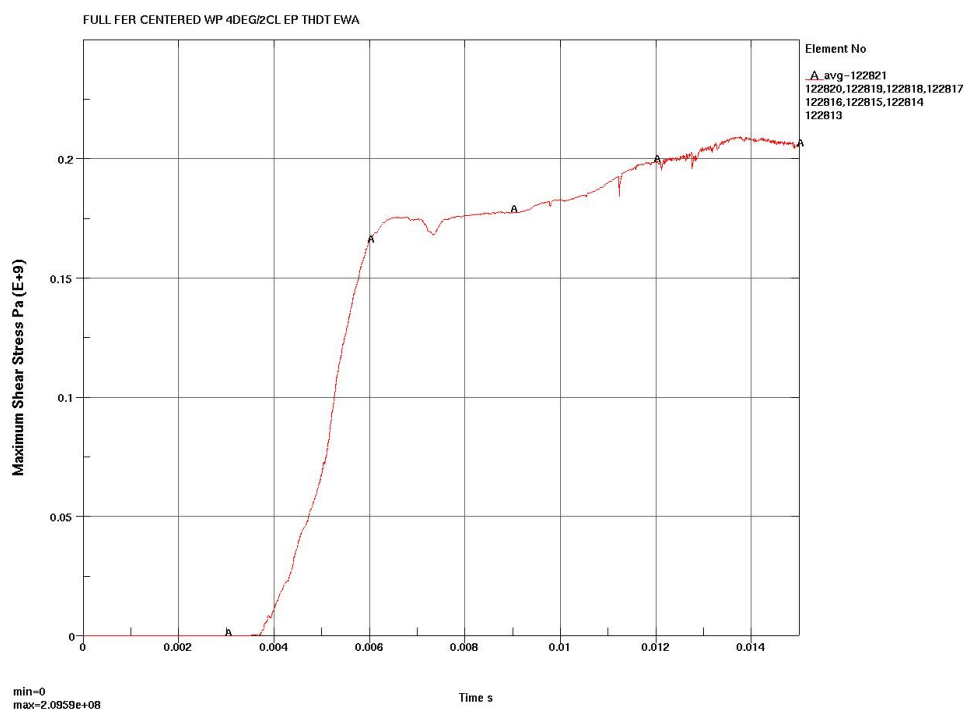


Figure 7-35 2 deg X-Axis, 4 deg Z-Axis EP Rotation, EWA MSS

Table 7-8 provides stress response comparisons between the individual cases, the combined case and the flat case. The combination of the two rotations reduces the stresses below those which exist in each rotation case.

Table 7-8 Comparative $\tau_{avg,max}$ Ratio to Flat for EP X-Axis Rotation

EP Rotation	$\tau_{avg,max}$	Ratio to Flat
Flat	241.2 MPa (see Figure 7-11)	1
2 deg X-axis	234.7 MPa (see Figure 7-34)	0.973
4 deg Z-Axis	253.5 MPa (see Figure 7-27)	1.051
2 deg X-Axis 4 deg Z-Axis	209.6 MPa (see Figure 7-35)	0.869

7.2.6 Angled WP Impacts

In this case, the WP is rotated about the X-axis while the EP remains flat. Visual representation of this case is shown in Figure 6-23. Figure 7-36 shows the governing EWA MSS of the OCB during the impact.

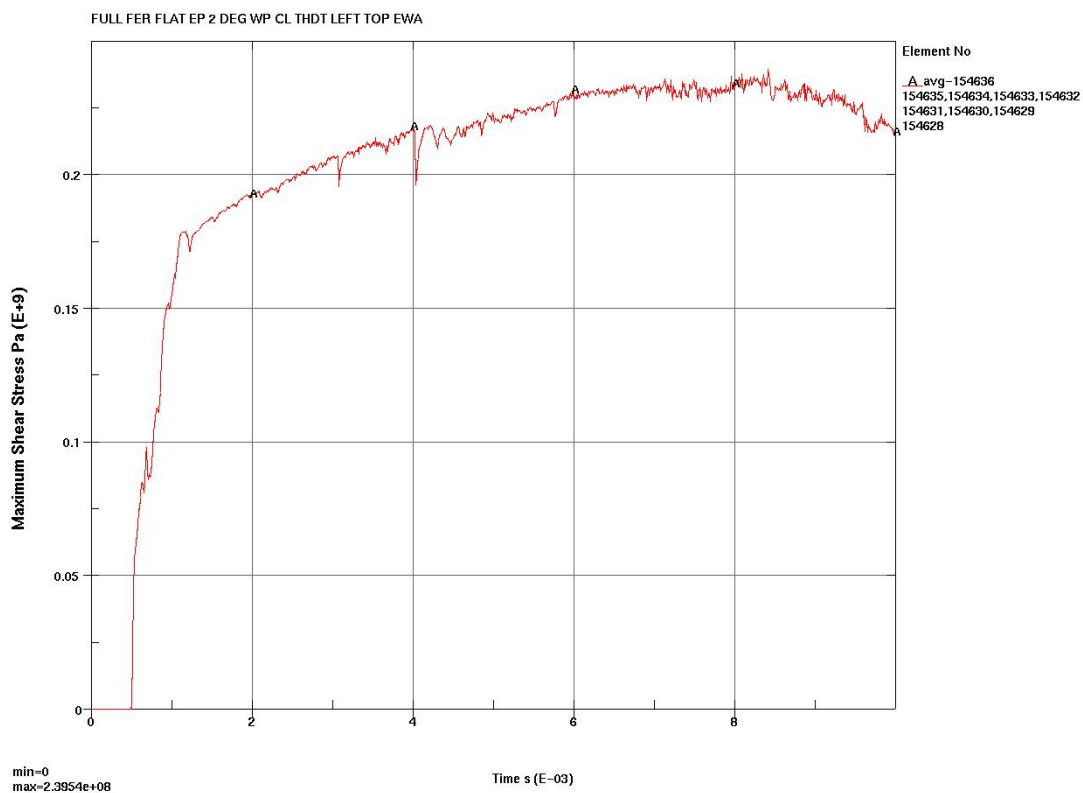


Figure 7-36 2 deg X-Axis WP Rotation, Flat EP, EWA MSS

Table 7-9 provides a stress response comparison between the rotated WP case and the flat impact case. The X-axis rotation of the WP reduces the stress response.

Table 7-9 Comparative $\tau_{avg,max}$ Ratio to Flat for WP X-Axis Rotation

WP Rotation	$\tau_{avg,max}$	Ratio to Flat
Flat	241.2 MPa (see Figure 7-11)	1
2 deg X-Axis	239.5 MPa (see Figure 7-36)	0.993

7.2.7 Worst Case Impacts

The worst case drop orientation is identified to be a rotated WP with respect to the Y-axis resulting in diagonal positioning on the EP (see Figure 6-24). The magnitude of the rotation is where the WP touches the EP at 2.8-in offset from the center. The 2.8-in (vertical) offset results in the highest stresses due to the “hard spot” created by the reinforcing tube on the EP end plate. The rotated WP results in a slightly more localized (more severe) edge loading at the location of EP contact. The worst case orientation has a flat impacting EP which results in higher stresses when the WP is not centered (as in this case). Figure 7-37 shows the governing EWA MSS of the OCB during the worst case orientation 1 m drop event.

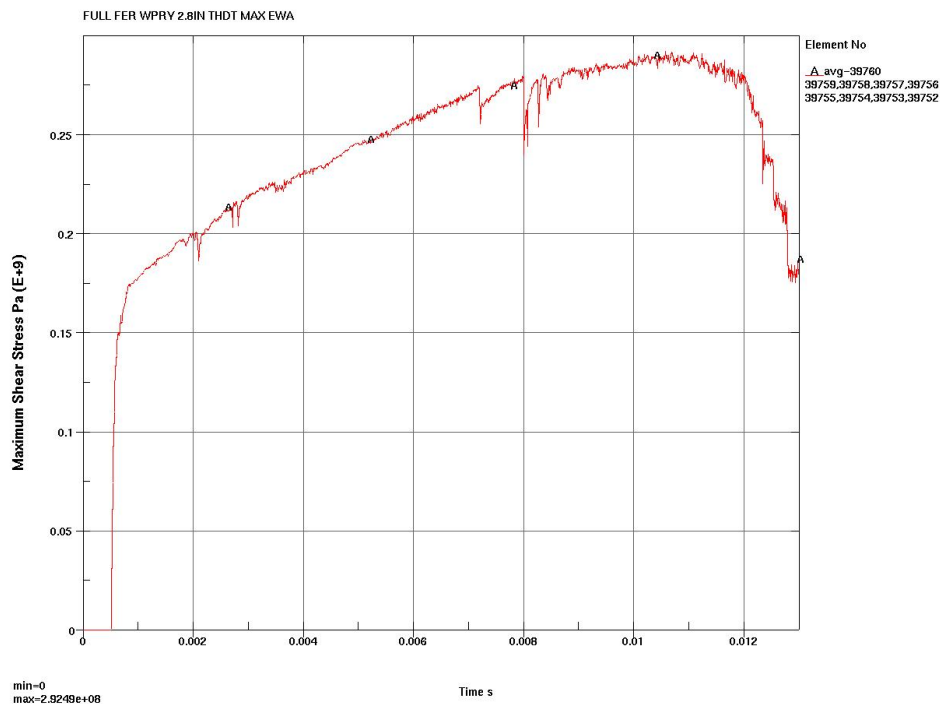


Figure 7-37 2.8 in Offset by Y-Axis WP Rotation, Flat EP, EWA MSS

The time-maximum of the EWA MSS stress on Figure 7-37 is greater than any previous analysis. To further investigate for higher stress values, the WP is offset along the Z-axis direction the maximum it can go before stopped by the trunnion sleeve (see Figure 6-25). Figure 7-38 shows the EWA MSS of the OCB during the impact for the rotated and translated WP.

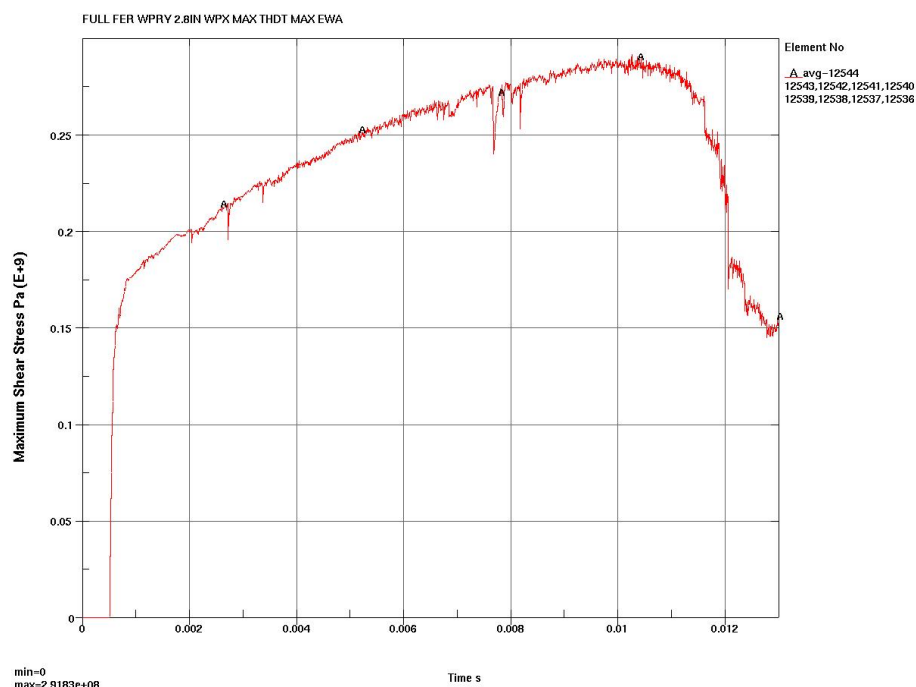


Figure 7-38 2.8 in Offset by Y-Axis Rotation of WP with Z-Axis Offset, EWA MSS

Table 7-10 indicates that the Z-axis offset has negligible effect on the OCB stresses.

Table 7-10 Comparison Table for Worst Case Drops

Case	$\tau_{avg,max}$	Ratio to Centered Flat
Centered Flat	241.2 MPa (see Figure 7-11)	1
2.8 in Offset by Y-Axis Rotation WP	292.5 MPa (see Figure 7-37)	1.213
2.8in Offset by Y-Axis Rotation WP w/ Z Offset	291.8 MPa (see Figure 7-38)	1.210

In summary, rotation of the EP (with a centered WP) about the X and Z axes (obviously Y-axis rotation or translations of the EP has no effect), translations of the WP relative to the EP in all three directions and rotations of the WP relative to the EP about the X and Y axes (obviously Z-axis rotation of the WP has no effect) were evaluated singularly and in combination. This covers

all reasonable WP and EP impact orientations given a centered WP horizontal EP starting position in a lifting device such as the proposed emplacement gantry. It is determined that the Z-axis rotation of the WP relative to the EP that leads to contact with the EP at 2.8 *in* vertical offset combined with a flat impact of the EP on the target plane leads to the highest OCB EWA MSS for a 1 *m* drop event.

This worst case orientation was then rerun for the current design details with a refined EP mesh for a 20 *in* (0.508 *m*) drop. Slightly higher OCB stresses were developed when the inner vessel was displaced as far as possible towards the bottom of the WP (see Figures 6-30 and 6-31). Figures 7-39 to 7-43 contain selective distortion and surface MSS plots near the time of maximum OCB EWA MSS. Recognize that the EP is more highly stressed and that the plotted surface MSS gradients change when the EP is deleted from the plots.

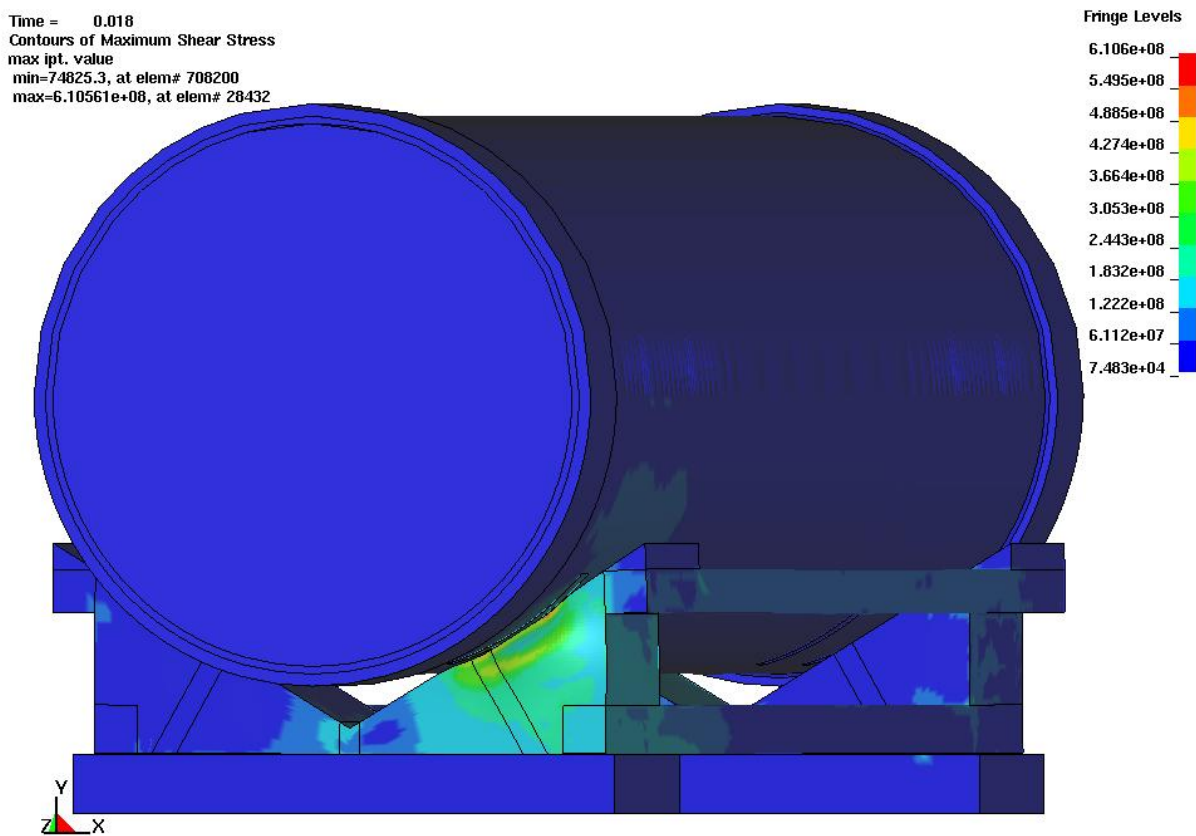


Figure 7-39 Worst Case Impact, 20 *in* Drop, Full View, *Pa*

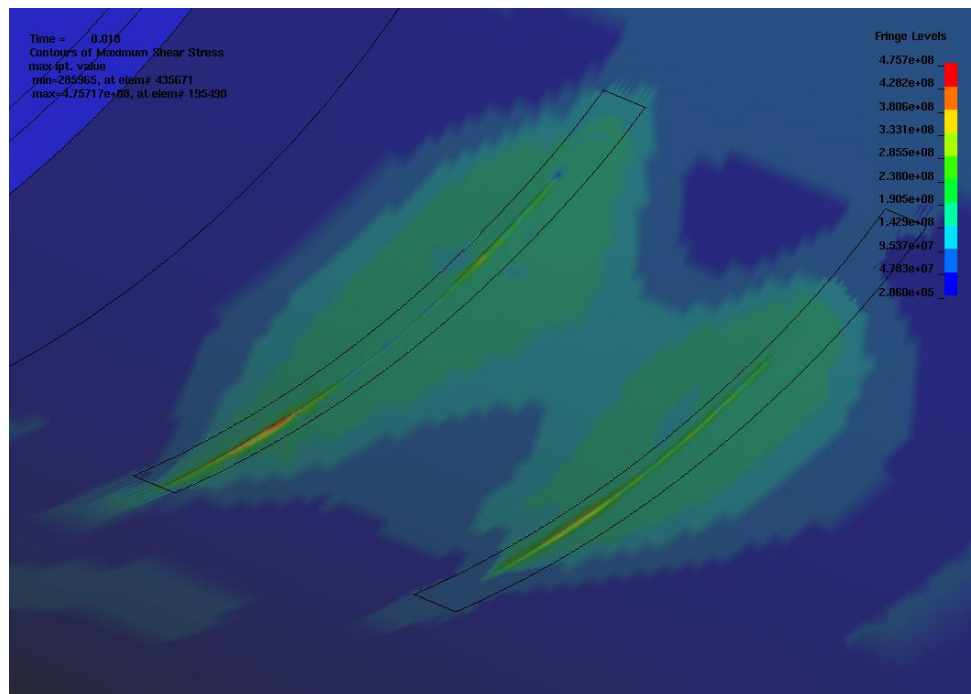


Figure 7-40 Worst Case Impact, 20 in Drop, OCB Impact Region, Pa

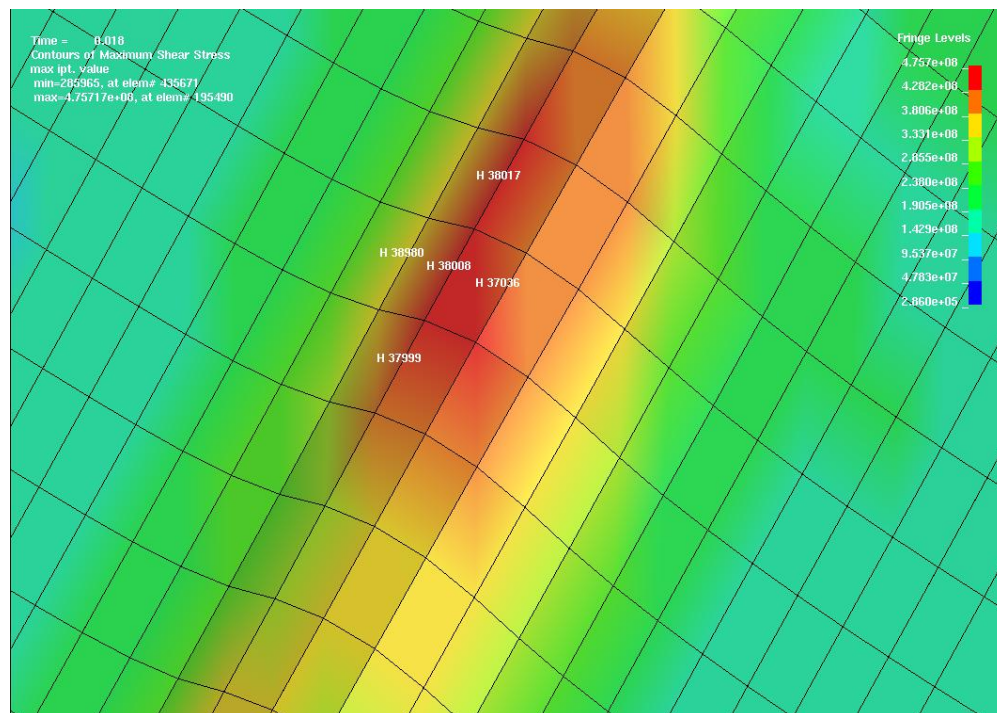


Figure 7-41 Worst Case Impact, 20 in Drop, OCB Governing Elements, Pa

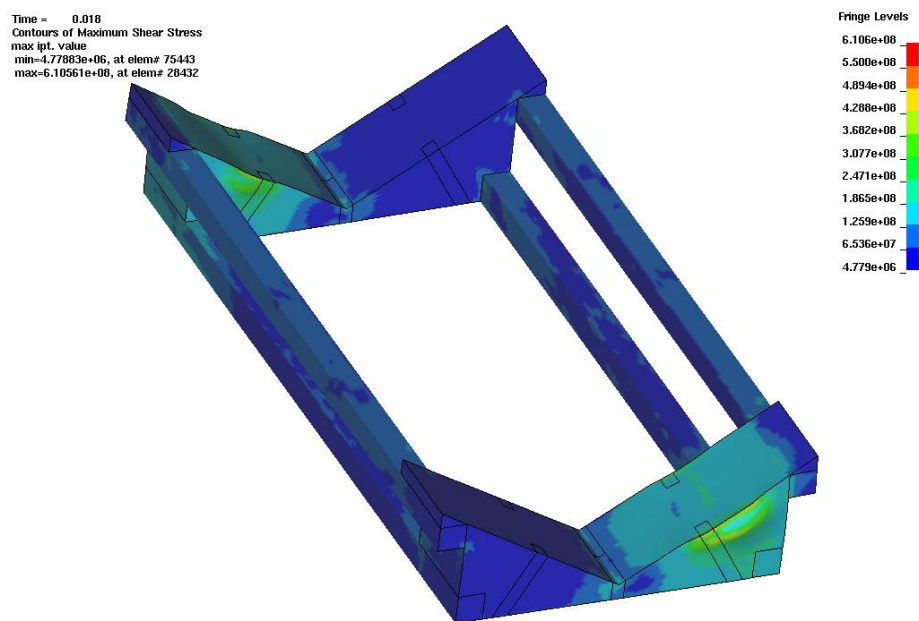


Figure 7-42 Worst Case Impact, 20 in Drop, EP Full View, Pa

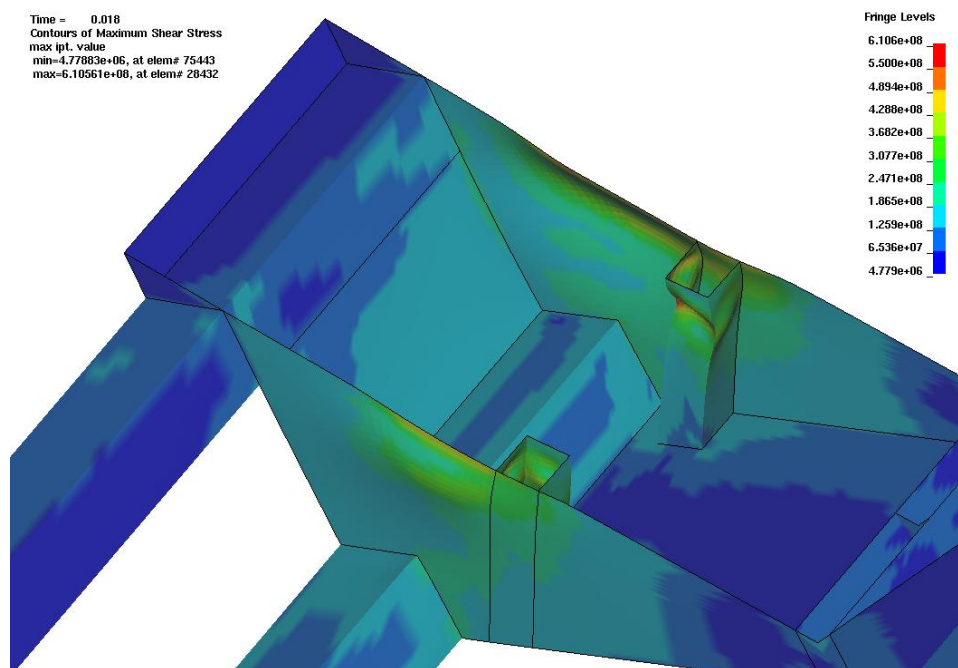


Figure 7-43 Worst Case Impact, 20 in Drop, Support Tube View, Pa

Care was taken to identify the governing through-wall location. Data collection rates were increased near the time of maximum response. Table 7-11 contains $\tau_{avg,max}$ values for that location and its surrounding elements, supported by Figures 7-44 to 7-48. Small differences in adjacent element values are a good indication of an adequate WP mesh.

Table 7-11 OCB Governing Location Stresses, 20 in Drop

OCB Outer Surface Element #	$\tau_{avg,max}$ (MPa)
H 38008 (Maximum Location)	293.63 (see Figure 7-44)
H 37999 (Adjacent Hoop Below)	288.74 (see Figure 7-45)
H 38017 (Adjacent Hoop Above)	293.49 (see Figure 7-46)
H 38980 (Adjacent Axial Towards Top)	235.08 (see Figure 7-47)
H 37036 (Adjacent Axial Towards Bottom)	293.50 (see Figure 7-48)

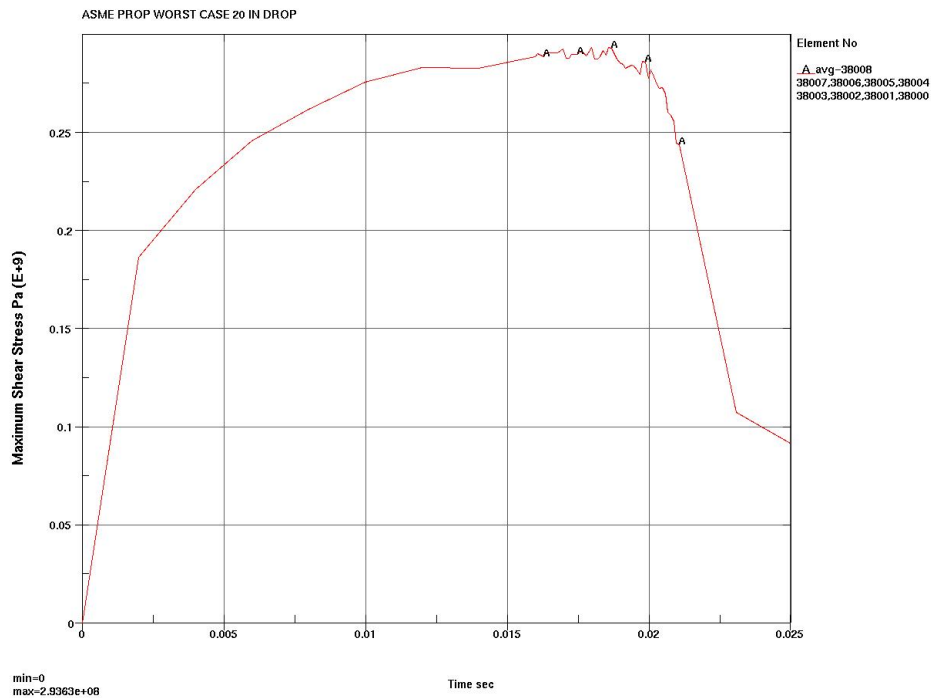


Figure 7-44 Worst Case Impact, 20 in Drop, Maximum Location, EWA MSS

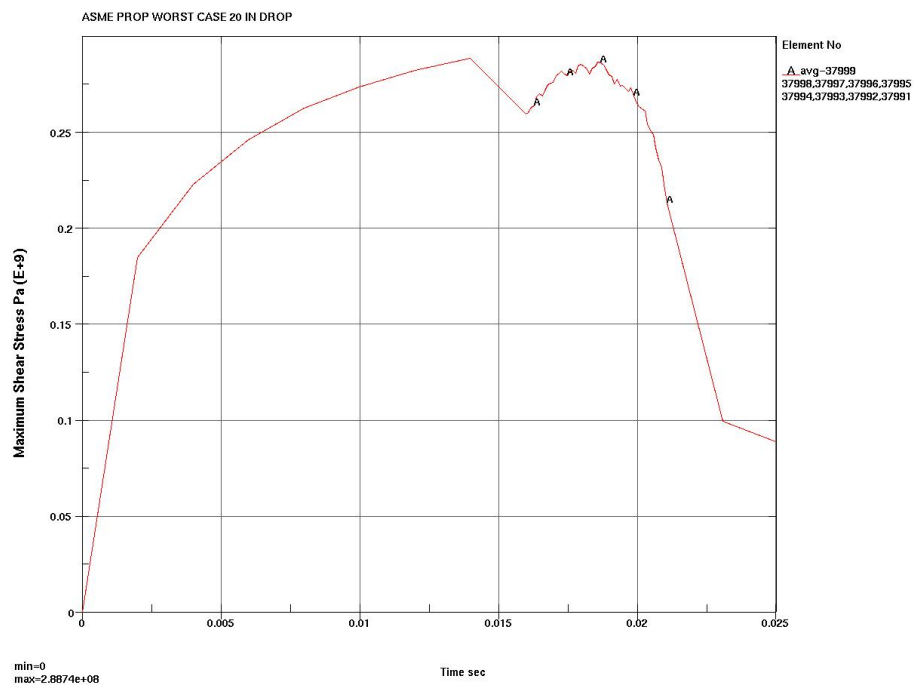


Figure 7-45 Worst Case Impact, 20 in Drop, Adjacent Hoop Below, EWA MSS

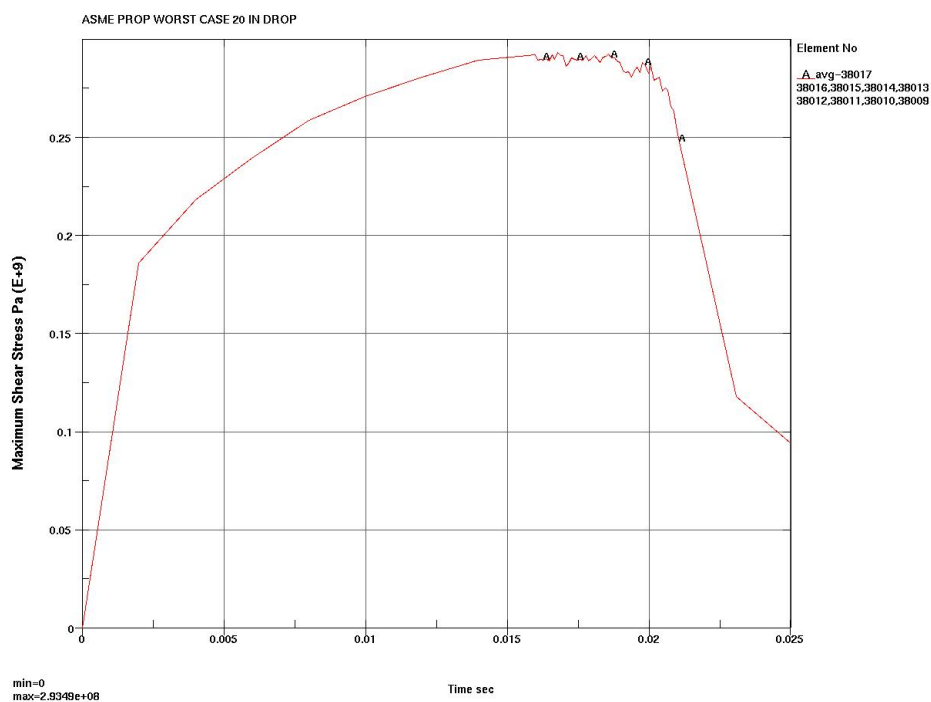


Figure 7-46 Worst Case Impact, 20 in Drop, Adjacent Hoop Above, EWA MSS

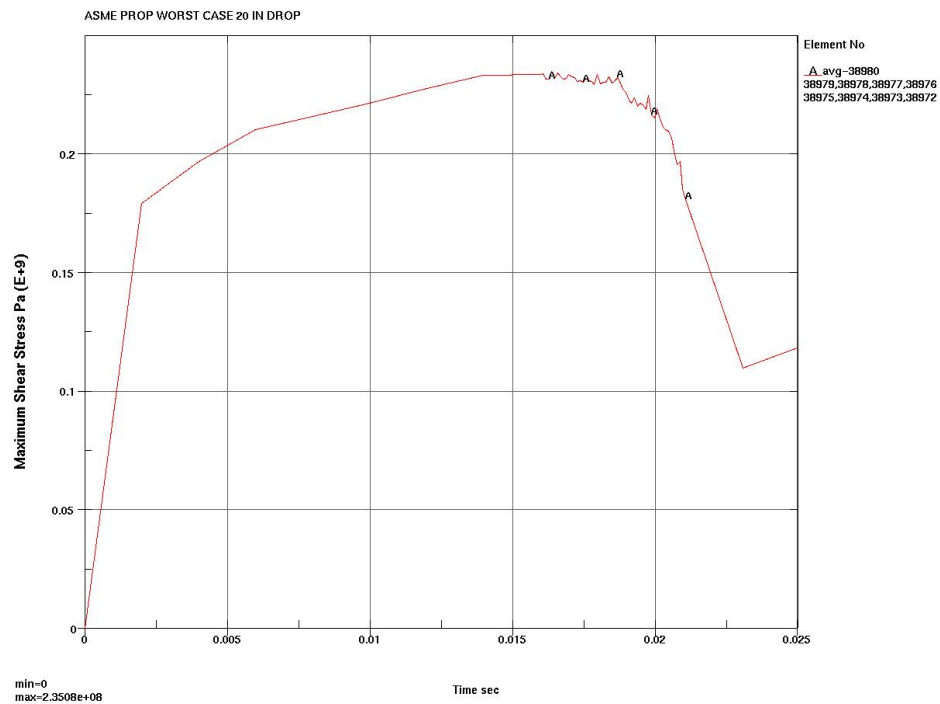


Figure 7-47 Worst Case Impact, 20 in Drop, Adjacent Axial Top, EWA MSS

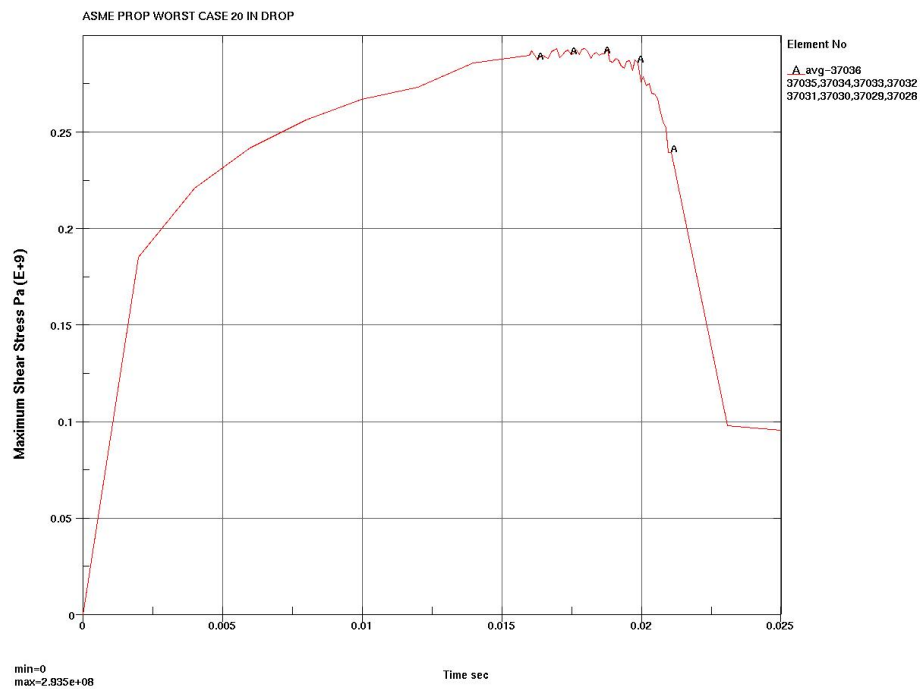


Figure 7-48 Worst Case Impact, 20 in Drop, Adjacent Axial Bottom, EWA MSS

The tiered screening criteria in Reference 2.2.15, Section 7.1.4 uses twice the value of $\tau_{avg,max}$ as a conservative bound on ASME primary membrane SI. If it is less than $0.7 \sigma_u$ (i.e., conservatively treated as general primary membrane stress intensity, P_M), the criteria is met.

The σ_u value of the OCB material (at RT) is 971 MPa (141 ksi) (see Section 6.1.1). Twice the Table 7-11 worst case OCB maximum $\tau_{avg,max}$ value is $(2)(293.63) = 587 \text{ MPa}$ (85 ksi). This is $0.6 \sigma_u$ and easily meets the tiered screening criteria.

Studies in the next section indicate that the RT evaluations govern over higher temperature cases and that the choices of friction coefficient and data collection rate are acceptable.

7.3 DETERMINISTIC CALCULATIONS SENSITIVITY STUDIES

Three deterministic calculation sensitivity studies are conducted for temperature, friction and data collection rate.

7.3.1 Temperature

The worst case orientated 2.8-in rotated WP is run at 300°C for a 1 m drop to observe its temperature sensitivity. Figure 7-49 shows the maximum EWA MSS in the OCB.

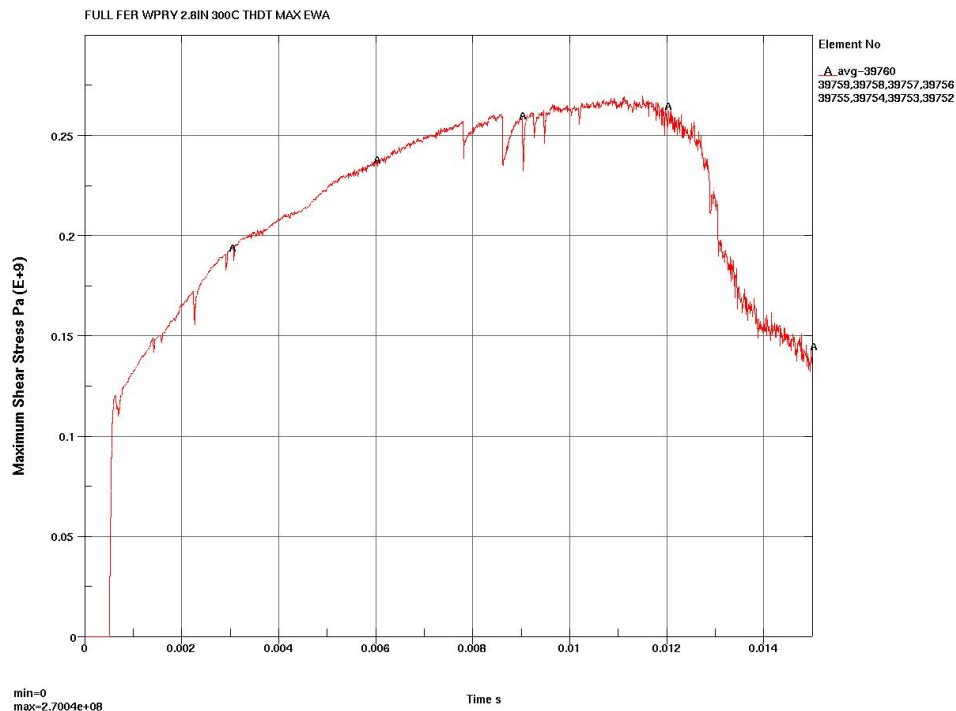


Figure 7-49 Worst Case Impact, 1 m Drop, EWA MSS, 300°C

Table 7-12 compares the ratio of twice $\tau_{avg,max}$ to the true ultimate tensile strength and the same ratio for the corresponding RT case (Table 7-10). The stress results for the 300°C temperature case are not governing. In this temperature range, the reduction in a stress ratio damage term is related to the lowering of the yield stress at the elevated temperature being more than the lowering of the true ultimate tensile strength at the elevated temperature. The amount of plasticity and energy dissipation increases at the elevated temperature, reducing the effectiveness of the impact loading.

Table 7-12 Temperature Sensitivity of OCB Stress Evaluation

Temperature	Twice $\tau_{avg,max}$ (see Section 7.1)	σ_u	Twice $\tau_{avg,max}$ $/\sigma_u$
RT	585 MPa (see Figure 7-37)	971 MPa	0.60
300°C	540 MPa (see Figure 7-49)	910 MPa	0.59

7.3.2 Friction

A friction coefficient study is conducted. This study was conducted before the worst case was identified and is for the 2.8 *in.* offset WP with flat EP contact (Figure 6-9) and a 1 *m* drop. Figure 7-50 contains the OCB maximum EWA MSS for a 0.2 friction coefficient between parts. High response oscillations occur.

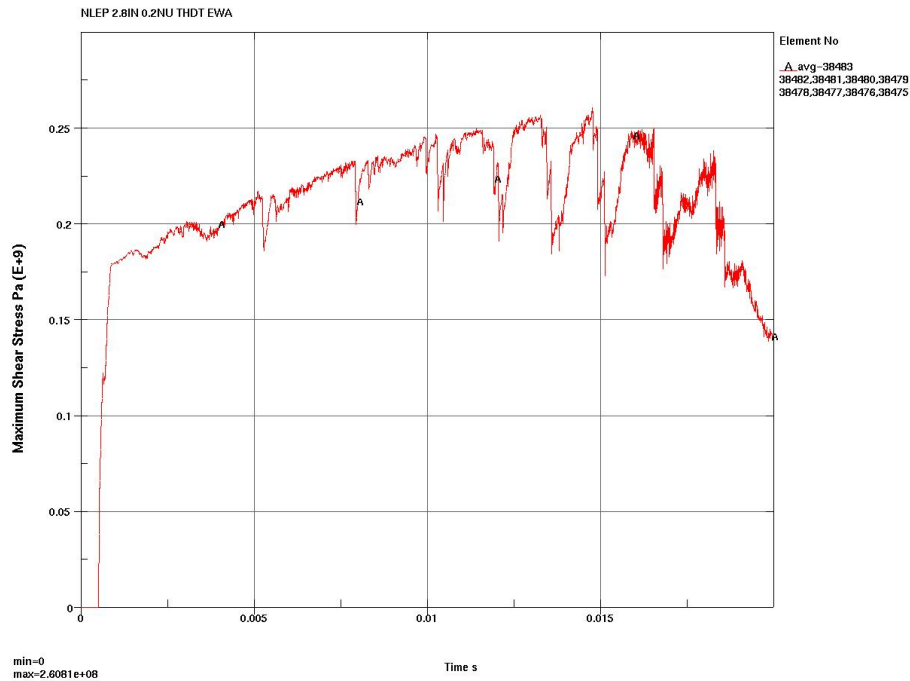
Figure 7-50 2.8 *in* WP Offset w/ Flat EP, 1 *m* Drop, EWA MSS, 0.2 Friction

Figure 7-51 contains the OCB maximum EWA MSS for the same case using a 1.0 friction coefficient between all parts. Table 7-13 compares the maximum OCB $\tau_{avg,max}$ values for these two cases and the nominal 0.4 friction coefficient case (Figure 7-18). The reduction in friction coefficient reduces the OCB stress response whereas the increase in friction coefficient provides essentially identical OCB stress response. This is reasonable because the reduced friction coefficient case permits slippage (and oscillatory instability) and can dissipate some of the potential impact energy as kinetic energy, whereas once there is adequate friction to prevent sliding (the contact surfaces lock-up), the value of friction coefficient doesn't matter.

Table 7-13 Friction Sensitivity of OCB Stress Evaluation

Friction Coefficient	$\tau_{avg,max}$	Ratio to Friction = 0.4
Friction = 0.4	279.96 MPa (see Figure 7-18)	1
Friction = 0.2	260.81 MPa (see Figure 7-50)	0.9316
Friction = 1.0	279.98 MPa (see Figure 7-51)	1.0001

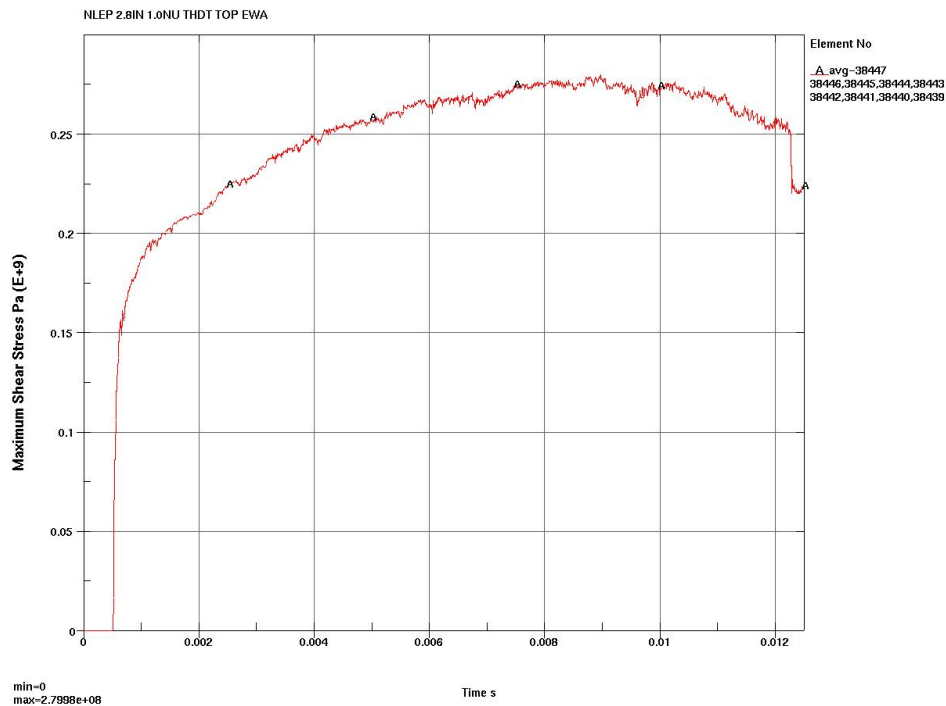


Figure 7-51 2.8 in WP Offset w/ Flat EP, 1 m Drop, EWA MSS, 1.0 Friction

7.3.3 Data Collection Rate

The last deterministic calculation sensitivity study is also conducted on the 1 *m* drop of the 2.8 *in* offset WP with a flat EP contact. Figure 7-52 contains the OCB maximum EWA MSS for a data collection rate of 10,000 data points per second (0.0001 seconds between data points). Figure 7-53 is for the same drop event with a much faster data collection rate of 0.000001 seconds between data points.

Table 7-14 compares the time-maximum value of these to the time-maximum value for the normal data collection rate (0.00001 seconds between data points) used in Figure 7-18. The comparison indicates that the normal data collection rate is adequate to capture the peak responses. It is also encouraging to note that all the significant data spikes are downward.

Table 7-14 Data Collection Rate Sensitivity of OCB Stress Evaluation

Data Collection Rate (time between data, seconds)	$\tau_{avg,max}$	Ratio to 0.00001 Rate
Rate = 0.0001 (Slower)	278.98 MPa (see Figure 7-52)	0.9965
Rate = 0.00001 (Normal)	279.96 MPa (see Figure 7-18)	1
Rate = 0.000001 (Faster)	280.08 MPa (see Figure 7-53)	1.0004

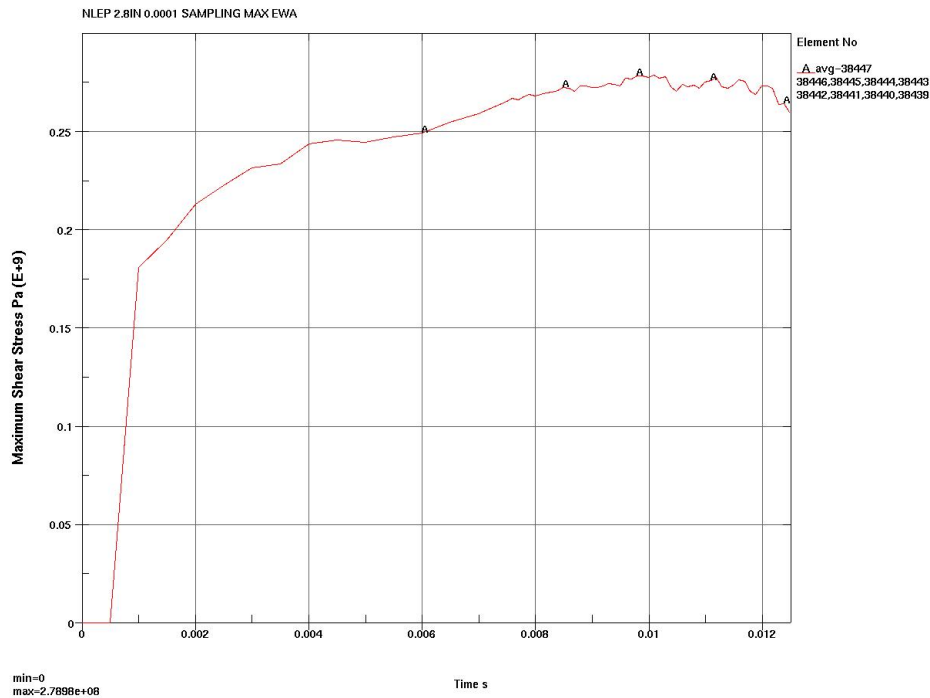


Figure 7-52 2.8 *in* WP Offset w/ Flat EP, 1 *m* Drop, EWA MSS, 0.0001 s Data

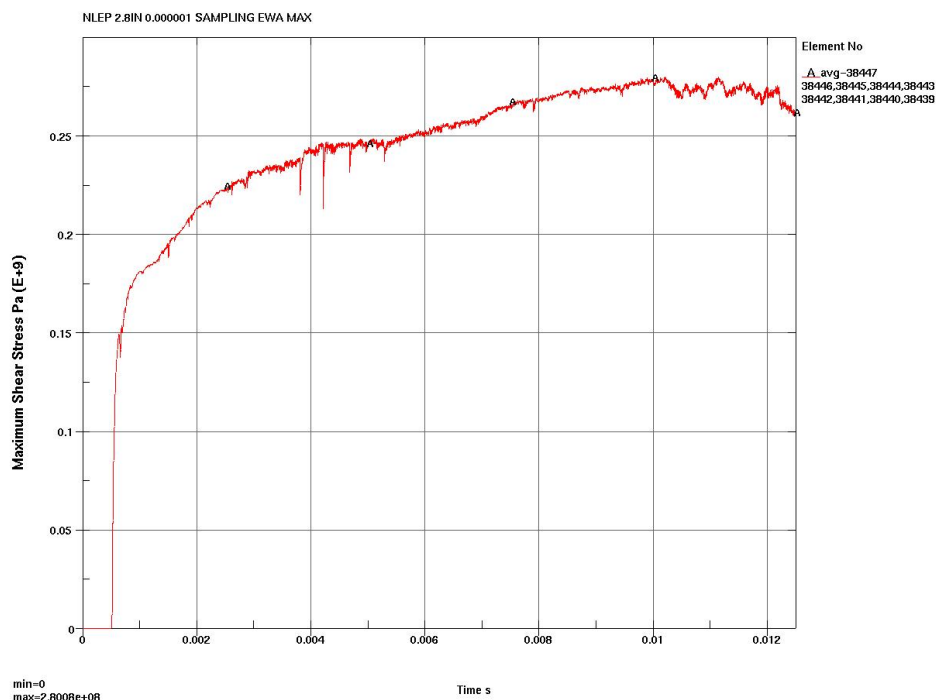


Figure 7-53 2.8 in WP Offset w/ Flat EP, 1 m Drop, EWA MSS, 0.000001 s Data

7.4 CAPABILITY CALCULATIONS

The worst-case-triaxiality-adjusted vendor-averaged strength properties presented in Section 6.1.2 were used as mean (most expected) strength properties of the OCB in Capability calculations for three basic event sequence orientations; WP on EP impact on flat surface, WP on EP bridging invert steel, and, WP direct impact on invert steel. Ten percent adjusted strength properties for other components were also used as discussed in Section 6.1.2.

The Alloy 22 mean material Toughness Index, I_T , using worst-case-triaxiality-adjusted vendor-averaged properties in Section 6.1.2 (see Equation 3, Section 7.1.7.2.2, Reference 2.2.15) is:

$$I_T = \varepsilon_u' \cdot (\sigma_y + \sigma_u')/2 = 0.28 \cdot (356 + 1006)/2 = 191 \text{ MPa}$$

The ratio I_T'/I_T is termed the Expended Toughness Fraction (ETF) and is a measure of the damage (Section 7.1.7.2.2, Reference 2.2.15). The wall-averaged toughness expended is I_T' , and when it is below I_T ($ETF < 1$), it is computed as:

$$I_T' = \varepsilon_{vm,tmax} \cdot (\sigma_y + \sigma_{vm,max})/2$$

ETF values less than 1.0 do not indicate failure and ETF values above 1.0 indicate failure. Simulations resulting in ETF values above 1.0 are not realistic because internal void initiation is not modeled in the simulation and localized thickness reduction (necking) is not realized. In

actuality, local strains would increase due to strain concentration effects (reduced thickness) and the voids would hook-up (coalescent) across the wall with sufficient porosity to lead to load-controlled rupture (bifurcation). Appendix I of Reference 2.2.15 discusses the phenomenon.

Nevertheless, ETF values above 1.0 are computed as a measure of the demand created by the impact. When the wall-section toughness expended, I_T' , is above I_T ($ETF > 1.0$), it is computed as:

$$I_T' = I_T + \sigma_{vm,max} \cdot (\epsilon_{vm,unload} - \epsilon_{vm,flow}), \text{ where}$$

$\epsilon_{vm,unload}$ is the EWA VM strain at the time of initiation of unloading, t_{unload} , and $\epsilon_{vm,flow}$ is the EWA VM strain at the time, t_{flow} , when most, if not all, of the elements in the wall section reach σ_u' , and the VM stress plot runs horizontal in time. This latter behavior (horizontal wall section VM stress plots at σ_u' level) is an indication of incipient failure. In some cases, a surface element on the wall section will be in bearing and/or shear contact with another structure and locally high hydrostatic stress states will prevent that element's VM stress from reaching σ_u' . This local strengthening will not prevent section failure.

For $ETF > 1.0$, at some time after "failure", the horizontal time plots of individual wall element VM stresses begin to separate and retract from σ_u' , indicating unloading. The time at initiation of stress plot separation is t_{unload} , and is the time used to determine $\epsilon_{vm,unload}$.

The governing wall section is the string of through-wall elements having the maximum ETF value. Exceptions can sometimes exist when local discontinuities at corners or welds introduce significant peak stresses. This was not the case for this calculation.

7.4.1 WP on EP on Flat Surface Impact

Table 7-15 presents a Capability calculation summary for the WP on EP (Section 7.3 determined worst case) impacting on a flat unyielding horizontal surface. Figures 7-54 to 7-61 provide the results of the simulations used to compute the ETF. The ETF values are all less than unity, therefore, only the EWA VM stress and strain states at t_{max} need to be evaluated. Figures 7-62 to 7-65 illustrate the deformation and stress profiles at t_{max} during the 14 m/s simulation.

Table 7-15 WP on EP on Flat Surface Impact Capability Summary

Impact Velocity, m/s	Element No.*	$\sigma_{vm,max}$ MPa	t_{max} sec	$\epsilon_{vm,tmax}$ m/m	I_T' MPa	ETF = I_T'/I_T
1.5	37018	486	0.01489	0.06093	26	0.14
3.16 (20 in drop)	38017	580	0.01600	0.10332	48	0.25
10	35083	603	0.00500	0.11424	55	0.29
15	37036	631	0.00320	0.12205	60	0.31

*Element number of solid element on inner surface of OCB for selected wall section

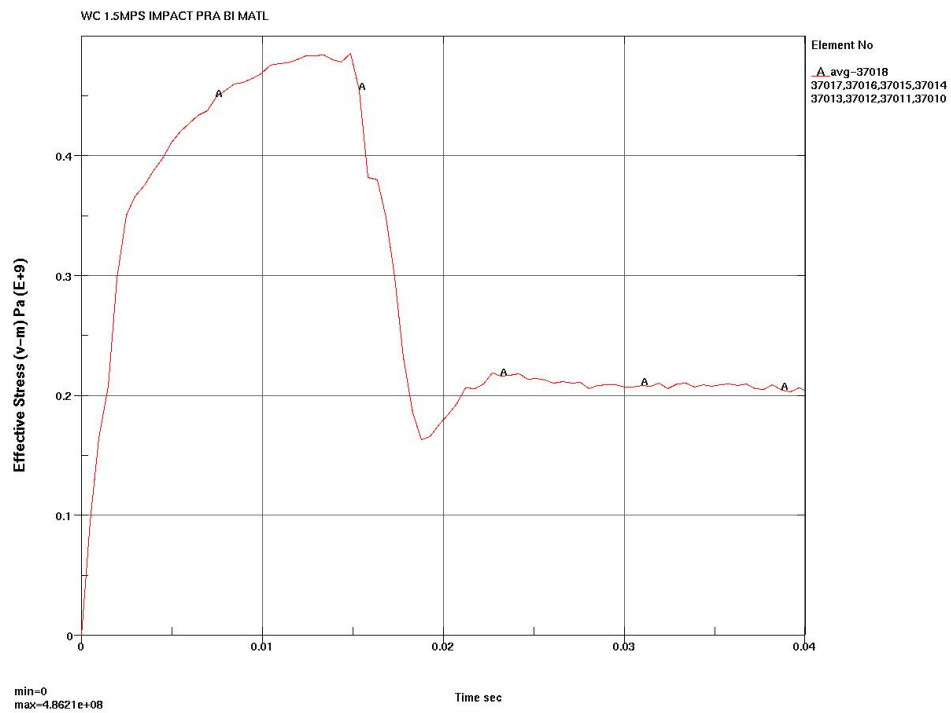


Figure 7-54 1.5 m/s, EWA VM Stress

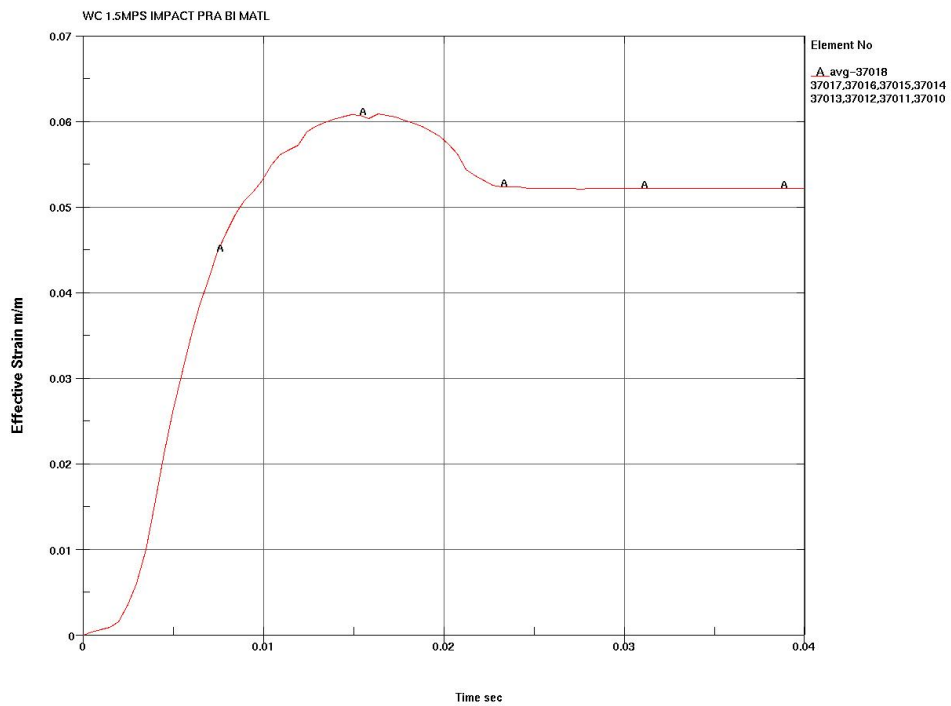


Figure 7-55 1.5 m/s EWA VM Strain

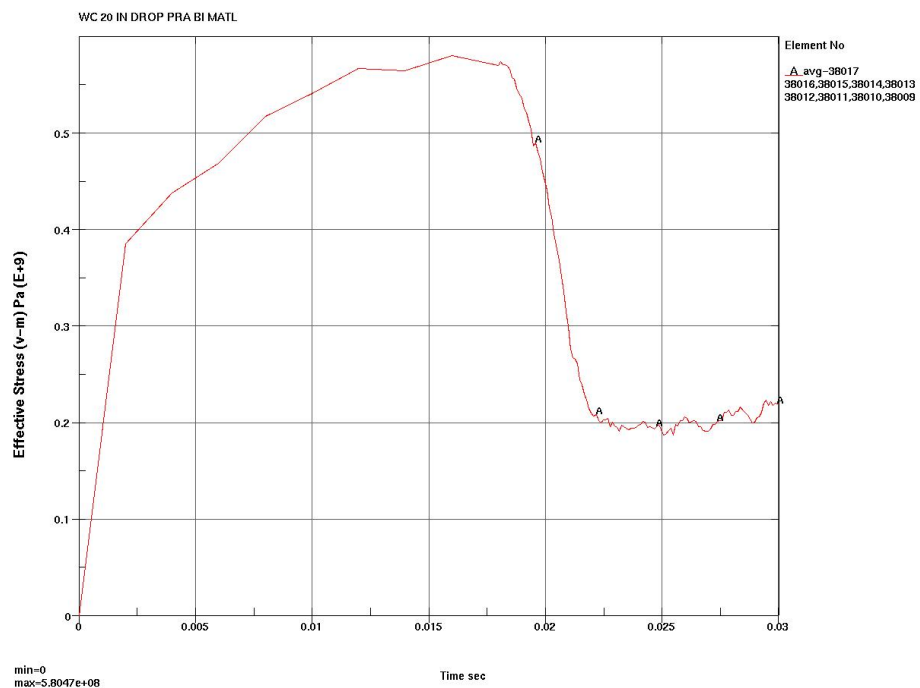


Figure 7-56 20 in Drop EWA VM Stress

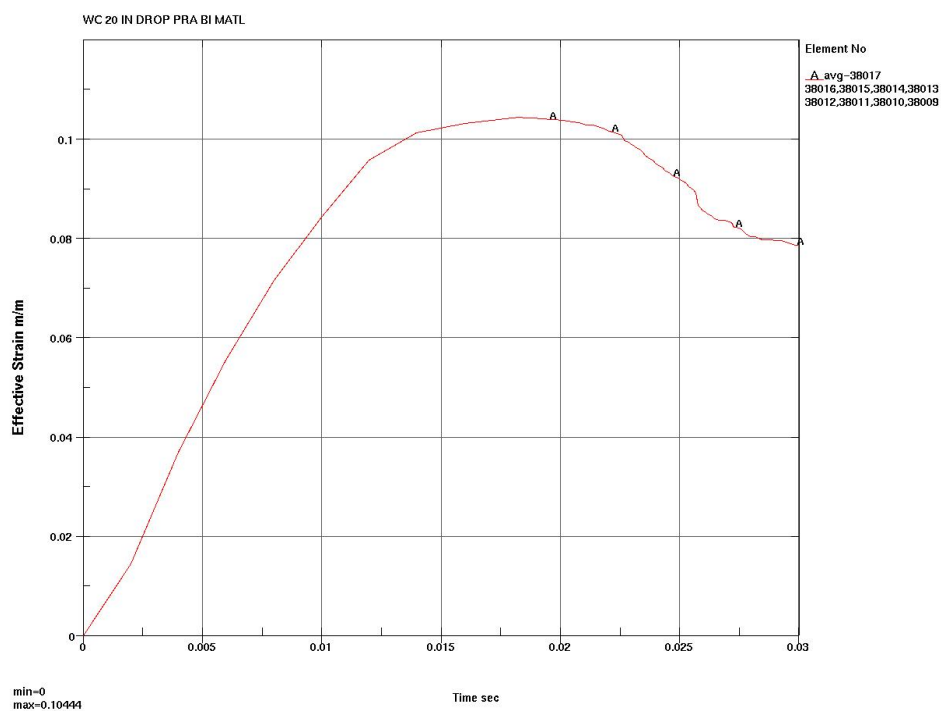


Figure 7-57 20 in Drop EWA VM Strain

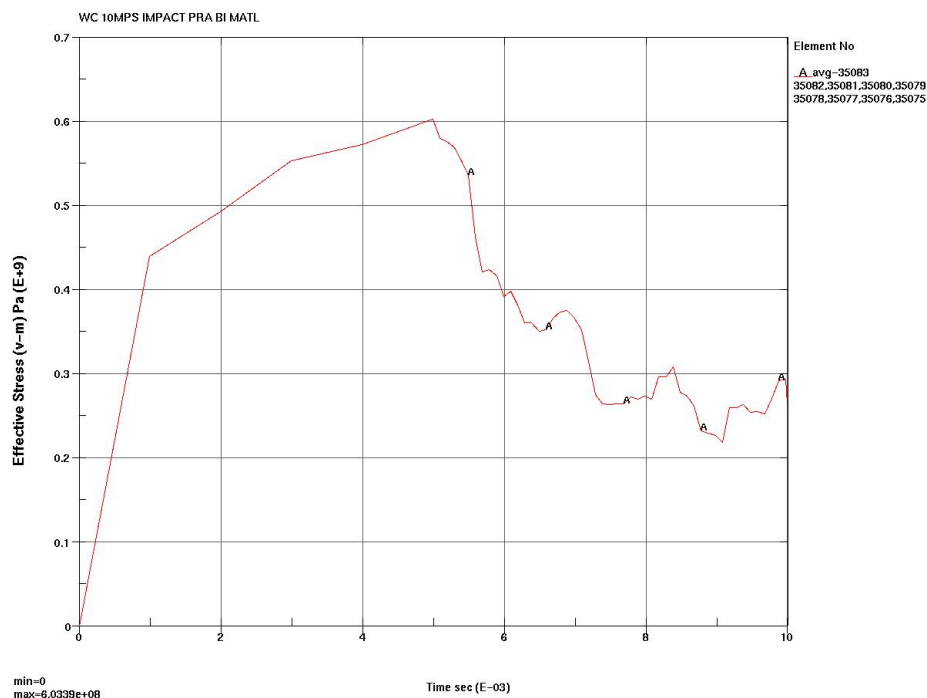


Figure 7-58 10 m/s EWA VM Stress

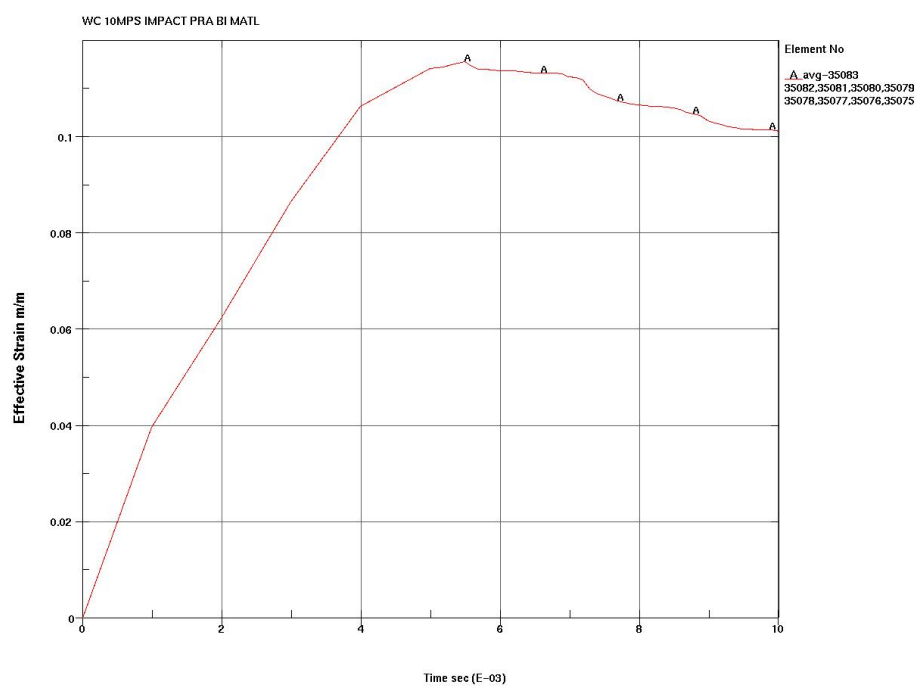


Figure 7-59 10 m/s EWA VM Strain

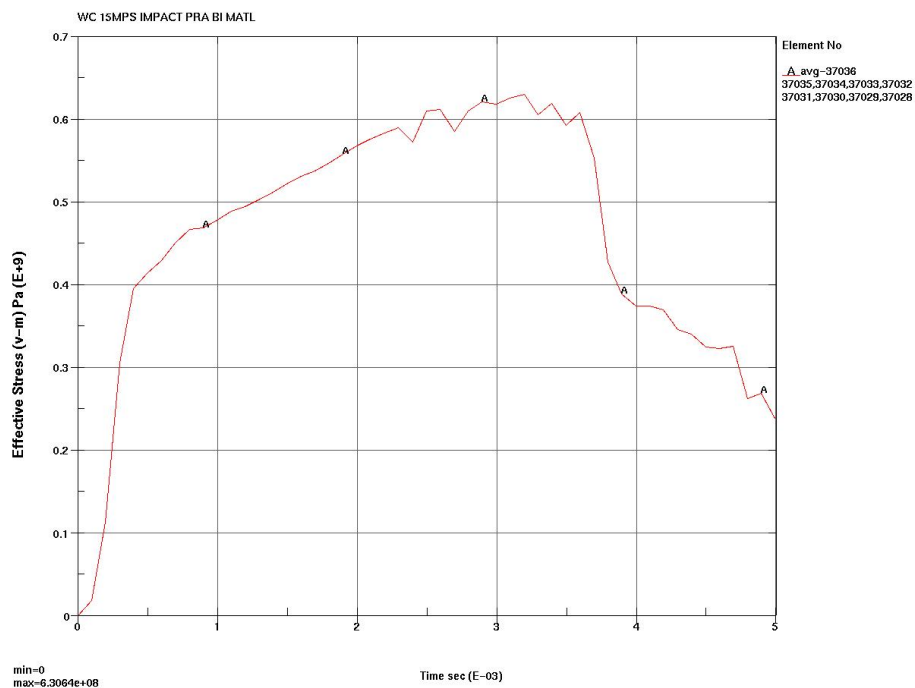


Figure 7-60 15 m/s EWA VM Stress

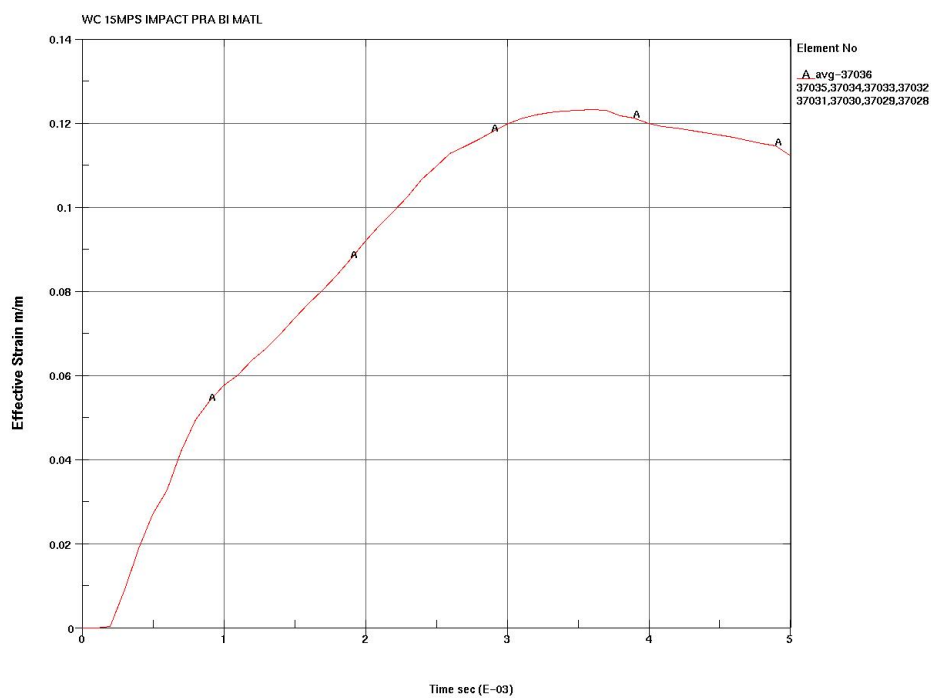


Figure 7-61 15 m/s EWA VM Strain

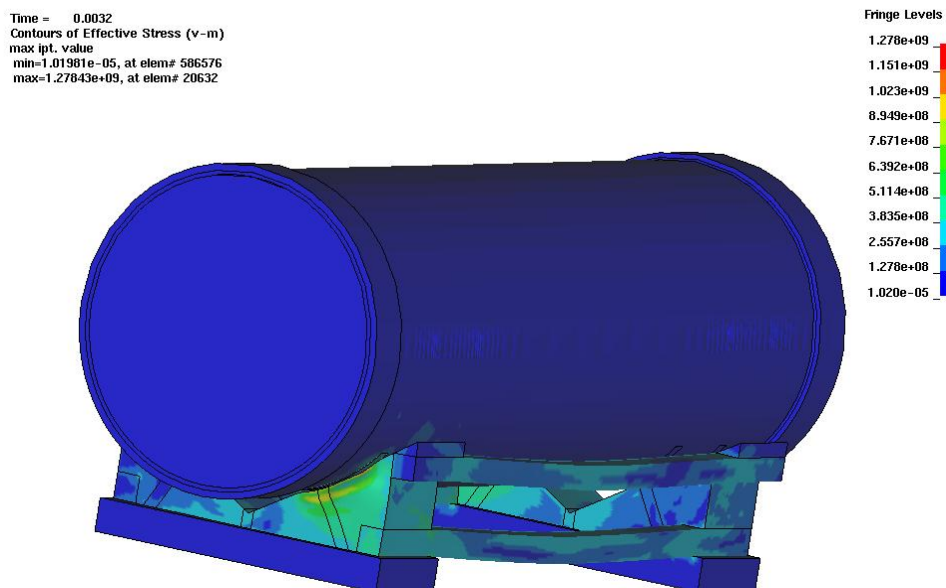


Figure 7-62 15 m/s Maximum EP VM Stresses (Pa) and Distortions

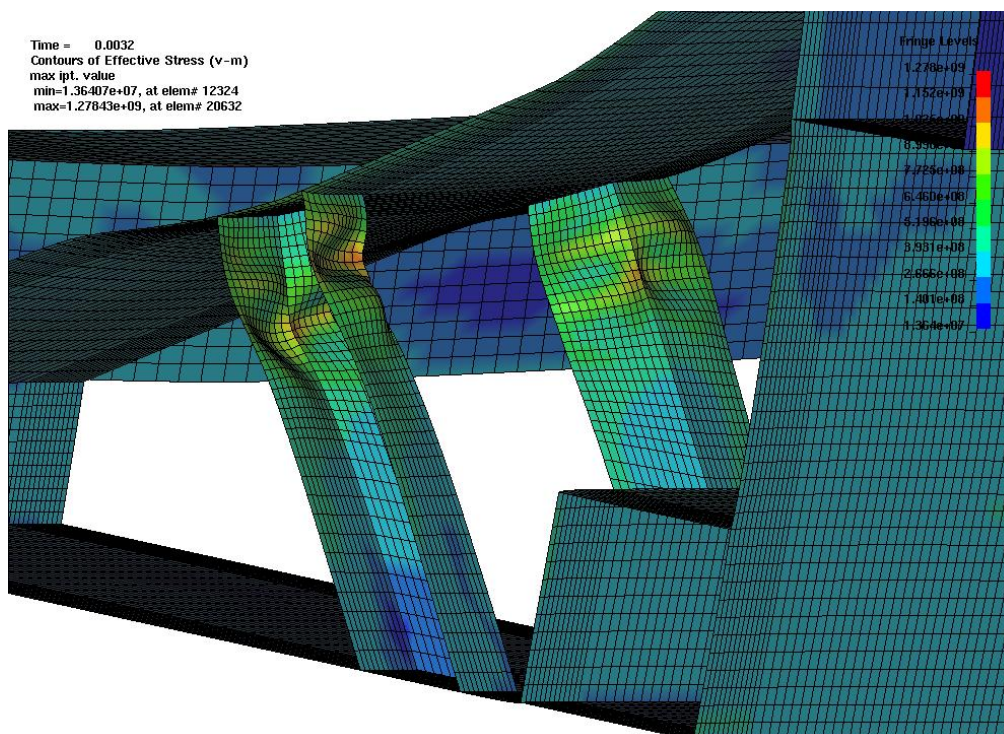


Figure 7-63 Cutaway, 15 m/s Maximum EP VM Stresses (Pa) and Distortions

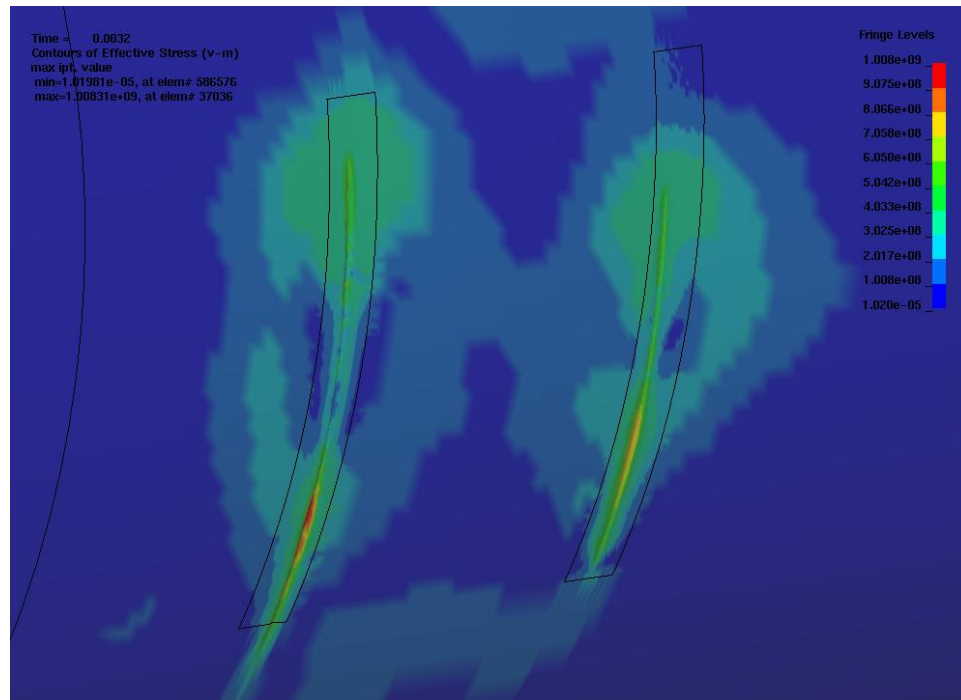


Figure 7-64 15 m/s Maximum WP VM Stresses (Pa) and Distortions

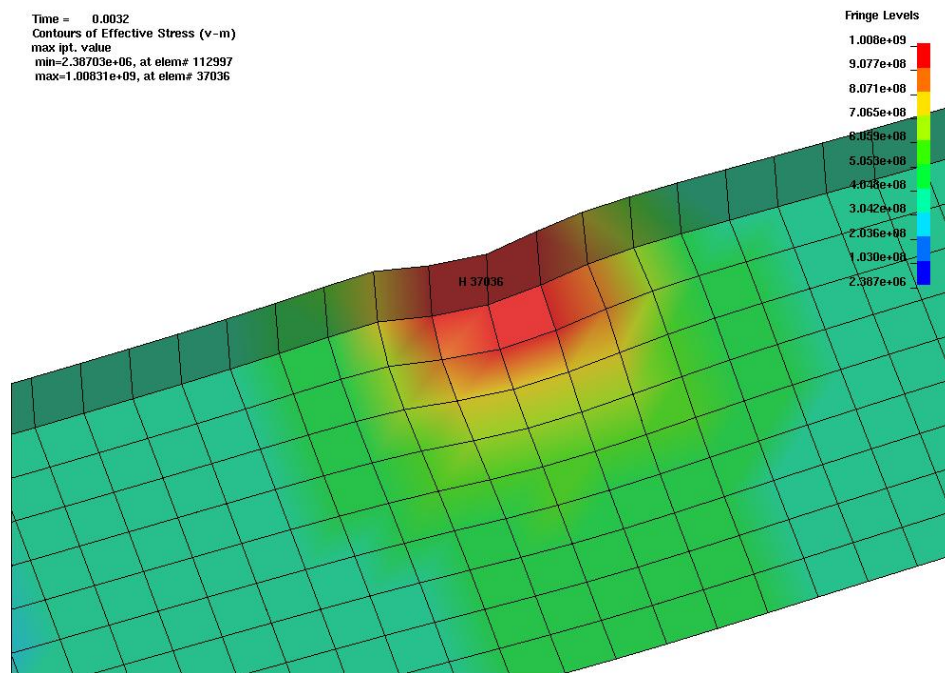


Figure 7-65 Wall Section Close-up 15 m/s Maximum WP VM Stresses (Pa) and Distortions

OCB failure is not predicted for any of the impact velocities (all ETF values < 1.0). The maximum single element VM stress in the governing wall section barely reaches σ_u' . In this situation, identical solution results are obtained using the bilinear version of the triaxiality adjusted OCB stress-strain material curve, i.e., without the horizontal shape past (σ_u', e_u') .

The EP is dissipating the kinetic energy of the impact through plastic distortions and even though stresses well above the EP ultimate strength are evident, the EP is not stiff enough to induce high contact zone stresses into the OCB. Additionally, the EP sidewalls and support tubes are plastically collapsing without significant stiffness change. Therefore, the contact zone stresses in the OCB are fairly constant, regardless of impact velocity. The 1.5 m/s case was needed to estimate the initiation of this EP plastic collapse mechanism. Figure 7-66 plots the Table 7-15 results. A failure level (ETF = 1.0) could be extrapolated from Figure 7-66, but the value of velocity would be well above any physically realistic level.

This indicates that the WP on EP impact will never fail at the contact zone between WP and EP. This is because at higher load levels, the WP will crush through the EP without significantly higher stresses and strike structure below the EP. This second impact on the WP sleeves or shell will transfer any further momentum loading away from the WP to EP contact zone load path.

This also indicates the conservatism in the deterministic calculation. The Table 7-15 ETF for the 20 inch drop is 0.25 while the governing EWA SI for the deterministic 20 inch drop is $0.6\sigma_u$ which has a minimum “damage fraction” of 0.67 (using the highest $0.9\sigma_u$ limit of Section 7.1.4 of Reference 2.2.15).

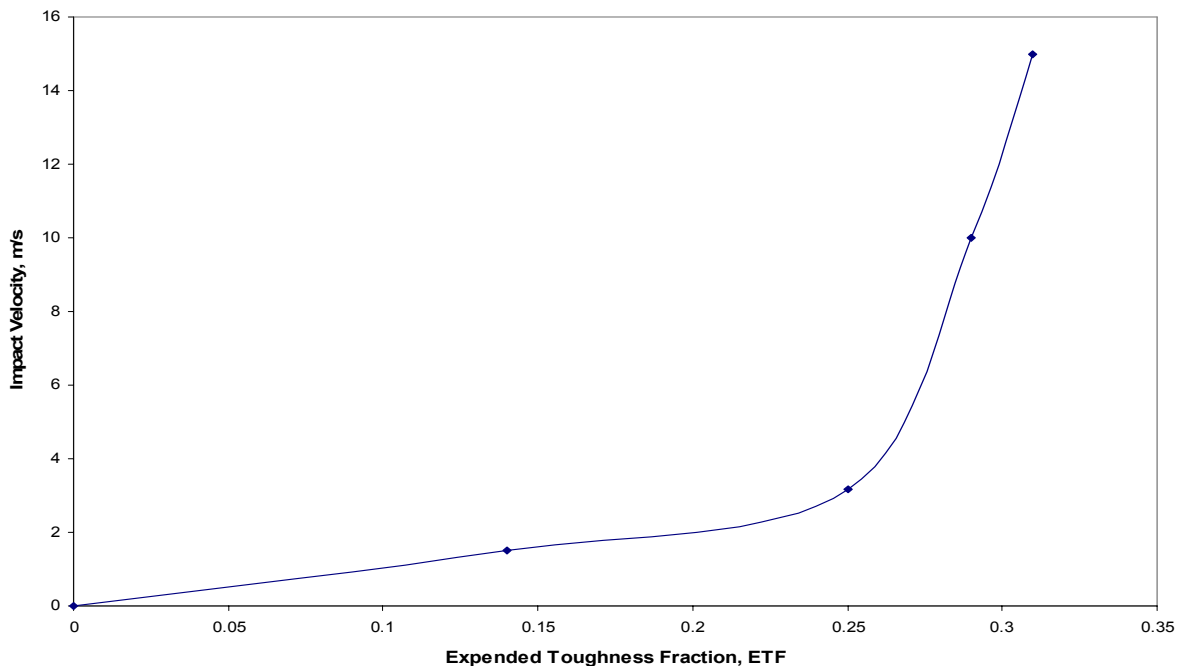


Figure 7-66 Summary Plot, WP on EP Impact on Flat Surface

7.4.2 Worst Case WP on EP on Invert Impact

Table 7-16 presents a summary of the Capability calculation for the WP centered on the EP bridging the invert structure's longitudinal steel beams and the WP impacting the transverse steel beams after the EP crushes. The worst case orientation depicted in Figures 6-43 to 6-45 is evaluated for three impact velocities. Figures 7-67 to 7-77 provide the results of the simulations used to compute the ETF. Note the delay in significant stresses until the EP has collapsed and the WP finally reaches the invert steel. Expanded time scale plots of the VM stresses are needed for the 14 m/s calculation to determine t_{flow} and t_{unload} and are used for the EWA VM strain plot to facilitate $\epsilon_{\text{vm,flow}}$ and $\epsilon_{\text{vm,unload}}$ determination. Figures 7-78 to 7-89 illustrate the deformation and stress profiles at different times during the 14 m/s simulation.

Table 7-16 Worst Case WP on EP on Invert Impact Capability Summary

Impact Velocity, m/s	Element No.*	$\sigma_{\text{vm,max}}$ MPa	t_{max} or t_{flow} sec	$\epsilon_{\text{vm,tmax}}$ or $\epsilon_{\text{vm,flow}}$ m/m	t_{unload} sec	ϵ_{unload} m/m	I_T' MPa	ETF = I_T'/I_T
10	79075	640	0.0427	0.1234	-	-	61.4	0.32
12	79102	947	0.0330	0.2427	-	-	158	0.83
14	79057	1000	0.0245	0.2658	0.0285	0.3420	267	1.40

* Element number of solid element on inner surface of OCB for selected wall section

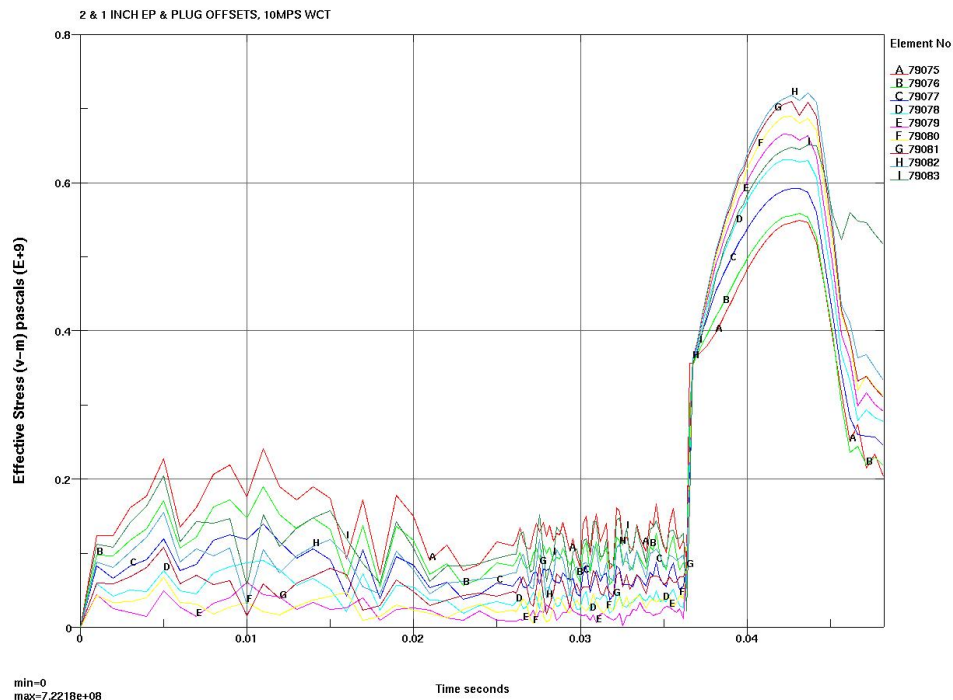


Figure 7-67 10 m/s VM Stresses

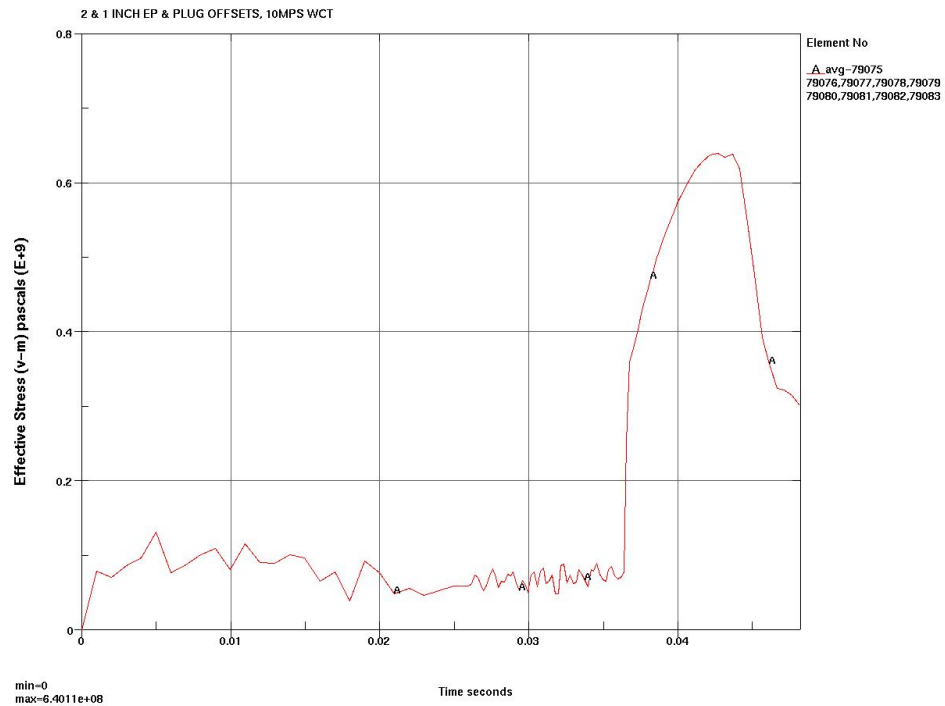


Figure 7-68 10 m/s EWA VM Stress

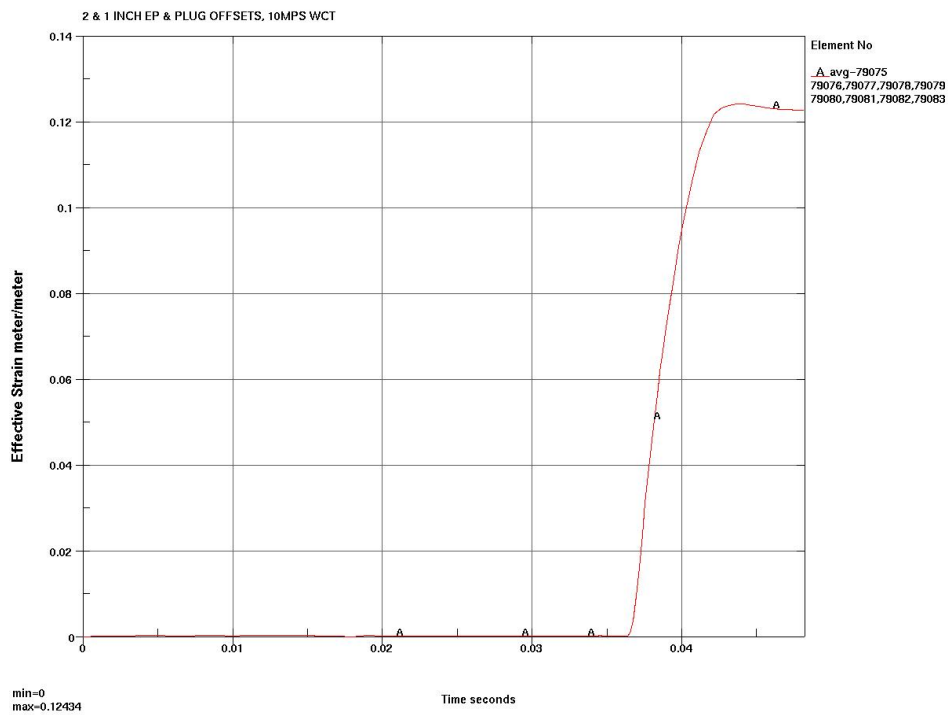


Figure 7-69 10 m/s EWA VM Strain

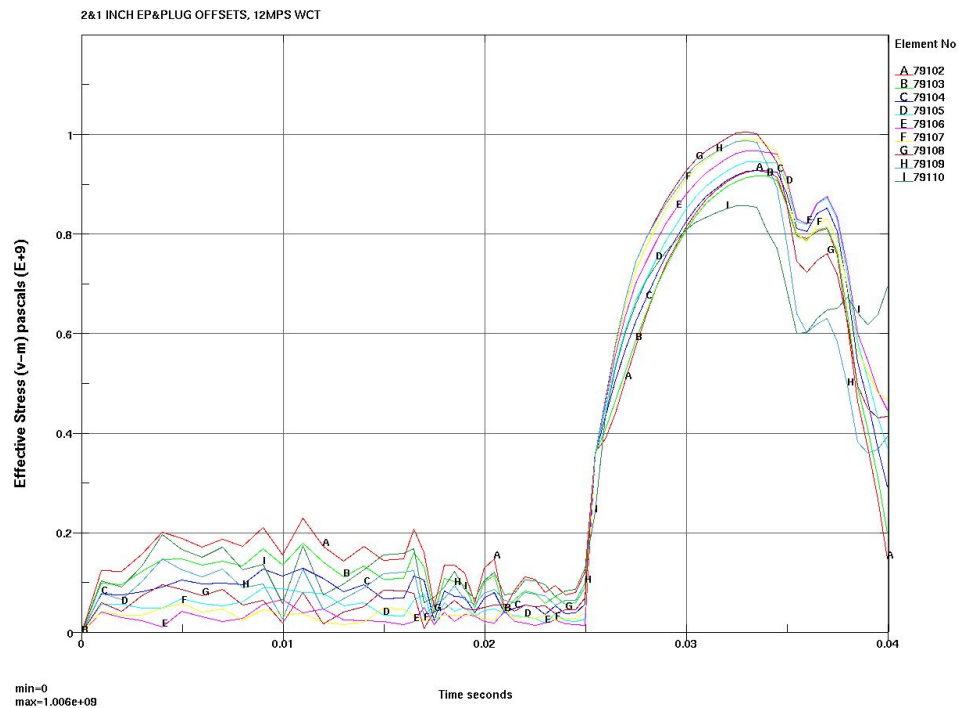


Figure 7-70 12 m/s VM Stresses

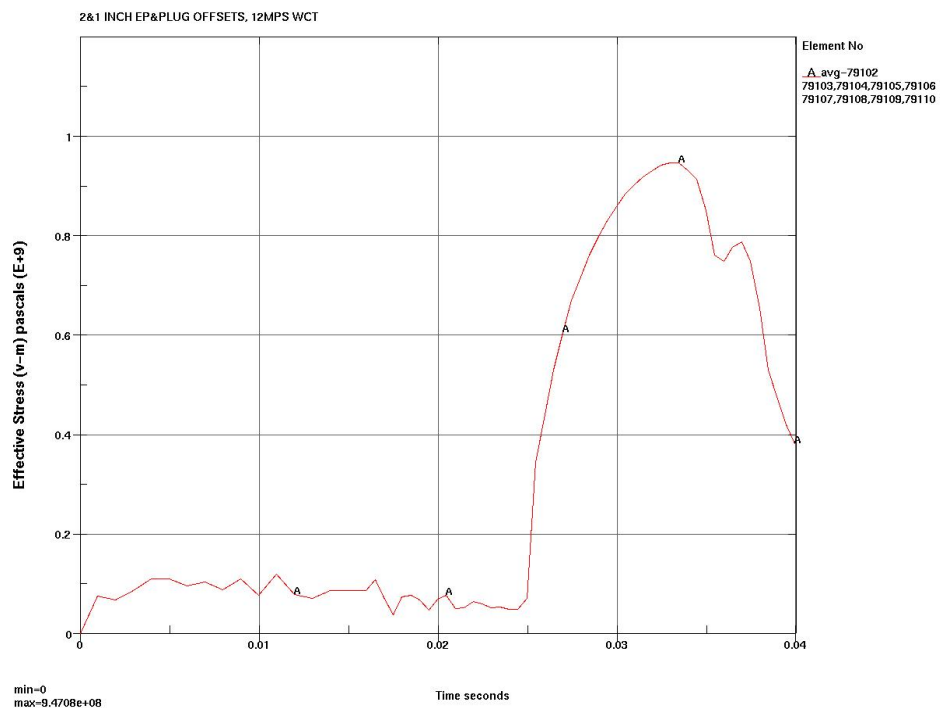


Figure 7-71 12 m/s EWA VM Stress

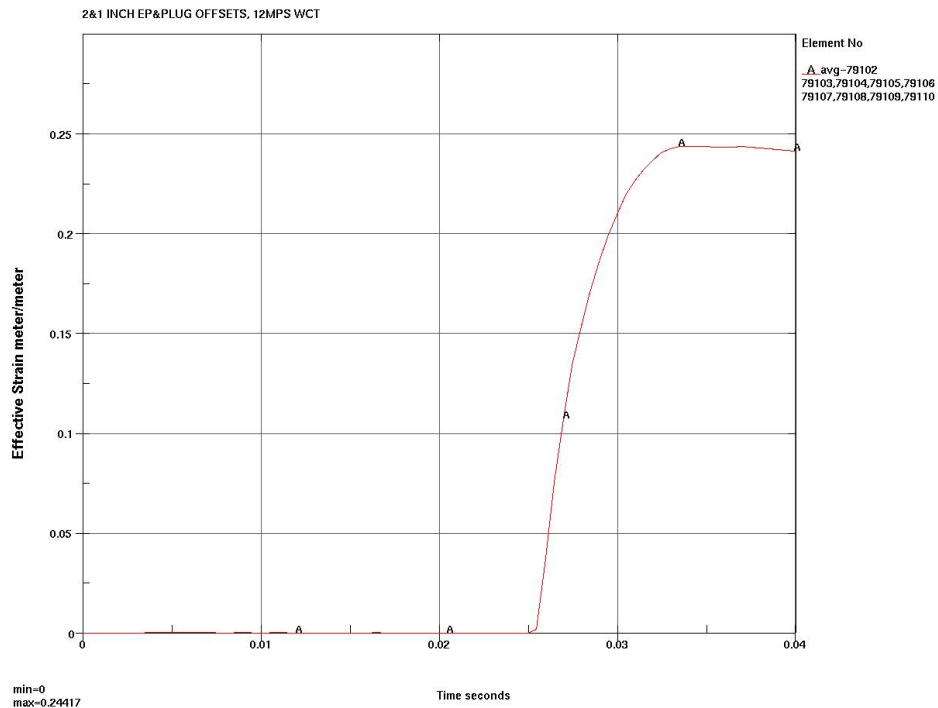


Figure 7-72 12 m/s EWA VM Strain

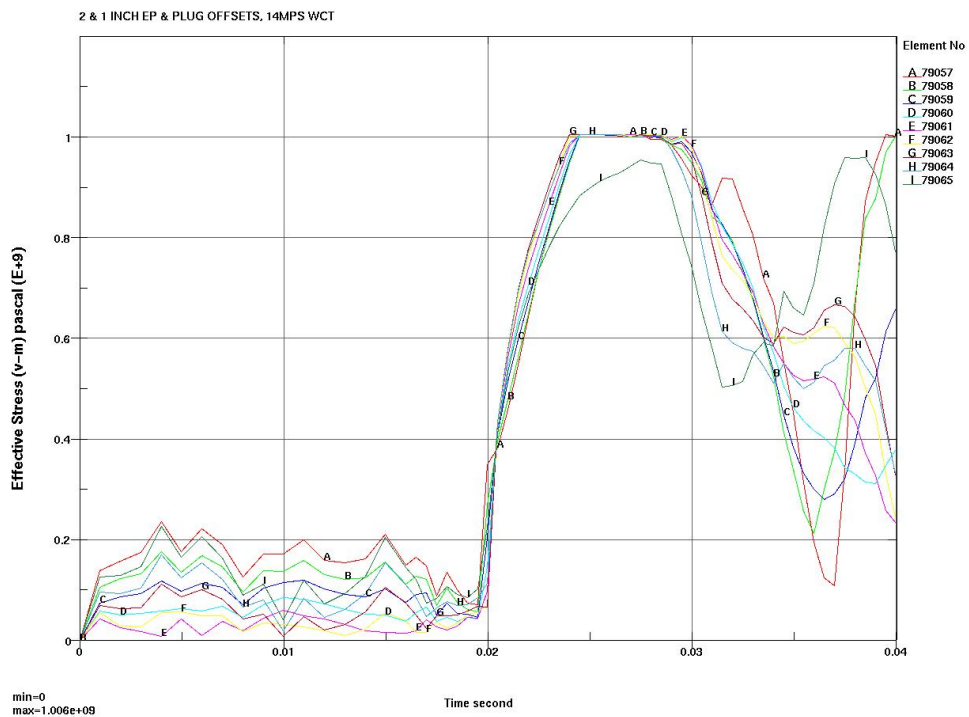


Figure 7-73 14 m/s VM Stresses

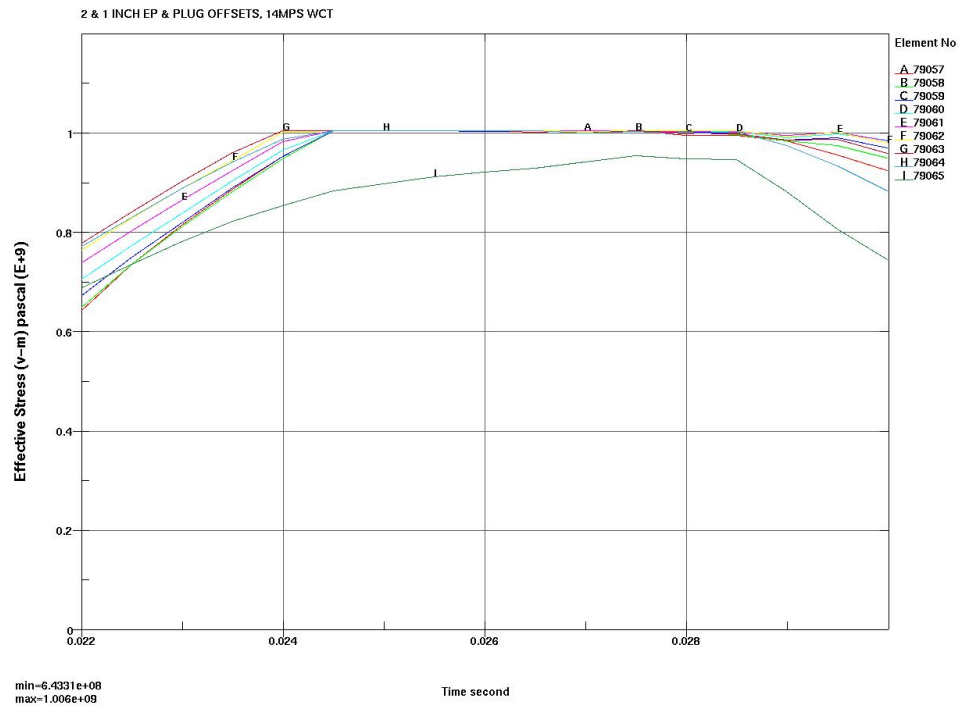


Figure 7-74 14 m/s VM Stresses, Expanded Time Scale

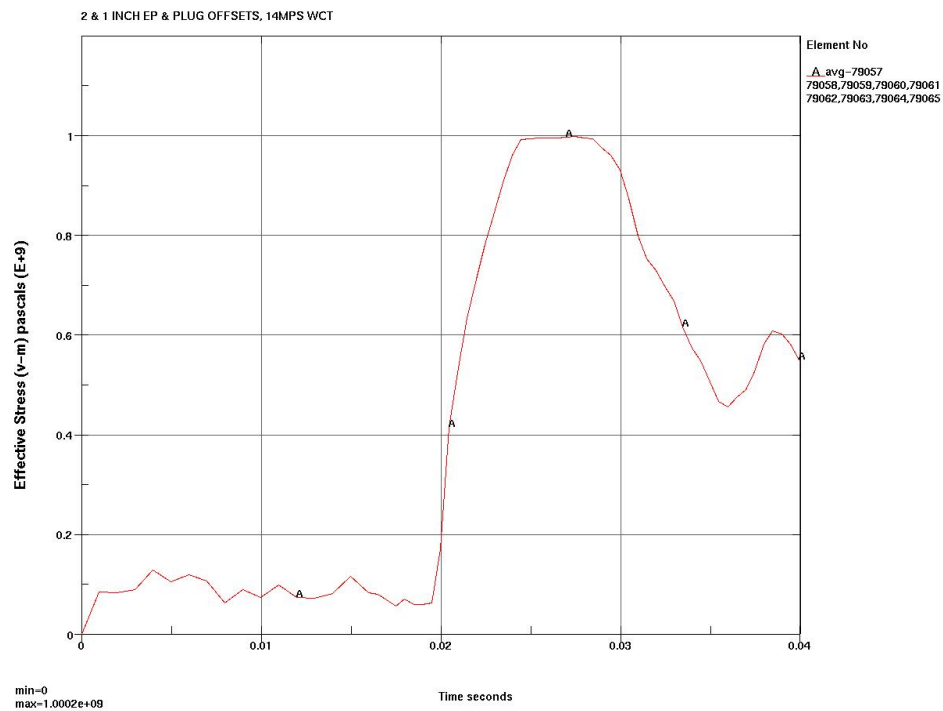


Figure 7-75 14 m/s EWA VM Stress

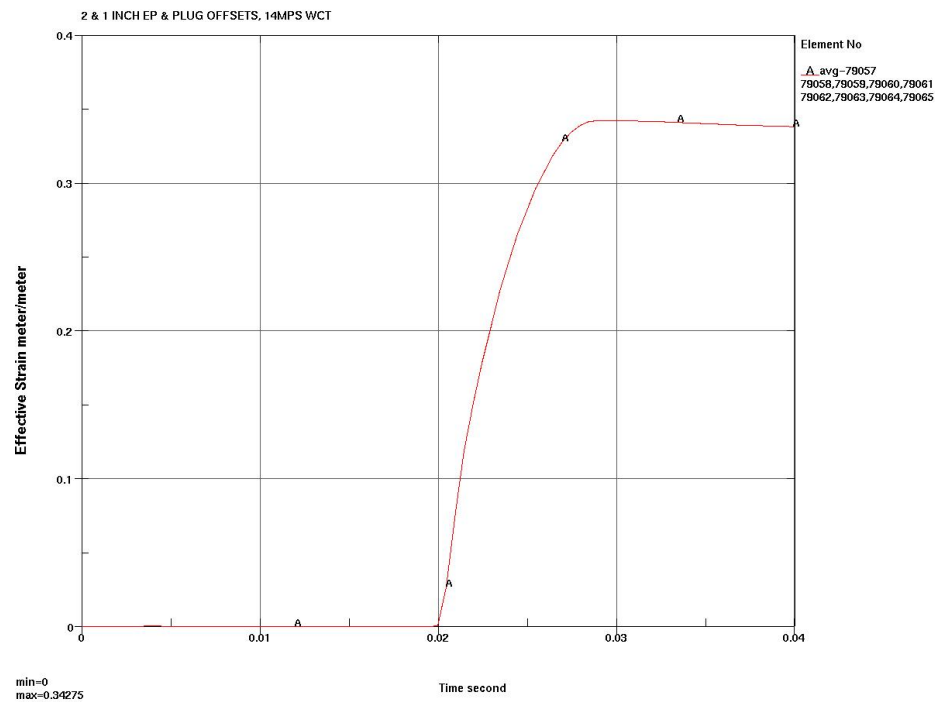


Figure 7-76 14 m/s EWA VM Strain

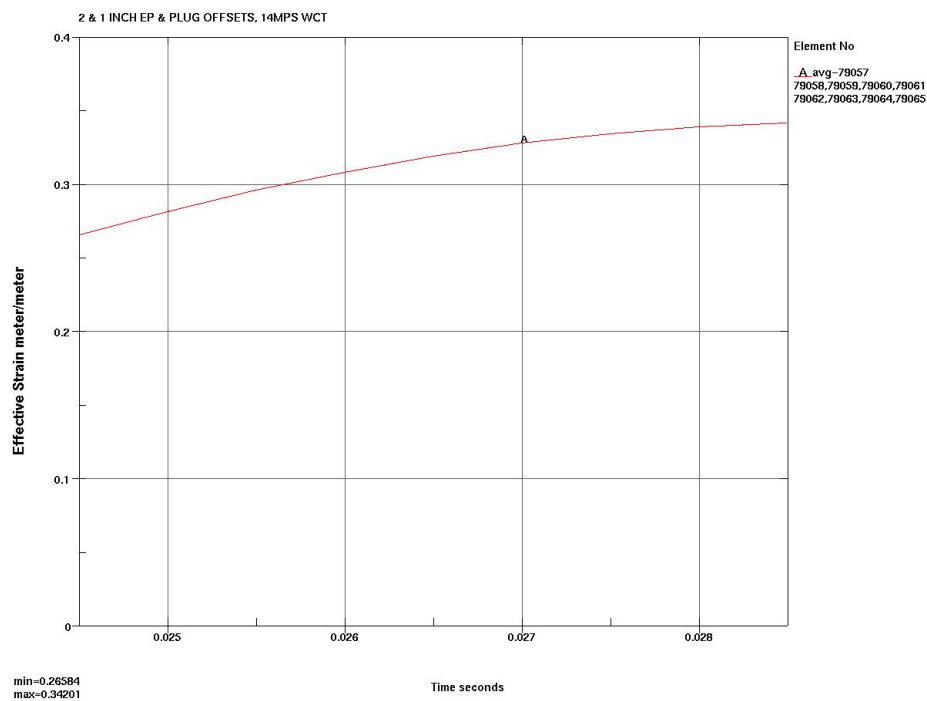


Figure 7-77 14 m/s EWA VM Strain, Expanded Time Scale

2 & 1 INCH EP & PLUG OFFSETS, 14MPS WCT
Time = 0.0049999

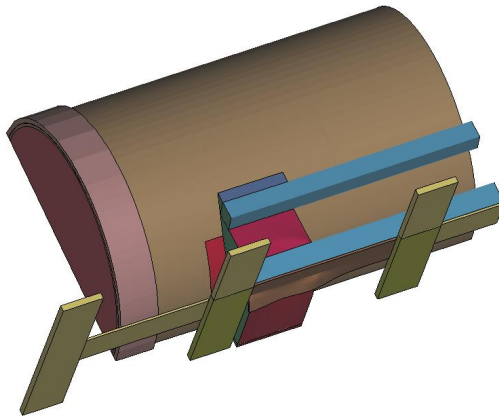


Figure 7-78 14 m/s WP on EP on Invert Impact, 5 ms Back View

2 & 1 INCH EP & PLUG OFFSETS, 14MPS WCT
Time = 0.01

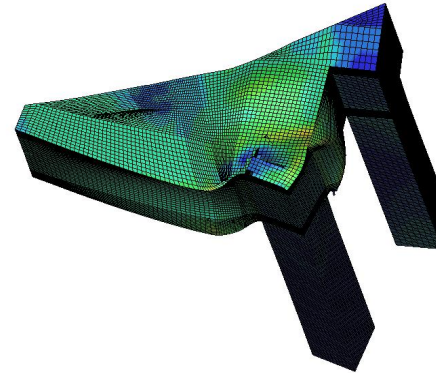


Figure 7-80 14 m/s WP on EP on Invert Impact, 10 ms, EP Only

2 & 1 INCH EP & PLUG OFFSETS, 14MPS WCT
Time = 0.025

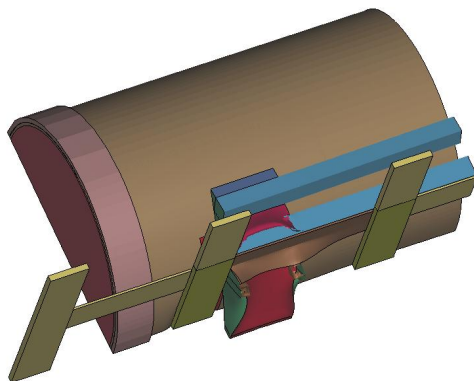


Figure 7-79 14 m/s WP on EP on Invert Impact, 25 ms Back View

2 & 1 INCH EP & PLUG OFFSETS, 14MPS WCT
Time = 0.0255

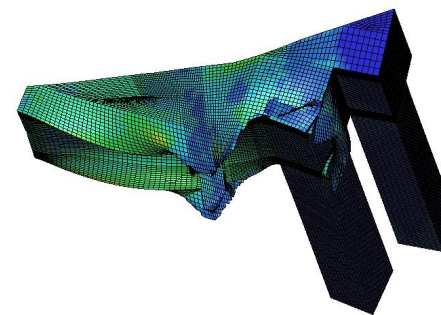


Figure 7-81 14 m/s WP on EP on Invert Impact, t_{unload} , EP Only

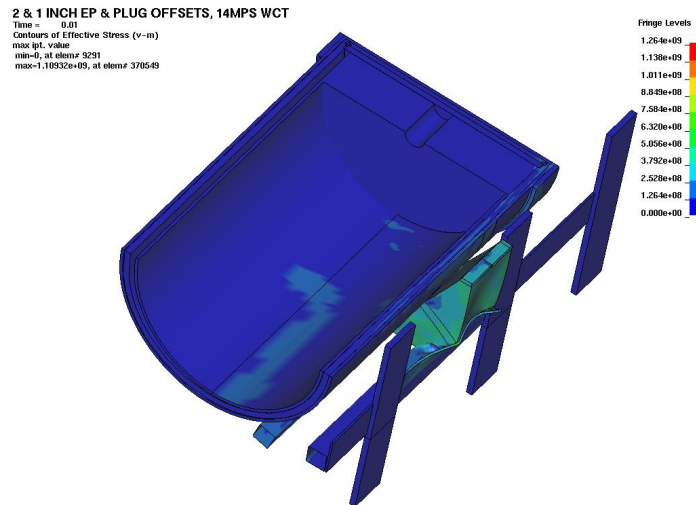
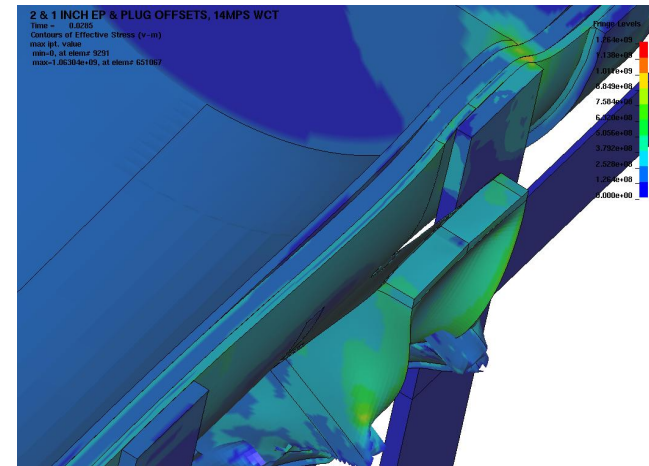
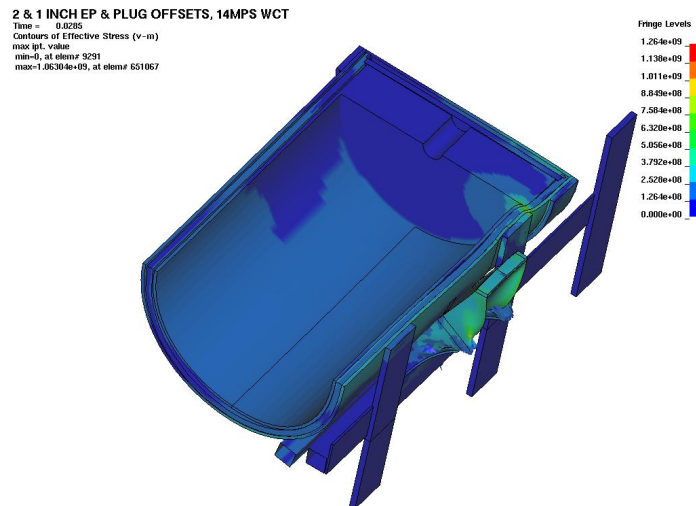
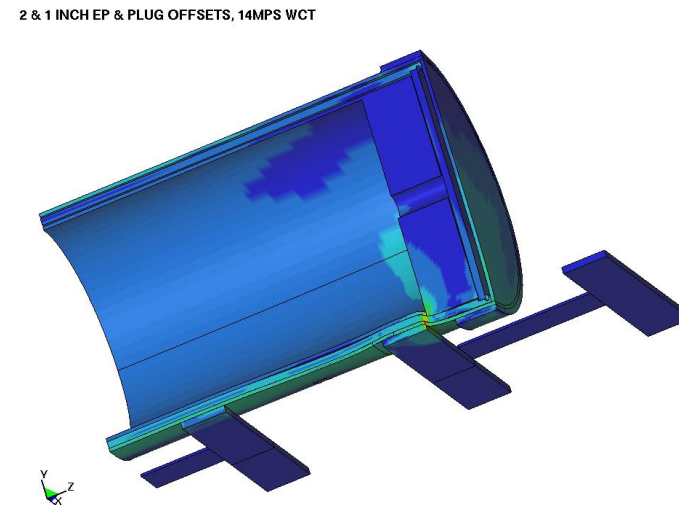


Figure 7-82 14 m/s WP on EP on Invert Impact, 10 ms, Pa

Figure 7-84 14 m/s WP on EP on Invert Impact, t_{unload} , PaFigure 7-83 14 m/s WP on EP on Invert Impact, t_{unload} , PaFigure 7-85 14 m/s WP on EP on Invert Impact, t_{unload}

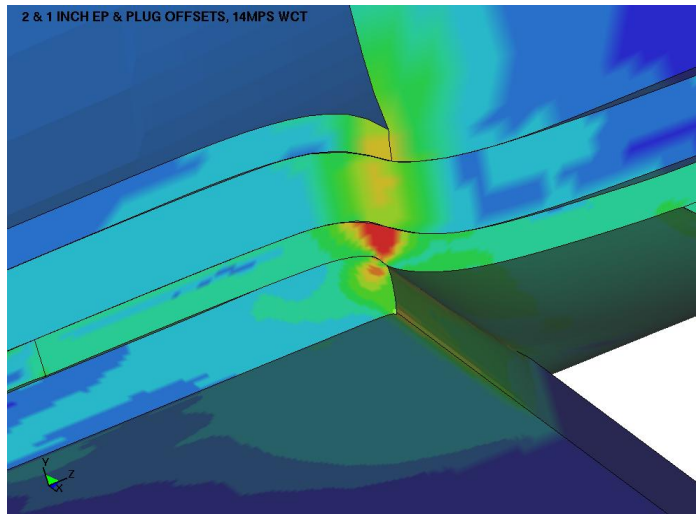


Figure 7-86 14 m/s WP on EP on Invert Impact, t_{unload} , Failure Zone

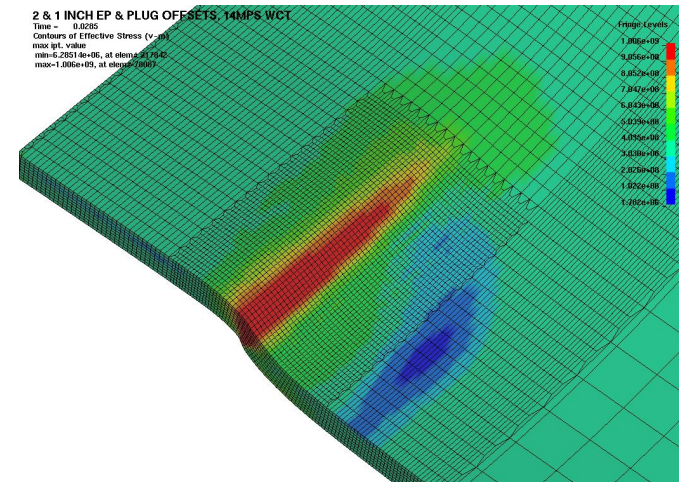


Figure 7-88 14 m/s WP on EP on Invert Impact, t_{unload} , OCB, Pa

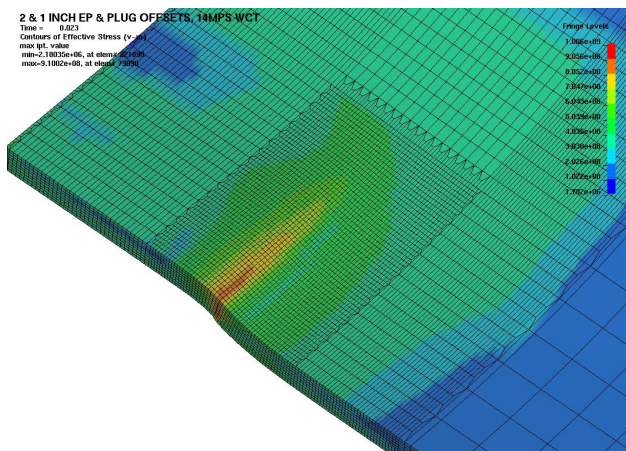


Figure 7-87 14 m/s WP on EP on Invert Impact, 23 ms, OCB, Pa

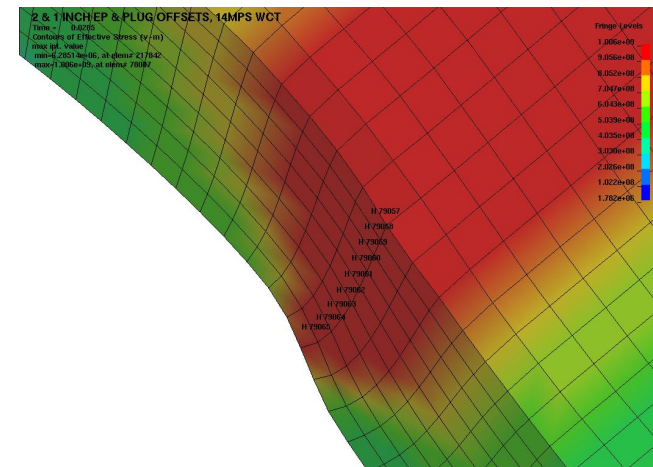


Figure 7-89 14 m/s WP on EP on Invert Impact, t_{unload} , OCB, Pa

The EP severely distorts the longitudinal beam's top flange and a significant amount of the EP is eroded. Figure 7-90 is a plot of the Table 7-16 velocities versus ETF and indicates that the (mean) velocity Capability for this event sequence is 12.6 *m/s*.

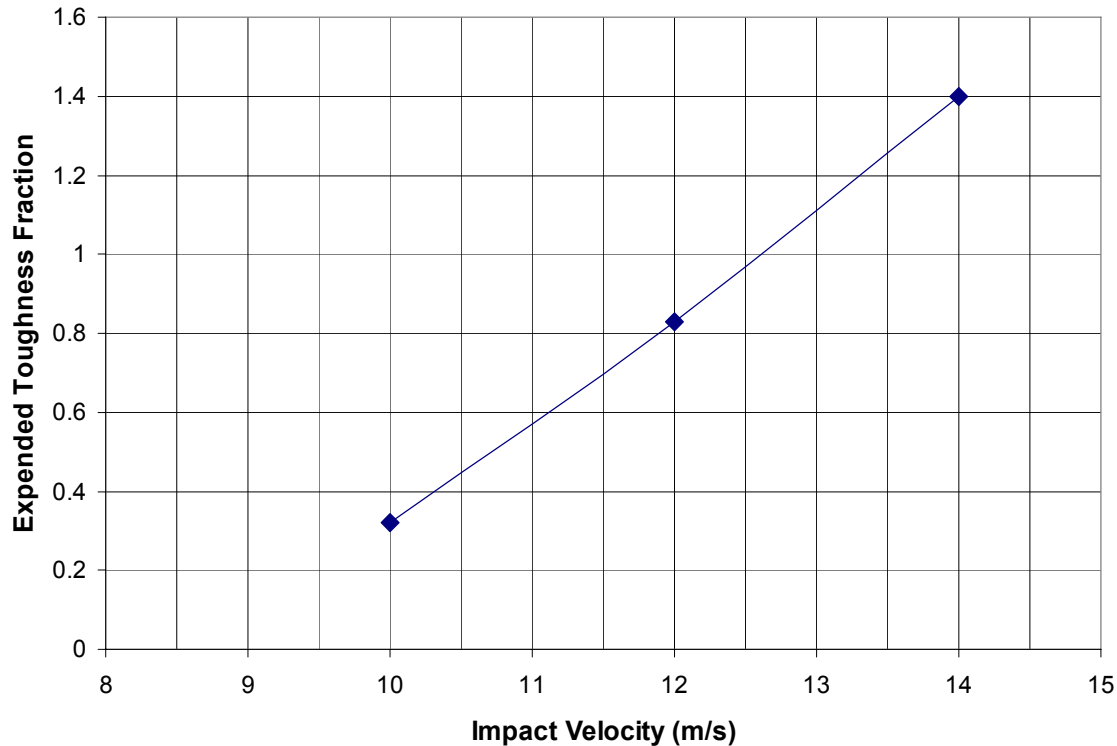


Figure 7-90 WP on EP on Invert Worst Case Impact Velocity Capability Trend

7.4.3 WP on Invert Impact

Table 7-17 presents a summary of the Capability calculation for the WP impacting the invert steel structure's transverse beams without any intervening EP. The various orientations depicted in Figures 6-47, 6-48, and 6-50 to 6-53 are evaluated for different impact velocities. Figures 7-91 to 7-120 provide the results of the simulations used to compute the ETF.

Truncated time plots of the VM stresses are presented to graphically define times t_{\max} , t_{flow} and t_{unload} used to construct truncated EWA VM strain plots with $\epsilon_{\text{vm},t_{\max}}$, $\epsilon_{\text{vm},t_{\text{flow}}}$ and $\epsilon_{\text{vm},t_{\text{unload}}}$ as posted extremes. Figures 7-121 to 7-125 illustrate the overall behavior and the governing wall section's deformation and VM stress component profiles (in pascals) at time t_{unload} during the 18 degree tilted 5 *m/s* impact simulation.

Table 7-17 WP on Invert Impact Capability Summary

deg / in*	Figs 7-x to 7-y	m/s	Element No.**	$\sigma_{vm,max}$ MPa	t_{max} or t_{flow} sec	$\epsilon_{vm,tmax}$ or $\epsilon_{vm,flow}$ m/m	t_{unload} sec	ϵ_{unload} m/m	I_T' MPa	ETF = I_T'/I_T
0 / 8	91-94	8	117451	637.8	0.0230	0.1194	-	-	59	0.31
0 / 1	95-98	4	79084	678.8	0.0075	0.1391	-	-	72	0.38
0 / 1	99-102	8	79102	990.4	0.0086	0.2697	-	-	182	0.95
0 / 1	103-107	10	79084	1002.2	0.0048	0.2732	0.0086	0.3358	253	1.33
5 / 1	108-111	4	79093	909.5	0.0124	0.2321	-	-	147	0.77
10 / 1	112-115	4	79102	937.1	0.0124	0.2448	-	-	158	0.83
18 / 1	6-7	4	79570	957.7	0.0136	0.2472	-	-	162	0.85
18 / 1	116-120	5	79561	993.1	0.0104	0.2659	0.0130	0.2787	203	1.07

* Orientation: Degrees WP angled on invert / Inches top plug offset from edge invert steel flange

** Element number of solid element on inner surface of OCB at governing wall section

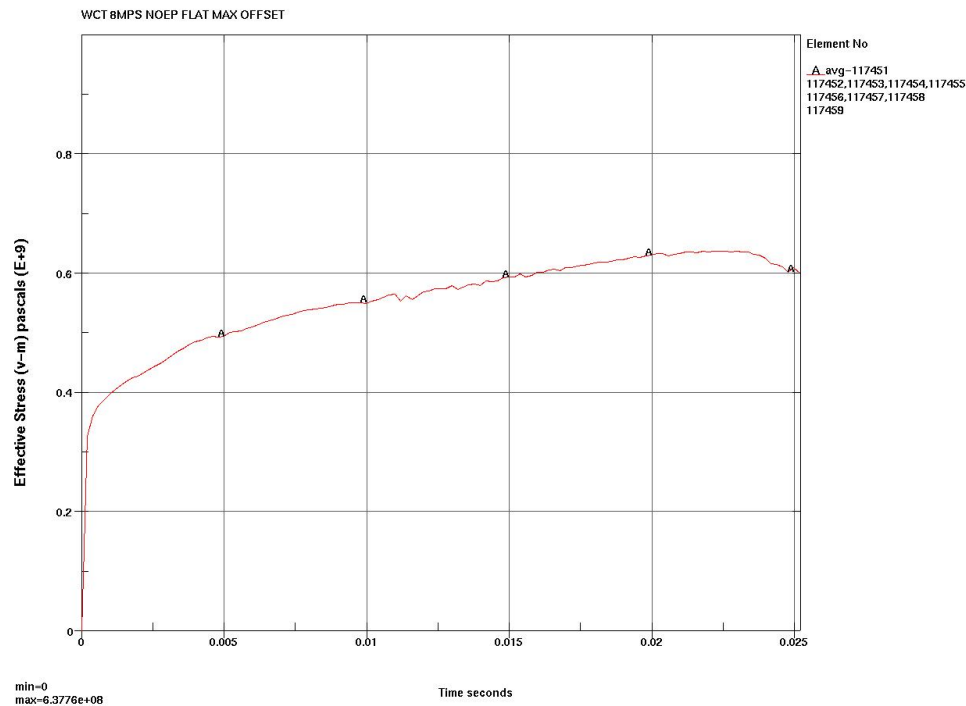


Figure 7-91 Flat 8 m/s Impact, 8 in Offset, EWA VM Stress

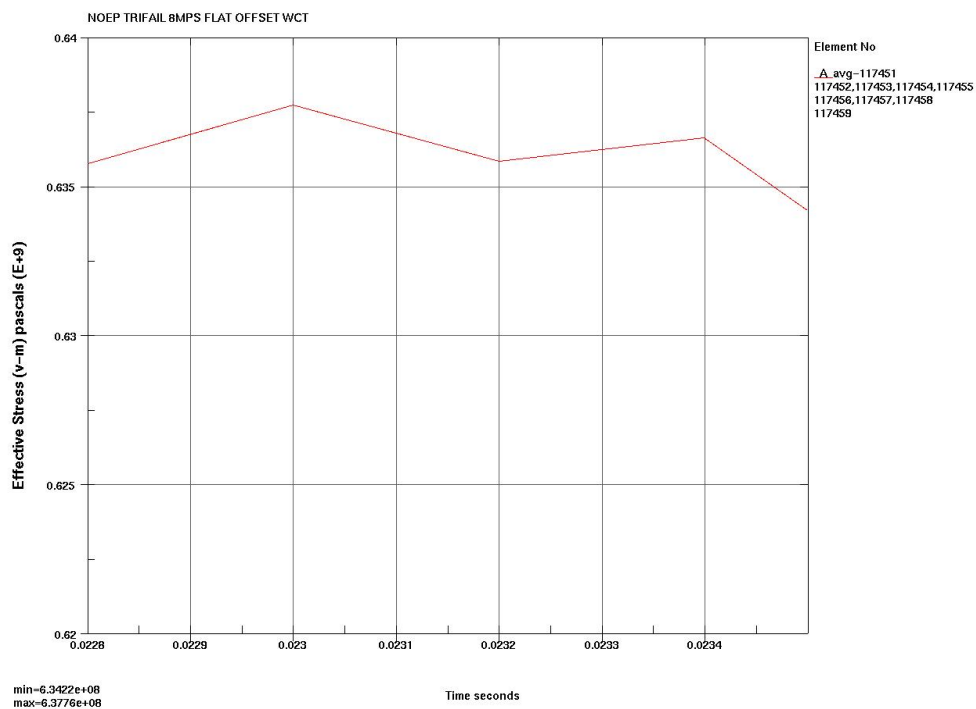
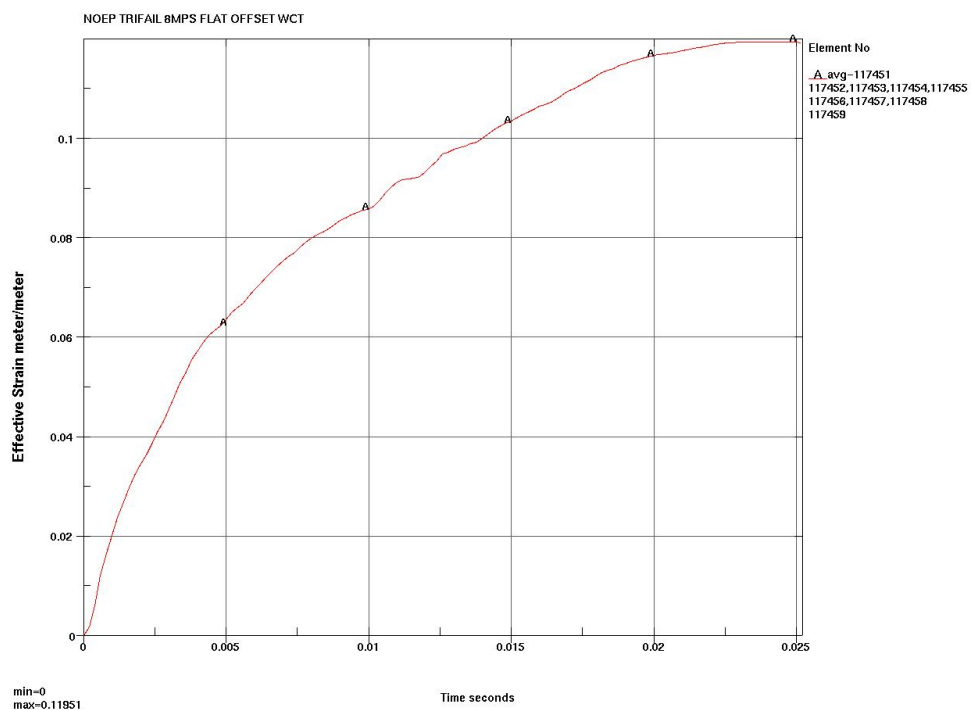
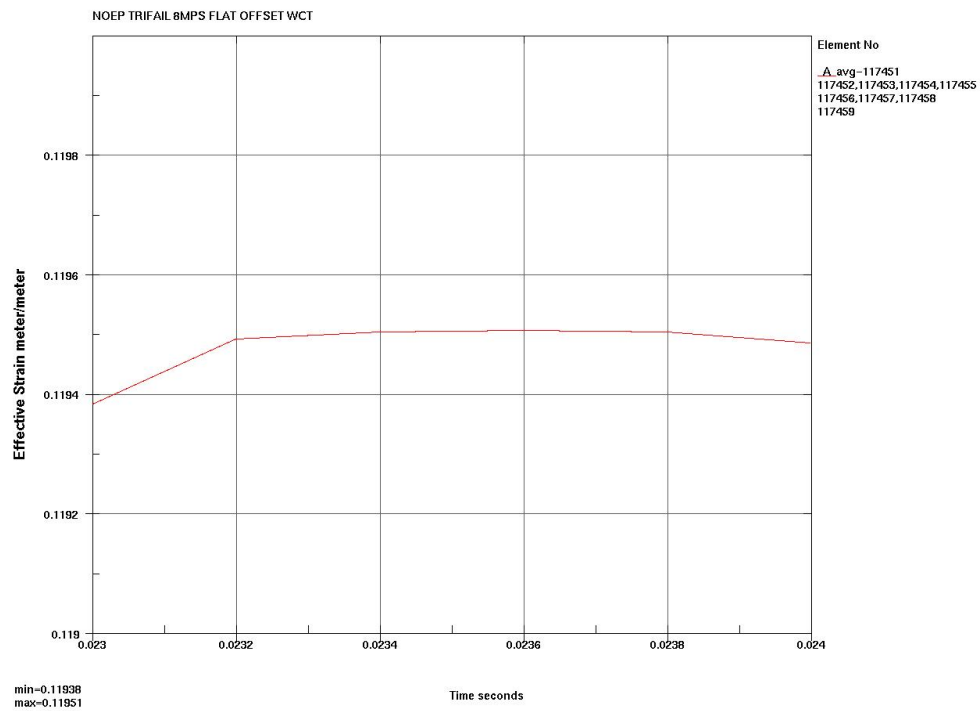
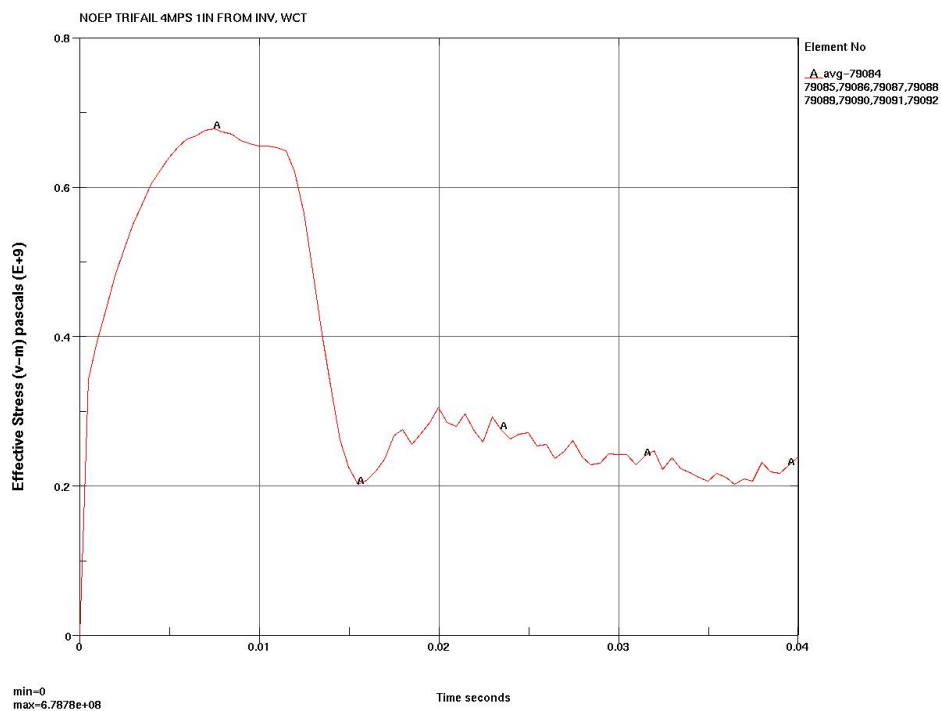
Figure 7-92 Flat 8 m/s Impact, 8 in Offset, t_{\max} of EWA VM Stress

Figure 7-93 Flat 8 m/s Impact, 8 in Offset, EWA VM Strain

Figure 7-94 Flat 8 *m/s* Impact, 8 *in* Offset, EWA VM Strain at t_{\max} Figure 7-95 Flat 4 *m/s* Impact, 1 *in* Offset, EWA VM Stress

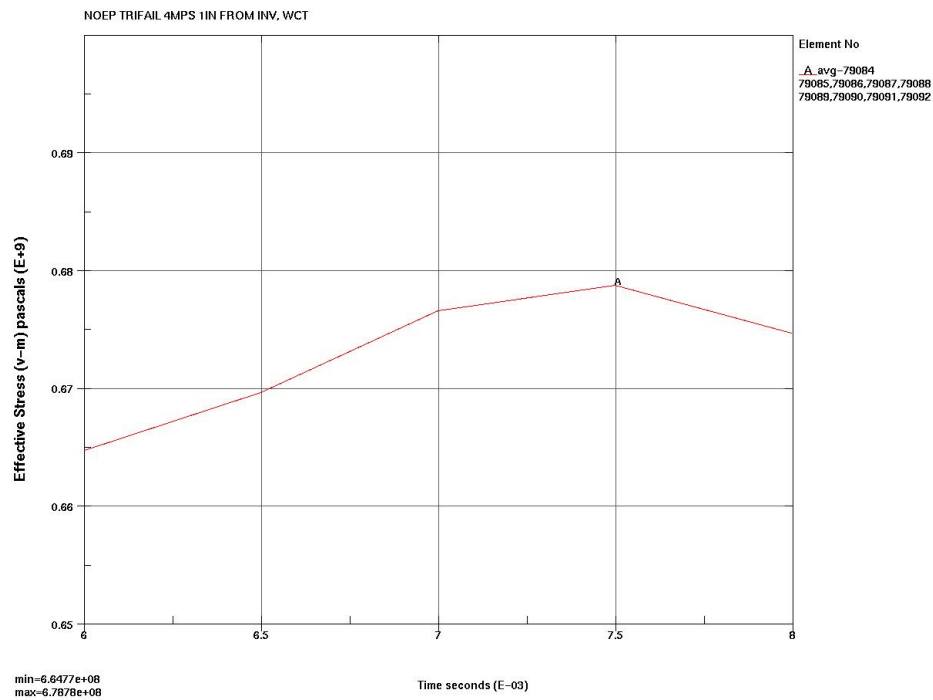
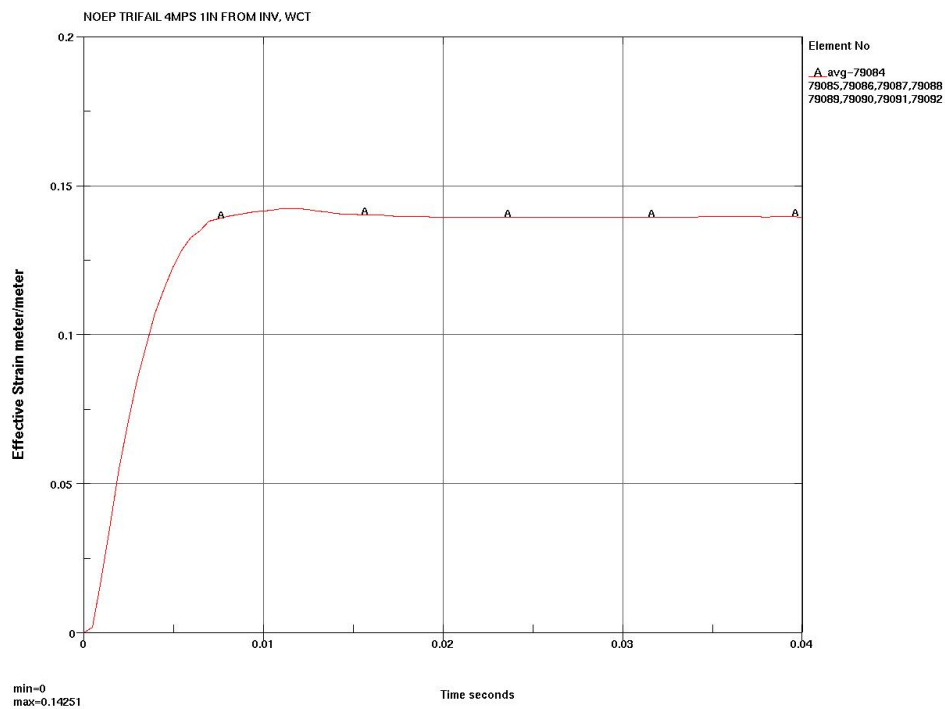
Figure 7-96 Flat 4 m/s Impact, 1 in Offset, t_{\max} of EWA VM Stress

Figure 7-97 Flat 4 m/s Impact, 1 in Offset, EWA VM Strain

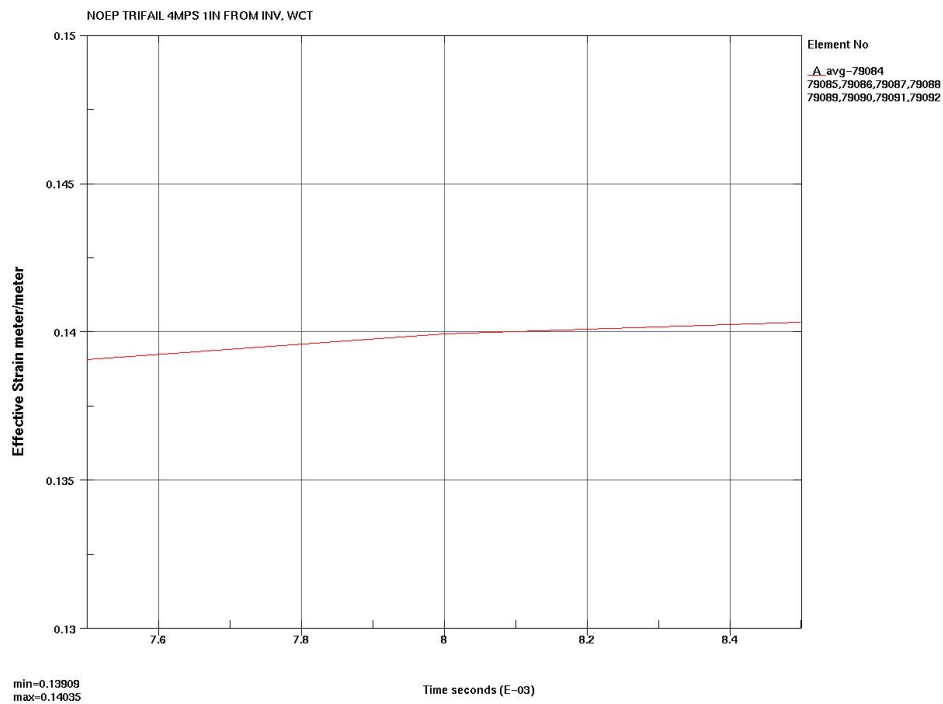
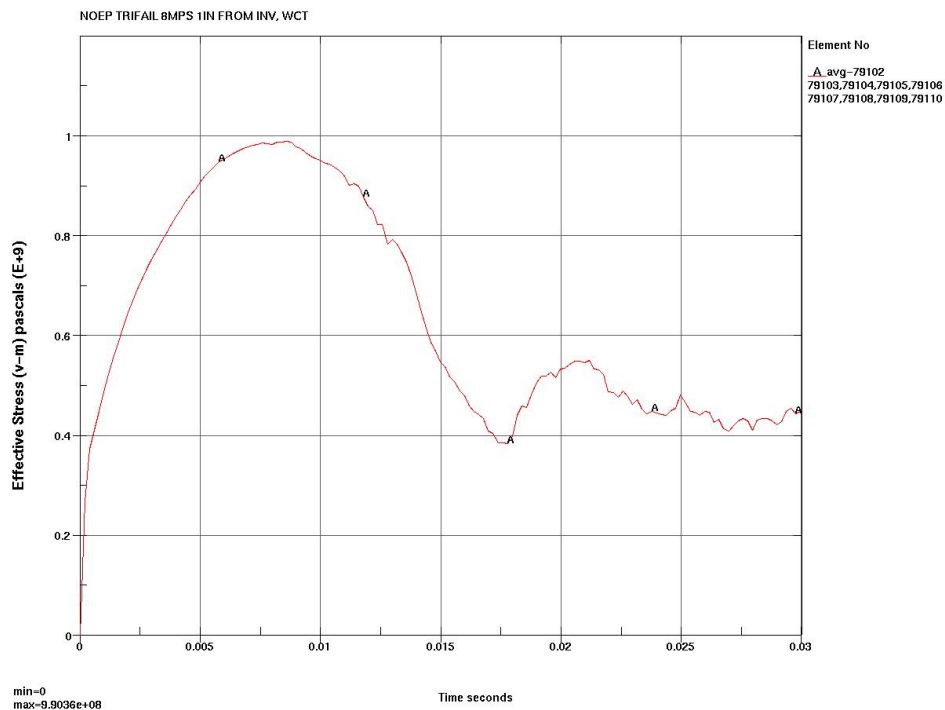
Figure 7-98 Flat 4 m/s Impact, 1 in Offset, EWA VM Strain at t_{\max} 

Figure 7-99 Flat 8 m/s Impact, 1 in Offset, EWA VM Stress

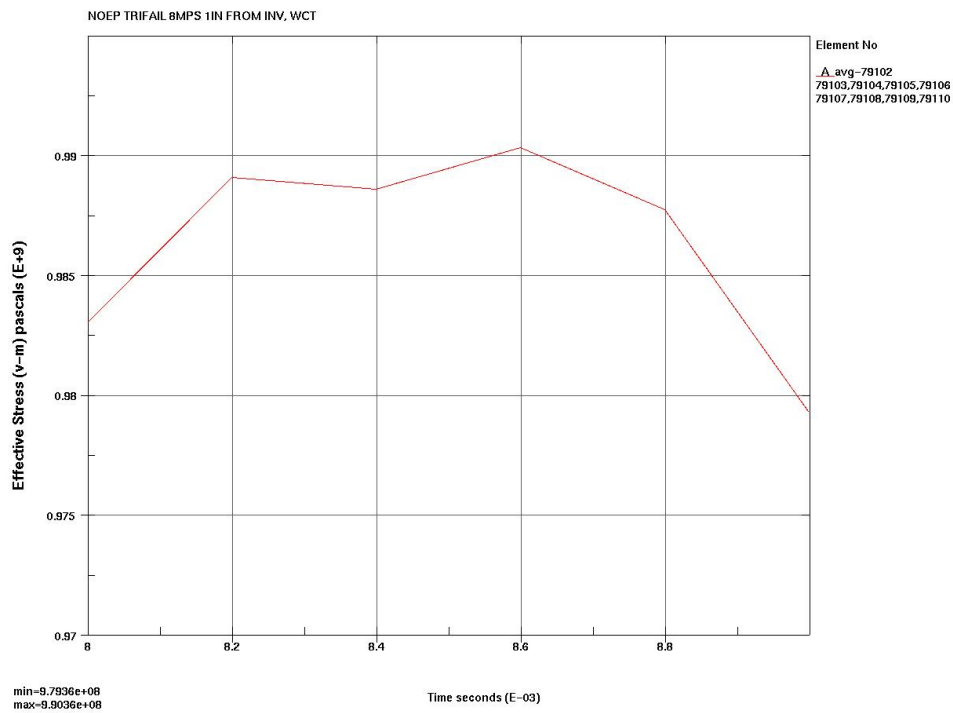
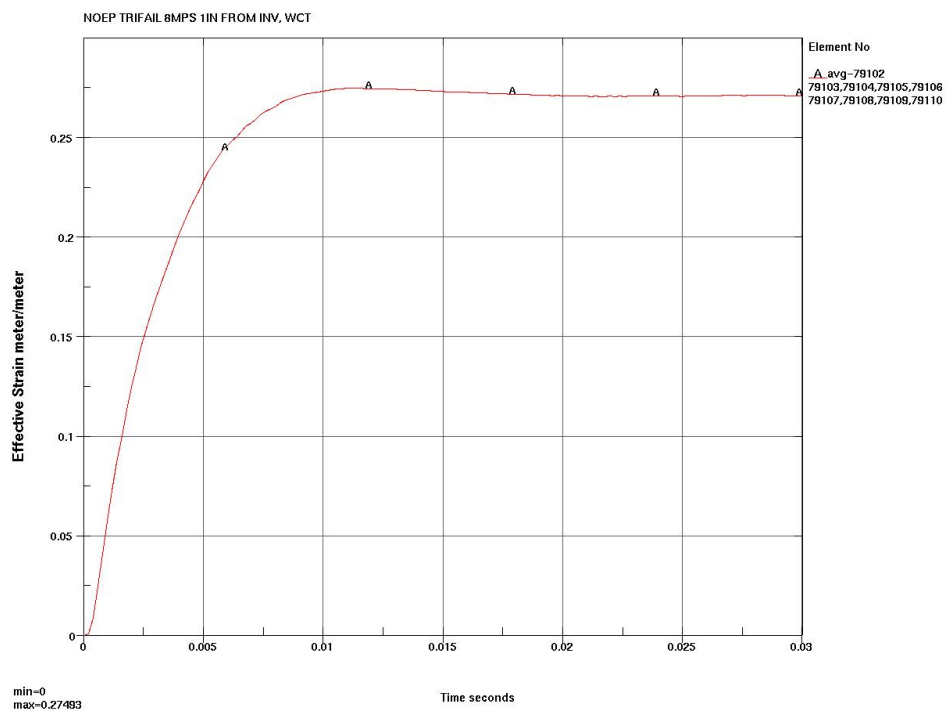
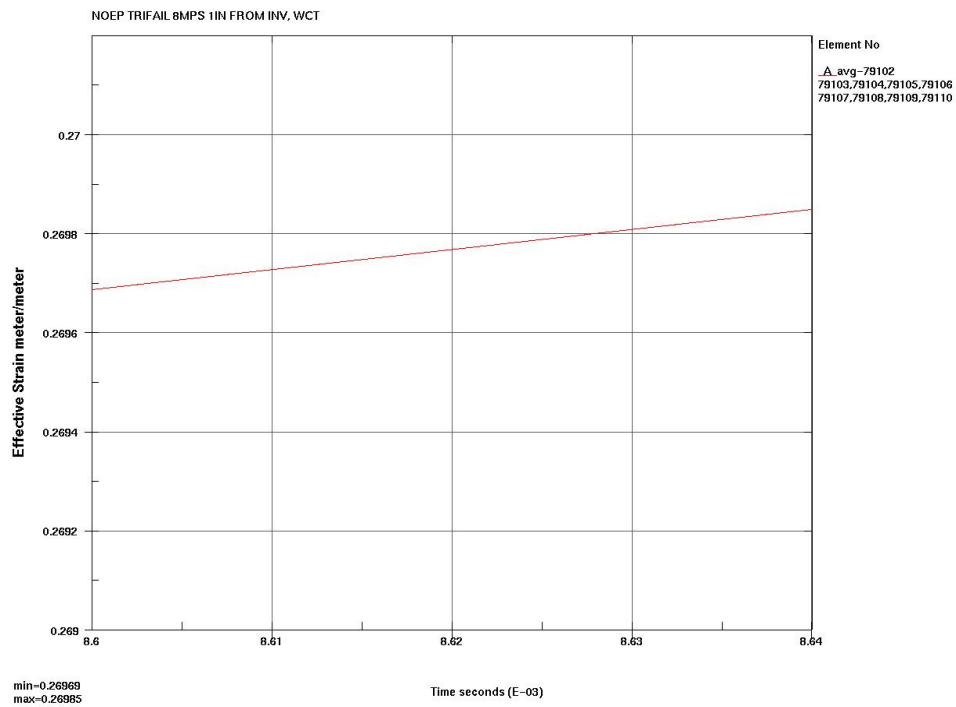
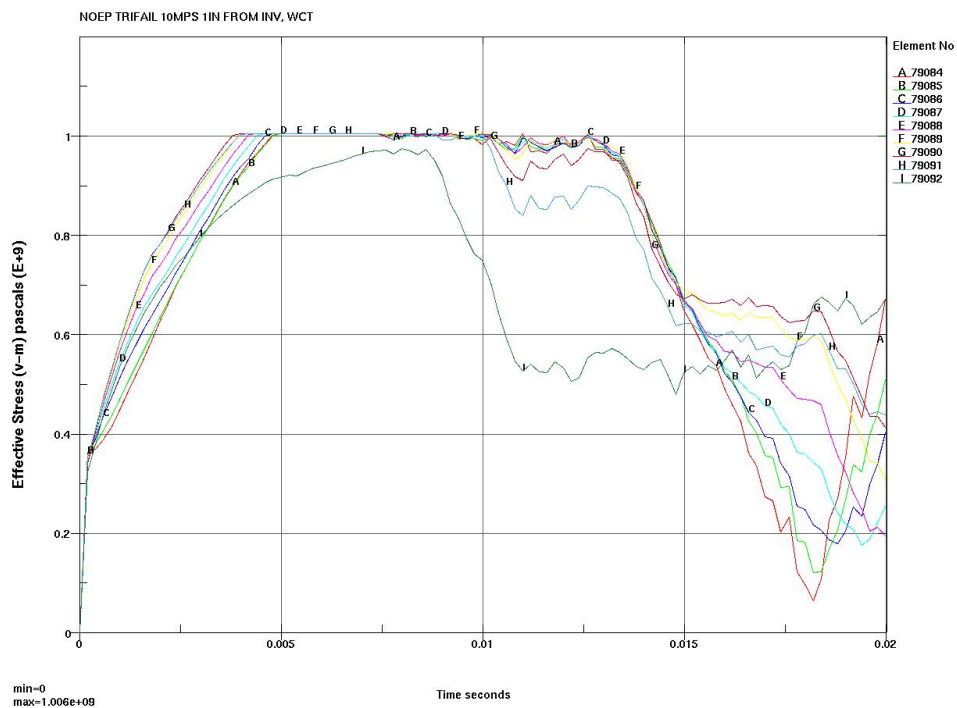
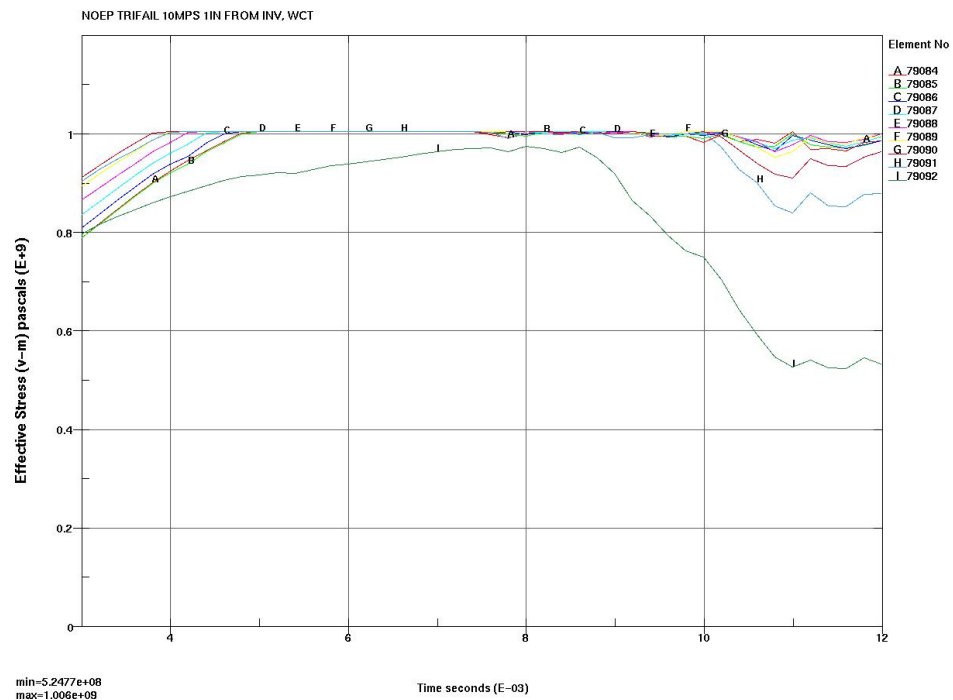
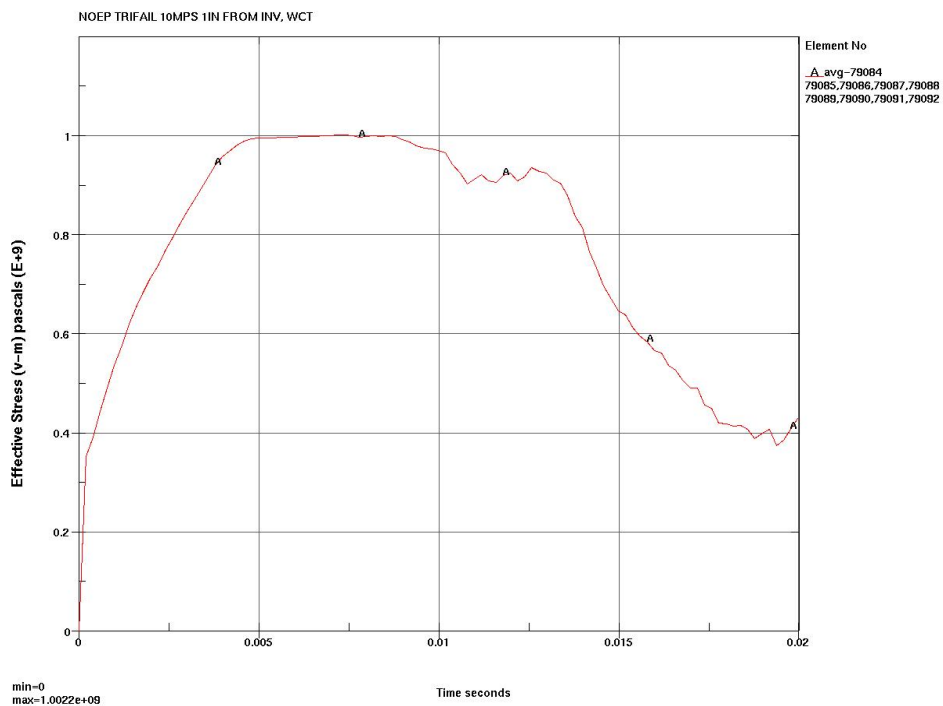
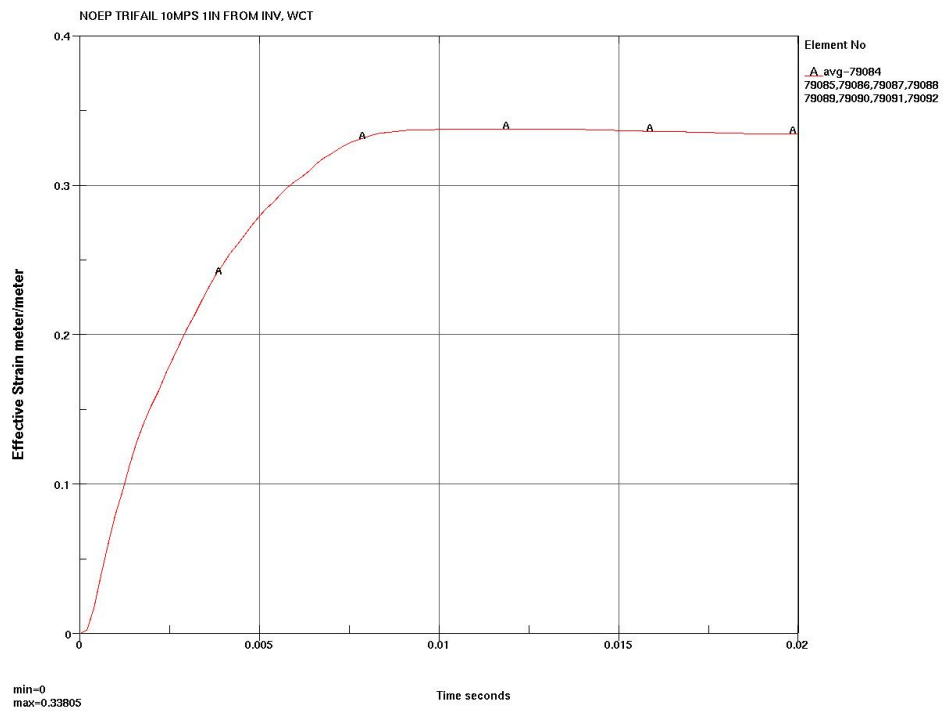
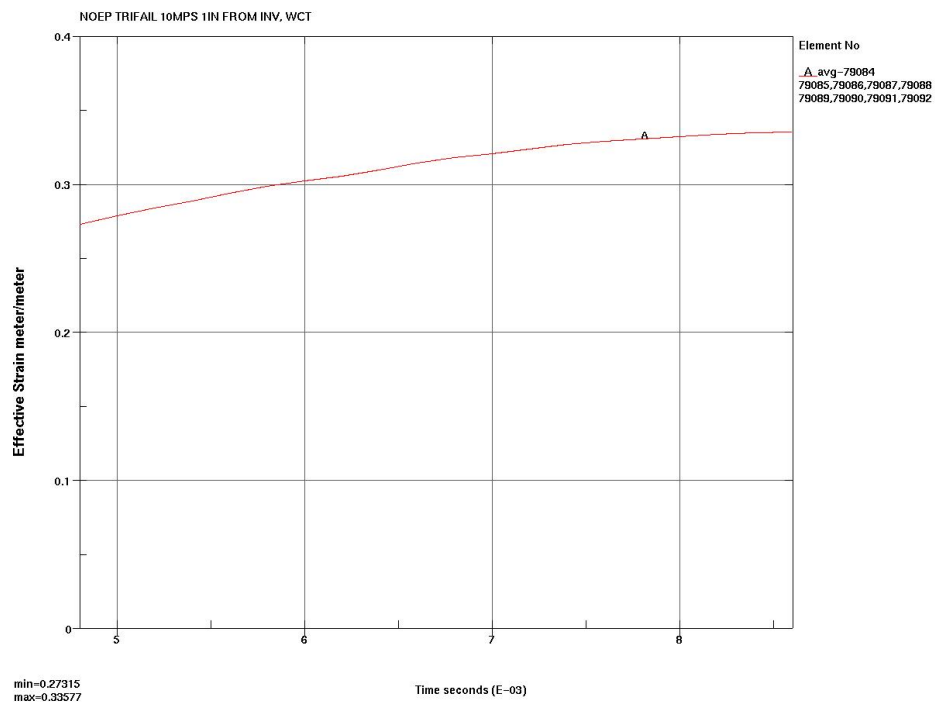
Figure 7-100 Flat 8 m/s Impact, 1 in Offset, t_{\max} of EWA VM Stress

Figure 7-101 Flat 8 m/s Impact, 1 in Offset, EWA VM Strain

Figure 7-102 Flat 8 *m/s* Impact, 1 *in* Offset, EWA VM Strain at t_{\max} Figure 7-103 Flat 10 *m/s* Impact, 1 *in* Offset, VM Stresses

Figure 7-104 Flat 10 *m/s* Impact, 1 *in* Offset, t_{flow} and t_{unload} of VM StressesFigure 7-105 Flat 10 *m/s* Impact, 1 *in* Offset, EWA VM Stress

Figure 7-106 Flat 10 *m/s* Impact, 1 *in* Offset, EWA VM StrainFigure 7-107 Flat 10 *m/s* Impact, 1 *in* Offset, EWA VM Strains at t_{flow} and t_{unload}

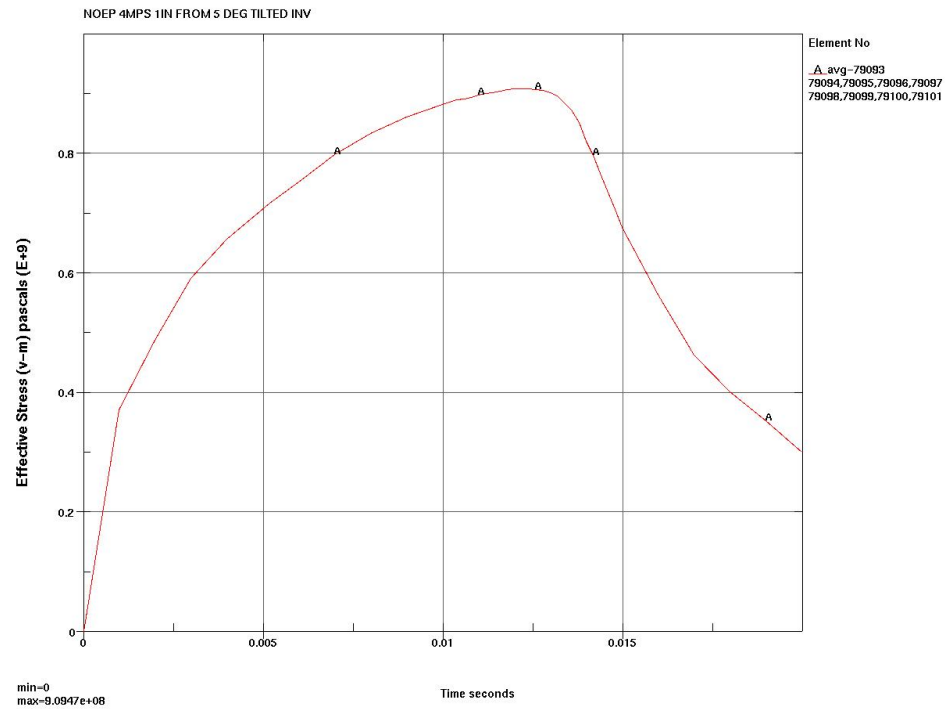
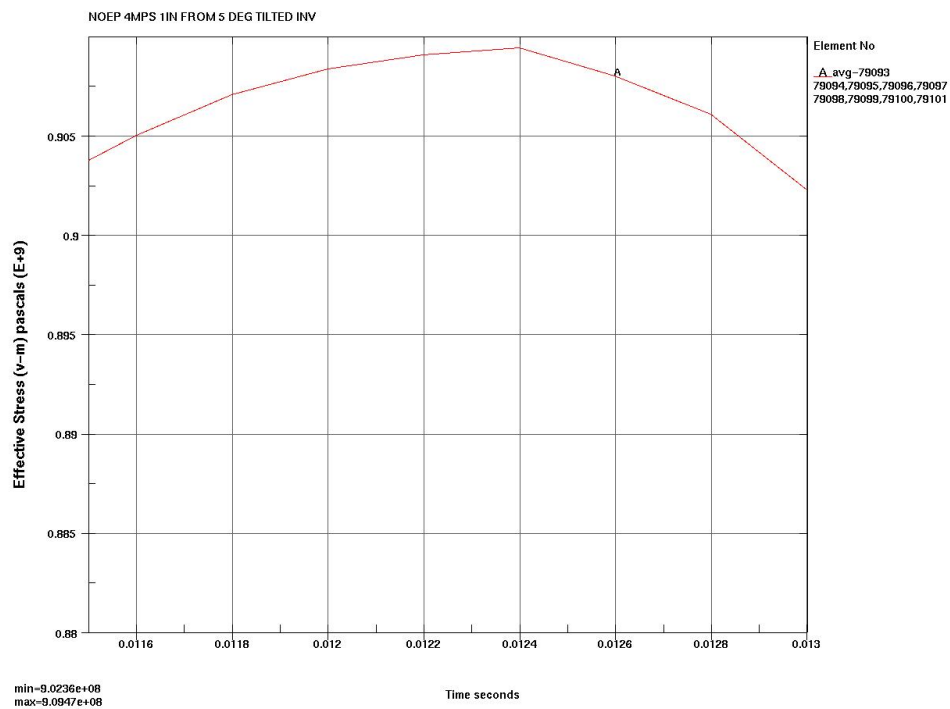


Figure 7-108 5 deg 4 m/s Impact, 1 in Offset, EWA VM Stress

Figure 7-109 5 deg 4 m/s Impact, 1 in Offset, t_{\max} of EWA VM Stress

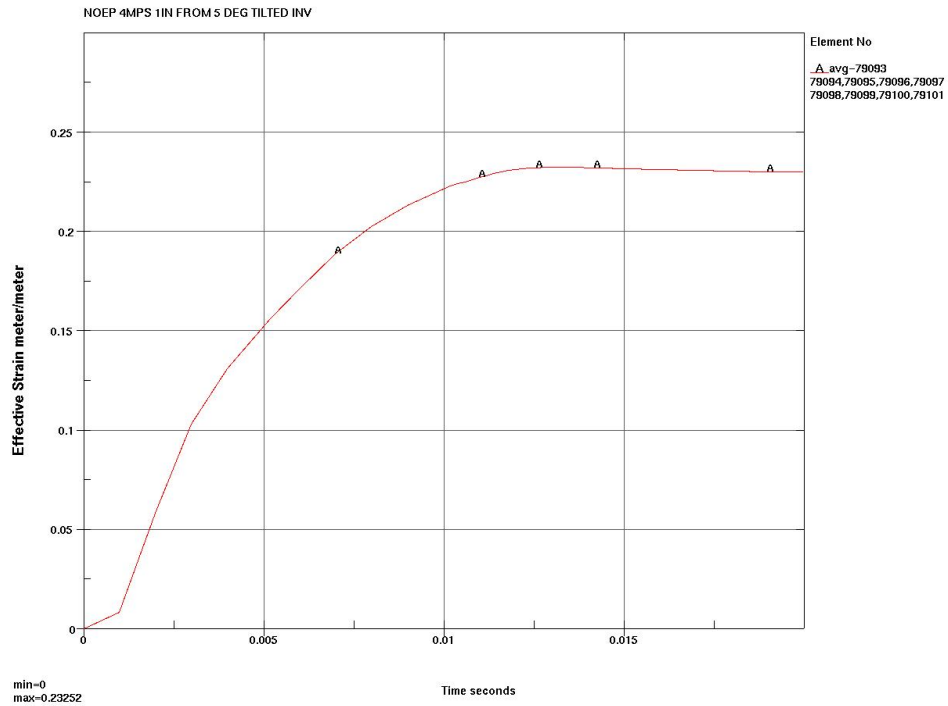
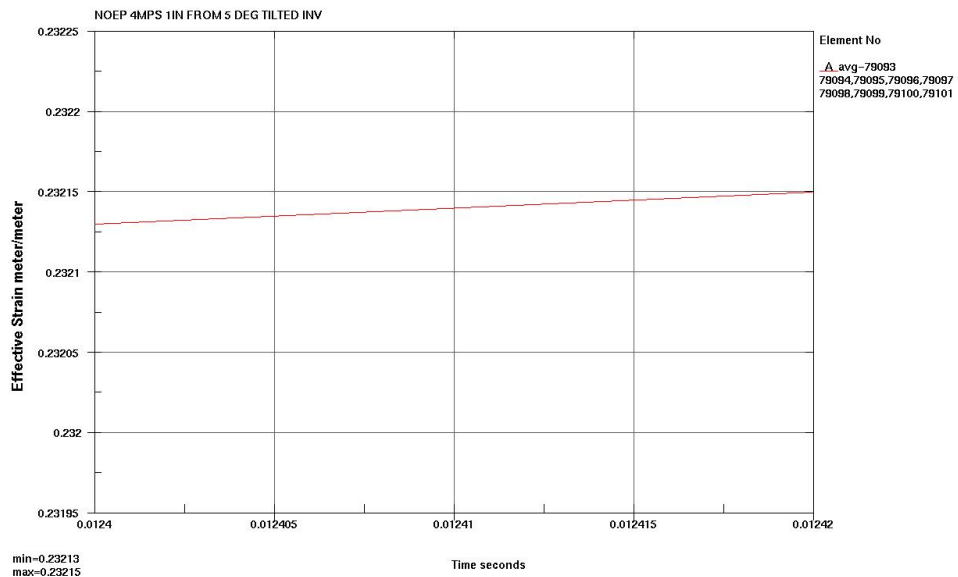


Figure 7-110 5 deg 4 m/s Impact, 1 in Offset, EWA VM Strain

Figure 7-111 5 deg 4 m/s Impact, 1 in Offset, EWA VM Strain at t_{\max}

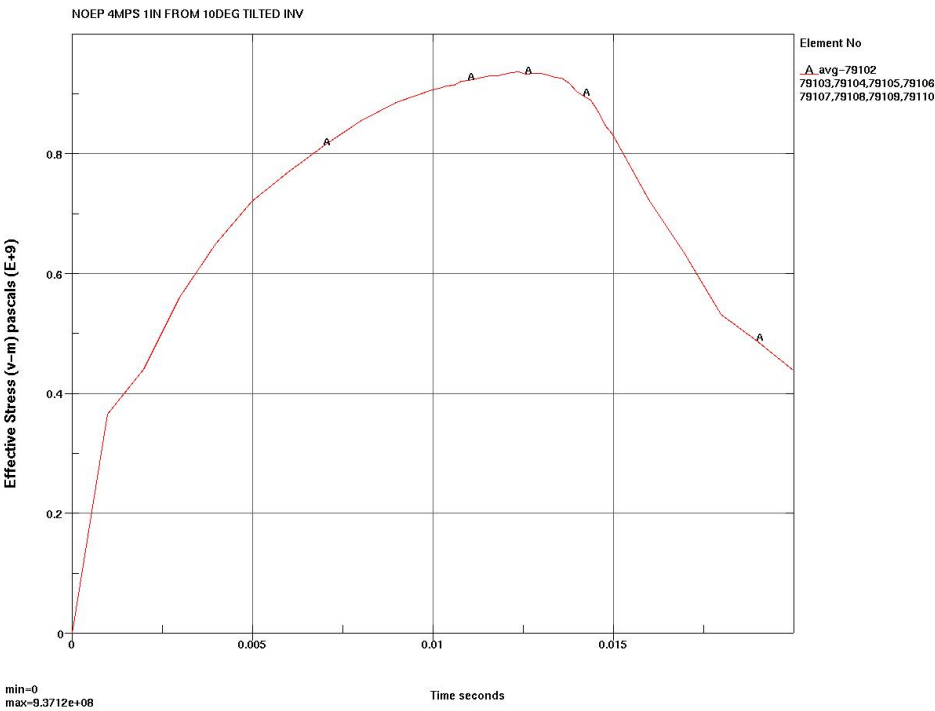


Figure 7-112 10 deg 4 m/s Impact, 1 in Offset, EWA VM Stress

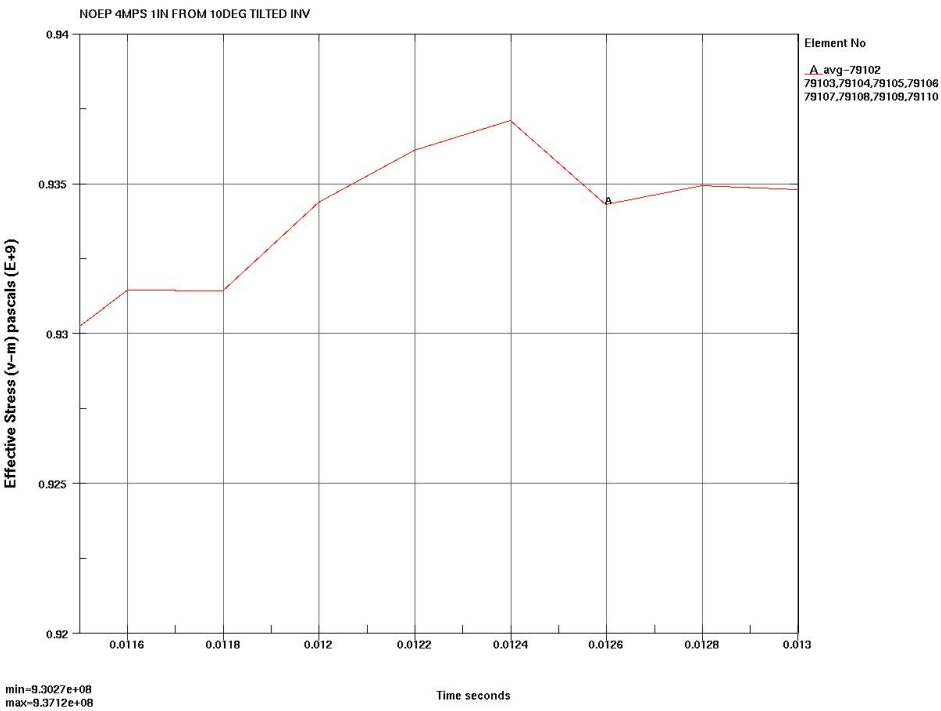


Figure 7-113 10 deg 4 m/s Impact, 1 in Offset, t_{\max} of EWA VM Stress

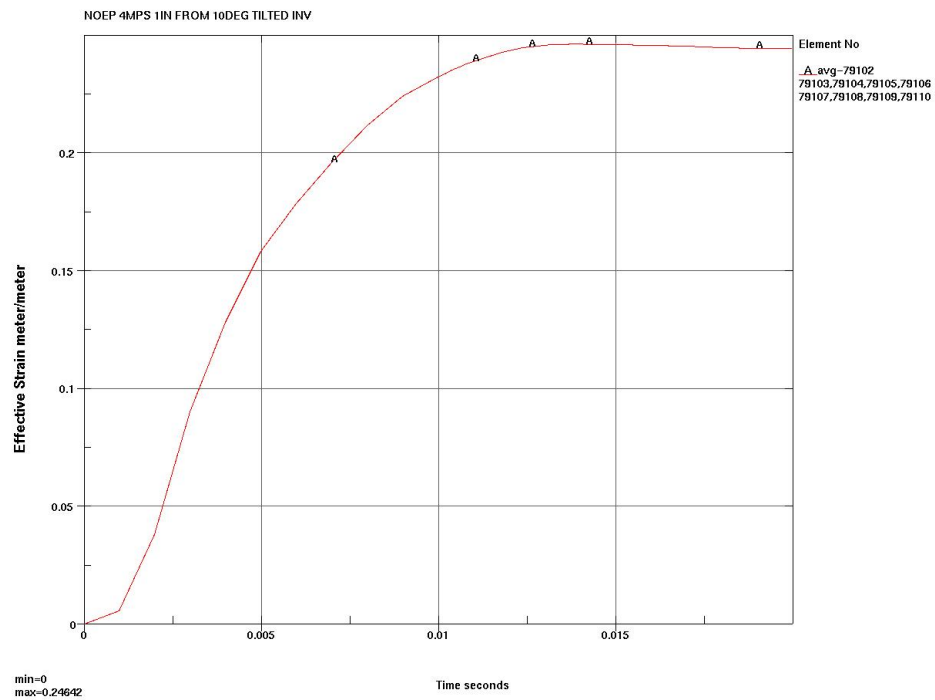
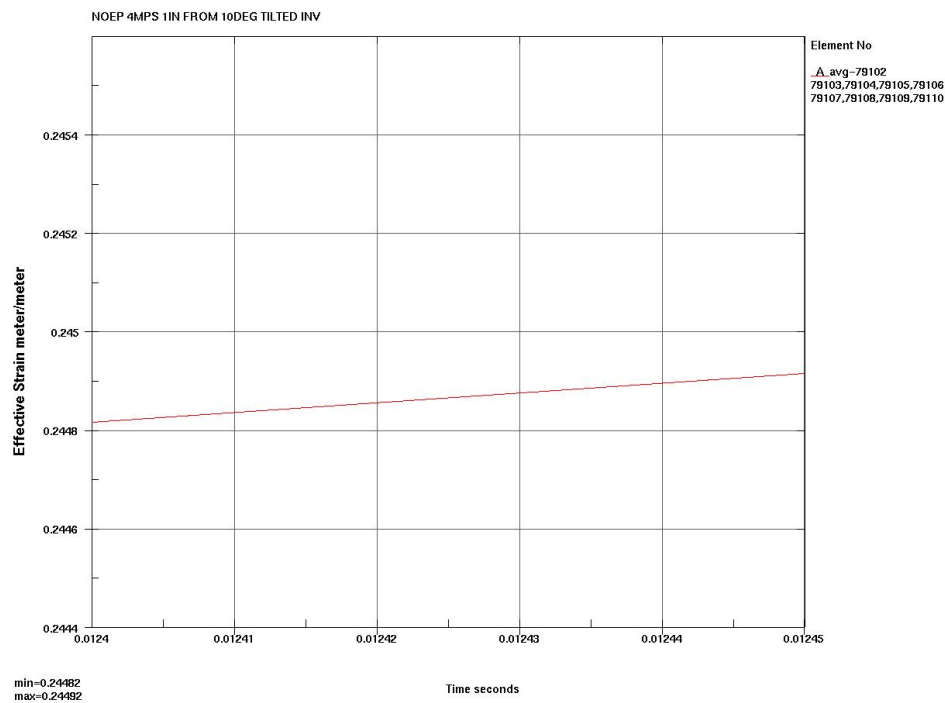


Figure 7-114 10 deg 4 m/s Impact, 1 in Offset, EWA VM Strain

Figure 7-115 10 deg 4 m/s Impact, 1 in Offset, EWA VM Strain at t_{\max}

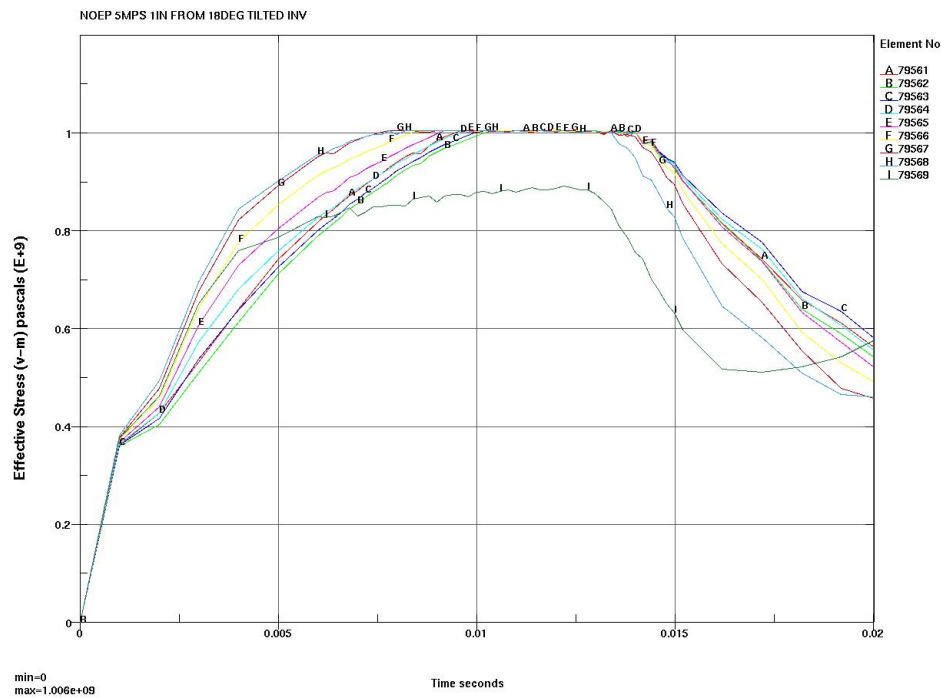
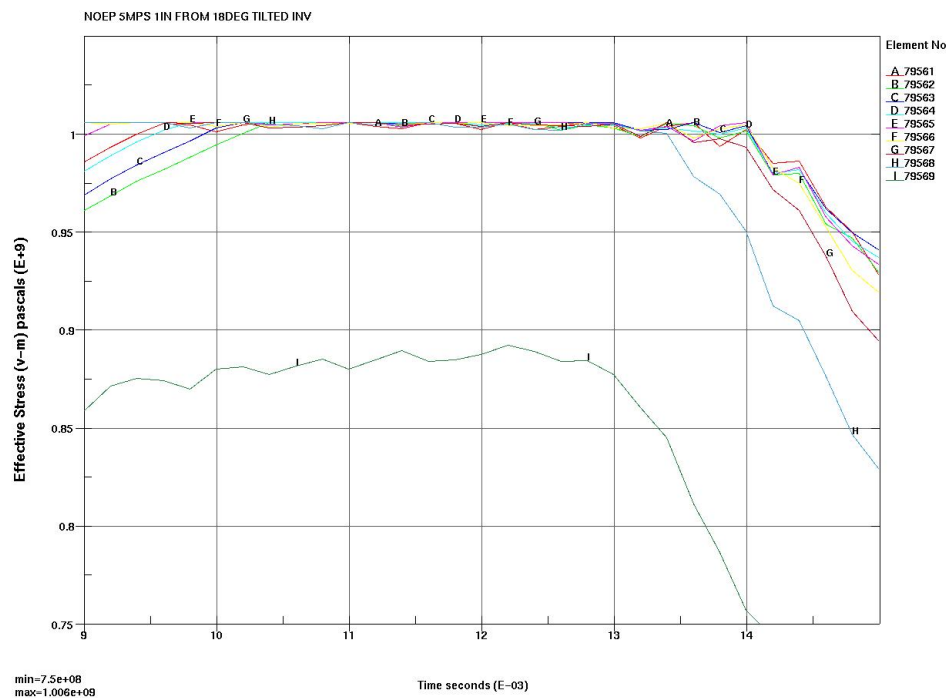


Figure 7-116 18 deg 5 m/s Impact, 1 in Offset, VM Stresses

Figure 7-117 18 deg 5 m/s Impact, 1 in Offset, t_{flow} and t_{unload} of VM Stresses

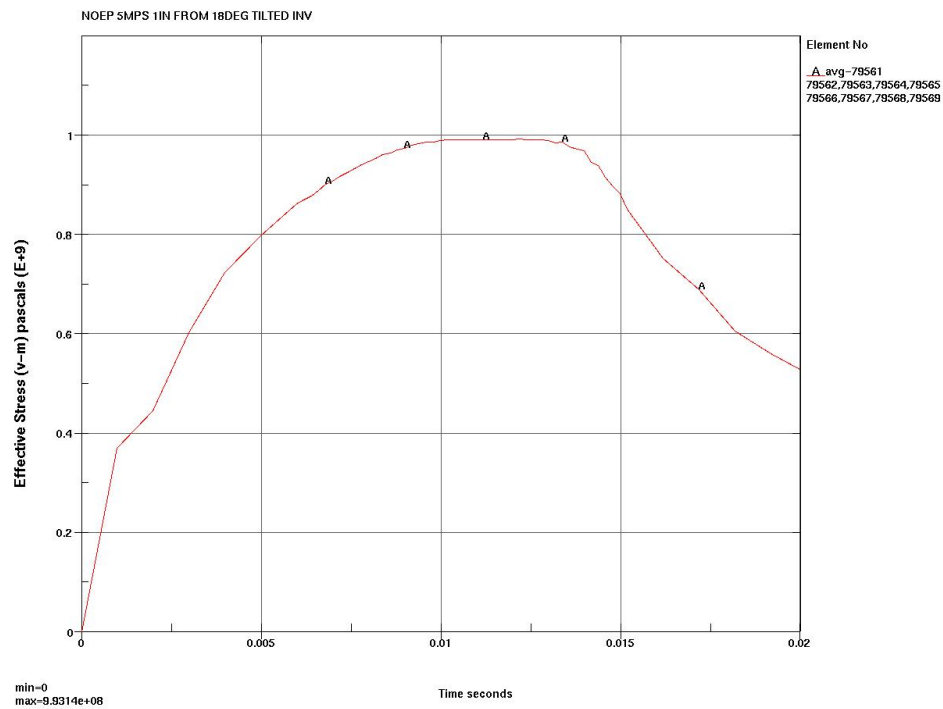


Figure 7-118 18 deg 5 m/s Impact, 1 in Offset, EWA VM Stress

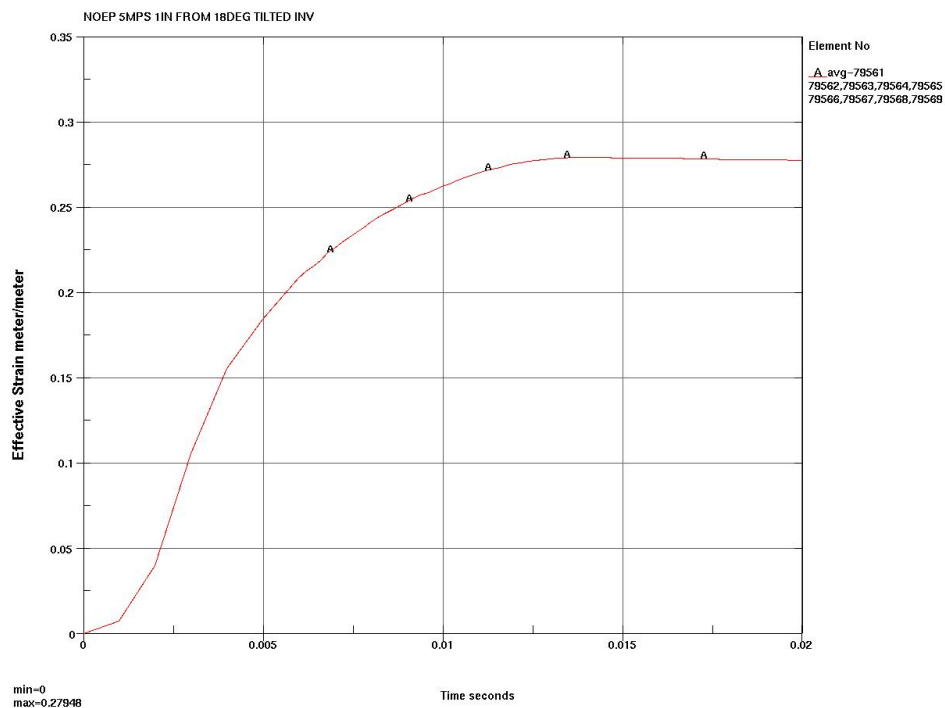
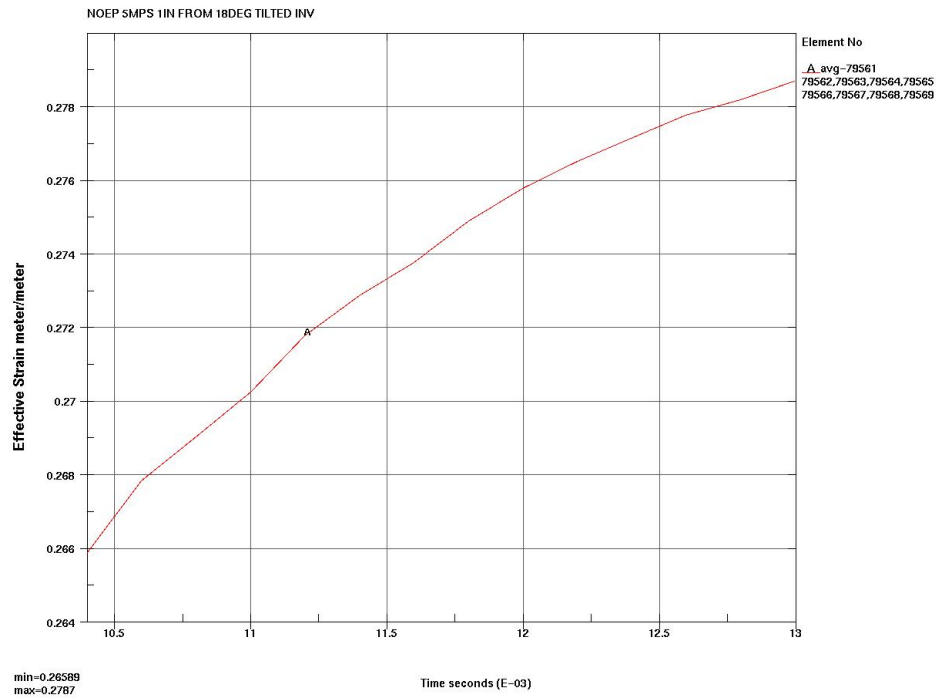
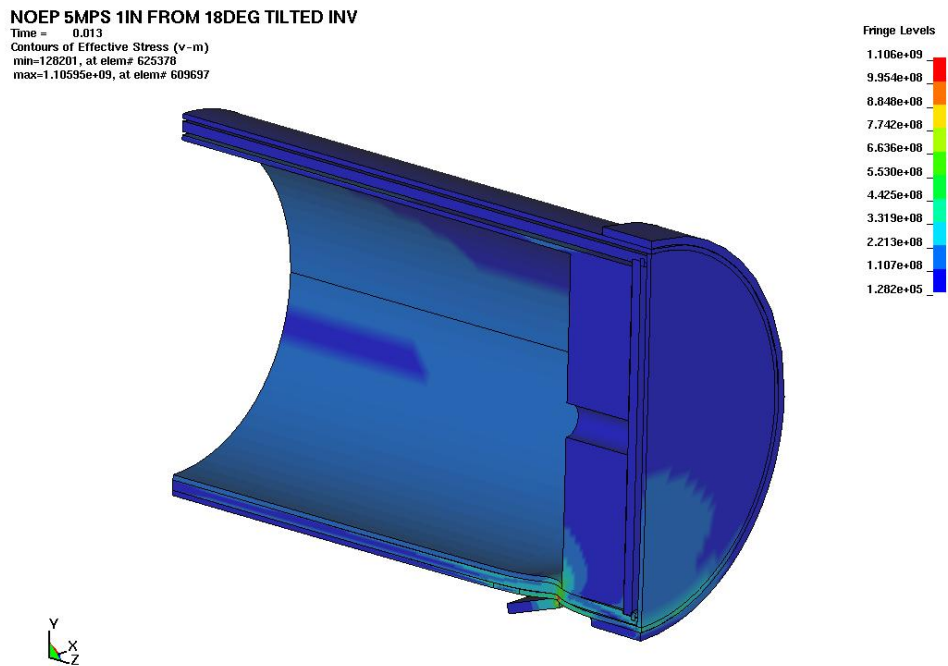
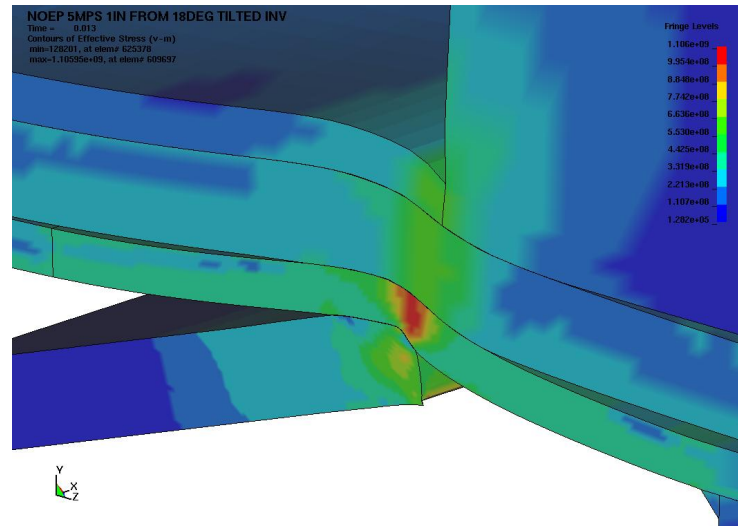
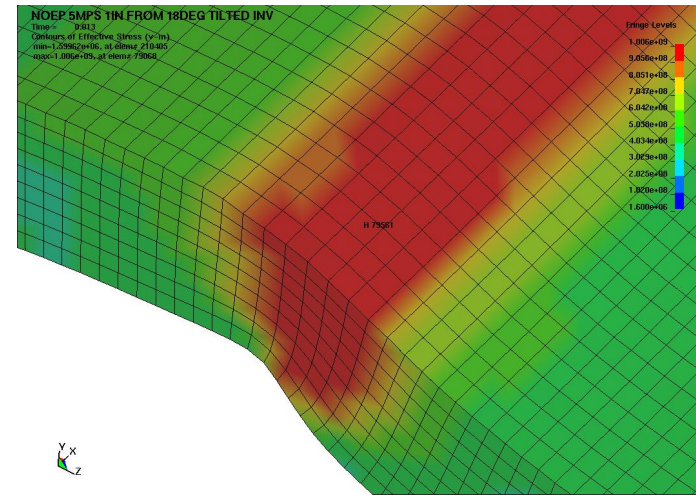
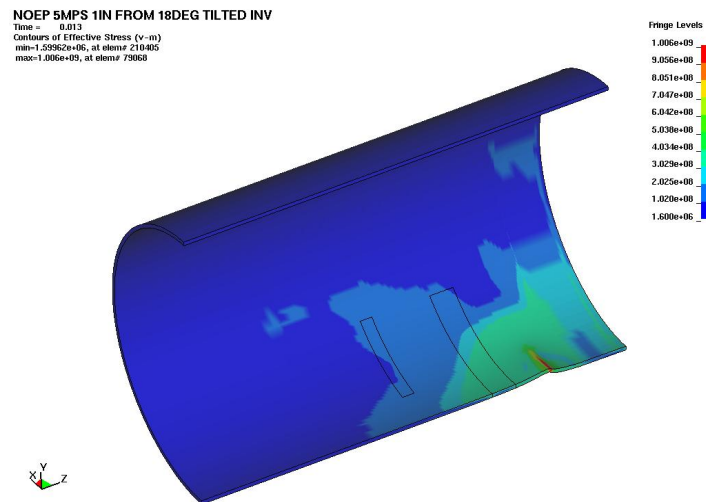
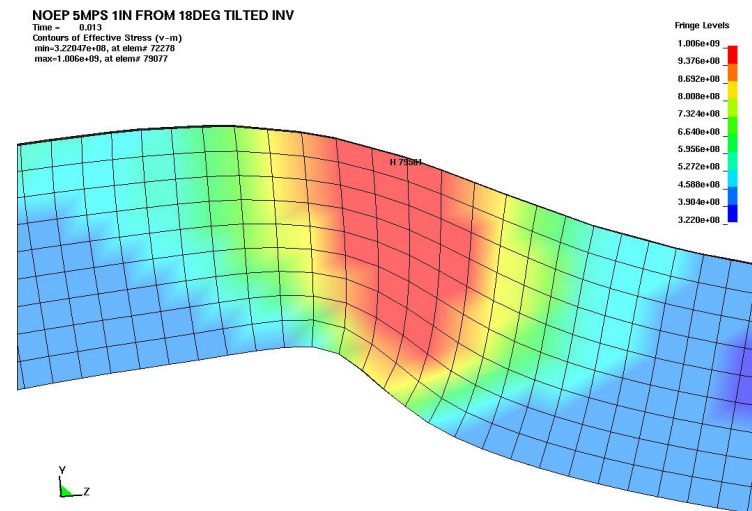


Figure 7-119 18 deg 5 m/s Impact, 1 in Offset, EWA VM Strain

Figure 7-120 18 deg 5 m/s Impact, 1 in Offset, EWA VM Strain at t_{flow} and t_{unload} Figure 7-121 VM Stresses at t_{unload} , Full FER, Pa

Figure 7-122 VM Stresses at t_{unload} , Full FER, Failure Location, PaFigure 7-124 VM Stresses at t_{unload} , OCB Close-up, PaFigure 7-123 VM Stresses at t_{unload} , OCB, Inner View, PaFigure 7-125 VM Stress at t_{unload} , OCB, Section View, Pa

The effect of tilt angle is small if the rare perfect flat hit is ignored. The location of impact has a moderate effect while the velocity of impact is the most dominant parameter. Plots of the Table 7-17 impact velocity versus ETF for the flat impacts and the 18 *deg* tilted impacts are provided in Figure 7-126. The (mean) velocity capabilities for the flat impact and 18 *deg* tilted impact sequence events are 8.4 and 4.7 *m/s*, respectively.

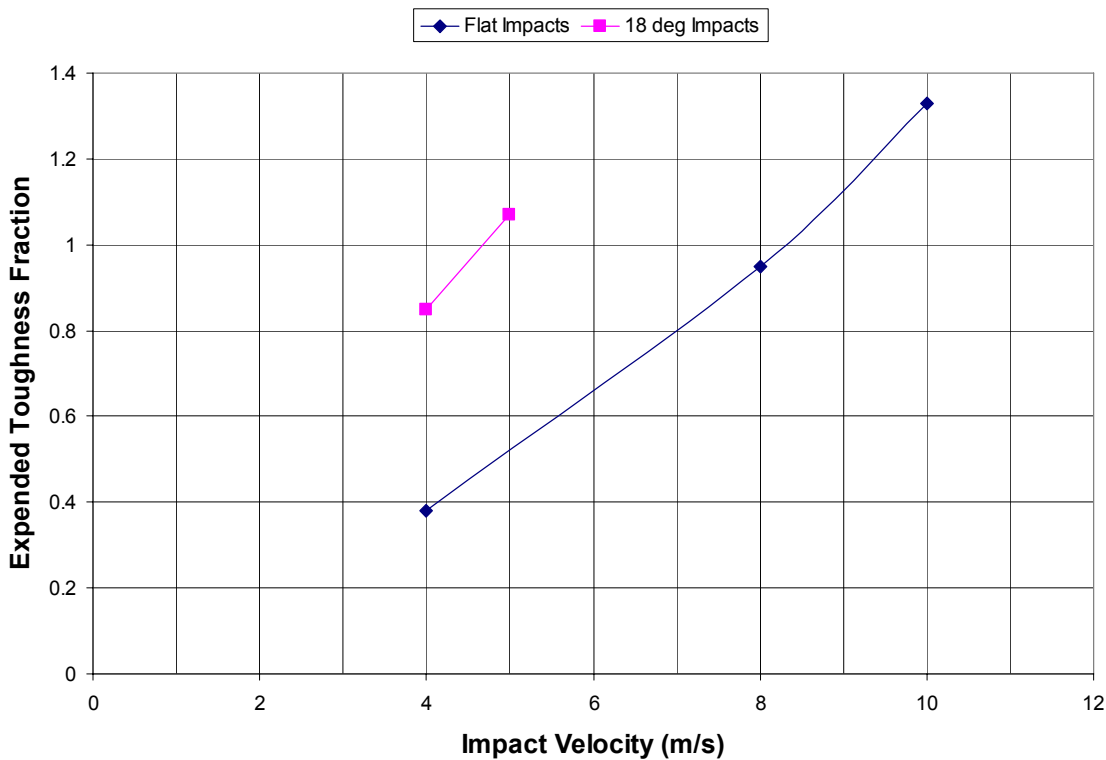


Figure 7-126 WP on Invert Impact Velocity Capability Trend

7.5 CAPABILITY CALCULATIONS SENSITIVITY STUDIES

Two parameters are studied, temperature and invert steel material.

7.5.1 Temperature

The 18 *deg* tilted impacts of the WP on the EP were rerun at 300°C. Table 7-18 contains the comparable RT data reductions from Table 7-17 and the 300°C data reductions supported by Figures 7-127 to 7-135. Figures 7-132 and 7-135 together indicate that the 5 *m/s* load level exactly results in failure (EWA VM strain = 0.028) at t_{\max} ($= t_{\text{flow}} = t_{\text{unload}}$) = 0.0110 *s*. Figure 7-136 plots the four cases and indicates temperature effects are minor and depend on load level. The RT cases reach failure at lower velocities than the 300°C cases when the load levels approach failure levels. Therefore, using RT data reductions for Capability in this calculation is conservative and it is expected to be a general trend for all impact Capability calculations as it was shown to be for deterministic impact calculations.

Table 7-18 Temperature Effect on WP on Invert Impact Capability

Temp	Figs 7-x to 7-y	m/s	Element No.*	$\sigma_{vm,max}$ MPa	t_{max} or t_{flow} sec	$\epsilon_{vm,tmax}$ Or $\epsilon_{vm,flow}$ m/m	t_{unload} sec	ϵ_{unload} m/m	I_T' MPa	ETF =** I_T'/I_T
RT	6-7	4	79570	957.7	0.0136	0.2472	-	-	162	0.85
RT	116-120	5	79561	993.1	0.0104	0.2659	0.0130	0.2787	203	1.07
300°C	127-130	4	79570	854.7	0.0142	0.2576	-	-	142	0.90
300°C	131-135	5	79561	869.8	0.0110	0.2817	0.0110	0.2817	158	1.00

* Element number of solid element on inner surface of OCB at governing wall section

** The 300°C Alloy 22 mean material Toughness Index, I_T , using worst-case-triaxiality-adjusted vendor-averaged properties in Section 6.1.2 (see Equation 3, Section 7.1.7.2.2, Reference 2.2.15) is:

$$I_T = \epsilon_u' \cdot (\sigma_y + \sigma_u')/2 = 0.28 \cdot (250 + 876)/2 = 158 \text{ MPa}$$

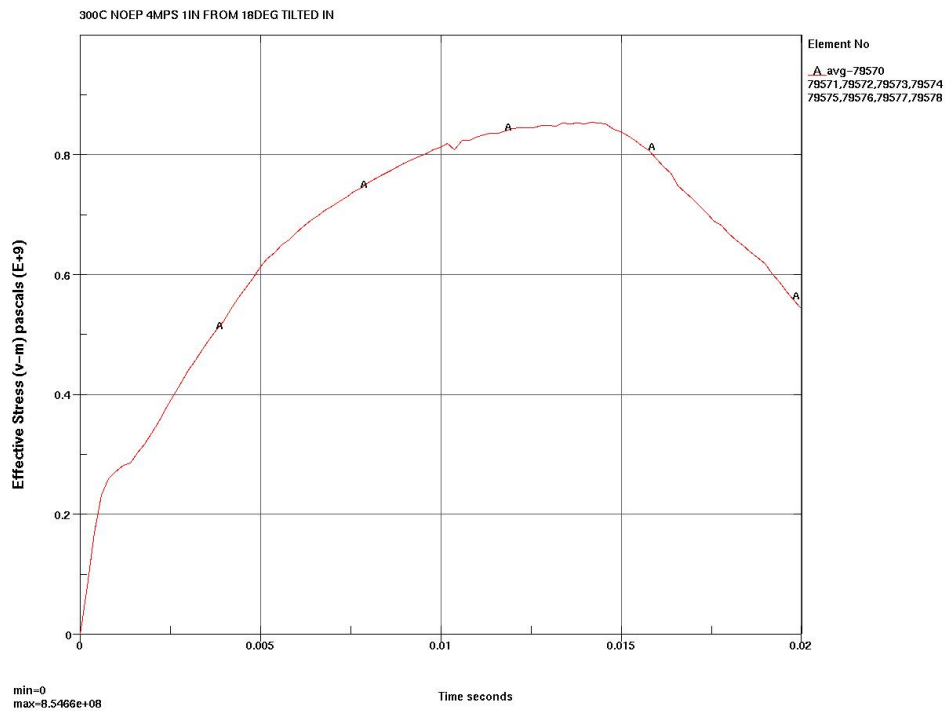


Figure 7-127 300°C WP on Invert 4 m/s Impact, EWA VM Stress

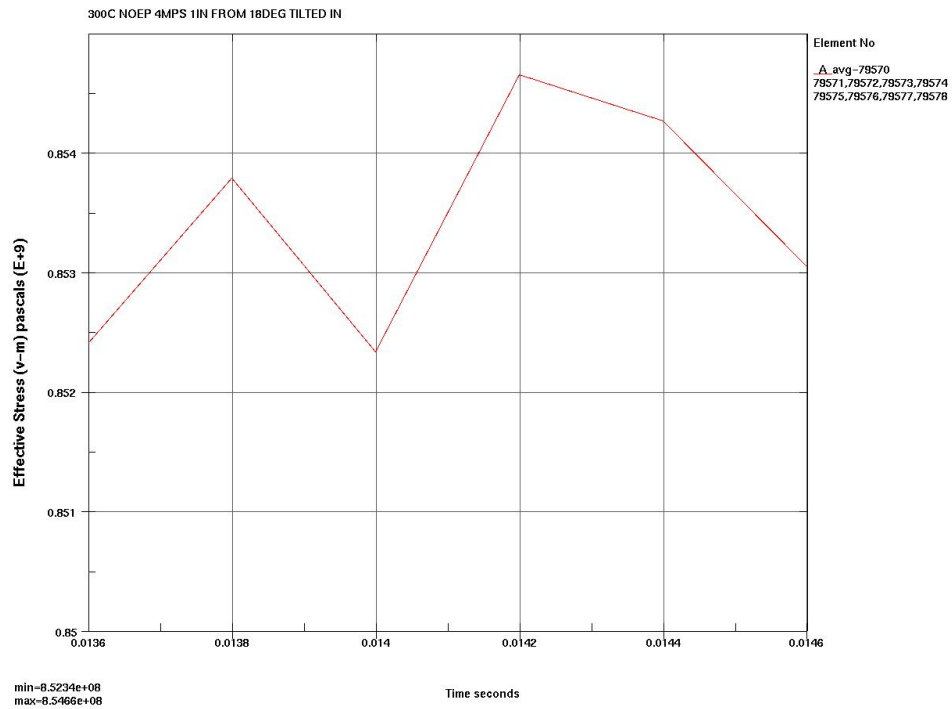
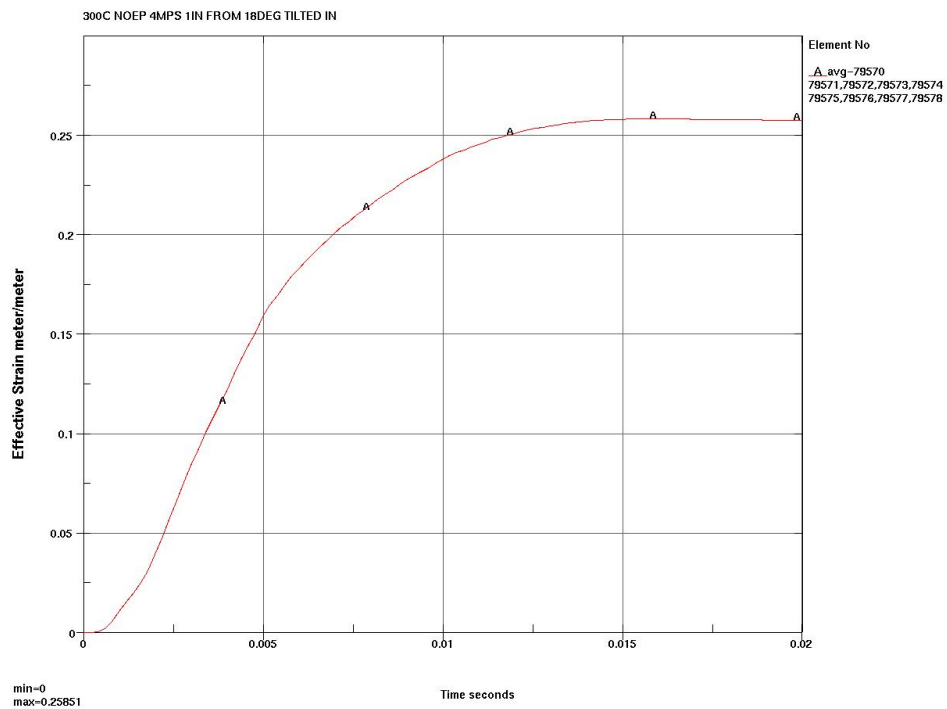
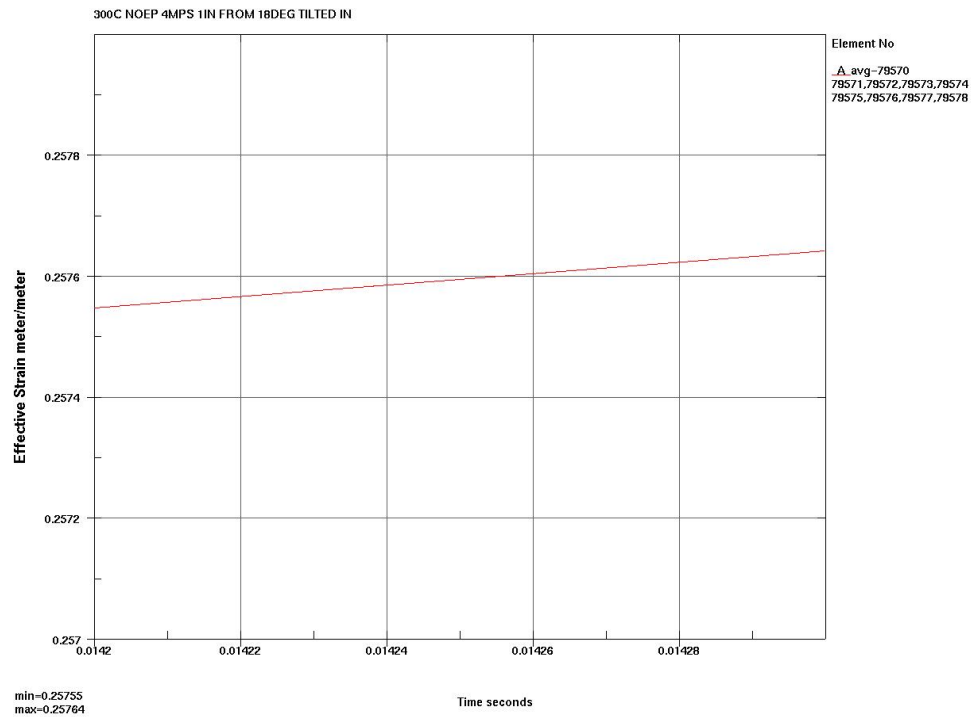
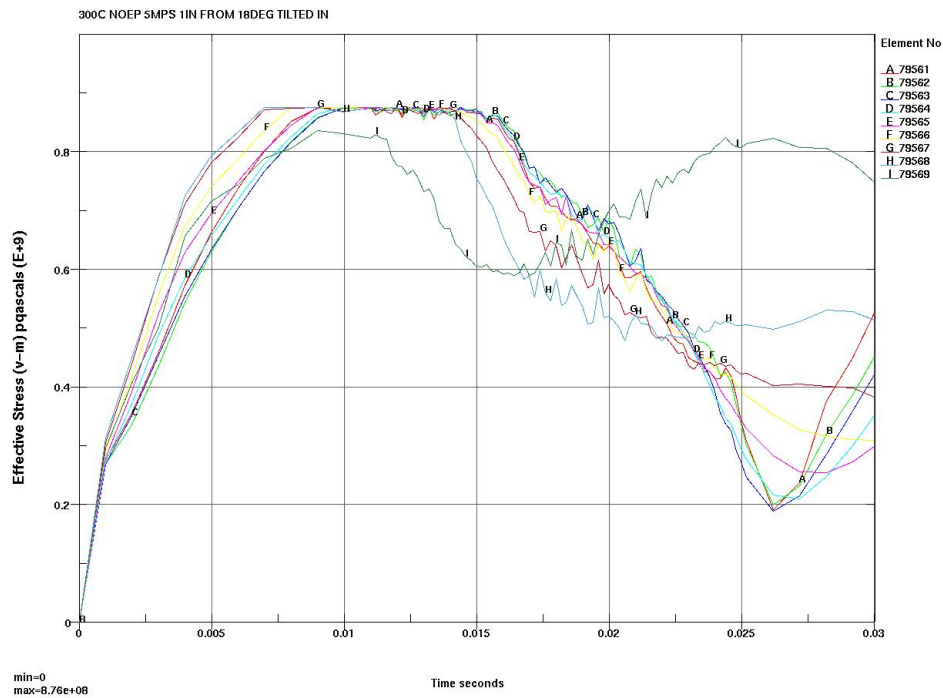
Figure 7-128 300°C WP on Invert 4 m/s Impact, t_{\max} of EWA VM Stress

Figure 7-129 300°C WP on Invert 4 m/s Impact, EWA VM Strain

Figure 7-130 300°C WP on Invert 4 *m/s* Impact, EWA VM StrainFigure 7-131 300°C WP on Invert 5 *m/s* Impact, VM Stresses

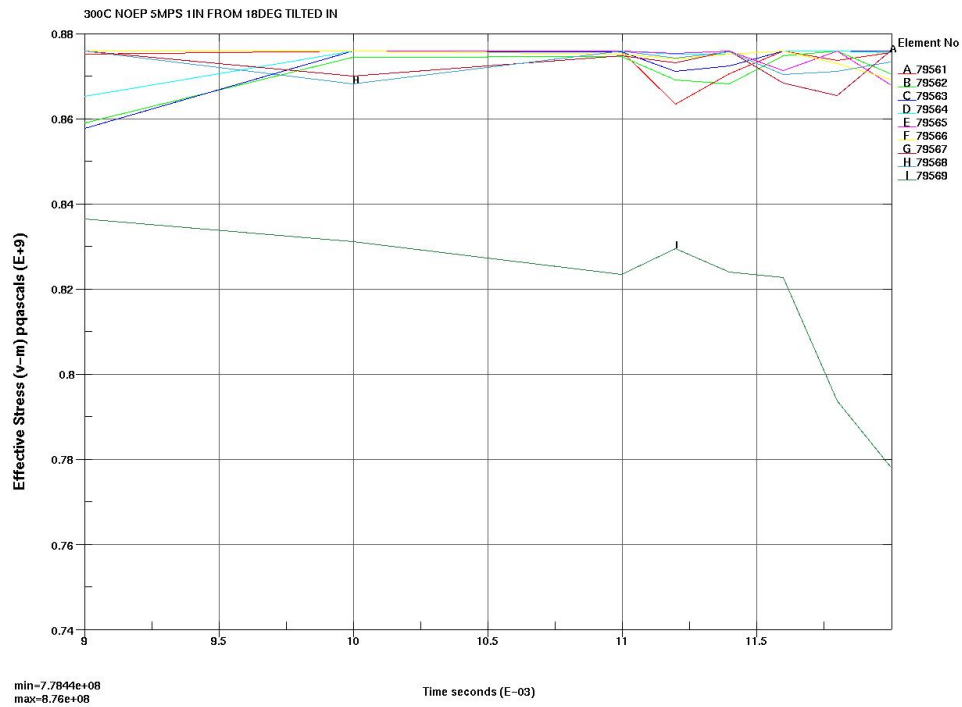
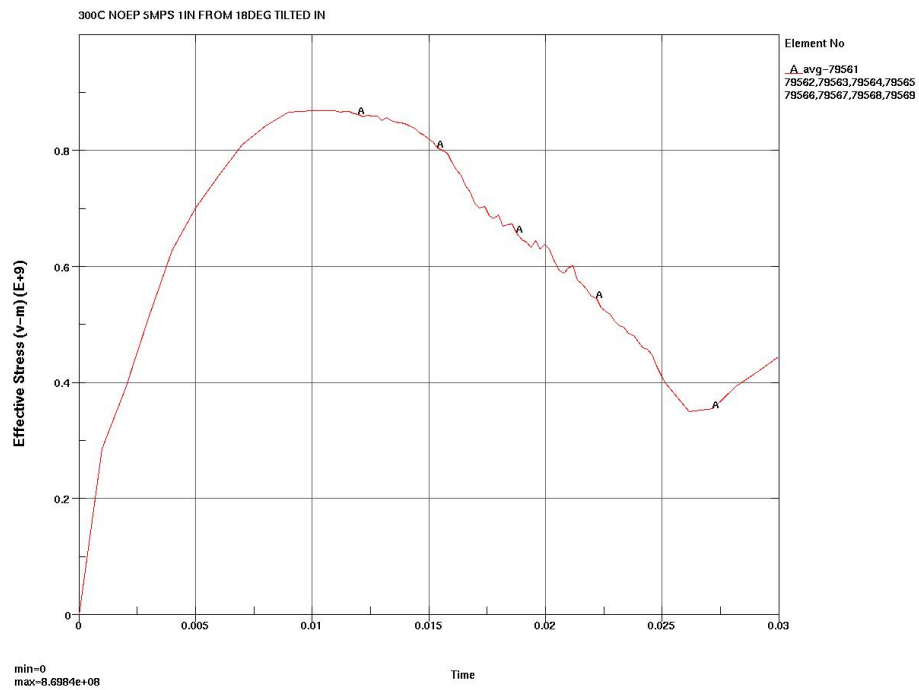
Figure 7-132 300°C WP on Invert 5 m/s Impact, t_{\max} of VM Stresses

Figure 7-133 300°C WP on Invert 5 m/s Impact, EWA VM Stress

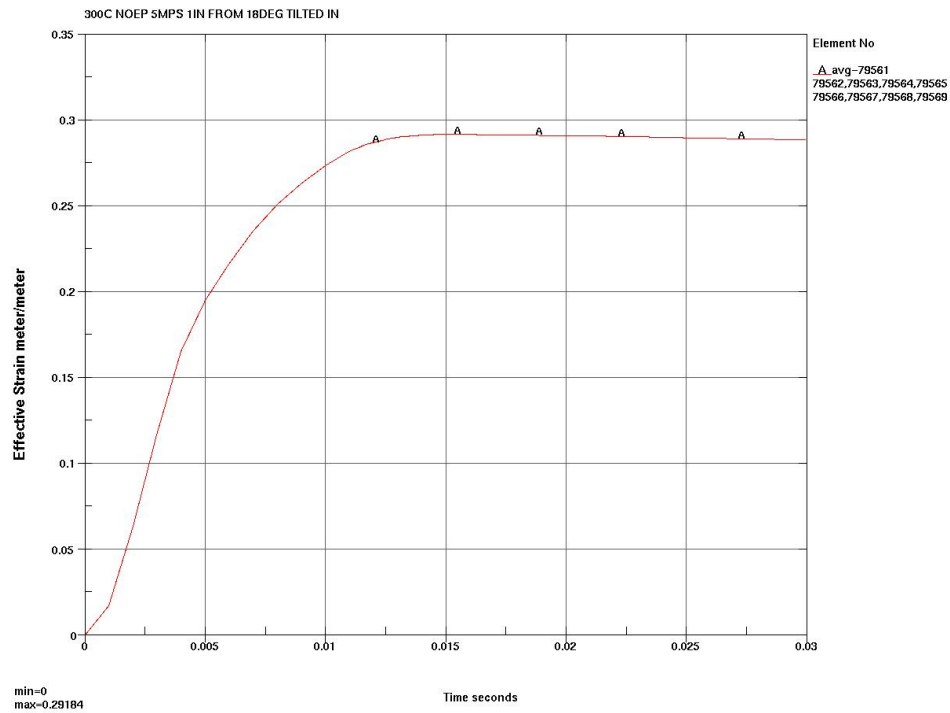
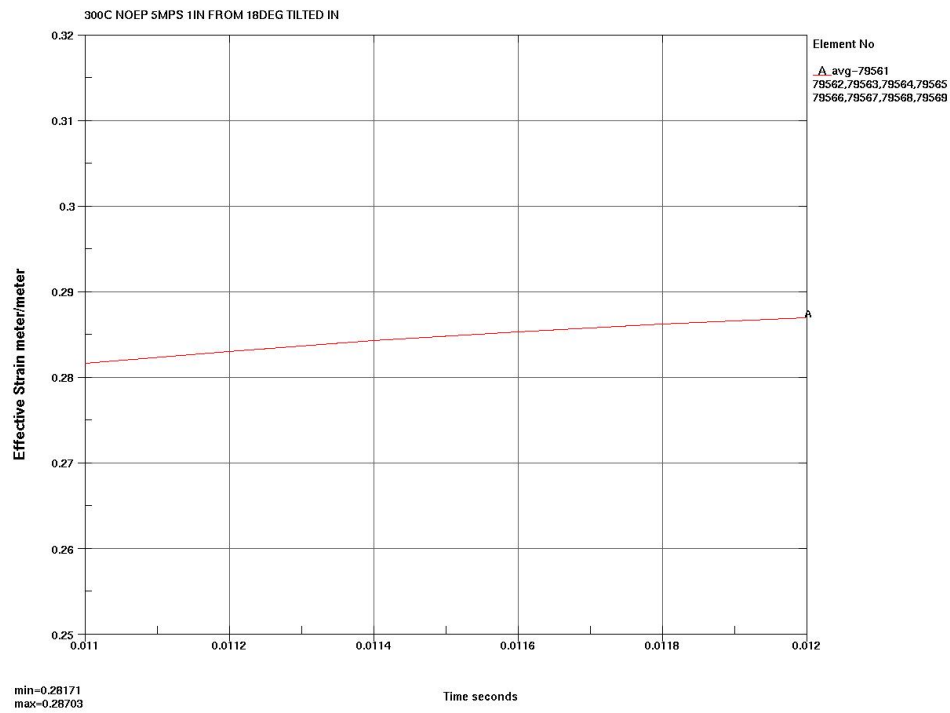


Figure 7-134 300°C WP on Invert 5 m/s Impact, EWA VM Strain

Figure 7-135 300°C WP on Invert 5 m/s Impact, EWA VM Stress at t_{\max}

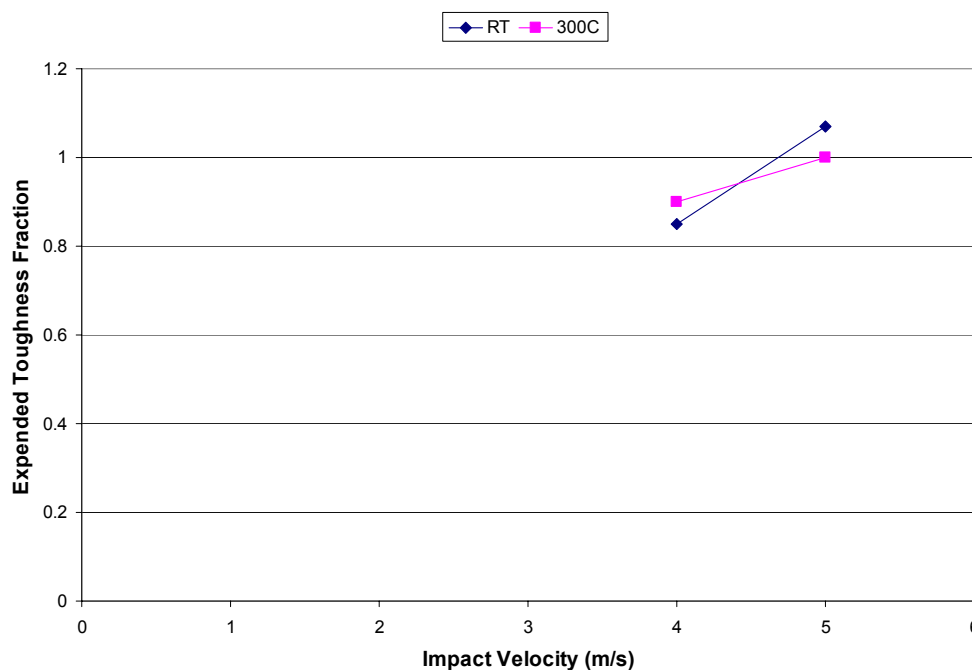


Figure 7-136 Sensitivity of RT versus 300°C WP on Impact Capability

7.5.2 Invert Steel Material

The 18 deg tilted impacts of the WP on the EP were rerun at 5 *m/s* using invert steel material properties based on A588 steel. Table 7-19 contains the comparable A36 steel invert data reductions from Table 7-17 and the A588 steel invert data reductions supported by Figures 7-137 to 7-141. The higher yield A588 material results in a noisier response and a slightly earlier peak response in the OCB (compare Figures 7-117 and 7-138). However, the amount of corner rounding of the upper flange edge is comparable (compare Figures 7-122 and 7-142). The Table 7-19 ETF values are nearly the same (within 6%) making the choice of invert steel material for the FER a minor effect on Capability prediction compared to other variations, e.g., material strength scatter in Section 7.6.

Table 7-19 Invert Steel Material Choice Effect on WP on Invert Impact Capability

Invert Steel Matl	Figs 7-x to 7-y	<i>m/s</i>	Element No.*	$\sigma_{vm,max}$ MPa	t_{flow} sec	$\epsilon_{vm,flow}$ m/m	t_{unload} sec	ϵ_{unload} m/m	I_T' MPa	ETF = I_T'/I_T
A36	116-120	5	79561	993.1	0.0104	0.2659	0.0130	0.2787	203	1.07
A588	137-141	5	79561	1001	0.0095	0.2713	0.0130	0.2966	216	1.13

* Element number of solid element on inner surface of OCB at governing wall section

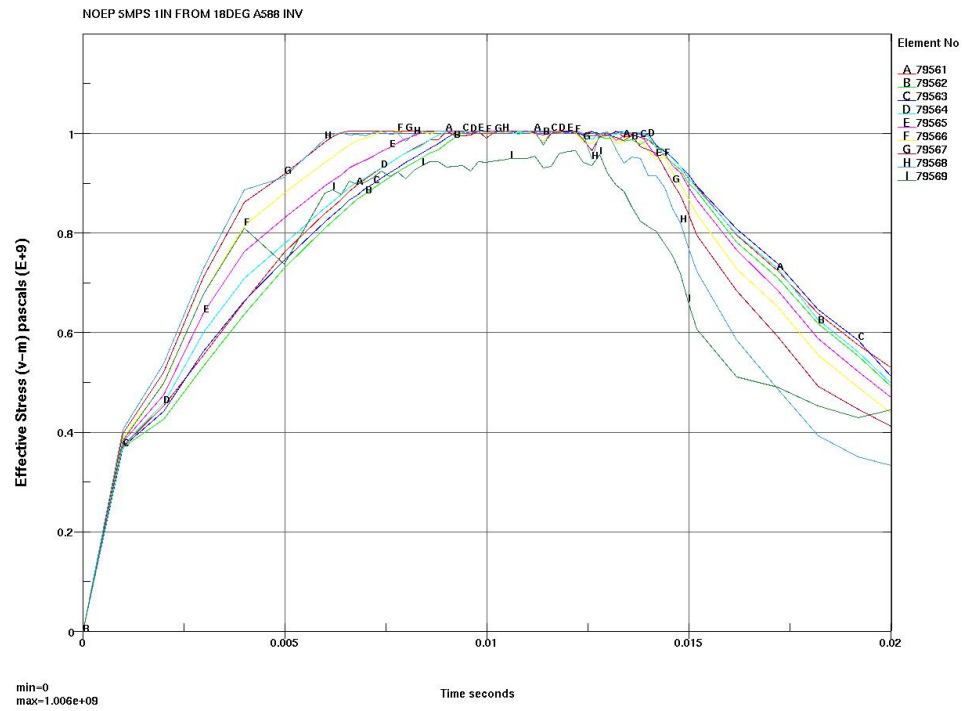
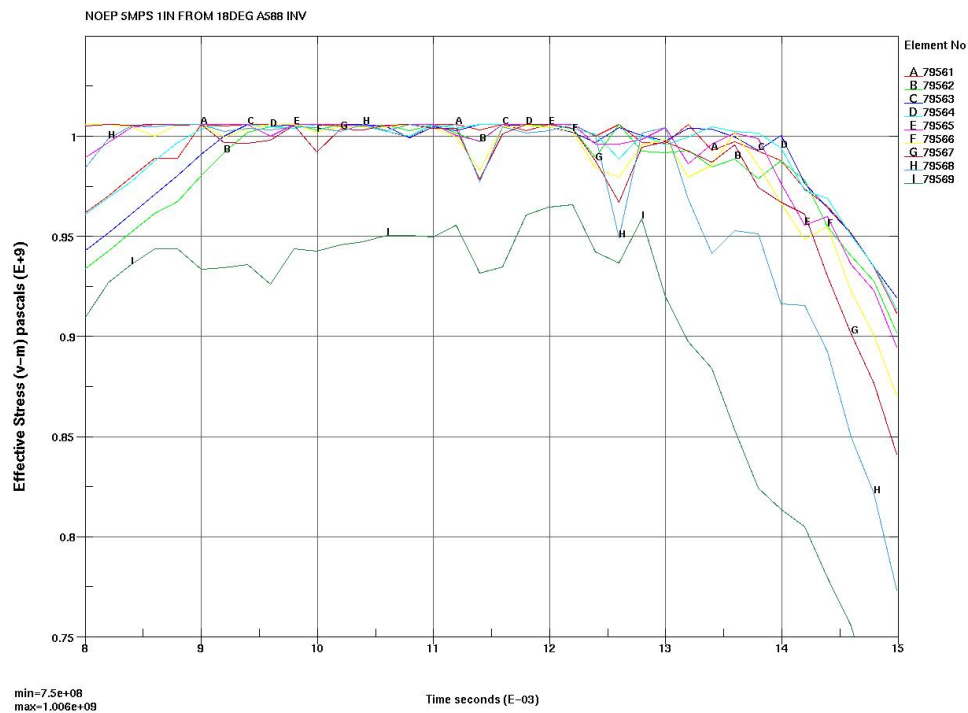


Figure 7-137 WP on A588 Invert 5 m/s Impact, VM Stresses

Figure 7-138 WP on A588 Invert 5 m/s Impact, t_{flow} and t_{unload} of VM Stresses

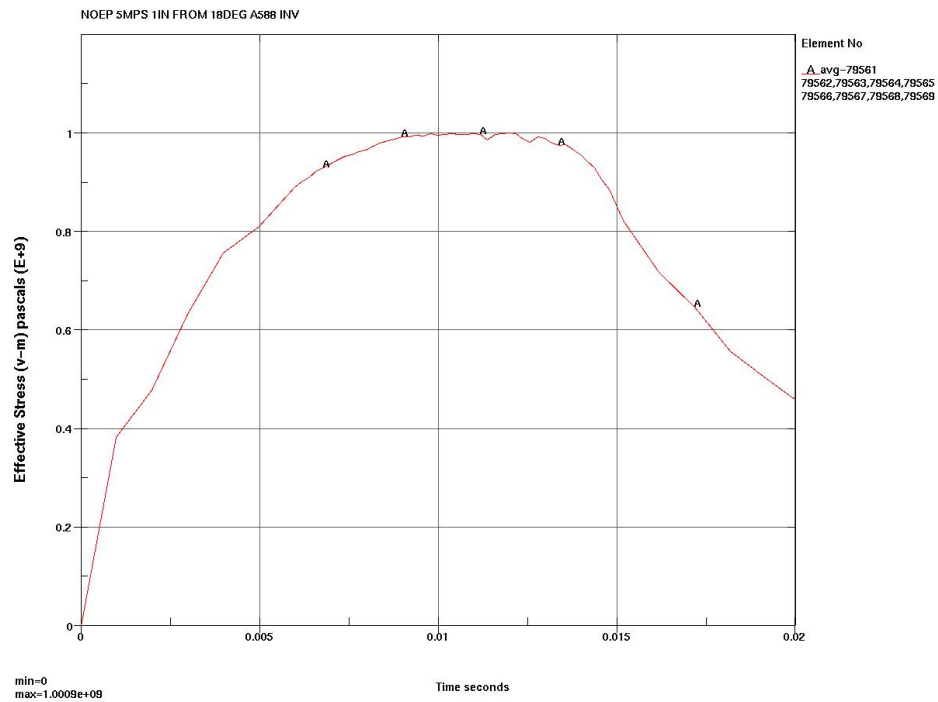


Figure 7-139 WP on A588 Invert 5 m/s Impact, EWA VM Stress

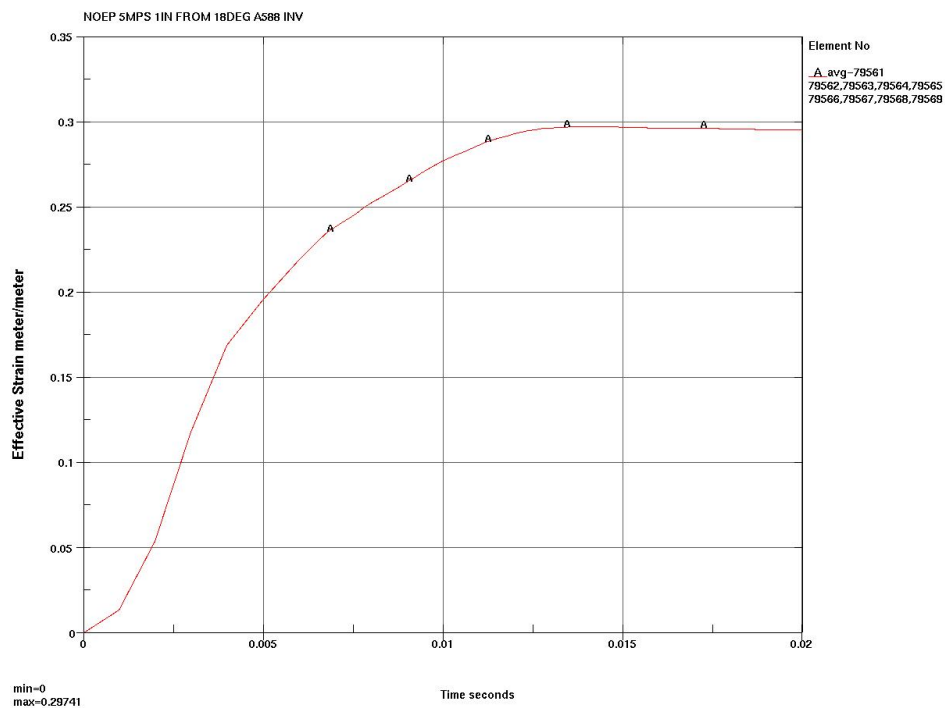
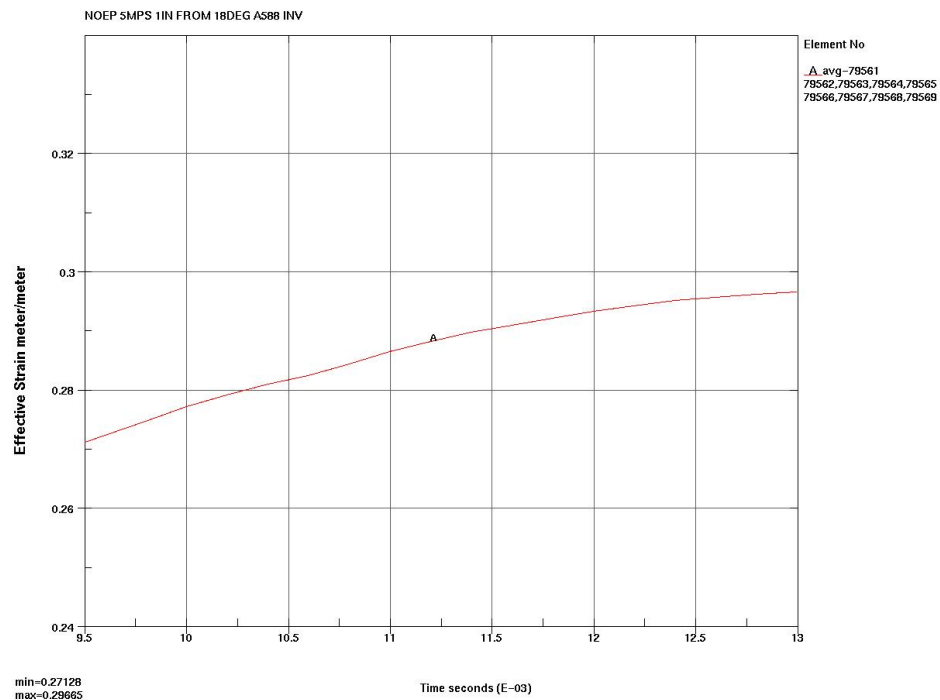
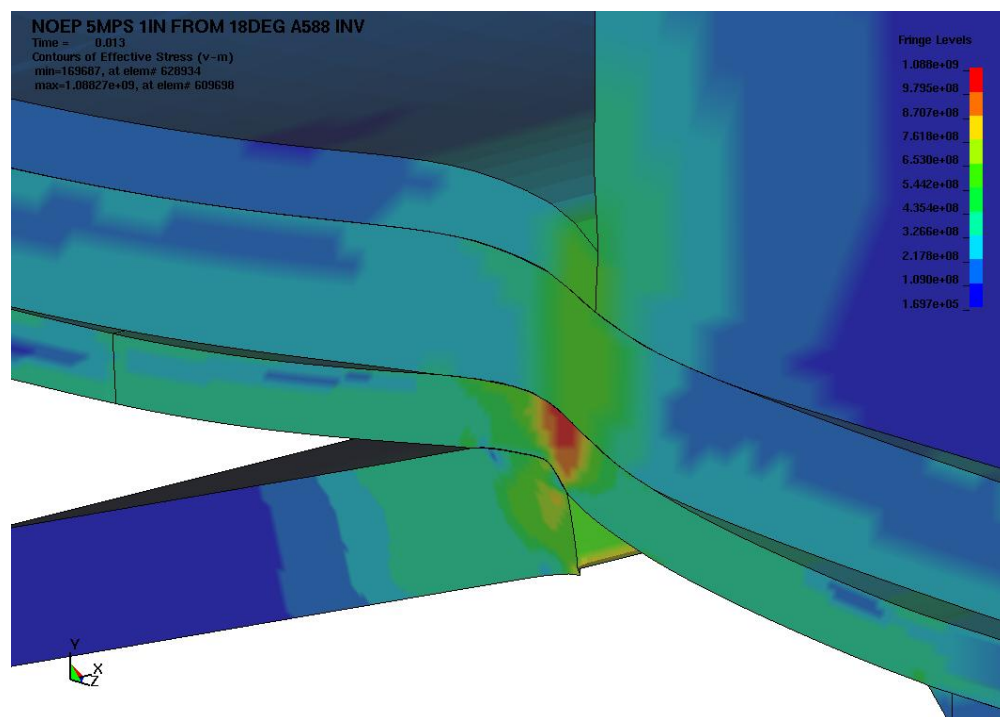


Figure 7-140 WP on A588 Invert 5 m/s Impact, EWA VM Strain

Figure 7-141 WP on A588 Invert 5 m/s Impact, VM Strain at t_{flow} and t_{unload} Figure 7-142 WP on A588 Invert 5 m/s Impact, Deformation and VM Stresses at t_{unload} , Pa

7.6 MATERIAL STRENGTH VARIABILITY

The vendor-averaged OCB Alloy 22 material strength data used in the FER simulations represents a mean (expected) value. Information on Alloy 22 strength variability is limited in traditional sources. Reference 2.2.47 processes strength variation data contained in Reference 2.2.48 based on an assumed Normal Distribution. This includes a computation of the variability in Toughness Index, I_T , values computed without triaxiality adjustments (uniaxial test data) and expressed as the standard deviation (σ) from the mean in percent. The average standard deviation of I_T in Table 7-4 of Reference 2.2.47 is 25%. This is rather high strength variability definitely due in part to the small number of data samples and possibly also due in part to the chemistry extremes used in the Reference 2.2.48 test program. The trend plots of computed ETF values versus velocity are broadened using this variability in the next section.

7.7 DETERMINISTIC AND CAPABILITY CALCULATIONS SUMMARY

The deterministic ASME minimum property simulation for a 20 *in* RT drop (3.15 *m/s* impact) of the WP onto the worst case location of the EP on a flat surface (Figure 6-24) had a time maximum EWA SI value of 587 *MPa* (see Section 7.2.7 and Figure 7-44). The ratio of this value to ASME minimum RT true tensile strength ($\sigma_u = 971$ *MPa*) is 0.60. This easily satisfies the acceptance criteria in Section 7.1.4 of Reference 2.2.15.

A comparative deterministic ASME minimum property simulation was run for a 20 *in* RT drop (3.16 *m/s* impact) of the worst case 18 *deg* tilted WP directly onto the invert steel at the worst case offset. The time maximum EWA SI value of 863 *MPa* (see Figure 7-143) occurs at the element string 79084 which is adjacent to the maximum 4 *mps* Capability simulation element string 79570. The ratio of this value to ASME minimum RT true tensile strength ($\sigma_u = 971$ *MPa*) is 0.89, very close to the $0.9\sigma_u$ limit allowed if the EWA SI drops below $0.77\sigma_u$ at a distance of $\sqrt{R \cdot t}$ (see Section 7.1.4 of Reference 2.2.15). Element 79084 is 0.0133 *m* from the symmetry plane, therefore the EWA SI value at $\sqrt{0.927 \cdot 0.0254} - 0.0133 = 0.14$ *m* from the symmetry plane must be below $0.77 \cdot 971 = 748$ *MPa*. This is element string 79336 whose maximum EWA SI value in Figure 7-144 is 694 *MPa*. Therefore, this deterministic calculation meets the ASME acceptance criteria, but with little margin.

The results of the worst case Capability evaluations in Tables 7-15, 7-16 and 7-17, presented on Figures 7-66, 7-90 and 7-126, respectively, are collected on Figure 7-145. The maximum offset flat impact without EP data point and intermediate tilt angle data points are included for comparison. Incipient failure is indicated when the ETF reaches unity, therefore the two data points above $ETF = 1.0$ are not valid (voiding and localized strains are not correctly simulated above the failure level). The data also logically trends towards zero ETF at an impact velocity of zero, except for the w/ EP data trend. In this case the OCB ETF being tracked is that for the eventual contact region with the invert steel and it is near zero until the velocity is high enough for the EP to collapse and allow the WP to strike the invert steel.

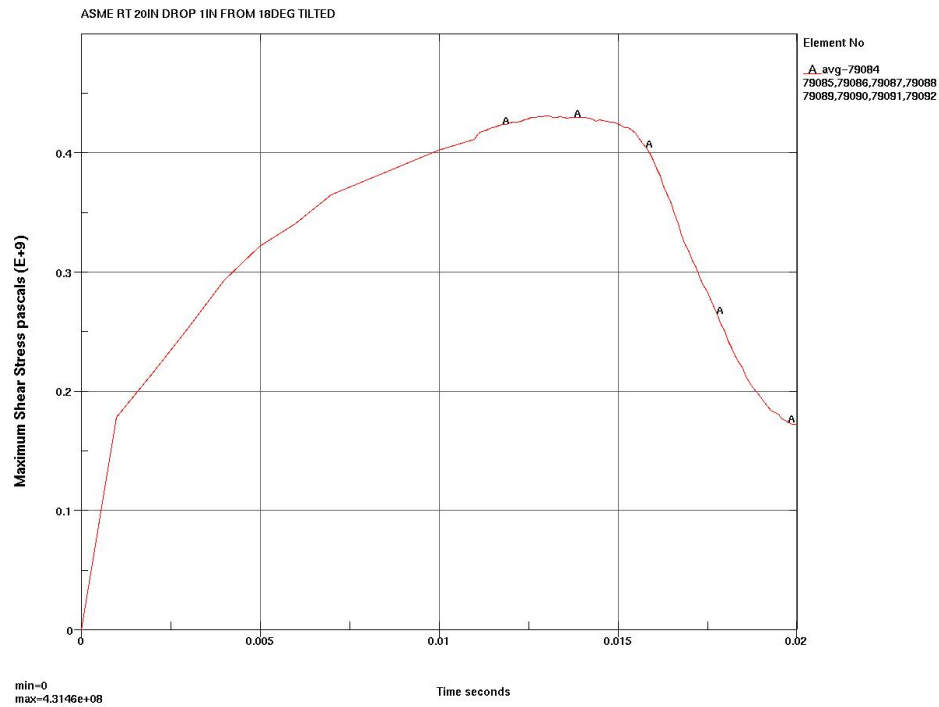
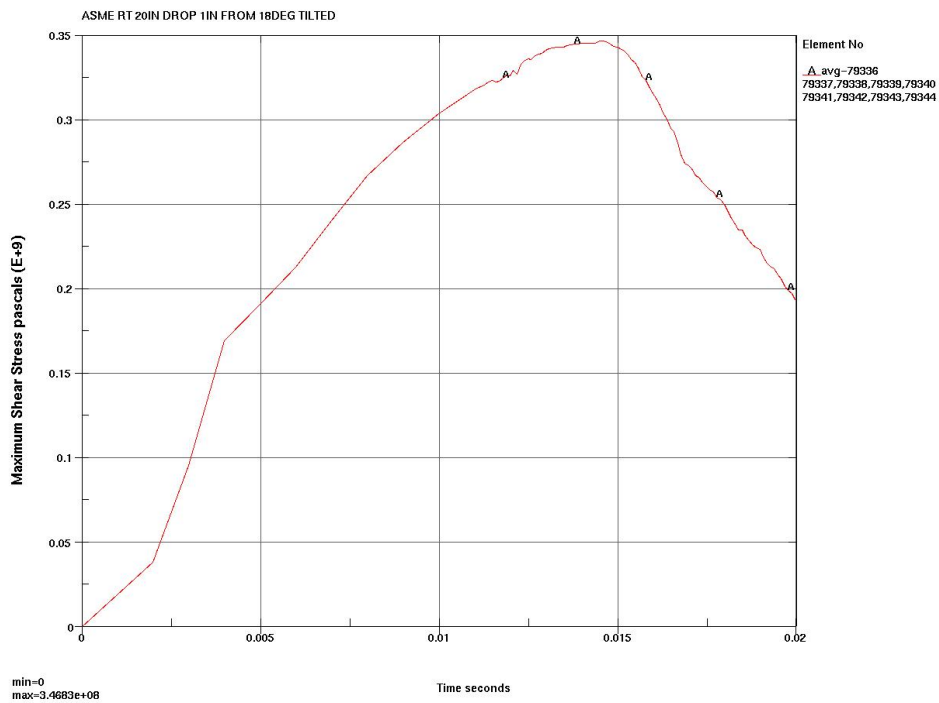


Figure 7-143 18 deg tilted 20 in drop on Invert, ASME Properties, Governing Location

Figure 7-144 18 deg tilted 20 in drop on Invert, ASME Properties, $\sqrt{R \cdot t}$ Location

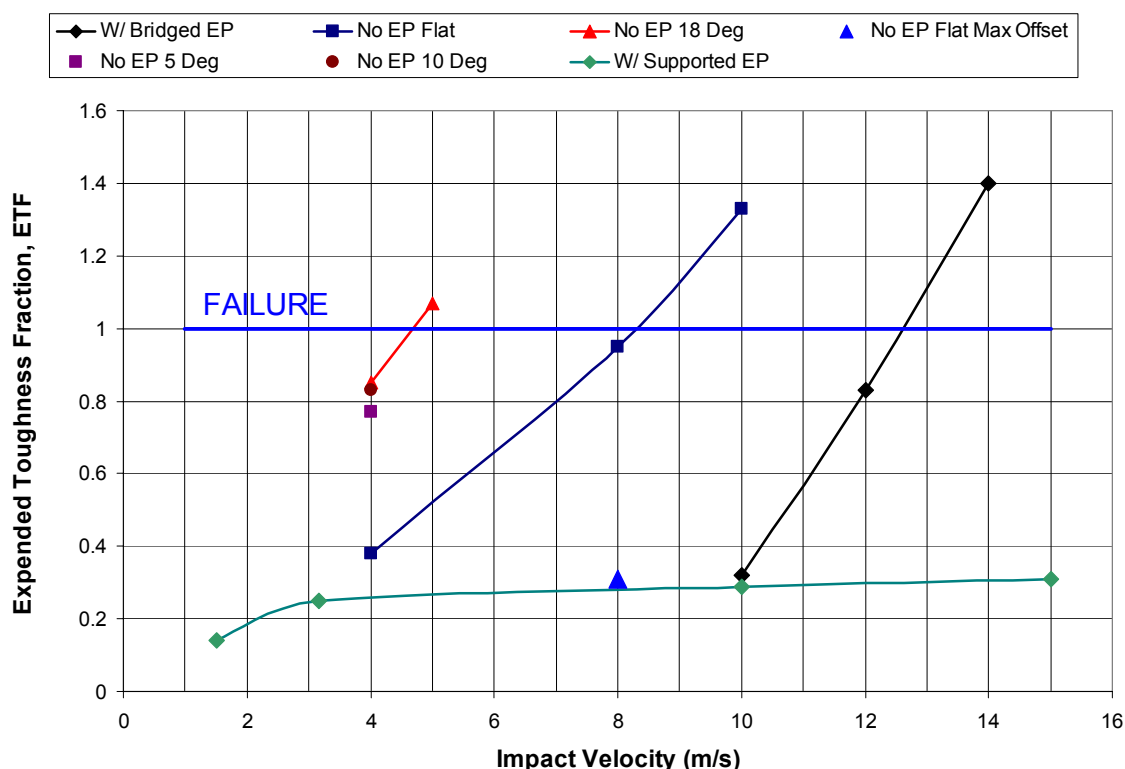
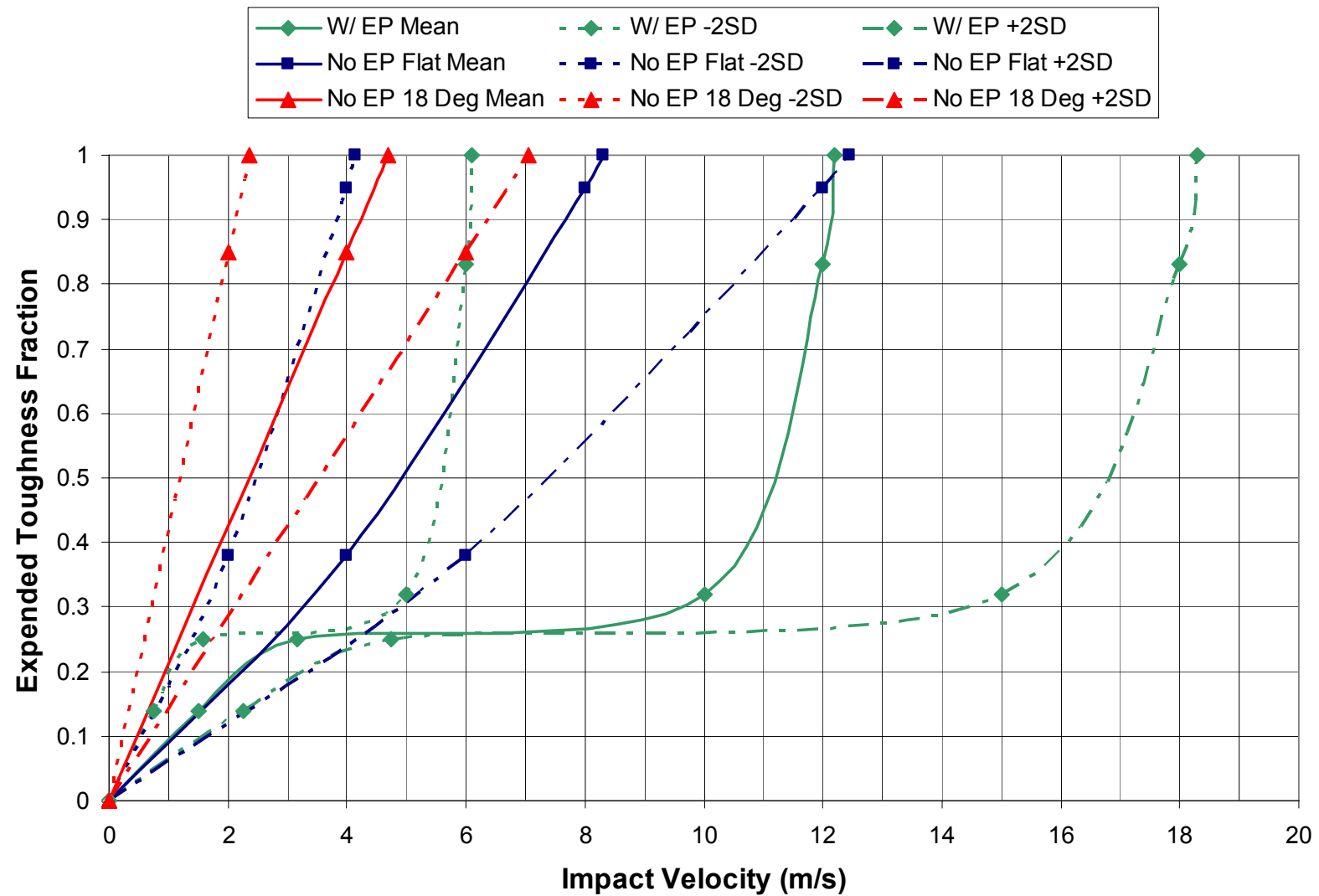


Figure 7-145 Mean Capability for Worst Case Impacts

Two additional data trends are used to adjust the four plotted trends on Figure 7-145. The first is the merging of the two trends for the WP on the EP impacts. The initial trend in both cases is that the highest stresses are at the WP to EP contact region. These stresses are highest for the fully supported EP. The minimum velocity for the WP to strike the floor or invert is for the bridged EP case and the stresses at the WP to invert steel contact region then become governing. The merging of the two trends provides a conservative composite of the two behaviors.

The spread due to material strength variability can be handled many ways. The linearity of the two “no EP” data trends with zero intercept indicates that the toughness expended for a given velocity is linearly related to the Toughness Index value, i.e., material with twice the Toughness Index of another material will require twice the impact velocity to expend the same fraction of available toughness (the two sets of time-maximum EWA VM stresses and strains develop the same ETF values). Therefore, one of the simplest material strength variability adjustments is to proportionately broaden the mean velocity trends linearly by the Toughness Index variability.

Values at two standard deviation (2σ or $2SD$) from the mean on normal Gaussian distributions provide 95% confidence limits. From Section 7.6, the standard deviation from the mean of the Alloy 22 annealed weldment Toughness Index is 25%. Therefore, decreasing and increasing the mean velocity trends by 0.5 and 1.5 can provide 95% confidence bounds on the failure velocity. Figure 7-146 provides these adjustments.

Figure 7-146 Mean and 2σ Capability for WP Worst Case Impacts

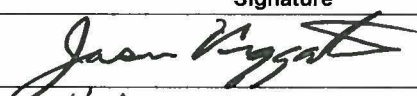

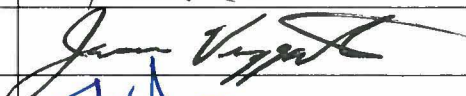
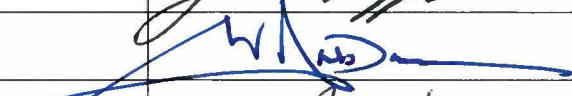

The comparative deterministic ASME material case to the No EP 18 Deg distribution indicates ASME acceptance criteria failure near 3.2 *m/s* whereas the Capability failure velocities vary between 2.3 *m/s* at $-2\sigma I_T$, 4.6 *m/s* at mean I_T and 7.0 *m/s* at $+2\sigma I_T$.

It is expected that a more refined statistical tuning of the Capability will be employed by Pre-Closure Safety using the herein contained impact location and orientation dependent mean failure levels, and material strength variability, convolved with the deterministic evaluations.

BSC**Calculation/Analysis Change Notice**

Complete only applicable items.

1. QA: QA
2. Page 1 of 5

3. Document Identifier: 000-00C-DNF0-00100-000		4. Rev.: 00C	5. CACN: 002
6. Title: Naval Long Waste Package Vertical Impact on Emplacement Pallet and Invert			
7. Reason for Change: CACN 002 is being issued to change the draft designator from QA:NA in CACN 001 to QA:QA to resolve CR 11897. CACN 001: Corrects originator error. Units for a released BSC calculation for standard deviation from mean were incorrectly believed to be percentage values, when actually, as labeled, were physical units of change. This did not affect the calculation of mean structural response, which is the objective of this calculation. The error affected an illustration of the potential variability in failure margin of the waste package to uncertainty in the structural properties of Alloy 22. This CACN has been initiated to help resolve Condition Report 11390.			
8. Supersedes Change Notice:		<input checked="" type="checkbox"/> Yes If, Yes, CACN No.: CACN 001 <input type="checkbox"/> No	
9. Change Impact:			
Inputs Changed: <input type="checkbox"/> Yes <input checked="" type="checkbox"/> No		Results Impacted: <input checked="" type="checkbox"/> Yes <input type="checkbox"/> No	
Assumptions Changed: <input type="checkbox"/> Yes <input checked="" type="checkbox"/> No		Design Impacted: <input type="checkbox"/> Yes <input checked="" type="checkbox"/> No	
10. Description of Change: CACN 001: Use re-computed average percent standard deviation from mean of Alloy 22 Toughness Index (7.3 % versus 25 %). Change-out pages attached (162,164,165 and 166) with revision bars. In Section 7.6 (page 162), reduce the amount of Outer Corrossion Barrier material toughness scatter from a standard deviation from mean of 25 % to a standard deviation from mean of 7.3 %. This is carried forward to page 164, last paragraph. Change the 2SD adjustments on the bottom of page 164 and in Figure 7-146 (page 165) from 0.5 and 1.5 to 0.85 and 1.15, respectively. Change the 95 % confidence PRA Capability failure velocity range on top of page 166 from 2.3 m/s and. 7.0 m/s to 4.0 m/s and 5.4 m/s, respectively.			
11. REVIEWS AND APPROVAL			
Printed Name	Signature	Date	
11a. Originator: Jason Viggato		3/31/08	
11b. Checker: Mohan Durani		3/31/08	
11c. EGS: Jason Viggato		3/31/08	
11d. DEM: Michael Anderson		3/31/08	
11e. Design Authority: Barbara Rusinko		3/31/08	

7.6 MATERIAL STRENGTH VARIABILITY

The vendor-averaged OCB Alloy 22 material strength data used in the FER simulations represents a mean (expected) value. Information on Alloy 22 strength variability is limited in traditional sources. Reference 2.2.47 processes strength variation data contained in Reference 2.2.48 based on an assumed Normal Distribution. This includes a computation of the variability in Toughness Index, I_T , values computed without triaxiality adjustments (uniaxial test data) and expressed as the standard deviation (σ) from the mean in percent. The average standard deviation of I_T in Table 7-4 of Reference 2.2.47 is 7.3 %. The trend plots of computed ETF values versus velocity are broadened using this variability in the next section.

7.7 DETERMINISTIC AND CAPABILITY CALCULATIONS SUMMARY

The deterministic ASME minimum property simulation for a 20 in RT drop (3.15 m/s impact) of the WP onto the worst case location of the EP on a flat surface (Figure 6-24) had a time maximum EWA SI value of 587 MPa (see Section 7.2.7 and Figure 7-44). The ratio of this value to ASME minimum RT true tensile strength ($\sigma_u = 971$ MPa) is 0.60. This easily satisfies the acceptance criteria in Section 7.1.4 of Reference 2.2.15.

A comparative deterministic ASME minimum property simulation was run for a 20 in RT drop (3.16 m/s impact) of the worst case 18 deg tilted WP directly onto the invert steel at the worst case offset. The time maximum EWA SI value of 863 MPa (see Figure 7-143) occurs at the element string 79084 which is adjacent to the maximum 4 mps Capability simulation element string 79570. The ratio of this value to ASME minimum RT true tensile strength ($\sigma_u = 971$ MPa) is 0.89, very close to the $0.9\sigma_u$ limit allowed if the EWA SI drops below $0.77\sigma_u$ at a distance of $\sqrt{R \cdot t}$ (see Section 7.1.4 of Reference 2.2.15). Element 79084 is 0.0133 m from the symmetry plane, therefore the EWA SI value at $\sqrt{0.927 \cdot 0.0254} - 0.0133 = 0.14$ m from the symmetry plane must be below $0.77 \cdot 971 = 748$ MPa. This is element string 79336 whose maximum EWA SI value in Figure 7-144 is 694 MPa. Therefore, this deterministic calculation meets the ASME acceptance criteria, but with little margin.

The results of the worst case Capability evaluations in Tables 7-15, 7-16 and 7-17, presented on Figures 7-66, 7-90 and 7-126, respectively, are collected on Figure 7-145. The maximum offset flat impact without EP data point and intermediate tilt angle data points are included for comparison. Incipient failure is indicated when the ETF reaches unity, therefore the two data points above $ETF = 1.0$ are not valid (voiding and localized strains are not correctly simulated above the failure level). The data also logically trends towards zero ETF at an impact velocity of zero, except for the w/ EP data trend. In this case the OCB ETF being tracked is that for the eventual contact region with the invert steel and it is near zero until the velocity is high enough for the EP to collapse and allow the WP to strike the invert steel.

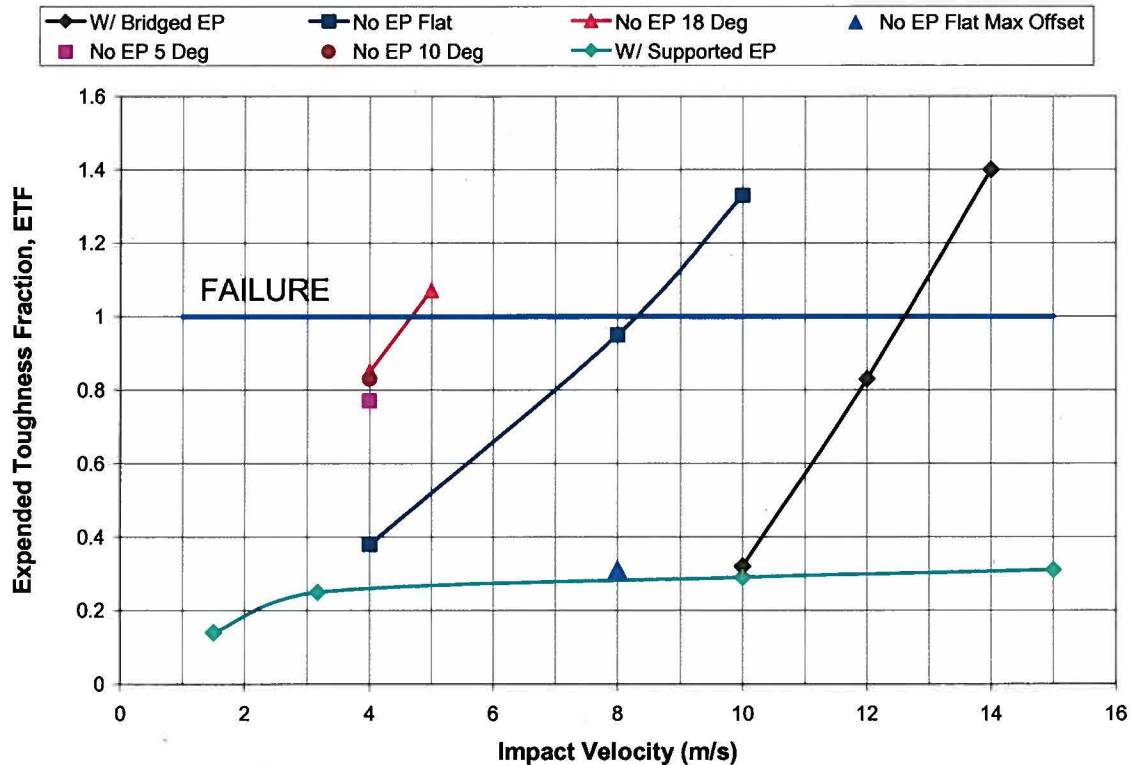
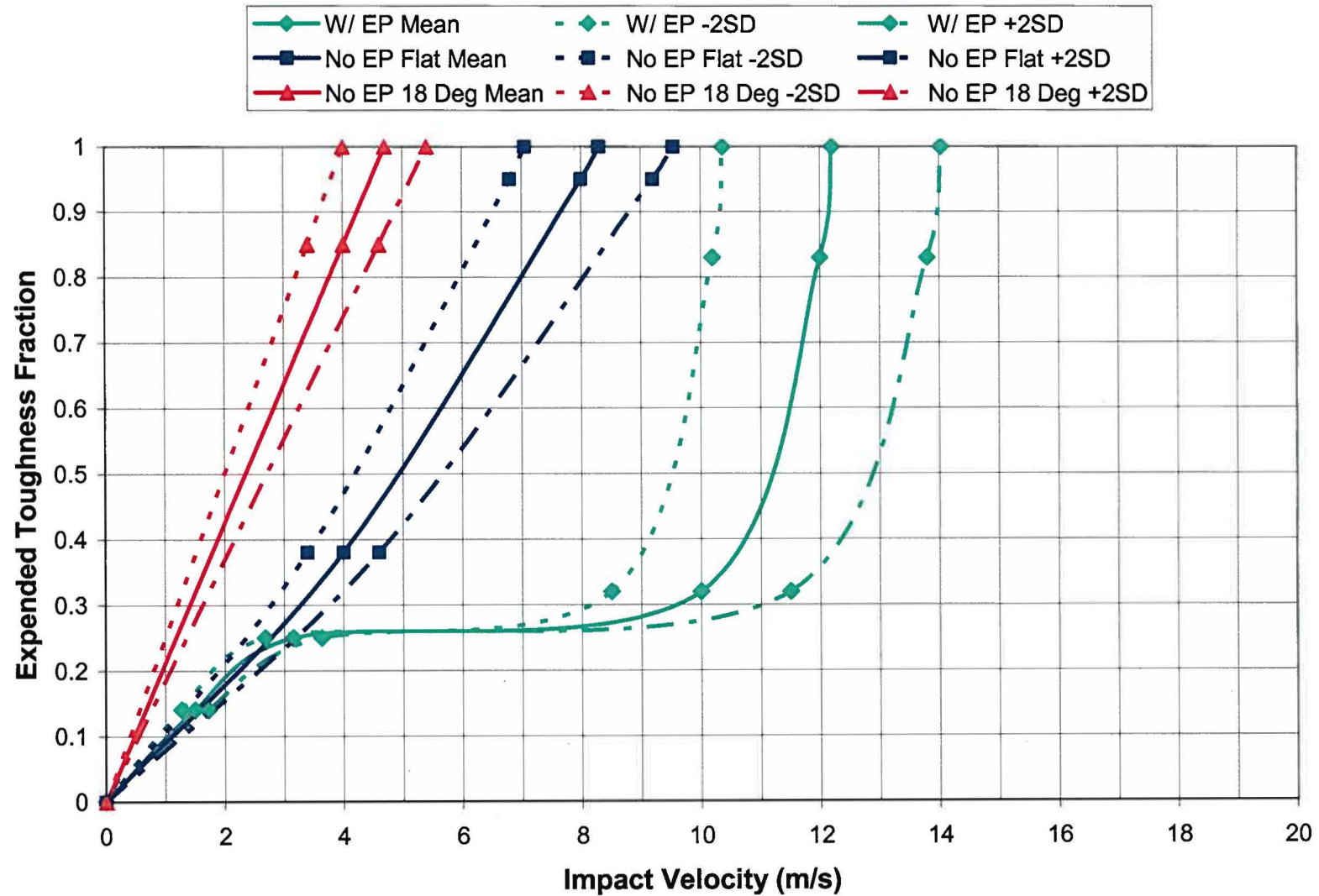


Figure 7-145 Mean Capability for Worst Case Impacts

Two additional data trends are used to adjust the four plotted trends on Figure 7-145. The first is the merging of the two trends for the WP on the EP impacts. The initial trend in both cases is that the highest stresses are at the WP to EP contact region. These stresses are highest for the fully supported EP. The minimum velocity for the WP to strike the floor or invert is for the bridged EP case and the stresses at the WP to invert steel contact region then become governing. The merging of the two trends provides a conservative composite of the two behaviors.

The spread due to material strength variability can be handled many ways. The linearity of the two “no EP” data trends with zero intercept indicates that the toughness expended for a given velocity is linearly related to the Toughness Index value, i.e., material with twice the Toughness Index of another material will require twice the impact velocity to expend the same fraction of available toughness (the two sets of time-maximum EWA VM stresses and strains develop the same ETF values). Therefore, one of the simplest material strength variability adjustments is to proportionately broaden the mean velocity trends linearly by the Toughness Index variability.

Values at two standard deviation (2σ or $2SD$) from the mean on normal Gaussian distributions provide 95% confidence limits. From Section 7.6, the standard deviation from the mean of the Alloy 22 annealed weldment Toughness Index is 7.3 %. Therefore, decreasing and increasing the mean velocity trends by the factors 0.85 and 1.15 can provide 95% confidence bounds on the failure velocity. Figure 7-146 provides these adjustments.

Figure 7-146 Mean and 2σ Capability for WP Worst Case Impacts

The comparative deterministic ASME material case to the No EP 18 Deg distribution indicates ASME acceptance criteria failure near 3.2 *m/s* whereas the Capability failure velocities vary between 4.0 *m/s* at -2σ I_T , 4.6 *m/s* at mean I_T and 5.4 *m/s* at $+2\sigma$ I_T .

It is expected that a more refined statistical tuning of the Capability will be employed by Pre-Closure Safety using the herein contained impact location and orientation dependent mean failure levels, and material strength variability, convolved with the deterministic evaluations.